DESIGN AND IMPLEMENTATION OF ANN BASED PHASE COMPARATORS APPLIED TO TRANSMISSION LINE PROTECTION

A Thesis Submitted to
The College of Graduate Studies and Research
for the Partial Fulfillment of the Requirements
for the Degree of Doctor of Philosophy
in the Department of Electrical and Computer Engineering
University of Saskatchewan, Saskatoon, Saskatchewan, Canada

By

GAGANPREET CHAWLA

PERMISSION TO USE

In presenting this thesis in partial fulfillment of the requirements for a Doctor of Philosophy degree from the University of Saskatchewan, the author agrees that the Libraries of this University may make it freely available for inspection. The author further agrees that permission for copying of this thesis in any manner, in whole or in part, for scholarly purposes may be granted by the professors who supervised the thesis work or, in their absence, by the Head of the Department of Electrical Engineering or the Dean of the College of Engineering. It is understood that any copying or publication or use of this thesis or part thereof for financial gain shall not be allowed without the author's written permission. It is also understood that due recognition shall be given to the author and the University of Saskatchewan in any scholarly use which may be made of any material in this thesis.

Request for permission to copy or to make other use of material in this thesis in whole or in part should be addressed to:

Head of the Department of Electrical and Computer Engineering,
University of Saskatchewan,
Saskatoon, Saskatchewan, Canada S7N 5A9

ABSTRACT

There has been significant development in the area of neural network based power system protection in the previous decade. Neural network technology has been applied for various protective relaying functions including distance protection. The reliability and efficiency of ANN based distance relays is improving with the developing digital technologies. There are, however, some inherent deficiencies that still exist in the way these relays are designed. This research addresses some of these issues and proposes an improved protective relaying scheme.

The traditional ANN distance relay designs use parameter estimation algorithms to determine the phasors of currents and voltages. These phasors are used as inputs to determine the distance of a fault from relay location. The relays are trained and tested on this criterion; however, no specific relay characteristic has been defined. There is a need for development of a new methodology that will enable designing of an ANN that works as a generic distance relay with clearly defined operating boundary.

This research work presents a modified distance relaying algorithm that has been combined with a neural network approach to eliminate the use of phasors. The neural network is trained to recognize faults on basis of a specific relay characteristic. The algorithm is flexible and has been extended for the design of other relays. The neural network has been trained using pure sinusoidal values and has been tested on a 17-bus power system simulated in PSCAD™. The training and testing of the neural network on different systems ensures that the relay is generic in nature. The proposed relay can be used on any transmission line without re-training the neural network.

The design has been tested for different fault conditions including different fault resistances and fault inception angles. The test results show that the relay is able to detect faults in lesser time as compared to conventional relay algorithms while maintaining the integrity of relay boundaries.

ACKNOWLEDGEMENTS

I am extremely grateful to Dr. Mohindar Singh Sachdev for the guidance and supervision provided during this research project. The suggestions and help in the preparation of this thesis are also thankfully acknowledged. I would also like to express my gratitude towards Dr. Ramakrishna Gokaraju for co-supervision of this work.

I thank all the advisory committee members, cognate member, Dr. Richard Burton and external examiner, Dr. Sukumar Brahma for their valuable suggestions.

I would also like to thank the secretarial and technical staff at the Electrical Engineering Department and the computer staff at the Engineering Computer Center at the University of Saskatchewan for all the support provided during this research. Financial support provided by the Natural Sciences and Engineering Research Council (NSERC) of Canada and College of Engineering at the University of Saskatchewan is thankfully acknowledged.

A special thank you to my dear husband, Rishabh – I could not have done this without you! The completion of this work would not have been possible without the support of my family and family-in-law; thank you for being there for me.

TABLE OF CONTENTS

LIST OF FIGURES

LIST OF TABLES

LIST OF ACRONYMS AND SYMBOLS

ANN	Artificial Neural Network
A/D	Analog to Digital
A-B	Phase A and Phase B (Fault or Relay)
ABC-G	Phase A, Phase B and Phase C (Fault or Relay)
A-G	Phase A to Ground (Fault or Relay)
B-C	Phase B and Phase C (Fault or Relay)
B-G	Phase B to Ground (Fault or Relay)
C-A	Phase C and Phase A (Fault or Relay)
C-G	Phase C to Ground (Fault or Relay)
CT	Current Transformer
DC	Direct Current
DFT	Discrete Fourier Transform
EMTDC	Electromagnetic Transient
EMTP	Electromagnetic Transient Program
FFT	Fast Fourier Transform
FIRANN	Finite Impulse Response Artificial Neural Network
FNN	Fuzzy Neural Network
Hz	Hertz
IEEE	The Institute of Electrical and Electronics Engineers
km	kilometers
kV	Kilo-volts
LP	Low Pass Filter
MUX	Multiplexer
MVA	Mega Volt-amperes
NN	Neural Network
O/C	Overcurrent
OP-Amp	Operational Amplifier
p.u.	Per unit

PSCAD	Power System Computer Aided Design
PT or VT	Potential or Voltage Transformer
R	Resistance on an Impedance Plane
SLG	Single Line to Ground Fault
SNR	Signal to Noise Ratio
TCC	Time Current Curve
X	Reactance on an Impedance Plane
Z	Impedance seen at the Relay Location
Z_r	Impedance Reach of a Relay
θ_z	Impedance Reach Angle or Maximum Torque Angle
Z_{r1} or $\overline{Z}_r$	Positive Sequence Impedance reach of a relay
ms	Milliseconds
μs	Microseconds
I_a or $\vec{I}_a$	Current or phasor of Current flowing in Phase A
I_b or $\vec{I}_b$	Current or phasor of Current flowing in Phase B
I_c or $\vec{I}_c$	Current or phasor of Current flowing in Phase C
V_a or $\vec{V}_a$	Voltage or phasor of Current of Phase A
V_b or $\vec{V}_b$	Voltage or phasor of Current of Phase B
V_c or $\vec{V}_c$	Voltage or phasor of Current of Phase C
I_{comp}	Zero Sequence Compensation Current
$\vec{V}_r$ or $\vec{V}$	Fault Voltage measured at the Relay Location
$\vec{I}_f$	Fault Current as seen at the Relay Location
$\overline{X}_{r1}$ or X_{react}	Positive Sequence Reactance Reach
θ_{react}	Reactance Reach angle
μP	Microprocessor
ΔT	Sampling Time Interval
N	Number of samples in a Data Window
LSQ	Least Square Technique

$x_{1,2....n}$	n-dimensional Input Vector
$w_{1,2....n}$	n-dimensional Weight Vector
$z_{1,2....n}$	n-dimensional Output Vector
Φ	Angle between Inputs of the Relay
$Input_1$ or $Input_{1\,\mathrm{mod}}$	First Input of the Relay
$Input_2$ or $Input_{2\,\mathrm{mod}}$	Second Input of the Relay
$Z_r^{'}$	Modified Impedance Reach of a Relay
Z_{rb1} or X_{rb1}	Impedance or Reactance reach for Blinder on the positive side of X-axis
θ_{rb1}	Reach Angle for Blinder on the positive side of X-axis
Z_{rb2} or X_{rb2}	Impedance or Reactance reach for Blinder on the negative side of X-axis
θ_{rb2}	Reach Angle for Blinder on the negative side of X-axis
+ve seq.	Positive Sequence
$Z_{apparent}$	Apparent Impedance seen at Relay Location

1. INTRODUCTION

1.1 Power System Protection

Power systems are complex in nature because they include a large number of generators, transmission lines and protection & control equipment that makes them susceptible to electrical, insulation and mechanical failures [1]. The operation of these components is crucial to ensure availability of electrical energy to all loads connected to the system. A power system protection scheme cannot prevent these failures, but can ensure that any faulted equipment in a power system is isolated as soon as possible to avoid serious outages and spreading the damage to the electrical equipment.

Any protection scheme should be able to maintain a balance between some essential features. Three main features of a protection system are:

(a) Speed: A fault in a power system should be isolated as soon as possible to limit the damage and prevent it from spreading into the system. Widespread faults can result in loss of synchronism and voltage collapse of the system.

(b) Selectivity: A protective relay system should be able to determine if a fault is within its zone of protection or not. Further, the protection scheme should only trip the circuit breakers within its protection zone. Relay communications are helpful in achieving this function.

(c) Reliability: A protection system should be reliable to operate under fault conditions. Incorrect design/settings and deterioration in service are main factors for unreliability of a protection system. The reliability of the system can be increased by using back-up protection; however, this may reduce the speed because of time delay of the back-up protection zone.

Protective relays are one of the most economical, reliable and flexible protective devices. Relays, in conjunction with circuit breakers, are used to protect power system components including generators, transformers and transmission lines. Typical relays

used in a power system for protecting the system components can be categorized on the basis of their performance characteristics as [1, 4]:

- Distance Relay
- Definite Time Relay
- Inverse time Relay
- Over-Current Relay
- Directional Over-Current Relay
- Directional Power Relay
- Differential Relay
- Under-Voltage/Over-Voltage Relay

All these relays except differential relays use inputs from only one side of the line, also known as a non-unit scheme. A differential relay compares inputs from two ends of the protection zone to detect faults. Some of these relays are discussed briefly.

(a) Distance Relays: The most commonly used relays for protecting transmission and sub-transmission lines belong to the family of distance relays. Over the past eighty years successful designs based on electromechanical, solid-state and digital electronics technologies have been produced and marketed. Distance relays are expected to provide instantaneous trip coverage for faults on transmission and sub-transmission lines [1]. These relays implement various characteristics, such as impedance, offset-impedance, admittance, reactance and blinders.

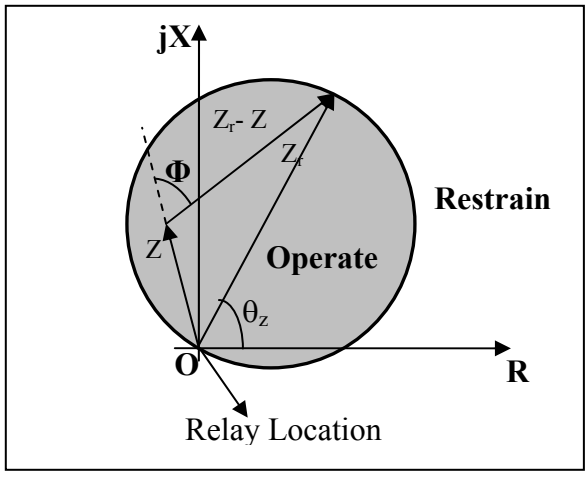

Figure 1.1: Ideal Characteristics of a Mho Relay

Distance relays are based on the principle that the impedance of the system seen at a relay location is proportional to the distance between the relay and the fault location. These relays detect faults by comparing two inputs either in terms of magnitude or the

phase. The impedance as seen at the relay location is measured to determine if the fault lies within or outside the relay characteristic boundary that are plotted on an impedance plane. Figure 1 shows the ideal operating characteristics of a mho relay installed at a line terminal represented in the figure at the origin of the impedance diagram. The maximum reach of the relay is $\overline{Z}_r$. The impedance reach $\overline{Z}_r$ is the positive sequence impedance of the transmission line. For a fault on the line, the apparent impedance measured at the relay location is inside the relay characteristic. By geometry, the angle Φ between the impedances $\overline{Z}_r - \overline{Z}$ and $\overline{Z}$ is less than ninety degrees. On the other hand, this angle is more than ninety degrees if the fault is outside the reach of the relay. These conditions can be mathematically expressed as:

$$-90° < \Phi < +90° \quad \text{for fault on the line} \tag{1.1a}$$

$$-90° > \Phi > +90° \quad \text{for fault outside line} \tag{1.1b}$$

When a fault occurs on a transmission line, the impedance seen by the relay cannot be measured directly. The current and voltage at the point of relay installation are measured and the positive sequence impedance is calculated. These relays are further discussed in Section 2.6.

(b) Overcurrent Relays: These relays are one of the simplest forms of protective relays that use the current in a circuit to detect a fault. The overcurrent relay setting depends on the full load current of a circuit. Relay pick-up time depends on the increase of this current in the circuit. These characteristics are represented by time-current curves (TCCs). These relays can be used either as instantaneous overcurrent with delay timers or as inverse overcurrent relay. An instantaneous overcurrent relay detects the fault current in its primary protection zone and trips the primary zone without any intentional delay. If the primary relay fails to perform, an instantaneous back-up relay trips the circuit after a desired time delay.

The current/time grading of an inverse overcurrent relay for primary and secondary protection zones is done by "nesting" the TCCs. The pick-up time of this type of relay is inversely proportional to the circuit current. For a fault in the primary zone, the current

seen by the primary relay is greater; therefore, the pick-up time of primary relay is lesser than the pick-up time of the back-up zone. This type of grading is useful in radial distribution systems.

The time delay between different zones of protection depends on the accuracy of the relay, primary zone circuit breaker and an appropriate safety margin between primary and backup protection zones. These relays are discussed in detail in Section 2.3.

(c) Directional Relays: Both terminals of a line in a transmission or subtransmission network are usually connected to energy sources that contribute to the flow of currents when a fault is experienced on the line. The flow of excessive current alone cannot be used to distinguish between faults on the line from faults on adjacent lines. Directional relays are used in such cases. These relays preserve the directionality of a system by discriminating between reverse and forward faults. They compare the current in the line and voltage at the relay location and detect forward faults based on the phase angle between the voltage and the current. Directional relays can be used as independent units or as additional elements to provide directionality to other protection systems. These relays and their coordination are discussed in Section 2.4.

(d) Differential Relays: Differential relays compare current "going into" and "coming out" of a protection zone. The criterion of operation of these relays is based on the fact that current flowing into a protected circuit is equal to the current flowing out of the circuit during normal operation. This criterion is not valid when a fault is in the protection zone; the current flowing into the zone is greater than the current flowing out of the zone. Differential relays are widely used to protect transformers, generators, lines and buses. These relays are discussed in detail in Section 2.5.

Electromechanical and solid-state technologies were used in producing protection systems during the previous century. Digital electronics and application of numerical techniques received considerable attention by power system protection engineers during the previous thirty years [3]. Numerical relays have provided performance superior to the

performance of most electromechanical and solid-state relays due to their higher speed, more flexibility, increased reliability and precise information. Algorithms such as Discrete Fourier transform, Least Squares technique, Kalman Filtering etc. [21, 22] are used in numerical relays to detect faults. Most of these techniques calculate phasors from the samples and quantized values of the voltages and currents [5, 23]. The calculation time of most of algorithms is about one period of the fundamental frequency and therefore, a final decision is made usually in about one period of the fundamental frequency.

1.2 Introduction to Artificial Neural Networks

Artificial neural networks (ANNs) are inspired by biological neural systems and have been modeled based on a human brain. ANNs are information-processing paradigms that are capable of recognizing different patterns and perform according to the way they are trained. They have the ability to learn and adapt to the conditions they are subjected to just like a human brain.

Neural Networks can simulate multiple layers of inter-connected neurons that process information. These neurons have the ability to train, learn and recognize patterns similar to biological neurons. They have an ability of self-organizing and self-learning. ANNs have proven to be highly successful in solving non-linear complex problems that could not be handled by conventional numerical algorithms. Different structures and learning algorithms of ANNs are discussed in detail in Chapter 3.

ANN technology had rapid development in the early 1990's. Substantial in-depth research regarding the properties of ANNs and their applications to non-linear problems has been conducted. Power system protection, like any other real-life complex problem, is non-linear in nature. Numerous applications of ANNs for protecting power system components have been proposed in the previous few years. Some of these applications are discussed in the Sections 1.3 and 1.4.

1.3 Artificial Neural Networks for Power System Protection

Most numerical relaying algorithms used until 1990s processed samples of voltages and currents using conventional digital signal processing techniques. In the last decade, ANNs have been applied in various engineering applications, including power system protection. The ability of ANNs to act as non-linear, non-parametric estimators has helped to unravel power system protection problems that were otherwise difficult to solve with conventional numerical methods. Specifically, ANNs have been used for fault detection, directional discrimination of the faults on the transmission lines [6, 7], fault classification on double circuit lines [8], distance protection of transmission lines [9], differential protection of power transformers [10] and generators [11], detection of high-impedance faults [14] and adaptive reclosing [15].

Even though ANNs are gaining popularity for power system protection applications, protection engineers are doubtful about the use of neural networks for relaying applications due to lack of analytical methods that can explain the design and internal processes of neural networks [5]. Some of the issues associated with the competence and reliability of the ANNs have been addressed by analyzing an ANN based fault discriminator. This analysis, developed by using MATLAB neural network toolbox [12], is described in references [13] and [35].

1.4 Literature Review of Neural Network Based Protective Relays

Extensive research work has been carried out for applying ANNs for specific protective relaying functions. One of the earliest applications of neural networks, proposed by S. Ebron, D.L. Lubkeman and M. White, detects high impedance faults by separating it from normal transients using a feed-forward network [25]. This study discusses the importance of data preprocessing before its application to the ANN. In this work, an electromagnetic transient program (EMTP) [27] generated training cases in which faults were simulated on a 12 kV distribution line. Samples of current waveforms in case of high impedance faults and normal transient events were obtained from these simulations. A preprocessor module separated each current waveform into separate cycle and extracted pertinent information that included peak of transient current, pre- and post

transient currents and amount of imbalance between phases. The neural network was trained and tested using these simulations. This design primarily demonstrates the potential of neural networks as an effective strategy for detecting incipient faults.

H.Singh, T.S. Sidhu and M.S. Sachdev proposed the design and implementation of a three-layer neural network for directional discrimination of faults [6, 40] in 1995. The design used instantaneous values of currents and voltages from a three-phase transmission line connected at each terminal to a power system represented by an equivalent generator. The voltages and currents were pre-processed by removing higher-order frequency components by using 4^{th} order anti-aliasing filters and the decaying dc component from the fault currents. A 12-4-1 configuration neural network trained with the voltages and currents representing single phase to ground, phase-to-phase and three phase faults successfully identified forward faults from reverse faults. The directional discriminator was implemented on a TMS320C30-based system.

T. Dalstain and B. Kulicke presented a neural network approach for classifying faults on parallel transmission lines in 1995 [20]. The design uses a 30-20-15-11 neural network for classifying single line to ground, double phase to ground and three phase to ground faults on a 2-bus, 2 source system. Training has been done using 2268 fault patterns derived by simulating faults on a 380 kV transmission line using an electromagnetic transient simulation program [26]. A fault location module has been used in addition to the trained ANN. The system has been tested with 240 independent test patterns from the same power system. The algorithm has been extended for detection and classification of arcing faults for implementing auto-reclosing; a 20-15-10-1 neural network has been used. The work reports that ANN detects an arcing fault in less than 30 ms in most cases.

Qi Weiguo, G.W. Swift, P. G. McLaren and A.V. Castro proposed an ANN for distance protection in the presence of fault resistance in 1996 [16, 41]. This design uses a 4-5-1 configuration neural network to detect faults when a non-linear arcing fault resistance is present. Simulated current and voltage samples from a 2-source, 4-bus power system have been pre-processed to obtain four ANN training inputs; resistance, reactance, X/R

ratio and system equivalent reactance. Testing patterns have been simulated by running tests for different fault locations. The ANN results have been compared with a conventional relay. The neural network has also been tested for acceptable criteria by applying "running" data that has more samples than the usual testing data.

S.A. Khaparde, N. Warke and S.H. Agarwal presented an ANN based adaptive relaying technique in 1996 [18]. The relay uses a multi-layer perceptron to implement a quadrilateral relay on a 2-bus, two source system. This work assumes that the phase angle between voltage and current is available as an input. Three inputs that include voltage, current and the phase angle between the voltage and current have been used for offline training of a 2-8-1 network. Inputs close to the relay characteristics' boundaries generated by varying voltage, phase angle and fault resistance, have also been added to the training set. It has been reported that the proposed relay failed to perform accurately near the relay boundaries. It has been noted that the proposed relay is a first step in designing an ANN relay for adaptive relaying.

Ioni T. Fernando, P.G. McLaren and A.V. Castro integrated ANNs and distance relaying for double circuit transmission line protection in 1997. This research project [42] investigates parallel usage of neural networks to validate or invalidate the trip signals issued by individual impedance elements of a numerical relay in double circuit and six-phase transmission systems. Current and voltage samples obtained by simulating 120 fault cases on a 2-source, double line system have been pre-processed using a FFT technique. These current and voltage phasors, that are devoid of higher order frequency and d.c. components, are then used for ANN training. Each training data set has 32 fault and 8 pre-fault data points. The ANN relay includes six "sub-ANNs" that have been trained with same inputs; each ANN is trained to identify a different faulted phase. The ANN has been tested using a different data set, primarily for 10%, 80% and 90% fault locations on a transmission line. This work reports that the relay is able to pick up the close-in faults accurately, however, shows performance deterioration for remote faults.

D. V. Coury and D. C. Jorge [28] presented a neural network relay for zone-1 protection of transmission lines in 1998. A 2-source, 2-bus system has been considered and faults have been simulated for a 400kV, 100km transmission line. The fundamental frequency magnitudes of voltages and currents of the three phases have been obtained using a half-cycle Discrete Fourier Transform (DFT). The design uses thirty-two data samples of each input at a sampling frequency of 4 kHz. The MATLAB NN toolbox has been used to train a 6-2-1 ANN network. Weights of the trained ANN have been used to implement the design on a microprocessor. The neural network has been tested for 0º and 90º fault inception angles and fault resistances ranging between 0Ω and 100Ω. The tests have been conducted for single phase to ground faults only.

F. Zahra, B. Jeyasurya and J. E. Quaicoe proposed a ANN based fault indication and location technique for transmission lines in 2000 [17, 43]. The neural network inputs have been obtained by simulating faults on a 345kV, 160 mile transmission line in a 2-source, 2 bus power system using EMTP [27]. Faults have been applied at 23 fault locations to simulate a total of 344 cases. The design uses Fast Fourier Transform (FFT) to obtain the frequency spectrum of voltages and currents and normalizes these inputs with respect to the 60 Hz component. One-cycle data window at a sampling rate of 960 Hz has been used. Two different ANNs, with configurations 32-4-2-1 and 32-5-3-1 have been used for detecting single line to ground faults and per-unit fault distance respectively. These configurations have been changed to 48-3-3-1 and 48-5-4-2 respectively for three phase faults. The ANNs have been tested for 160 different cases on the same power system. It has been reported that the neural network is able to detect a fault in less than one cycle after fault inception for 84% of test cases not seen by the network previously.

A.L.O Fernandez and N.K.I Ghonaim presented a finite impulse response neural network (FIRANN) for fault detection and direction estimation on high voltage transmission lines in 2002 [7]. A FIRANN with a 45-35-5 configuration has been trained and tested on a five bus system using temporal back propagation algorithm [34]. Each fault pattern has one cycle of pre-fault samples and 1.25 cycles of post fault samples. The five outputs of

the trained ANN indicate the presence of fault, the faulted phase, the fault direction, and whether the applied fault is an under-voltage/undercurrent or over-current fault. The same approach has been extended for designing a differential relay for a three phase transformer [10].

M. Sanaye-Pasand and H. Khorashadi-Zadeh proposed a fault detection and phase selection technique using an ANN in 2003 [19]. A 230 kV power system has been simulated using PSCAD/EMTDC™ [36] and magnitudes of currents have been used to train and test a 5-10-4 neural network. A DFT Technique has been employed to calculate the magnitudes of currents. Negative sequence current and zero sequence current, along with currents of three phases are used as five inputs to the ANN. The four outputs of the ANN detect the fault in each phase and the neutral. The fault type, fault location, fault inception time, source impedance and pre-fault power flow direction have been changed for testing the ANN. It has been reported that the ANN detects a fault in about 60ms in most cases.

A. H. Osman, Tamer Abdelazim and O. P. Malik presented a transmission line distance relaying scheme using on-line trained neural networks in 2005 [33]. The scheme has been implemented on a DSP board to perform real-time analysis. The technique is based on a modified differential equation of a transmission line model for estimating fault location. The neural network uses an adaptive data window technique [24, 37] employing a four-sample window algorithm. It has been trained and tested for different fault conditions during single line to ground, double line and three phase faults. Some of these conditions include fault locations that vary from 50km to 200km with 20Ω fault resistance and -20° loading angle; fault resistances varying from 0Ω to 200Ω with 180km line length; loading angles ranging from -10° to 30°. It has been reported that the neural network is able to estimate the fault distance in one cycle of fundamental frequency.

Many other approaches that use fuzzy neural networks for power system protection applications have also been proposed [29-31]. A fuzzy neural network combines the

™ Trademark of Manitoba Hydro HVDC Research Center

learning and generalization capability of a neural network with the robustness of fuzzy logic. One such approach has been presented by P. K. Dash, A. K. Pradhan and G. Panda in 2000 [32]. The neural network inputs have been obtained by simulating faults on a 230kV, 190 mile transmission line in a 2-source, 2 bus power system using EMTDC. The ANN inputs are post-fault peak values of fundamental frequency components of voltages and currents. Four different fuzzy neural networks (FNNs) have been used to detect single line to ground, line to line, double line to ground and three phase faults respectively. Separate FNNs have been used to estimate fault type and location. The FNNs have been tested for fault inception angles ranging from 30° to 90° and fault resistances ranging from 0 to 100 ohms.

1.5 Discussion

The literature review in the previous section discusses ANN based relaying applications that have been proposed in the previous decade. ANNs have been applied for detecting onset of faults, classification of faults and other protection functions such as estimating fault locations. Most ANN distance relay designs discussed in literature review use phase currents and voltages as neural network inputs and are expected to determine if a fault is within a certain distance of the relay location. However, none of these designs are trained for any generic relay characteristic with a defined operating boundary. Further, none of these relays have been designed for a specific relay function; the current and voltage inputs of a generic distance relay vary depending on the relay function.

The following deficiencies have been observed in the work listed in the previous section.

a. The neural network relays have been trained and tested to detect faults based on "distance to fault" from relay location; however, none of the designs define clear boundaries of the relay characteristic.
b. The relay performance close to boundaries of protection zone has not been evaluated since a specific relay characteristic has not been defined.
c. The proposed relays have been trained and tested on the same power system; therefore, they can be implemented only on the systems they are trained for. It would be necessary to re-train the ANNs before applying them on a different system.

d. Most of these relays use DFT or FFT to extract fundamental frequency components of currents and voltages that are applied as inputs to the ANN. The ANN is, therefore, being used only to perform logic of the relay that can be easily performed using trigonometric functions.
e. Some of the relays have been tested in the presence of fault resistance but without defining the relay characteristic. It cannot, therefore, be determined whether the apparent impedance in the presence of fault resistance lies inside or outside the relay operating characteristic.
f. The designs do not address the cases when inputs are not available or when the levels of the inputs are low, such as, re-closing of a circuit breaker on a close-in fault.

1.6 Objectives of the Research

The ANN relays that have been proposed for protecting transmission lines were analyzed. The performance of these relays was examined to set a research objective. Development of new strategies for designing ANNs that would work as generic distance relays with clearly defined operating boundaries needs to be performed.

The first objective of this research work is to develop a methodology that fully exploits the potential of ANNs to implement admittance relay characteristic with acceptable integrity of its boundaries. The second objective is to make the design flexible for the development of other distance relays and directional relays. The third objective is that the designed ANN should be suitable for applying to any power system without having to retrain it. The fourth objective is to use sampled and quantized values of current and voltage waveforms as inputs without converting them into phasors. The fifth objective of this research is to design a relay that performs adequately for different types of faults, with and without fault resistance. The final objective is that the relay should be able to detect close-in faults.

1.7 Outline of the Dissertation

The dissertation is divided into seven chapters and seven appendices. A general introduction to protective relaying and ANN applications in power systems is given in Chapter one. Various proposed ANN relays for power system protection are discussed and the literature review for these relays is presented.

The principles of power system protection are discussed in Chapter two. The different distance relays and their amplitude and phase comparison characteristics are discussed in detail. It also discusses the polarization techniques used to detect zero and low voltage faults. Numerical Protection and the numerical protective algorithms used in power systems are described. The factors affecting the detection of faults in power systems are also discussed.

The theory and principles of neural networks is detailed in Chapter three. The emulation of an artificial neuron and ANNs from a biological neuron is described. Different types of neural networks are discussed. Learning algorithms used for training neural networks are explained. The application of ANNs as pattern classifiers is described in this chapter as well. The application of ANNs in power systems for fault classification, fault detection and estimation of fault location is also discussed.

The issues associated with the conventional design of distance relays are discussed in Chapter four. The deficiencies related to the existing methods of fault detection using distance relay algorithms; electromechanical, static and numerical are discussed. This chapter proposes a new algorithm for the design of distance relays using instantaneous values of currents and voltages instead of phasors. The mathematical equations and calculations involved in the implementation of the design are presented. A full cycle DFT algorithm was used to prove the veracity of the proposed algorithm and the test results are presented.

The design and implementation of different distance relays that includes admittance relay, reactance relay, directional relay and quadrilateral relay are discussed in Chapter

five. The mathematical calculations involved in the design of each of these relays are presented. This chapter also discusses the polarization techniques that were used along with the proposed design to detect faults very close to the bus where the relay is installed. The proposed design was tested for accuracy in the presence of different levels of noise and the results are presented in this chapter.

The designed relays were tested on a seventeen-bus power system simulated using PSCAD/EMTDC and the results are presented in Chapter six. The faults were applied at the different percentages of a transmission line at two different fault inception angles. The ANNs were tested according to their applications; therefore, the quadrilateral ANN relay was also tested for different fault resistances. Some of the results from these tests are shown and discussed in this chapter. This chapter also presents the results obtained by applying polarization for different faults. A comparative analysis of some results with a conventional Discrete Fourier Transform algorithm is presented.

Chapter seven concludes the dissertation and summarizes the issues that have come forward during this research project. It also discusses the contributions made by this research and presents future directions to further enhance the new approach that is presented in this dissertation.

Appendix A provides the details of the Discrete Fourier Transform (DFT) technique that was used to test the proposed algorithm. The sine and cosine weights and the impedance used for testing are given. The parameters of the neural networks are shown in Appendix B. The impedance reach values used for training the quadrilateral relay have been given.

Appendix C shows the design process of the ANNs. Appendix D gives the data of the 17-bus power system simulated in PSCAD/EMTDC that was used to test the designed neural network based relays. This includes data for transmission lines, loads, generator and other sources.

Appendix E shows the calculation of positive sequence voltage during the occurrence of single line to ground, line to line, double line to ground and a three line to ground faults using the principle of symmetrical components. Appendix F shows the noisy inputs used to test the proposed algorithm. These inputs were obtained by adding white Gaussian noise to pure sinusoidal currents and voltages. Appendix G gives the extra results of ANN testing for different faults. These results are not included in the main body of the dissertation due to space constraints.

1.7 Summary

This chapter introduces the general concepts of power system protection and the application of neural networks in power systems. Recent works done in the area of neural network based protective relaying are detailed in this chapter. The issues and deficiencies existing in the current relays are discussed. The objectives of this research project and thesis are outlined. Further, this chapter also provides the organization of the thesis.

2. TRANSMISSION LINE PROTECTION

2.1 Introduction

The basic concepts of power system protection, ANNs and applications of ANNs in power systems are introduced in Chapter 1. The literature review on ANN based distance relays and the deficiencies existing in proposed designs are discussed. The research objectives and outline of the dissertation are presented.

This chapter gives an overview of power system protection philosophy and the factors affecting a protective relaying scheme. Transmission line protection schemes based on overcurrent, directional, differential and distance protection principles are discussed. Distance relay amplitude and phase comparators are discussed in detail. The principles of numerical relaying, including the theories of parameter estimation techniques are presented.

2.2 Protective Relays

2.2.1 The Principle of Protective Relaying

Power system protection schemes can be divided into two groups, primary relaying and back-up relaying. Figure 2.1 illustrates primary relaying zones of protection for different power system components [3]. A separate zone of protection is set up for each element of the power system. The power system elements are interconnected through circuit breakers and a fault on one of the component causes the circuit breaker of only that particular zone to trip (open). This provides the selectivity aspect of protective relaying. Reliability is another very important requirement of a power system protection scheme. For this purpose, the zones of protection overlap so that no area of a power system is left unprotected. The circuit breakers are usually controlled by tripping devices such as relays. The time taken to isolate faulted equipment from a system depends on the relay tripping time and the circuit breaker opening time.

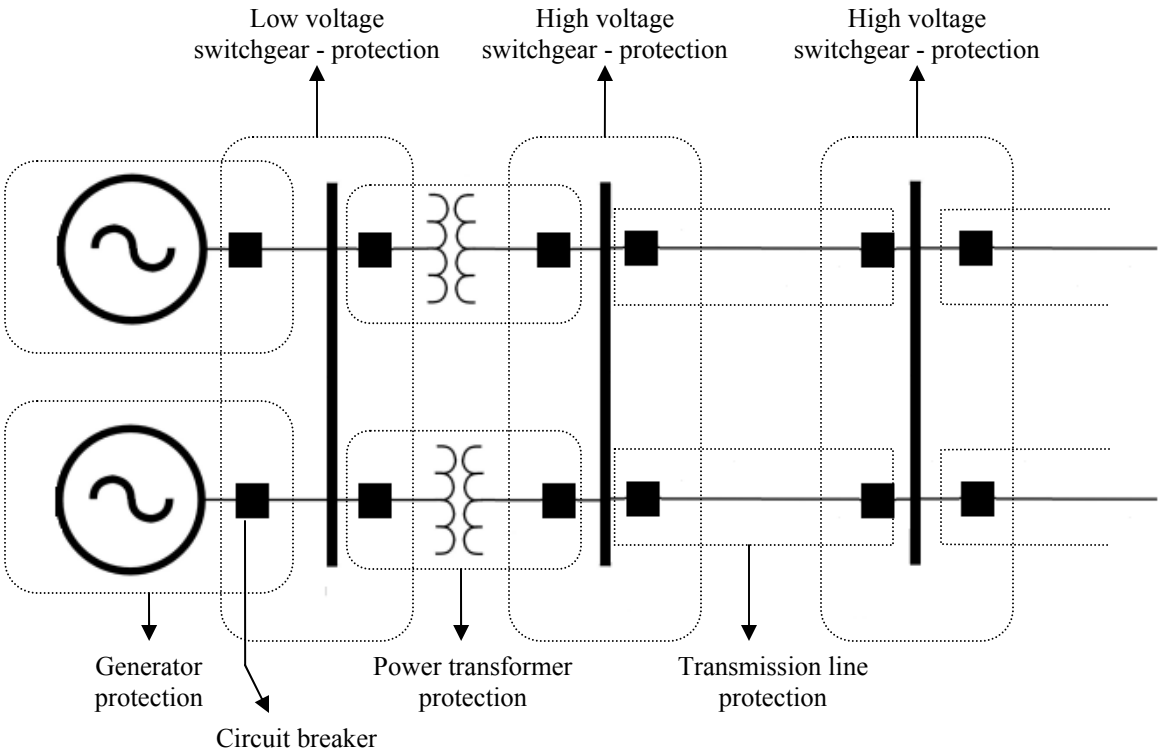

Figure 2.1: Primary Relaying for Power System Components

Back up relaying protects power system equipment in case of failure of primary protection. Primary protection of one zone usually acts as back up protection for the adjacent zones with appropriate time delays. For example, in Figure 2.1, the bus protection relay can act as a back up relay in case the transmission line protection fails. The time delay between the two zones usually accounts for the relay tripping time, circuit breaker opening time and a safety margin.

2.2.2 Types of relays

Relays can be categorized by different principles and performance characteristics. Table 2.1 gives the different classifications of protective relays [4]. These have been classified on the basis of their input, operating principle and characteristics. Modern numerical relays are sophisticated and are able to perform other functions such as monitoring, metering, regulating and producing sequence of events.

This chapter explains the theory and principle of relays based on their characteristics. Sections 2.3 to 2.5 explain the theory and principles of overcurrent, directional and differential relays respectively. This research project focuses mainly on the design and implementation of the distance relay characteristics for transmission line protection; therefore, the theory and principles of this relay are explained in detail in Section 2.6.

Table 2.1: Classification of Protective Relays [4]

Relays - Classification Criteria		
By input	**By operating principle**	**By characteristic**
• Current • Voltage • Power • Frequency • Flow • Temperature	• Electromechanical • Solid-state • Balanced beam • Harmonic restraint • Percentage differential • Thermal • Gas accumulator	• Definite time • Inverse time • Overcurrent • Directional overcurrent • Directional power • Differential • Distance

2.3 Overcurrent Relays

Overcurrent relay protection is one of the most fundamental and economical forms of protective relaying. Overcurrent relays (also represented as O/C relays) use only one input, the fault current to detect a fault. The relay tripping time is usually a function of the fault current. These characteristics are represented on time-current diagrams using time-current curves (TCCs). The TCCs are usually plotted on log-log scale with time on the ordinate and current on the abscissa.

The setting of this relay depends on the full load amperage of a circuit. This relay can be used only when the minimum fault current is significantly higher than the maximum load current. A time delay is used for coordinating overcurrent relays and is dependent on the following factors.

- Accuracy of the relay characteristics: This may vary by relay manufacturer and type of relay, whether the relay is an electromechanical, solid-state or numerical relay
- Circuit Breaker Opening time: This is a combination of mechanical time and arc quenching time. The total time taken by a circuit breaker to isolate a fault is usually close to 50 ms.
- Over-travel time of upstream relay: This factor is considered in case of electromechanical disc-type relays that have a tendency to over travel.
- Safety Margin: A 10-20% safety factor is usually considered for good protective device coordination.

These relays are categorized into two types on the basis of protection principles. They can be used either as instantaneous overcurrent with delay timers or as inverse overcurrent relays.

2.3.1 Instantaneous Overcurrent Relays

Instantaneous Overcurrent relays are used for tripping a circuit breaker without any intentional delay. These are mostly used for primary protection zones, where fault current is the highest. These relays can be combined with delay timers as needed, for coordination with upstream relays and for back-up protection. Most numerical relays have multiple functions that enable a user to set these relays with and without delays, as required for protection and coordination purposes.

Figure 2.3 shows the characteristics of an instantaneous overcurrent relay without and with a delay timer of T_0 seconds. An ideal instantaneous function without delay is independent of time and is represented by a dotted line perpendicular to the X-axis. The instantaneous O/C function with T_0 delay is time-independent after the T_0 time has

elapsed. The practical TCCs for instantaneous O/C relay with and without delay are shown by using solid lines. It can be seen that a practical TCC of an instantaneous O/C relay deviates slightly from an ideal curve, resulting in an asymptotic curve.

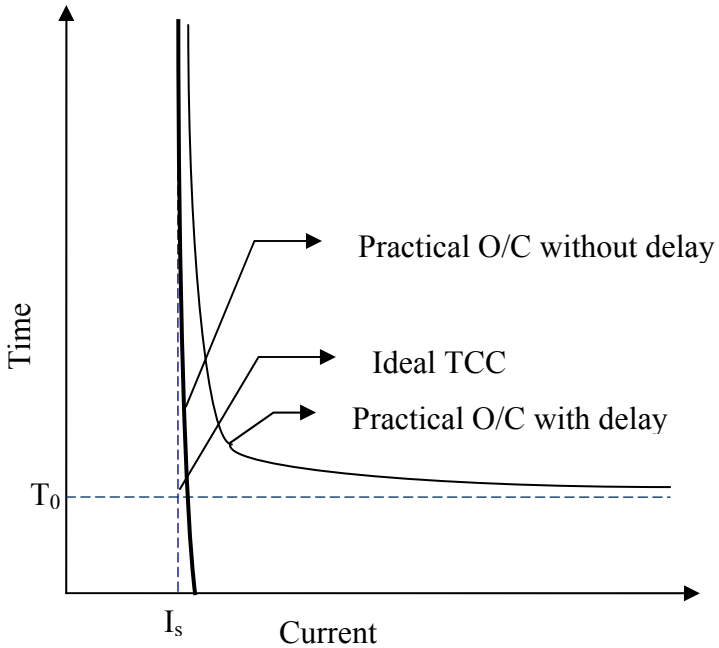

Figure 2.2: Overcurrent Relay Characteristics

The instantaneous setting of an overcurrent relay is dependent on the maximum current that flows in a circuit under normal conditions. This setting should account for cold load inrush i.e. the starting inrush current of motors, transformers, capacitor banks etc. The setting should be higher than the total inrush but lower than the maximum fault current in the circuit.

2.3.2 Inverse Overcurrent Relays

Inverse time overcurrent relays are dependent on the magnitude of fault current. The pick-up time of a relay increases with decrease in fault current. Figure 2.3 shows the characteristics of a typical inverse relay. The relays can be set with different time dial settings according to the desired operating time for proper device coordination. These relay characteristics are nested in a time-graded scheme for different zones of protection.

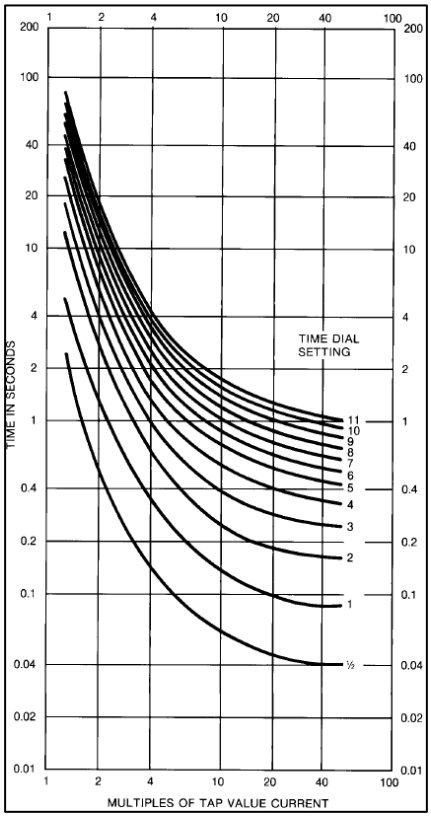

Figure 2.3: Typical Time-Current Curves for an Inverse Relay [75]

2.4 Directional Relays

Overcurrent relays are meant to see a fault in any direction. The time grading done in O/C relays is, therefore, useful in radial systems. This time grading does not apply when there is in-feed into a line from more than one source. In such cases, O/C relays cannot provide selective protection in a specific direction. This limitation can be overcome by using a directional relay. Directional relays compare the currents and voltages of a transmission line and deliver a trip signal in a fault condition based on the phase angle between the two inputs. This enables the relay to differentiate between the reverse and forward faults on the transmission line.

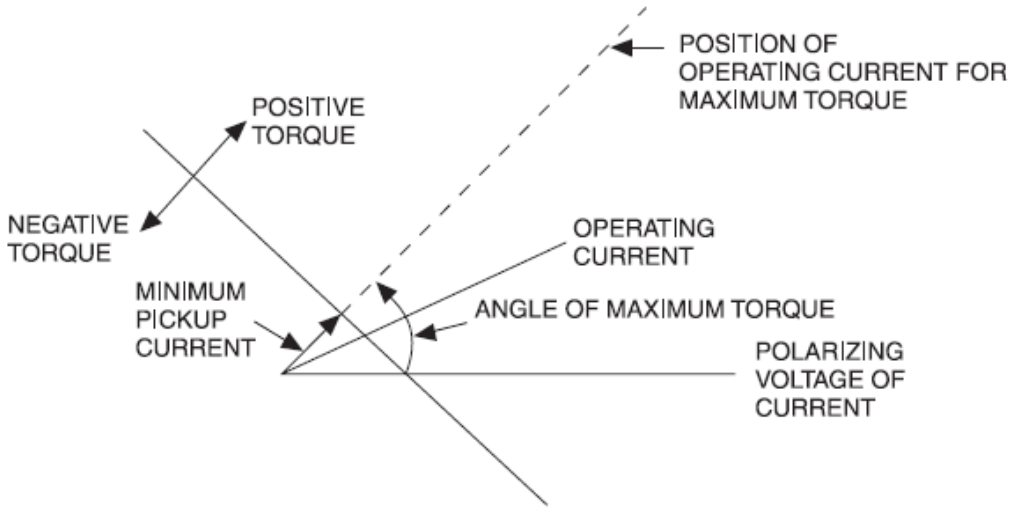

Figure 2.4: Characteristics of a Directional Element [75]

Figure 2.4 shows the characteristics of a directional element, as applied to an electromechanical relay. The same principle has been extended to solid-state and numerical relays. Each directional element has an operating element and a polarizing element. The current seen at the relay location is the operating element. The polarizing element is energized by voltage to determine the direction of current flow. The fault is considered to be in the operating area when the angle between the operating and polarizing elements is equal to the maximum torque angle of the electromechanical relay. In solid-state and numerical relays, these inputs are given to an Op-Amp type comparator or a microprocessor respectively and the relay trips if the measured values are above the

pickup settings and in the required tripping direction (usually forward direction). Some directional schemes are dual polarized and use both current and voltage as the polarizing element.

Directional relays can be used as an independent unit or as an additional element to provide directionality to an existing protective coordination scheme. Figure 2.5 shows a coordination scheme for directional overcurrent protection. Directional relays are time-graded according to the zones of implementation. In the shown figure, for a fault on line L_1, the relay at Circuit breaker 2 will pick up the fault. The relay at circuit breaker # 4 should act as a back-up relay for faults on line L_1. Therefore, the relays should be coordinated so that, $T_2 < T_4 < T_6 < T_8 < T_{10}$.

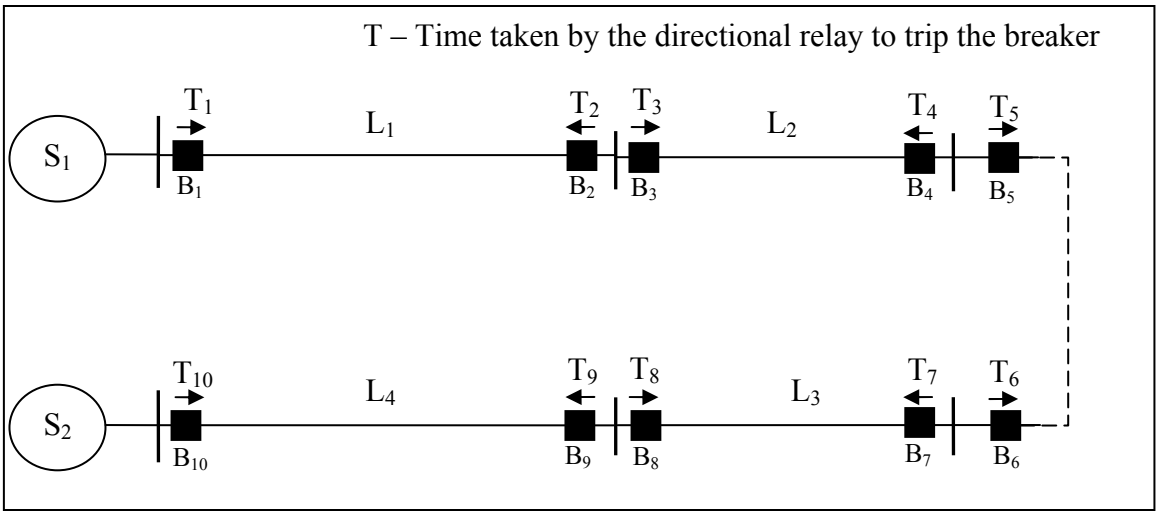

Figure 2.5: Coordination Scheme of a Directional Overcurrent Relay

Considering another case where the fault is at line 4. In this case, the relay at circuit breaker 9 should pick up the fault with relay #7 providing the back up protection. In such a scenario, the relays should be time graded so that $T_9 < T_7 < T_5 < T_3 < T_1$. Modern numerical relays have the provision to set up multiple zones for primary and backup protection. The setting for these is done according to the available fault currents in the respective zone. The relays are time-graded; therefore, no communication links between the relays are generally required. Another scheme where a directional element has been added to a distance relay is discussed in Chapter 5.

2.5 Differential Relays

In normal circumstances, the current flowing into a protected circuit is equal to the current flowing out of the circuit. In case of a fault inside the protected zone, part of the current contributes to the fault. The ingoing current, in such cases, is greater than out coming current, leading to an unbalance. The operation of a differential relay is based on this differential current between the two ends of a protected zone. The differential relay operates if the differential current exceeds a preset value.

Differential protection is generally applied to detect and isolate the faults in large motors, generators, lines or cables, transformers, and buses. Figure 2.6 shows the application of a typical differential protection scheme. The dotted box denoted by "87" indicates a differential relay; 87 is the ANSI device code for a differential protective device. The current transformers (CTs) on both sides of the equipment winding feed into the relay where the current going into and out of the equipment is compared. In case of transformer differential protection, the CTs on both sides are set to compensate for

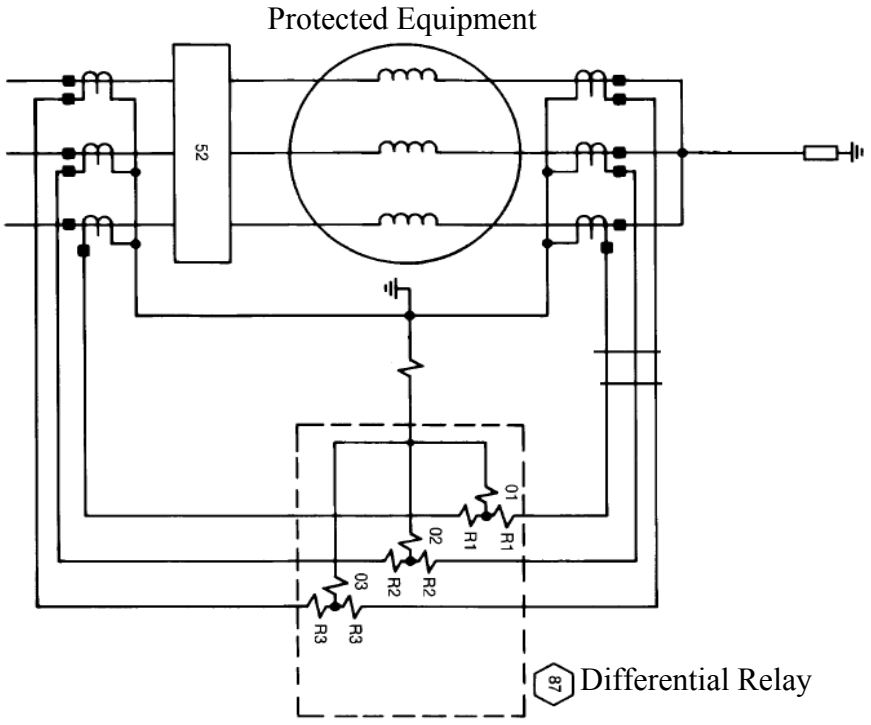

Figure 2.6: Typical Differential Protection Scheme [75]

voltage difference and delta/wye connections so that the secondary current from both the CTs can be matched. This is done by a set of taps that scale the current inputs from the two sets of CTs to match. Accurate selection and application (i.e. polarity and connections) of CTs is one of the critical factors for any differential protection scheme. Numerical relays have the provision to account for these changes internally.

Differential relays provide high-speed fault detection and are set to isolate the protective equipment instantaneously as soon as a fault is detected. Differential relays are sensitive and inherently selective and are designed to be insensitive to overloads or faults outside the protected zone. The two main types of differential protection schemes [75] are:

2.5.1 Overcurrent Differential Relay

An overcurrent differential relay is the least expensive and most widely used form of differential protection. It operates on a fixed differential current setting. The current input of this relay is given via the CTs on both sides. The accuracy of this relay is dependent on the type of relay, proper CT connections and errors. The current in secondary windings of the CTs is equal under normal circumstances, leading to zero current flow through the relay. When the differential current passing through the relay exceeds the pickup settings, the relay sends a trip signal to the circuit breaker to isolate the protected equipment.

CT saturation is one of the main caused that affects the performance of this protection. An exponentially decaying DC component is a part of a fault current, especially when the fault is close to a source such as a generator. During an external fault, a prolonged DC component can cause unequal saturation of CTs and lead to a substantial operating current. Another factor that can cause unwanted tripping of the equipment is the CT performance. Two same ratio CTs from different manufactures may not perform exactly in the same manner. This may cause a slight change in CT ratios, leading to a differential current to pass through the relay even under normal circumstances.

The only solution to these limitations is the increase in the maximum pick up setting of the overcurrent differential relay. The increase in the pickup setting reduces the sensitivity of the relay, especially for ground faults, where the current magnitude is lower. Another option is to use a percentage differential relay.

2.5.2 Percentage Differential Protection

A percentage differential relay is comparatively insensitive to high fault currents outside its protection zone that lead to CT errors. This relay is designed to be sensitive to all faults only within its protection zone. There are three main types of differential protection relays. These are fixed percentage, variable percentage and harmonic restraint differential relays.

2.5.2.1 Fixed Percentage Differential Relay

The amount of operating current is fixed at a percentage of the restraining (or polarizing) current in this type of relay. The relay trips if the differential current passing through the relay exceeds the set value. This relay is better than a differential overcurrent relay because the CT errors (or faults outside the protection zone) affect both the differential and the restraining current by the same percentage. This avoids nuisance tripping of the relay due to external faults. A fixed percentage differential relay can be used for generator, motor and transformer protection.

2.5.2.2 Variable Percentage Differential Relay

The magnetizing inrush current of a transformer during energization is equal to 6-8 times its full load current. This inrush current flows through the transformer primary CTs only, causing a significant differential current to flow through the relay. A fixed percentage relay setting needs to be adjusted (increased) for such cases. This may make it less sensitive for low-current faults. A variable relay can provide better protection than a fixed percentage relay in such situations. A different setting for situations such as transformer energization or motor starting can be used. This makes the variable percentage relay more sensitive to detect low-level faults.

2.5.2.3 Harmonic-restraint Percentage Differential Relay

The harmonic restraint percentage differential relay is primarily used in transformers as it has provisions to offer more restraint to harmonics. Transformer magnetizing inrush current predominantly contains 2^{nd} and 5^{th} harmonic components, therefore, this relay can be set to specifically offer restrain to these harmonic components. This is done by setting a specific slope (or sensitivity) setting for different harmonics. The relay does not operate if a certain percentage or lower amount of harmonic content is present in the current input of the relay.

2.5.3 High Impedance Differential Protection

This type of differential protection is typically used for bus protection. It reduces the differential current for external faults by introducing high impedance (usually close to 2000Ω) in the circuit. For faults within the relay protection zone, the CT error currents are small, the CT magnetizing impedances appear to be almost infinite, and the current flows through the relay coil [75]. The high-impedance differential elements, therefore, result in fast tripping of the relay for in-zone faults, while providing security during heavy through-faults and CT saturation.

2.5.4 Pilot Wire Differential Protection

The differential relays presented in the previous sections cannot be used for protecting long transmission and distribution lines. This is because of practical difficulties that arise because of the length of the CT leads that have to brought from both ends of the line. Further, cables have to be run from the relay to the circuit breaker location. Pilot wire differential relaying is used in such cases.

2.6 Distance Protection

Distance protection is a relatively quicker mode of eliminating faults on a transmission line. It overcomes the drawbacks of over-current and directional over-current relays in terms of time delays. Distance protection implements the principle of protecting a

transmission line by calculating the impedance at the point of relay installation. Distance relays use current and voltage inputs for their operation. The impedance of the circuit between the relay and the fault location is proportional to the distance between them, provided that the actuating quantities (voltage and current) are properly chosen [45]. The operation of the relays is thus, dependent primarily on distance of a fault from the relay location. Other factors affecting the operation of distance relays are fault resistance, load currents, current sources on the line etc [4]. Because of its simplicity and reliability, distance protection has been used widely for transmission and sub-transmission line protection. The same distance protection principles have been used in electromechanical, solid state and numerical relays.

2.6.1 Zones of Distance Protection

A distance protection scheme is normally a multi-zone arrangement. The first zone of protection provides instantaneous tripping and subsequent zones incorporate time delayed tripping [38], [46]. Figure 2.2 shows a stepped time-distance characteristic with three protective zones. The impedance reach of each zone has been represented numerically with a subscript. The times T_1, T_2 and T_3 refer to the time-setting of each zone and D_1, D_2, D_3 and D_4 represent the distance relays for tripping the circuit breakers.

The impedance reach of zone-1 is usually set to 80-85% of the transmission line impedance. Zone-1 provides instantaneous tripping for all faults lying within this distance. Practically, it is not possible to set a protection zone reach of 100% due to the inaccuracies introduced in an impedance measurement by transformation errors. For a typical numerical distance relay, the operating time T_1 is usually 20-30 ms for medium and high voltage transmission lines and 15-25 ms for extra high-voltage (EHV) lines [46]. This is the time taken by the relay to accurately calculate phasors for faults.

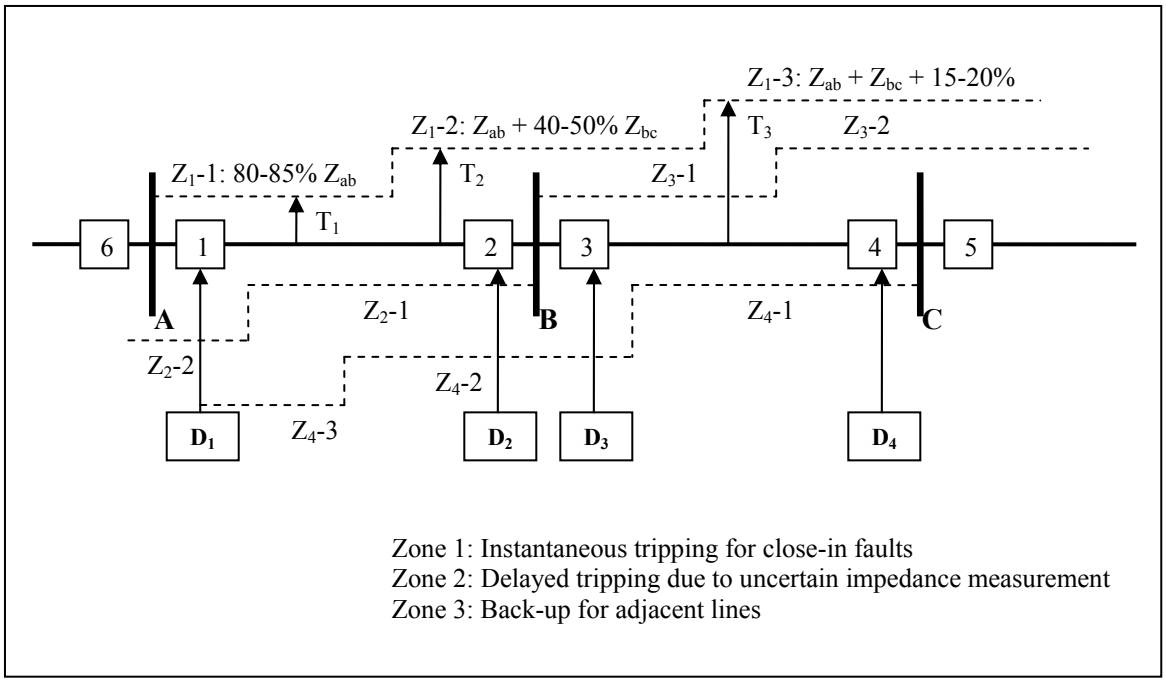

Figure 2.2: Stepped Zones for Transmission Line Distance Protection [38, 46]

Zone-2 provides time-graded protection for the remainder of the line and back-up protection for 40-50% of the shortest adjacent line. The time setting of zone-2 must initially allow the 1st zone relays on the neighboring line(s) to clear the fault. The zone-2 operating time for a numerical relay, therefore, is dependent on the operating time of the zone-1 relay, circuit breaker operating time on the neighboring line (~ 40 – 80 ms), distance relay re-setting time (~ 20ms), errors of distance relay internal timers (~ 10ms minimum), distance protection starting time (~ 15ms), circuit breaker opening time (~ 50ms) and an appropriate safety margin [46]. Zone-3 is primarily used for back-up protection for faults occurring in lines connected to the remote bus. The procedure for time grading for zone-3 is the same as zone-2, the only difference being that the operating time of zone-2 is taken into account instead of zone-1. Numerical relays have the capability to include more than three zones of protection.

2.6.2 Distance Relays

Distance relay measures the positive phase sequence impedance (Z_{1L}) between the relay location and the fault location. It is, therefore, important that the input currents and

voltages given to a distance relay accurately represent Z_{1L} during the occurrence of a fault. The six measuring elements (three from phase fault measurements and three from earth fault measurements) do not monitor the same impedance [38]. Distance relay characteristic is represented on an impedance plane. The measured impedance during a fault is influenced by a number of power system parameters and also by the fault type. Table 2.2 lists the voltage and current inputs given to distance relays for various fault conditions. This list can be found in references [4] [38] [39].

Distance relays detect faults by comparing two inputs either in terms of magnitude or the phase, resulting in amplitude or phase comparator respectively. Most of the numerical algorithms compare magnitude or phase angle of the calculated fault impedance with the transmission line impedance to determine if the fault lies within or outside the relay characteristic boundary. The following sections give a description of characteristics of various distance relays and their amplitude and phase comparison principles, that have been taken from reference [4].

Table 2.2 Inputs for Different Relay Functions

Fault	**Voltage (V_r)**	**Current (I_r)**
Phase Faults		
A – B, A – B – G and A – B – C	$V_a - V_b$	$I_a - I_b$
B – C, B – C – G and A – B – C	$V_b - V_c$	$I_b - I_c$
C – A, C – A – G and A – B – C	$V_c - V_a$	$I_c - I_a$
Earth Faults	$I_{comp} = 3k_0I_0$ where $k_0 = \frac{Z_{0L} - Z_{1L}}{3Z_{1L}}$	
A – G	V_a	$I_a + I_{comp}$
B – G	V_b	$I_b + I_{comp}$
C – G	V_c	$I_c + I_{comp}$

2.6.2.1 Admittance Relay

The characteristic of an admittance relay passes through the origin of the impedance plane. Given that Z_r is the impedance reach for the relay along the maximum torque line, the radius and center of the circle can be given as:

$$Radius_{mho} = \left| \frac{Z_r}{2} \right| \tag{2.1}$$

$$Center_{mho} = \frac{Z_r}{2} \tag{2.2}$$

(a) Amplitude Comparison Characteristic

Assuming Z to be the apparent impedance seen at the relay location, the amplitude comparison characteristic of the mho relay is:

$$\left| \frac{Z_r}{2} \right| \geq \left| Z - \frac{Z_r}{2} \right| \tag{2.3}$$

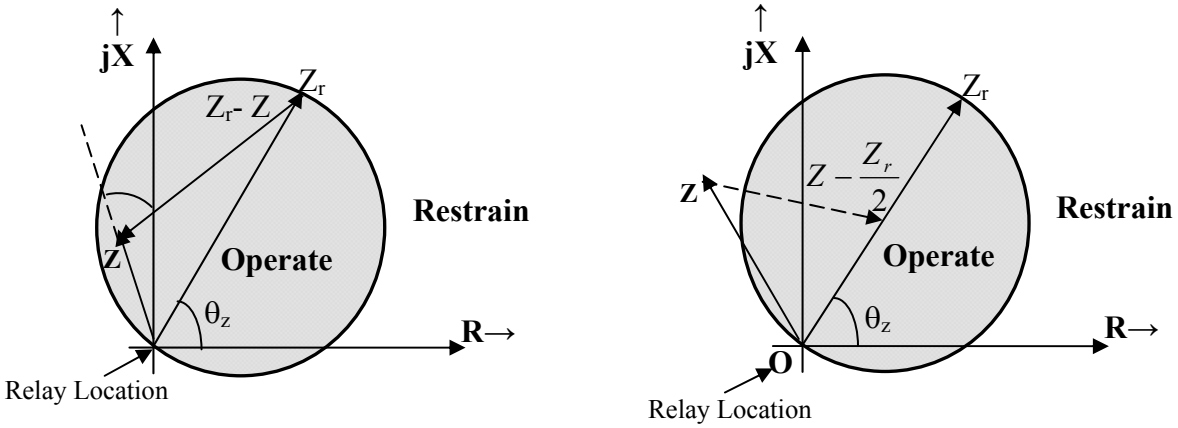

(a) Operating condition: $\left| \frac{Z_r}{2} \right| \geq \left| Z - \frac{Z_r}{2} \right|$ (b) Non-operating condition: $\left| \frac{Z_r}{2} \right| < \left| Z - \frac{Z_r}{2} \right|$

Figure 2.3: Admittance Relay: Amplitude Comparator Characteristic

Consider I_f to be the fault current and V to be the voltage at relay location during faults. Multiplying both sides by I_f and replacing $I_f Z$ by V, we get:

$$\left| I_f \frac{Z_r}{2} \right| \geq \left| V - I_f \frac{Z_r}{2} \right| \tag{2.4}$$

(b) Phase Comparison Characteristic

In terms of phase comparison, the characteristic can be described as:

$$-90° < ang(Z_r - Z) - ang(Z) < +90° \tag{2.5}$$

Considering Φ to be the angle (Z_r-Z) between (Z) as shown in Figure 2.4, and multiplying (Z) and (Z_r-Z) by I_f and replacing $I_f Z$ by V, it can be represented as:

$$|V||I_f Z_r - V|\cos(\phi) > 0 \tag{2.6}$$

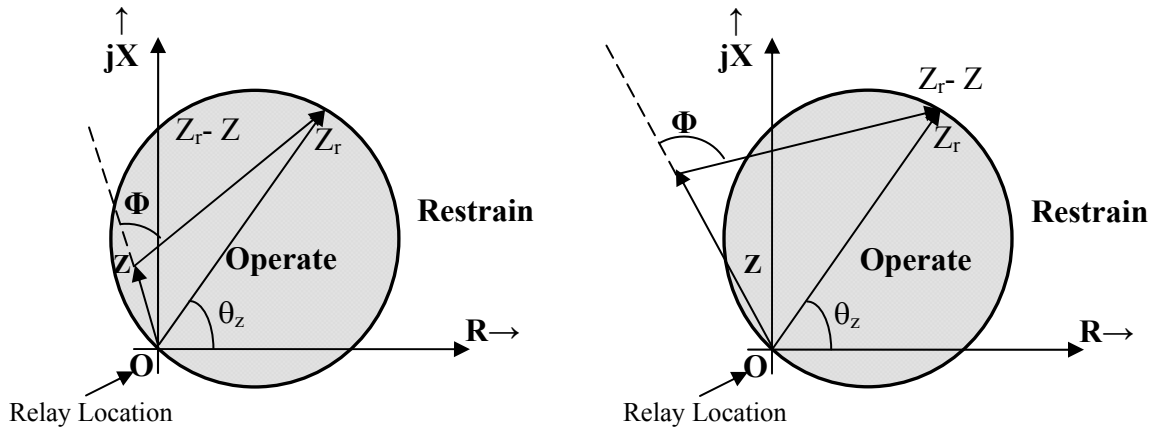

(a) Operating condition: -90º ≤ Φ ≤ 90º (b) Non-operating condition: -90º > Φ > 90º

Figure 2.4: Admittance Relay: Phase Comparator Characteristic

2.6.2.2 Reactance Relay

A reactance relay has a straight line characteristic parallel to real axis as shown in Figure 2.5 and 2.6. Therefore, the equations for the radius and center can be given as:

$$Radius_{react} = \infty \tag{2.7}$$

$$Center_{react} = -j\infty \tag{2.8}$$

(a) Amplitude Comparison Characteristic

The amplitude comparison inputs for a reactance relay are shown in Figure 2.5 and the operating condition can be represented in mathematical terms as:

$$\left|Z - 2X_{r1}\right| \geq \left|Z\right| \tag{2.9}$$

Multiplying the inputs by fault current I_f and replacing $I_f Z$ by V, the characteristic becomes:

$$\left|V - 2I_f X_{r1}\right| \geq \left|V\right| \tag{2.10}$$

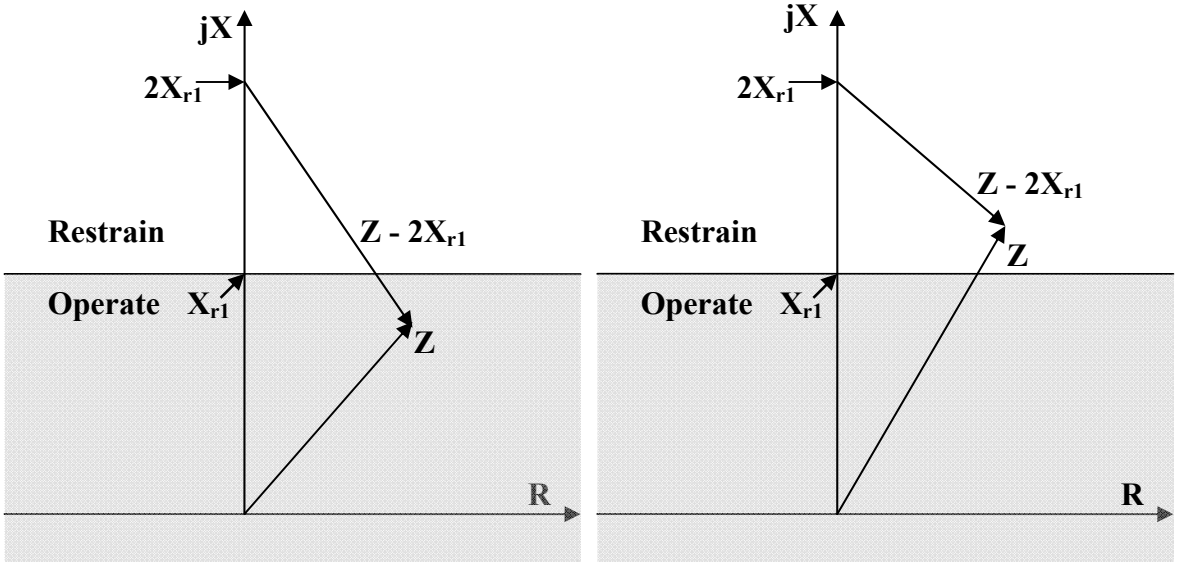

(a) Operating condition: $\left|Z - 2X_{r1}\right| \geq \left|Z\right|$ (b) Non-operating condition: $\left|Z - 2X_{r1}\right| < \left|Z\right|$

Figure 2.5: Reactance Relay: Amplitude Comparator Characteristic

(b) Phase Comparison Characteristic

The phase comparison characteristics of a reactance relay under operating and non operating conditions are shown in Figure 2.6. The condition for a reactance relay phase comparator to operate is:

$$X_{r1} \geq Z\sin(\theta) \tag{2.11}$$

$$-90° < ang(I_f X_{r1}) - ang(I_f X_{r1} - V) < +90° \tag{2.12}$$

where Φ is the angle between X_{r1}-Z and X_{r1}(or $I_f X_{r1} - V$ and $I_f X_{r1}$).

2.6.2.3 Impedance Relay

An impedance relay has a circular characteristic (refer to Fig 2.7(a)) with center at the origin of the impedance plane. This implies that $|Z_{r1}| = |Z_{r2}|$. Thus, radius and the center are equal to:

$$Radius_{impedance} = \left|\frac{Z_{r1} - Z_{r2}}{2}\right| = \left|\frac{2Z_{r1}}{2}\right| = \left|Z_{r1}\right| \tag{2.13}$$

$$Center_{impedance} = 0 \tag{2.14}$$

The amplitude and phase comparator characteristic of this relay are shown in Figure 2.7 and 2.8 respectively.

(a) Amplitude Comparison Characteristic

The amplitude characteristic of an impedance relay can be defined by:

$$\left|Z\right| \le \left|Z_{r1}\right| \tag{2.15}$$

Multiplying both sides by I_f, we get:

$$\left|I_f Z\right| \le \left|I_f Z_{r1}\right| \Rightarrow \left|V\right| \le \left|I_f Z_{r1}\right| \tag{2.16}$$

(b) Phase Comparison Characteristic

As seen in Figure 2.8, the phase comparator characteristic can be defined as:

$$-90° < ang(V - I_f Z_{r2}) - ang(I_f Z_{r1} - V) < 90° \tag{2.17}$$

If Φ is the angle between Z_{r1}-Z and Z-Z_{r2} (or $I_f Z_{r1} - V$ and $V - I_f Z_{r2}$), the phase comparator characteristic can be given as:

$$\left|V - I_f Z_{r2}\right|\left\|I_f Z_{r1} - V\right|\cos\phi > 0 \tag{2.18}$$

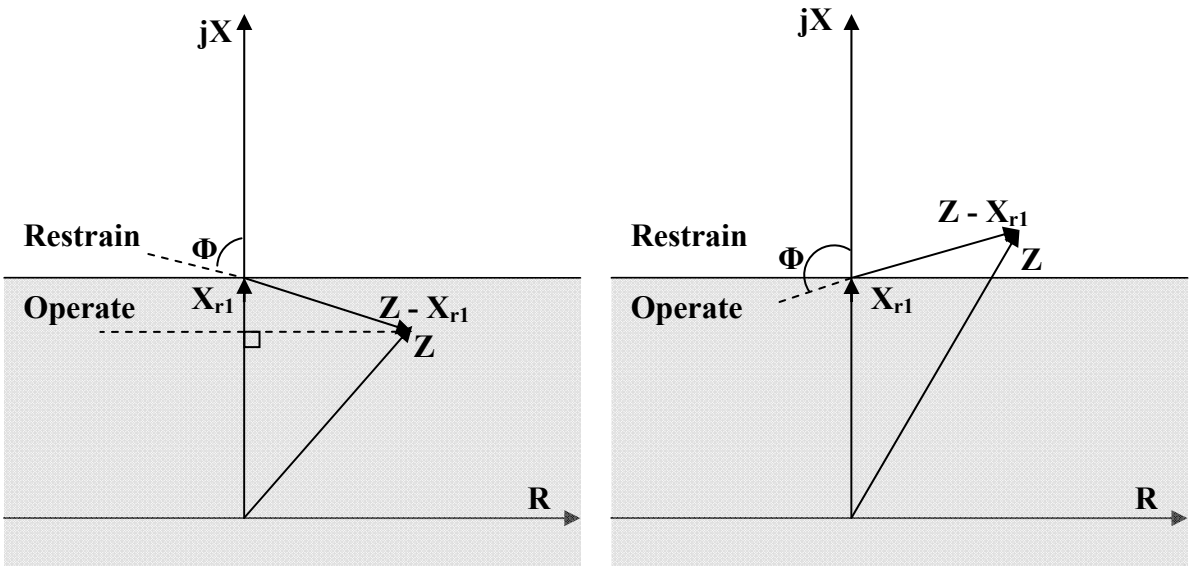

(a) Operating condition: -90º ≤ Φ ≤ 90º (b) Non-operating condition: -90º > Φ > 90º

Figure 2.6: Reactance Relay: Phase Comparator characteristic

2.6.2.4 Offset Impedance Relay

Offset impedance relay is a distance relay with circular characteristic like impedance relay; however, the center of the characteristic is offset from the origin. Figure 2.9 and 2.10 show the amplitude and phase characteristics of this relay respectively. By observing these characteristics, the radius and center of the circle can be determined as:

$$Radius_{offsetimp} = \left| \frac{Z_{r1} - Z_{r2}}{2} \right| \tag{2.19}$$

$$Center_{offsetimp} = \frac{Z_{r1} + Z_{r2}}{2} \tag{2.20}$$

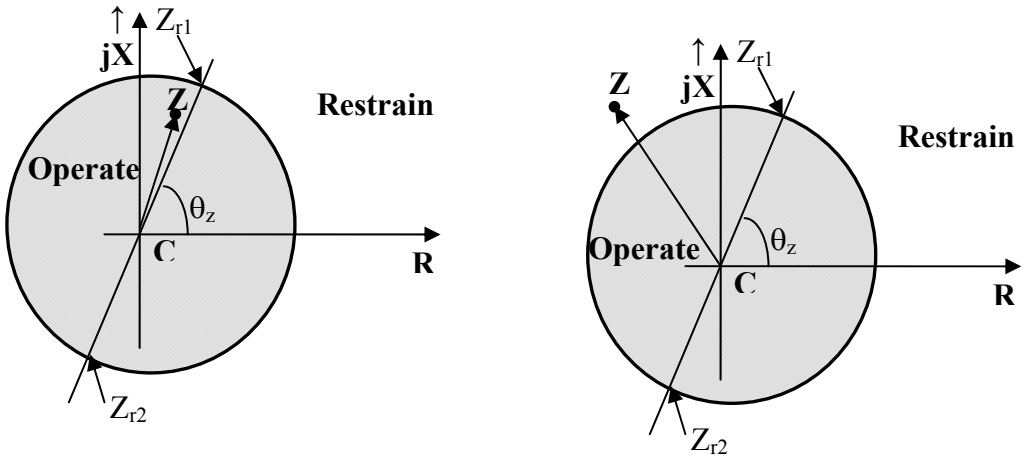

(a) Operating condition: $|V| \le |I_f Z_{r1}|$ (b) Non-operating condition: $|V| > |I_f Z_{r1}|$

Figure 2.7: Impedance Relay: Amplitude Comparator Characteristic

(a) Amplitude Comparison Characteristic

The amplitude characteristic of an offset impedance relay can be defined by:

$$\left|\frac{Z_{r1} - Z_{r2}}{2}\right| \ge \left|Z - \frac{Z_{r1} + Z_{r2}}{2}\right| \tag{2.21}$$

Multiplying both terms with I_f and replacing $I_f Z$ by V, we get:

$$\left|I_f \frac{Z_{r1} - Z_{r2}}{2}\right| \ge \left|V - I_f \frac{Z_{r1} + Z_{r2}}{2}\right| \tag{2.22}$$

The operating and non-operating conditions are shown in Figure 2.9.

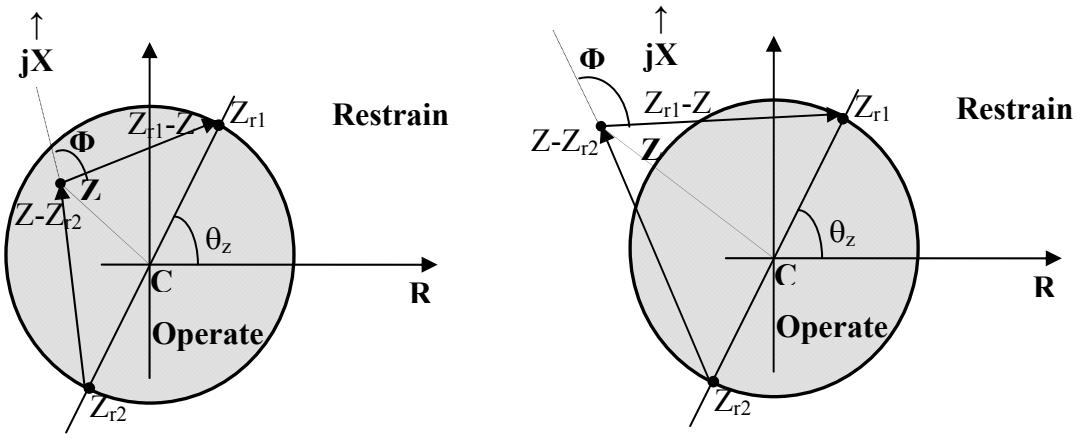

(a) Operating condition: $-90^{o} \leq \Phi \leq 90^{o}$ (b) Non-operating condition: $-90^{o} > \Phi > 90^{o}$

Figure 2.8: Impedance Relay: Phase Comparator Characteristic

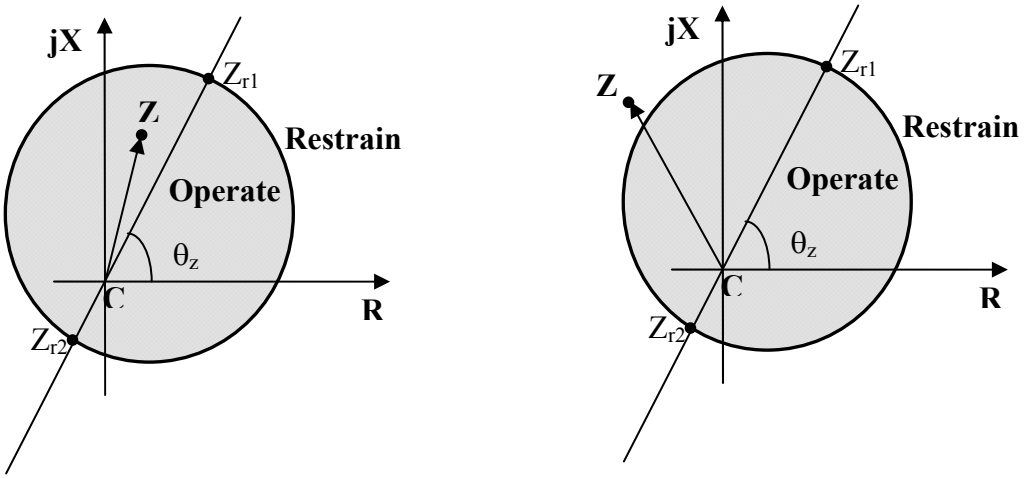

(a) Operating: $\left|V - I_f \frac{Z_{r1} + Z_{r2}}{2}\right| \leq \left|I_f \frac{Z_{r1} - Z_{r2}}{2}\right|$ (b) Non-operating: $\left|V - I_f \frac{Z_{r1} + Z_{r2}}{2}\right| > \left|I_f \frac{Z_{r1} - Z_{r2}}{2}\right|$

Figure 2.9: Offset Impedance Relay: Amplitude Comparator Characteristic

(b) Phase Comparison Characteristic

It can be seen by observing Figure 2.10 that the relay will operate if the resultant phase angle between is between -90º and +90º. The two inputs are multiplied by I_f and I_fZ is replaced by V, the equation for an offset impedance relay can be given as:

$$-90° < ang(I_f Z_{r1} - V) - ang(V - I_f Z_{r2}) < +90° \qquad (2.23)$$

Therefore, the characteristic can be given as:

$$| I_f Z_{r1} - V || V - I_f Z_{r2} | \cos\phi > 0 \quad (2.24)$$

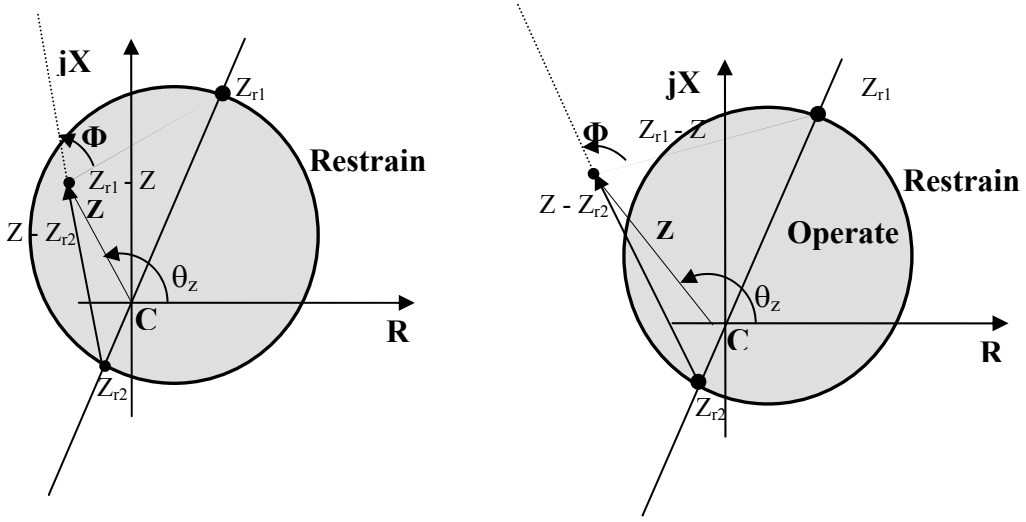

(a) Operating condition: -90º ≤ Φ ≤ 90º (b) Non-operating condition: -90º > Φ > 90º

Figure 2.10: Offset Impedance Relay: Phase Comparator Characteristic

2.6.2.5 Blinders

Blinders possess straight line characteristic. The amplitude and phase comparison characteristics of a blinder are shown in Figure 2.11 and 2.12 respectively. The equation for the radius and center can be given as:

$$Radius_{blinder} = \infty \quad (2.25)$$

$$Center_{blinder} = \infty \angle \delta \quad (2.26)$$

(a) Amplitude Comparison Characteristic

As can be seen in Figure 2.11, the amplitude characteristic can be given as:

$$|Z - 2Z_{r1}| \geq |Z| \quad (2.27)$$

Multiplying by I_f,

$$|V - 2I_f Z_{r1}| \geq |V| \quad (2.28)$$

(b) Phase Comparison Characteristic

The phase comparator characteristic of a blinder for the operating condition can be given as:

$$| Z_{r1} | - | Z | \cos(\theta_z - \delta) > 0 \tag{2.29}$$

$$-90° < ang(Z_{r1} - Z) - ang(Z_{r1}) < +90° \tag{2.30}$$

$$-90° < ang(I_f Z_{r1} - Z) - ang(I_f Z_{r1}) < +90° \tag{2.31}$$

The phase comparator characteristic for both operating and non-operating states are shown in Figure 2.12.

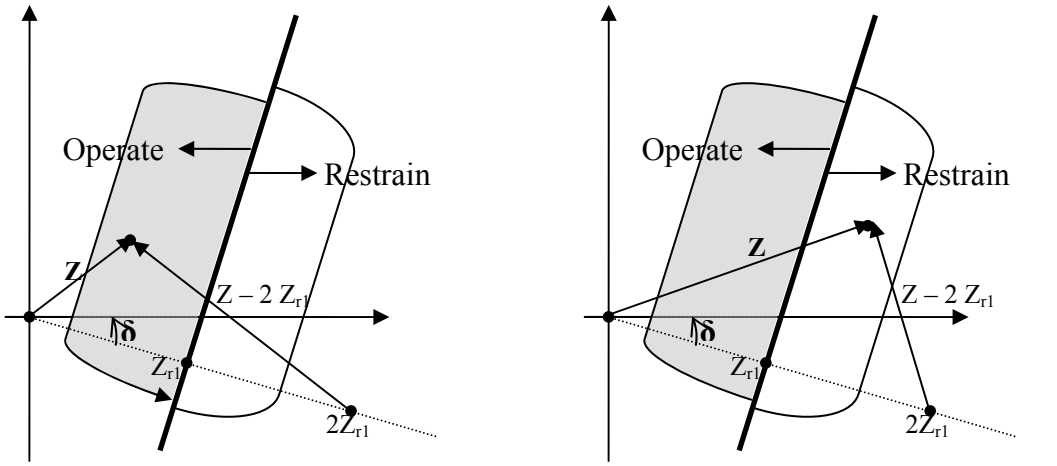

(a) Operating condition: $|Z - 2Z_{r1}| \geq |Z|$ (b) Non-operating condition: $|Z - 2Z_{r1}| < |Z|$

Figure 2.11: Blinder: Amplitude Comparator Characteristic

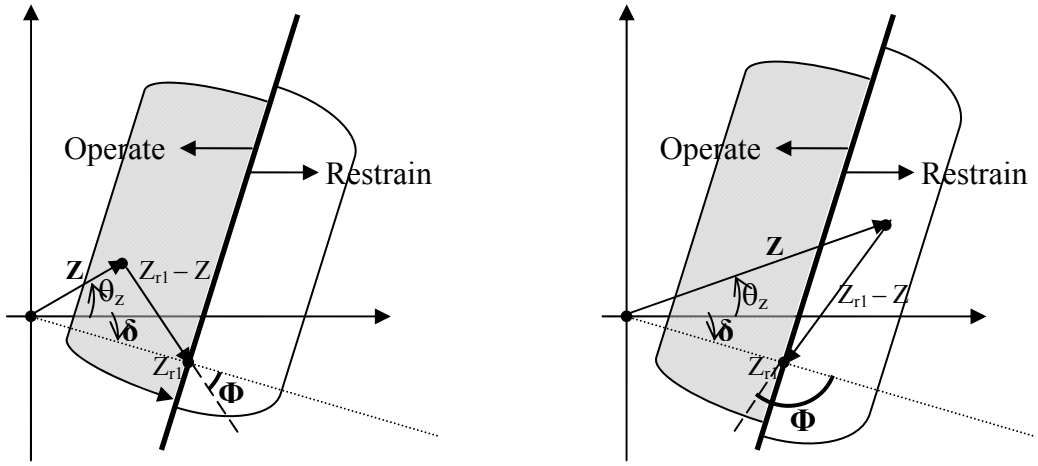

(a) Operating condition: -90º ≤ Φ ≤ 90º (b) Non-operating condition: -90º > Φ > 90º

Figure 2.12: Blinder: Phase Comparator Characteristic

2.6.2.6 Quadrilateral Relay

Quadrilateral relays have been termed as ideal distance relays for the protection of transmission lines [39]. Two factors are usually considered for settings these relays. These settings are relay fault resistance reach setting and relay impedance reach setting [38, 44]. The characteristic of a quadrilateral relay are generated by combining characteristics of different relays.

Figure 2.13 shows the characteristic of a quadrilateral relay that combines three blinders and a directional relay. The horizontal distance between the origin and Blinder 1 shows the fault resistance-reach setting. This parameter is set according to the system where the quadrilateral relay is installed. It is important to ensure that this reach does not overlap the load impedance zone. The relay impedance reach setting is dependent on the impedance of the transmission line and zone of protection.

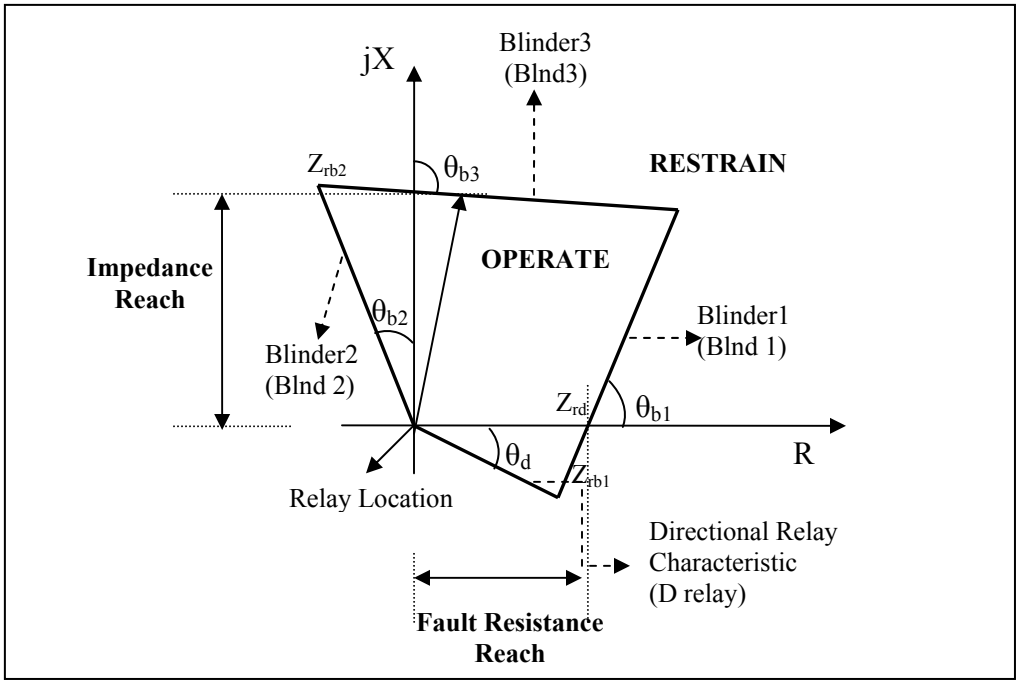

Figure 2.13: Quadrilateral Relay Characteristic

2.6.3 Polarization Techniques

As per IEEE [57], "A relay that consists of two elements, one of which operates as a neutral relay and the other of which operates as a polar relay can be termed as a polarized relay". A mho relay is a self polarized relay with $I_f Z_r - V_{phase}$ as the operating element and V_{phase} as the restraining or polarizing element. The phase comparator characteristic of distance relay show that it "sees" in one direction only; therefore it can discriminate between the forward and reverse faults. For faults very close to the relay location, the voltage V_{phase} may collapse to almost zero in some cases. This can lead to incorrect operation of the relay. This condition can be corrected by polarizing the relay by using either the healthy phase voltage or by using memorized voltage of the faulted phase. For unbalanced faults (or zero-voltage three phase faults) a polarizing component is introduced to produce either a single or dual polarization scheme [38]. Depending on the power system conditions, different types of polarizing quantities can be used for distance relays. There are two basic requirements [58] for any polarizing input:
(a) The phase angle of the polarizing input should be fixed relative to the restrain voltage.
(b) The magnitude of the polarizing input is unimportant so long as it is never zero, e.g. for terminal faults, when the restraint voltage is zero, the polarizing input must exist.

Sections 2.6.3.1 to 2.6.3.3 describe the different types of polarization techniques.

2.6.3.1 Self Polarization

Mho relay is a self-polarized relay. This implies that the relay uses a polarizing input from the faulted phase itself. As faulty phase voltage is the polarizing quantity in this case, the phase angle criteria between the restraint voltage and the polarizing quantity is always satisfied. For faults very close to the relay location, the relay may not be able to discriminate between reverse and forward faults as the fault voltage collapses to zero. It is beneficial to use a different polarizing input to maintain the directionality of the relay in such situations.

2.6.3.2 Cross Polarization

In a cross polarization scheme, phase voltage of one of the healthy phases or the voltage between the healthy phases is used as a polarizing input. The phase angle relativity of the

polarizing input with respect to the restraint voltage is maintained by applying appropriate phase shifts. This scheme, however, fails in case of a three-phase fault or if there is a fault on one of the phases from which the polarizing input is being derived.

Cross-polarizing inputs vary for different faults. The cross-polarizing input for a single line to ground fault (A-G) is the voltage between the other two healthy phases V_{bc}. This line voltage is shifted by 90º to bring it in phase with voltage of the faulted phase V_a. Table 2.3 lists the various cross polarizing inputs for different types of faults.

Table 2.3: Cross-Polarizing Voltages for Different Faults

Type of Fault	Cross-Polarizing Voltage
A – G	jV_{bc}
B – G	jV_{ca}
C – G	jV_{ab}
AB or AB – G	$-jV_c$
BC or BC – G	$-jV_a$
CA or CA – G	$-jV_b$

2.6.3.3. Memory Polarization

A memory polarization scheme uses the voltage input stored in memory before the occurrence of the fault. A memory polarizing input in the case of a mho relay is the phase voltage V_{phase} before the faults occurs. The phase angle of the polarizing input, thus, will be the same as the restraining input. Evidently, this scheme will fail in case a fault occurs at the instant a line is switched on and no memory inputs are available.

All the schemes described in this section have their advantages and disadvantages. A combination of two or more of these schemes, thus, may prove to be advantageous to incorporate all fault situations.

2.7 Numerical / Digital Protection

The first micro-processor relay was introduced in mid 1980s and there has been significant research and development of commercial micro-processor based relays since then. Today's protection systems widely use numerical relays. The structure of the numerical relays is general in nature and internal modules of the relays remain the same irrespective of the operating principle. Figure 2.14 shows the different hardware components and modules constituting a generalized numerical relay. These modules are broadly classified into three categories on the basis of functions performed by them.

- **Analog Input Sub-system:** There are four main components of an analog sub-system. These are isolation & scaling, filtering, sample & hold and analog to digital conversion [4]. Analog inputs obtained from current and voltage transformers (CTs and VTs) are scaled down to current and voltage inputs appropriate for relay levels as shown in Figure 2.14. These inputs pass through a low-pass anti-aliasing filter to remove high frequency components present in the inputs. Since a micro-processor can process only digital inputs, the currents and voltages are passed through an analog to digital sub-system (A/D sub-system) consisting of a sample and hold circuit, followed by an analog to digital converter. The digital inputs are then communicated through a multiplexer (MUX) to the micro-processor.
- **Parameter Estimation Algorithm:** A parameter estimation technique is implemented on the micro-processor. It calculates the required parameters as per the protection algorithm. The parameters are usually the current and voltage phasors. The different phasor algorithms have been discussed in more detail in Section 2.8. The micro-processor uses the calculated phasors to determine the presence of a fault on the system.
- **Relay Logic and Trip:** Once a signal is received from the microprocessor that a fault is present, a relay output is provided. Depending on the relay output, a trip/no trip signal is provided to control the circuit breakers.

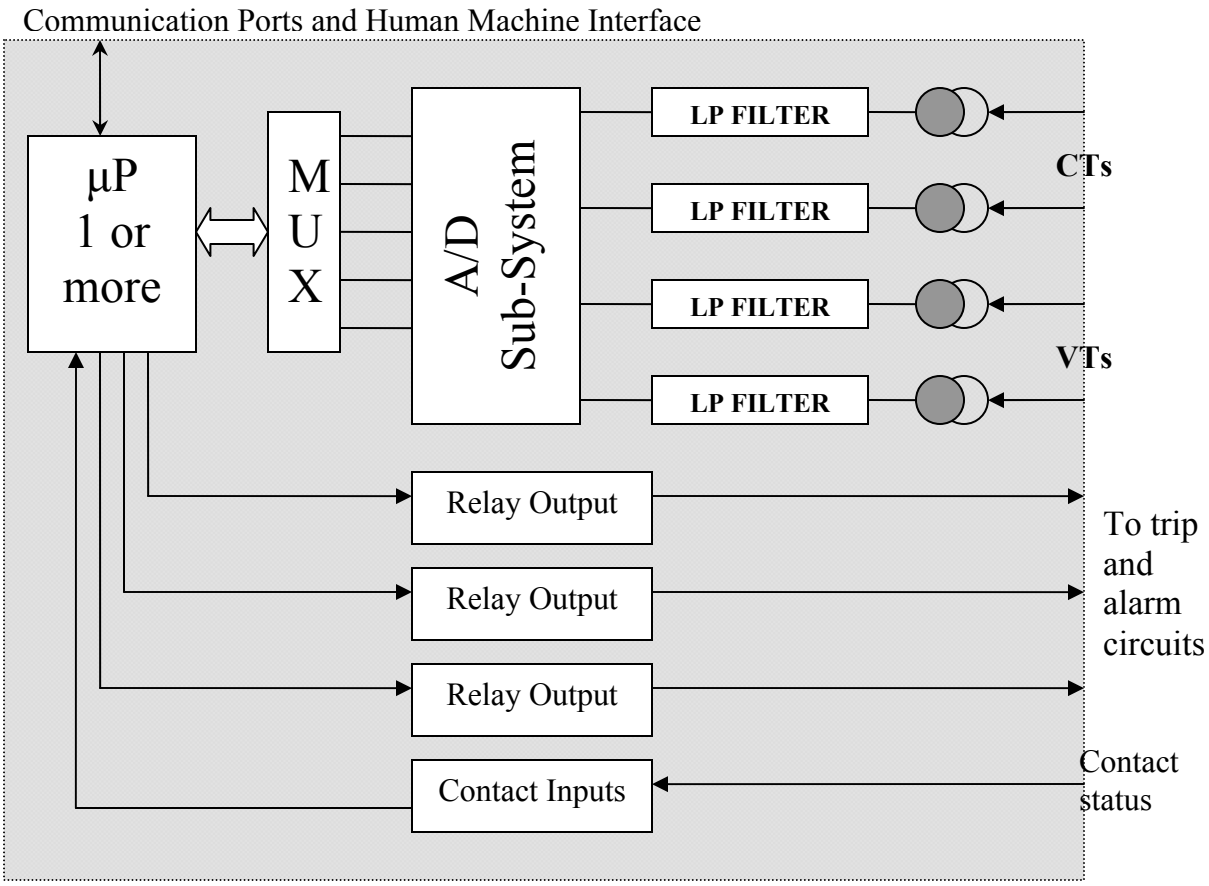

Figure 2.14: Block Diagram: Typical Arrangement of a Numerical Relay [4]

2.8 Parameter Estimation Techniques

There are essentially three types of numerical relaying algorithms that are used for various protective relaying functions such as measuring phasors, impedance, power flows, frequency, estimate distance of faults etc. These algorithms can be classified as:

1. Phasor Algorithms

- Non-Recursive
  - ◊ Short-window algorithm
    - Miki and Mikano
    - Mann and Morrison
    - Rockefeller and Udren
  - ◊ Long-window algorithm
    - Discrete Fourier Transform

        - Walsh Technique
        - Least Square Error Method
- Recursive
    - ◊ Recursive Least Square Error Method
    - ◊ Kalman Filtering

2. Modeling Algorithms

- Line models
- Transformer models

3. Alternative algorithms

- Neural Networks
- Fuzzy Logic
- Artificial Intelligence techniques using expert systems etc.

Some of these algorithms have been discussed in the following sections. The details of these algorithms can be found in references [4] and [5].

2.8.1 Non-Recursive Phasor Algorithms

Non-recursive algorithms use constant weights that are multiplied with input data window to calculate the phasor values. These algorithms can be further classified as short-window and long-window algorithms, as described in Sections 2.8.1.1 and 2.8.1.2 respectively. Mann & Morrison and Rockefeller & Udren are examples of short-window algorithms and Discrete Fourier transform [47] and Walsh functions are examples of some of the long-window non-recursive algorithms.

2.8.1.1 Short Window Techniques

These algorithms are based on the assumption that the waveform of the input under consideration is a sinusoid of nominal frequency. It also assumes that the frequency of the input does not vary with time. Short window algorithms usually use a data window of two or three samples. Figure 2.15 shows a three-sample window for a sinusoidal signal S. The time is zero in the middle of the window and the sampling time is considered as ΔT. The signal at time t = 0 is equal to s_0. The values of the signal one

sample before and after have been considered as s_{-1} and s_{+1} respectively. The subsequent windows are obtained by shifting the sample by one.

(a) Mann and Morrison Algorithm

According to the Mann and Morrison technique, the peak value of the signal can be estimated by calculating the first derivative of the signal. At time t = 0, signal $s = s_0$ and the first derivative s' is given as

$$s' \approx \frac{s_{+1} - s_{-1}}{2\Delta T} \tag{2.32}$$

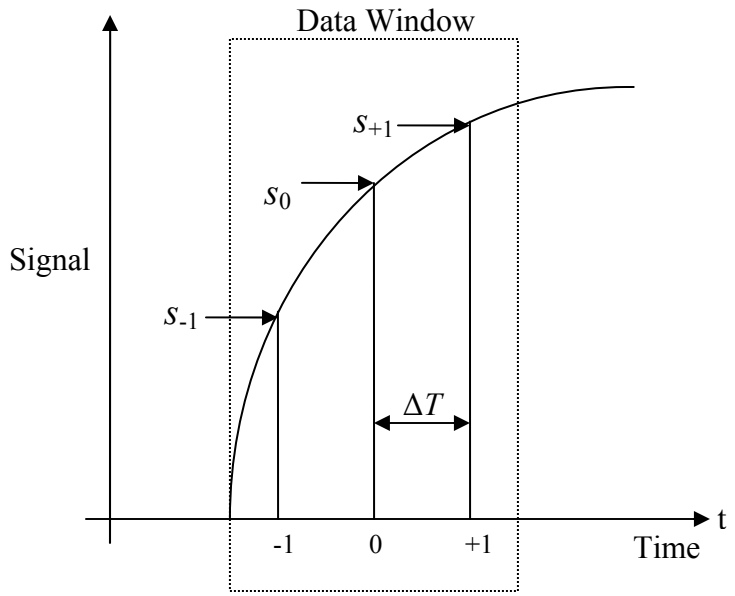

Figure 2.15: Three Sample Data Window for Short-window Algorithms

When the next sample is received, the oldest sample i.e. s_{-1} is discarded and the new values are calculated by moving the data window. Considering θ to be the displacement angle of the signal from the reference and S_p to be the peak value of the signal, s_{-1} can be represented as:

$$s_{-1} = S_p \sin(-\omega_o \Delta T + \theta) \tag{2.33}$$

Therefore, $$s' = \omega_o S_p \cos(\omega_o \Delta T + \theta) \tag{2.34}$$

At time t = 0, $$s' = \omega_o S_p \cos\theta \tag{2.35a}$$

Also, at 0^{th} sample, $$s_0 = S_p \sin\theta \tag{2.35b}$$

Therefore, the peak value of the signal can be calculated as:

$$S_p \cos\theta = \frac{s_{+1} - s_{-1}}{2\omega_o \Delta T} \tag{2.36a}$$

$$S_p \sin\theta = s_0 \tag{2.36a}$$

(b) Rockefeller and Udren Algorithm

Rockefeller and Udren technique uses the first two derivatives of the signal to calculate the peak value and the phase angle of the signal. The second derivative of a sinusoidal signal can be given as:

$$s'' = \frac{d}{dt}(S_p \sin(\omega_o t + \theta)) = -\omega_o^2 S_p \sin(\omega_o t + \theta) \tag{2.37}$$

Considering intermediate points $s_{-0.5}$ and $s_{+0.5}$ between three samples s_{-1}, s_0 and s_{+1} shown in Figure 2.15,

$$s_0' \approx \frac{s_{+1} - s_{-1}}{2\Delta T} \tag{2.38}$$

$$s'_{-0.5} \approx \frac{s_0 - s_{-1}}{\Delta T} \tag{2.39}$$

$$s'_{+0.5} \approx \frac{s_{+1} - s_0}{\Delta T} \tag{2.40}$$

Combining equations 2.34 and 2.35:

$$s_0'' \approx \frac{s'_{+0.5} - s'_{-0.5}}{(\Delta T)^2} \approx \frac{s_{+1} - 2s_0 + s_{-1}}{(\Delta T)^2} \tag{2.41}$$

Therefore, $$\omega_o^2 S_p \sin\theta = \frac{s_{+1} - 2s_0 + s_{-1}}{(\Delta T)^2} \tag{2.42}$$

$$\Rightarrow S_p \sin\theta = \frac{s_{+1} - 2s_0 + s_{-1}}{(\omega_o \Delta T)^2} \tag{2.43a}$$

From equation 2.36,

$$S_p \cos\theta = \frac{s_{+1} - s_{-1}}{2\omega_o \Delta T} \tag{2.43b}$$

2.8.1.2 Long Window Techniques

Long window algorithms generally use a data window of one or more cycles. For the implementation of long window algorithms, the input is assumed to be comprised of components of known frequencies. Two orthogonal functions are usually used to extract the components of the frequency of interest. Two long window non-recursive algorithms, using Discrete Fourier transform and Walsh functions have been described here.

(a) Discrete Fourier Transform Algorithm

The Discrete Fourier Transform algorithm (DFT) is a non-recursive algorithm that uses sine and cosine orthogonal functions to calculate magnitude and phase angle of a given signal [5, 47]. The basis of this algorithm for any signal S is given by equations 2.44 and 2.45.

$$S_p \cos(\theta) = \frac{1}{\pi} \int S_p \sin(\omega t + \theta) \sin(\omega t) d(\omega t) \tag{2.44}$$

$$S_p \sin(\theta) = \frac{1}{\pi} \int S_p \sin(\omega t + \theta) \cos(\omega t) d(\omega t) \tag{2.45}$$

The real and imaginary components of a phasor can be calculated as shown in equations 2.46 and 2.47 respectively.

$$S_p \cos(\theta) = \frac{2}{N} \sum_{k=m-N+1}^{k=m} s_k \sin[(k + N - m)\omega \Delta T] \tag{2.46}$$

$$S_p \sin(\theta) = \frac{2}{N} \sum_{k=m-N+1}^{k=m} s_k \cos[(k + N - m)\omega \Delta T] \tag{2.47}$$

In these equations, S_p is the peak value of any signal, N is the number of samples in one cycle data window, m is the current sample number, k is an integer ranging between (m-N+1) and m, s_k is the instantaneous value of the phasor at the k^{th} sampling instant and ΔT is the time interval between two consecutive samples. Equations 2.46 and 2.47 can be used to calculate the phase angle θ and signal S_p. The sine and cosine functions are sampled at the same time interval as the signal S. The first sample of the data window is multiplied with the first sample of the sine and cosine function. The weighted sine and

cosine samples are used to calculate the real and imaginary parts of the phasor; the magnitude and phase angle of the input are then calculated.

(b) Walsh Function Technique

Walsh Transform uses the Even and Odd rectangular orthogonal functions to calculate the magnitude and phase angle of any signal. The principle of this technique can be described using the following equations:

$$S_p \cos(\theta) = \frac{1}{4}\int_0^{2\pi} S_p \sin(\omega t + \theta) signum[\sin(\omega t)] d\omega t \tag{2.48}$$

$$S_p \sin(\theta) = \frac{1}{4}\int_0^{2\pi} S_p \sin(\omega t + \theta) signum[\cos(\omega t)] d\omega t \tag{2.49}$$

The real and imaginary components of a phasor can be calculated as:

$$S_p \cos(\theta) = \frac{\pi}{2N}\sum_{k=m-N+1}^{k=m} s_k signum\{\sin[(k+N-m)\omega\Delta T]\} \tag{2.50}$$

$$S_p \sin(\theta) = \frac{\pi}{2N}\sum_{k=m-N+1}^{k=m} s_k signum\{\cos[(k+N-m)\omega\Delta T]\} \tag{2.51}$$

S_p is the peak value of any signal, N is the number of samples in one cycle data window, m is the current sample number, k is an integer ranging between (m-N+1) and m, s_k is the instantaneous value of the phasor at the k^{th} sampling instant and ΔT is the time interval between two consecutive samples. The values of even and odd rectangular functions are equal to either +1 or -1. The discrete samples s_k are multiplied by one of these two numbers depending on the sample number. The real and imaginary values obtained from equations 2.50 and 2.51 are then used to calculate the phase angle θ and magnitude of signal S_p.

2.8.2 Recursive Phasor Algorithms

The main difference between non-recursive and recursive phasor algorithms is that the recursive algorithms are designed such that heavier weights are assigned to the recent inputs. As a result, the effect of the older inputs on the output diminishes as time goes on [22]. Recursive least squares techniques [22, 70] and Kalman filtering [21] are some examples of recursive phasor algorithm. Recursive least squares technique (LSQ) is a

modification of non-recursive LSQ technique. Least Squares Algorithm assumes that the composition of the waveforms is known. Various components such as the fundamental frequency, components of harmonic frequencies and decaying dc component can be included in the waveform composition. Kalman Filter Technique is based on the statistical properties of the signal. In addition to the fundamental frequency component, noise and other selected frequencies can also be included in the signal.

2.8.3 Modeling Algorithms

Modeling algorithms are based on the physical model of the system where the current and voltage samples are used to estimate parameters of the physical models [5]. Some of the examples of model algorithms are line models and transformer models. In line protection, the physical model is a series R-L circuit that represents the faulted line for different faults on the transmission line. In case of transformer protection, the magnetic flux circuit with associated inductance and resistance forms the model. These models have been used to detect core saturation and internal faults of a transformer.

2.8.4 Alternative Algorithms

- Neural Networks

  The theory, structure and learning algorithms of neural networks are discussed in detail in Chapter 3. ANNs have been widely used for various protection applications. Some of these applications include transmission line protection, transformer protection, generator protection, adaptive re-closing, estimation of fault location etc.

- Fuzzy Logic

  Fuzzy logic is derived from the theory of fuzzy sets that is a generalization of classical sets as discussed in reference [51]. It deals with objects that are a "matter of degree" or approximate rather than precise, with all possible grades from 0 to 1 [48, 50]. The ultimate goal of fuzzy logic is to form theoretical foundation for reasoning about imprecise propositions; such reasoning has been referred to as approximate reasoning [49]. Fuzzy logic systems have been used for digital distance protection [52] and other power system protection applications such as fault classification and detection [53].

- Other Artificial Intelligence Techniques

Various artificial intelligence techniques using expert systems [54, 55] have been used for fault diagnosis, fault classification and fault location in power systems. An expert system is an application of artificial intelligence that imitates the behavior of a human expert in solving a complex problem that requires knowledge – intensive and scarce expertise [54]. These knowledge base systems are usually based on a set of application-based rules that are followed to make a decision.

2.9 Factors Influencing the Detection of Faults

A distance comparator is provided with voltages and currents from one end only of the protected circuit and it assesses the location of a fault on the basis of these locally derived inputs [38]. Figure 2.16 shows a typical tripping scheme for distance protection of a transmission line. Because the relay inputs are calculated locally, there are various parameters and equipment associated with a protection scheme that can affect the detection of faults in a power system. Some of these factors are listed below. The subsequent sections describe some of these factors.

Transducer Errors

Estimation of apparent impedance

Effect of fault resistance

Source (X/L) ratio

Mutual coupling

2.9.1 Transducer Errors

The measuring element receives the currents and voltages from the secondary windings of the current and voltage (potential) transformer (CT and PT) respectively, as shown in Figure 2.16. The measurements obtained from the CTs and PTs, thus, affect the relay performance. Fault currents contain constant and/or exponentially decaying d.c. component. The characteristics of the d.c. component are dependent on the instant of the fault. The d.c. transient component is an important source of error that tends to reduce the impedance seen by a distance relay, causing the relay to overreach [38]. The presence of a d.c. component in the primary fault current may also lead to the saturation of the current transformer core [56], thus leading to an incorrect current estimation.

Voltage transformers, on the other hand, are adversely affected by abrupt changes in the primary voltage, leading to a distorted voltage output. The presence of frequency components higher than the fundamental frequency affects the output of the PTs, especially in case of capacitor voltage transformers (C.V.T.). The transients have a marked effect on the relay operating time, resulting in slower zone 1 operating times [38].

2.9.2 Estimation of Apparent Impedance

The distance relay measures the apparent impedance as seen at the relay location at the instant of fault occurrence. It is, therefore, important to give appropriate inputs to the relay (as stated in Table 2.1) depending on the fault. Proper residual compensation input should be given to earth fault measuring elements and differences between the phase voltages and the line currents should be given to phase fault measuring elements. The error in the compensating factor k_0 and/or calculation of proper phase inputs leads to miscalculation of the impedance seen at the relay location.

2.9.3 Presence of Fault Resistance

In presence of fault resistance, the faults lying inside the protection zone of the relay appear to be outside the zone and thus cause the relay to under-reach. Proper provisions have to be made in the numerical algorithm to account for fault resistance, if present. This is important to establish if the apparent impedance calculated at the relay location lies inside or outside the protection zone. The presence of a fault resistance makes the proper measurement of the impedance even more complicated in case of a double end feed, resulting in the over-reach of relay in certain cases [38].

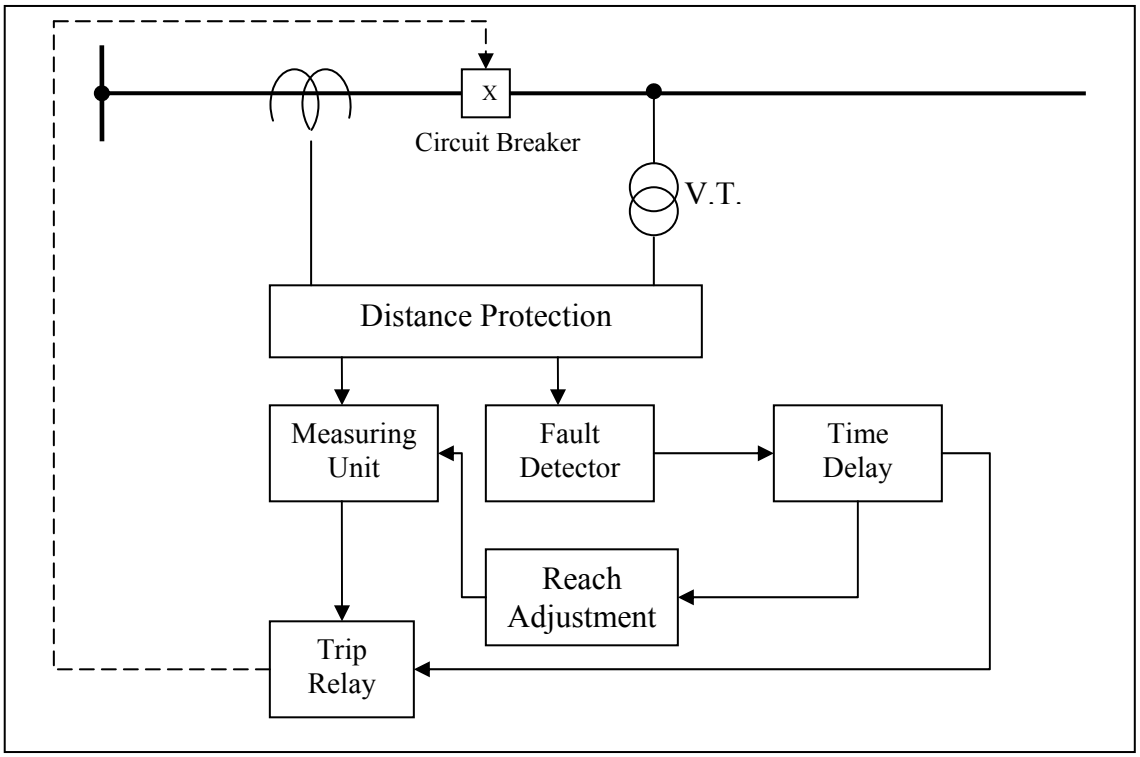

Figure 2.16: Simplified Tripping Arrangement for a Protection Scheme [38]

2.10 Summary

The principle of protective relaying is described in this chapter. Different types of protection and relays that are used for transmission lines are discussed. The operating principles and characteristics of distance relays and the polarization techniques associated with the operation of distance relays are discussed. This chapter also presents various important aspects of numerical relaying and different numerical relaying algorithms that include phasor estimation, modeling and alternative algorithms. The factors influencing the detection of faults in any protective scheme are also discussed.

3. ARTIFICIAL NEURAL NETWORKS

3.1 Introduction

The previous chapter gives an overview of the general protection principles and numerical relaying. The different types of protection used for transmission lines are discussed in detail. The amplitude and phase comparison characteristics of different distance relays are presented. Polarization techniques for different faults and the factors affecting the detection of faults are also addressed.

This research project combines the generic characteristics of distance relays with the learning and generalization capabilities of neural networks. The theory and principles of distance protection for transmission line protection are discussed in the last chapter. This chapter presents the theory and learning paradigms of neural network. The applications of neural networks for protective relaying are also discussed.

3.2 Structure of Neural Networks

An artificial neural network, also known as a neural network (ANN or NN) is a system modeled based on the structure of a human brain. This section describes the elements of a biological neuron and the derivation of an artificial neuron from the biological neuron.

3.2.1 A Biological Neuron

The most basic element of an artificial neural network is an artificial neuron. The components of an artificial neuron closely resemble their biological counterparts. A biological neuron has four basic components – dendrite(s), soma, axon and synapse(s). A simplified biological neuron and the functions of these four components are shown in Figure 3.1. Dendrites bring inputs from other neurons to the soma of the neuron. This information is processed in soma and is transferred through axon. The synaptic junction joins the neuron with dendrites of other neurons and is responsible for passing the information (as inputs) to other neurons.

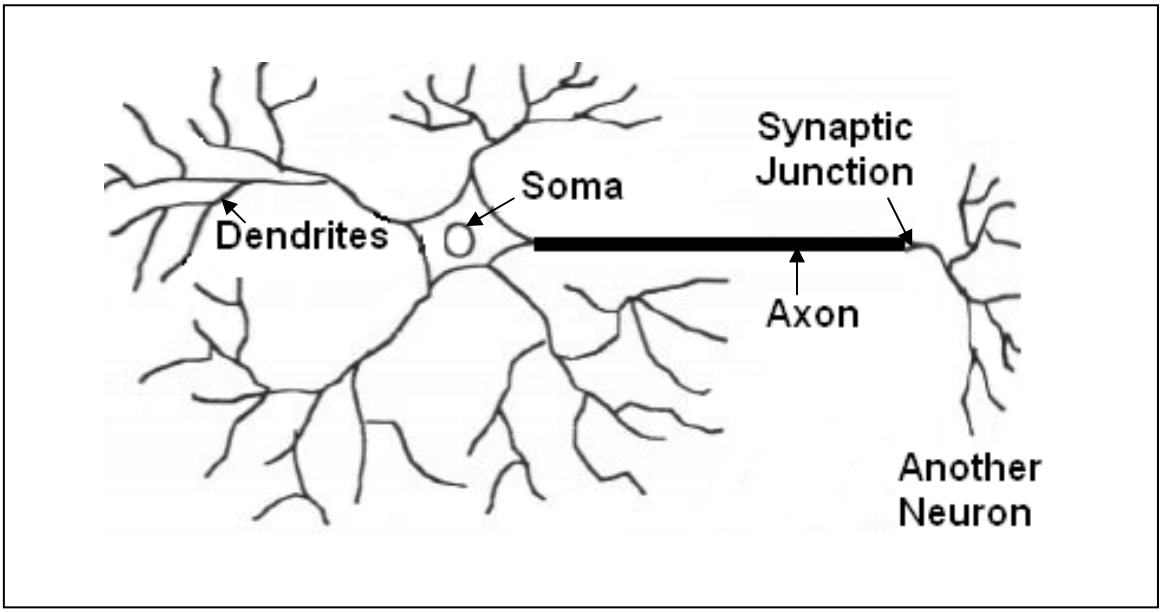

Figure 3.1: A Biological Neuron

3.2.2 Mathematical Model of a Neuron

An artificial neuron can be represented as a mathematical replica of a biological neuron. The actions performed by a biological neuron can be mapped in mathematical terms and are divided into two main operations, a synaptic operation and a somatic operation. These are discussed below.

3.2.2.1 Synaptic Operation

Each neuron receives several inputs through the dendrites, via the synaptic junction in this operation. This operation can be expressed mathematically for an artificial neuron. For an n-dimensional input vector x and an n-dimensional synaptic weights-vector w, the resultant z is expressed as:

$$z_i = w_i x_i \tag{3.1}$$

where $i = 1, 2, 3.....n.$

3.2.2.2 Somatic Operation

In this process, all the synaptic inputs are summed and the result is mapped with a threshold of a non-linear function. The sum of the weighted inputs can be given as:

$$u = \sum_{i=1}^{n} z_i \tag{3.2}$$

$$y = \phi(u - w_o) \tag{3.3}$$

where Φ [.] is a non-linear function, w_0 is the threshold and y is the output of the neuron. The choice of the non-linear function is dependent on the application for which the neural network is used. Some of the commonly used transfer functions are sigmoid function, hard-limiting function and linear function.

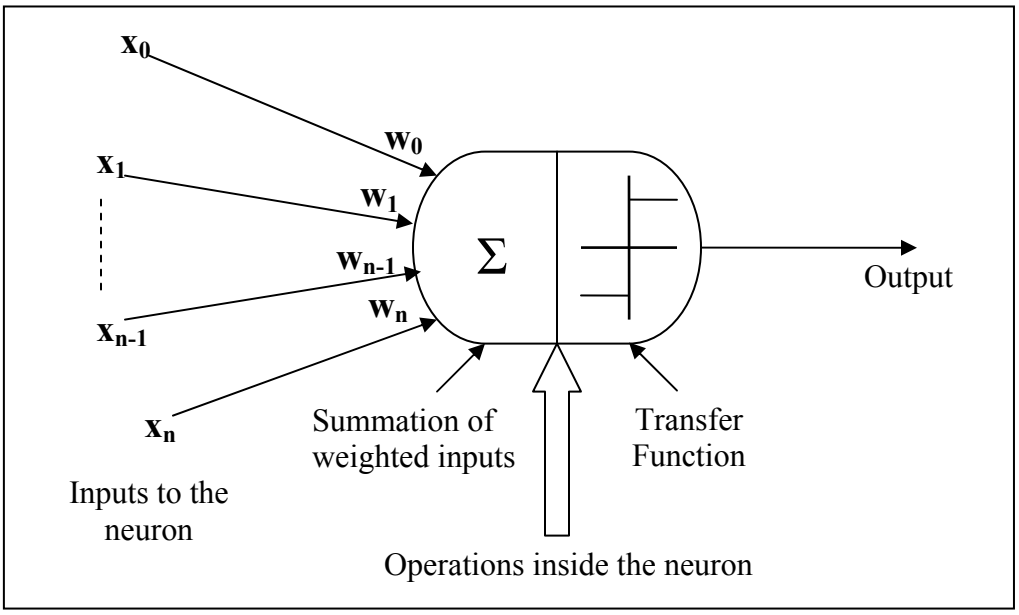

Figure 3.2: Structure of an Artificial Neuron

3.3 Types of Neural Networks

Artificial neural networks are classified into different categories depending on the neuron connections and the flow of data through the different layers of the neural network. Some of the different ANNs are discussed in subsequent sections.

3.3.1 Feed-forward Networks

The information in a feed-forward neural network moves only in the forward direction. The different layers of the neural network are either partially or fully connected. The output of the first layer is used as the input of the hidden layer and so on. The output of the last hidden layer is, thus the input of the output layer. Feed-forward networks are the most widely used neural networks because of the simplicity of their design. Feed forward networks can be broadly classified into three categories.

3.3.1.1 Single/Multi-layer Perceptron

A perceptron is the simplest form of a neural network used for classification of patterns that are said to be linearly separable [34]. It may consist of single or multi layer(s) of neurons depending on the complexity of the application for which it is being used. The inputs are given through a set of input weights and the output of the perceptron depends on the sum of weighted inputs and the mapping function (also known as activation function) used. Single unit perceptrons are used for simple pattern classification and learning problems that have only two linearly separable classes.

Multi-layer perceptrons consist of layers of neurons as computational units that are connected in a feed-forward manner. Each layer is either partially or fully connected to its adjacent layer. The most commonly used learning algorithm with these kinds of neural networks is the back-propagation algorithm. In a back-propagation algorithm, the output obtained from the neural net is compared with the desired output value and the errors are back-propagated to update the weights of the network. One of the main drawbacks of multi-layer perceptrons is the amount of time that it takes to train them. However, these neural networks have been successfully used in numerous pattern classification applications. The pattern classification abilities of these neural networks have been discussed further in Section 3.5.

3.3.1.2 Radial Basis Networks

Radial basis networks typically use one input layer using an input vector with different parameters, one hidden layer that uses a non-linear radial basis activation function and a

linear output layer. Radial basis networks require more neurons than standard feed-forward back-propagation networks, but often they can be designed in a fraction of the time it takes to train standard feed-forward networks [12]. Further, these networks do not get stuck in local minima problems like multi-layer neural networks. These networks are best optimized in applications where a high number of training data is available.

3.3.1.3 Self-Organizing Maps

Kohonen self-organizing maps (or simply self-organizing maps) are based on Kohonen's learning law where the neurons in different layers of the neural network compete for the opportunity to learn and update the weights accordingly. These networks possess the ability to detect correlations in the input data and respond to that particular input accordingly in the future. Only the output from the processing neuron with the largest output value is accepted and the connection weights of this neuron and all the other neurons connected to it are updated in that iteration. The neurons of competitive networks learn to recognize groups of similar input vectors [12]. Unlike perceptrons and radial basis networks, a self – organizing map does not need a target output value and uses a form of unsupervised learning, which has been discussed in Section 3.4.1.2.

3.3.2 Recurrent Networks

The neurons of a recurrent network are partially or fully connected and receive inputs from other neurons. However, the information in a recurrent network may not necessarily move in a feed – forward way. The neurons interact with each other depending on the target value of the output and adapt themselves accordingly. The hidden layer values from the latest iteration are usually saved, which enables these networks to be successfully applied to sequence prediction type applications. Fully connected recurrent networks are not arranged in layers because each neuron receives an input from every other neuron in the network. Some of the recurrent networks are Elman network, Hopfield network, echo state network etc.

3.3.3 Other Networks

Various other types of neural networks have been proposed for different applications in the last twenty years. Some of these networks are:

- Adaptive linear neuron network (ADALINE)
- Boltzmann Machine
- Cascade neural networks
- Finite Impulse response networks
- Fuzzy neural networks
- Probabilistic neural networks
- Time-delay neural networks or dynamic neural networks

3.4 Learning

Learning and adaptation is the most critical part of neural network training. Learning is a process by which the free parameters of an ANN are adapted through stimulation by the environment in which the network is embedded [34]. Various learning techniques and learning algorithms have been used to update the connection weights between the different layers of a neural network. Some of the algorithms and types of learning have been discussed in the next sections.

3.4.1 Learning Paradigms

A learning paradigm is defined as a procedure for modifying the weights and biases of a network [12]. The learning paradigm is classified by the method in which the parameters are updated during the training phase of the ANN. There are three main techniques of neural learning that are used according to the application.

3.4.1.1 Supervised Learning

Supervised learning is the most common form of learning that has been used in numerous real-life applications. It is used in systems where a target output is available. A block diagram of a supervised learning system is shown in Figure 3.3. It is a predictive measurement of performance type of system. ANN learns during training by adapting to

a dataset of inputs and the desired outputs corresponding to them. The network parameters such as the weights and biases are adjusted according to the error between the desired output and the obtained output in a closed-loop feedback type system.

Supervised learning has proven to be highly successful in multi-layer perceptrons. This type of training can be done offline or online, however, most of the networks are of the offline learning type. In offline training, once the weights and biases of the network are set according to the inputs and targets, they cannot be changed during the testing phase. Online learning type networks have a much more complex structure since the network continues to learn during the testing or decision phase as well.

The adjustment of the network parameters also depends on the learning algorithm used to train the network. The different learning algorithms are discussed in Section 3.4.2.

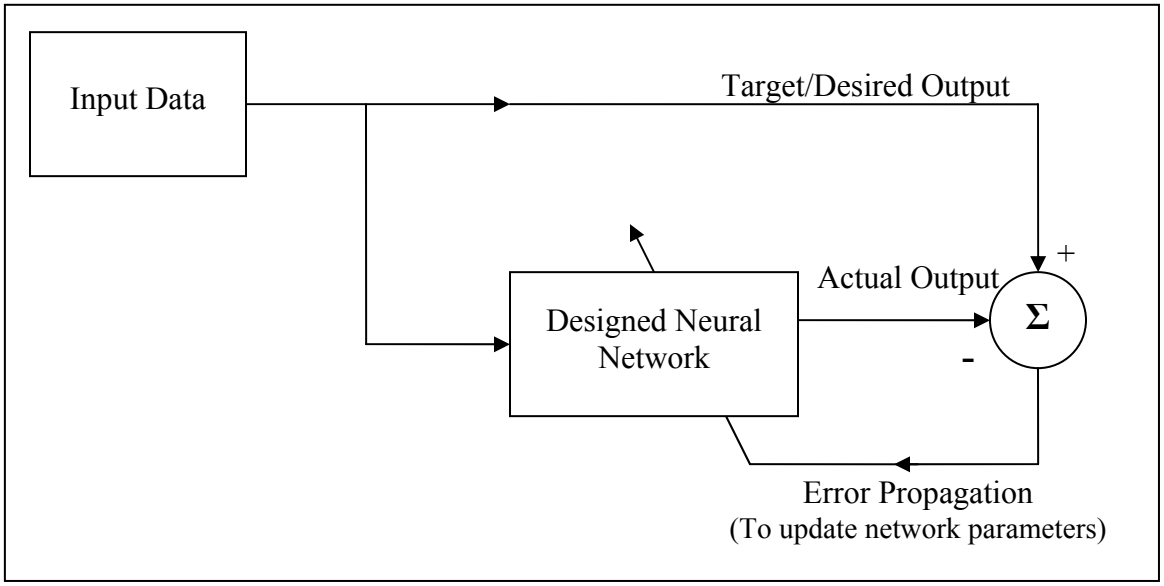

Figure 3.3 Block Diagram of Supervised Learning

3.4.1.2 Unsupervised Learning

In unsupervised learning, the neural network learns and adapts according to the inputs without any target outputs. The weights and biases are modified in response to the network inputs only and the input patterns are categorized into a finite number of classes [12]. No feedback is given in this type of learning. The hidden neurons of the neural

network using this type of learning find a way to organize themselves. This leads to a longer learning process that may tend to become relatively inefficient. Unsupervised learning is used with a competitive learning rule such as Kohonen's law that is discussed in Section 3.3.1.3.

3.4.1.3 Reinforcement Learning

In reinforcement learning, the network attempts to map the outputs according to the input data set. The input and desired outputs are not presented in pairs, unlike supervised learning. The learning is done by reinforcement from the environment (in the form of data or an observer) to minimize the performance error of the network. The training is carried out through a continual process of reshuffling the hidden layer neurons. Reinforcement learning can tend to take a long time due to the process of random selection of network parameters.

3.4.2 Learning Algorithms

A multi-layer perceptron has an input layer and an output layer and can have one or more hidden layers. The input data set is given to the input layer and it propagates forward through a set of mathematical calculations till it emerges as an output from the output layer. A learning algorithm is a procedure that is followed to determine the outputs that are propagated forward from one layer to the next during the training process. Further, a learning algorithm also determines the values of errors that are sent back in order to update the weights and biases of the network in between iterations.

Most of the learning algorithms use some form of gradient descent technique. Since this research project concentrates only on the use of a multi-layer feed forward network (MFNN) using a back-propagation algorithm, only back-propagation algorithms have been discussed in the subsequent sections.

3.4.2.1 Back-propagation Algorithm

The standard back-propagation algorithm is one of the most commonly used learning algorithms and is based on Delta or Widrow-Hoff learning rule. According to this rule,

the strengths of the inputs to each layer are modified in order to reduce the delta (difference) between the desired output and the actual response of the neural network. The input data given to each neuron is a product of the input and its corresponding weight. The back-propagation algorithm establishes a method to modify the connection weights to minimize the value of the performance error below an acceptable level. This algorithm is a gradient descent algorithm because the connection weights of the network are moved along the negative of the gradient of the error function. Mean square error function has been most commonly used for this algorithm. Considering w_i to be the weight vector matrix for any output neuron i, the weights are updated by Δw after an iteration as [59]:

$$\Delta w = -\alpha_k g_k \tag{3.4}$$

$$w_i(k+1) = w_i(k) + \Delta w_i \tag{3.5}$$

In equation 3.4, α_k is the learning rate and g_k is the current gradient, which is a function of the performance function (mean square error in most cases) and the negative sign indicates the direction of the negative of the gradient.

The transfer function used in the neurons is dependent on the application of the neural network. Linear and Sigmoid transfer functions are the most commonly used in output layer whereas sigmoid function is most commonly used in hidden layer of the network. Sigmoid function, often known as a squashing function, has the ability to restrict an infinite range of inputs to a specified range of outputs. Logarithmic sigmoid function has an output range of [0, 1] whereas a tangent sigmoid function limits the outputs to a [-1, 1] range. On the other hand, the output of linear functions is dependent on the input data.

Standard back-propagation algorithm suffers from certain disadvantages. It has the tendency to get stuck in local minima. The addition of a momentum parameter has been suggested to overcome this shortcoming [63]. Another limitation of this algorithm is the convergence time taken to train the network. Other faster algorithms such as resilient back propagation and conjugate gradient algorithms have been proposed to reduce the training time.

3.4.2.2 Resilient Back-propagation Algorithm

The standard back propagation algorithm is dependent on the steepest descent technique. Therefore, a small magnitude of gradient of the error function gradient leads to very small change in the weights and biases, leading to a longer convergence time. Further, when sigmoid neurons are used in gradient descent algorithms, the size of the derivative decreases exponentially with the distance between the weight and the output-layer, due to the limiting influence of the slope of the sigmoid activation function.

Resilient back propagation eliminates these inherent limitations of partial derivatives. It performs a local adaptation of the weight-updates according to the behavior of the error function and the adaptation process is only dependent on the temporal behavior of its sign [64]. According to this rule, if the partial derivative of a weight does not change its sign after an update, it implies that the algorithm is moving towards convergence and the update values can be increased further. On the other hand, if the derivative changes it sign, it implies that the algorithm has jumped a local minima and update values should be decreased.

This algorithm has proven better than a standard back-propagation algorithm, especially when used for sigmoid neurons. It prevents the ANN from getting stuck in local minima, which is highly possible when sigmoid neurons are employed. It further decreases the training time of the ANN. Because of these advantages, resilient back propagation has been used in all the ANN designs in this project.

3.4.2.3 Conjugate Gradient Algorithm

Conjugate gradient algorithm is based on numerical optimization techniques and produce faster convergence than standard gradient descent algorithms. This algorithm performs search to reduce the performance function in conjugate gradient direction. This is combined with an adaptive learning rate, which is adjusted between iterations. Various types of conjugate gradient algorithms have been proposed. Some of these algorithms are also available as functions in the MATLAB neural network tool box.

3.5 Artificial Neural Networks as Pattern Classifiers

A relay is used for the detection and classification of faults. This is essentially a pattern classification problem. ANNs have been successfully applied in various pattern classification applications in the fields of science and technology. Further, ANNs have the ability to learn from a representative set of patterns and apply the learning to different system conditions. This capability of an ANN to learn and generalize has been utilized in this project. A single neuron can be used for simple classification problems whereas multiple layers of neurons are required for more complex and non-linear applications like protective relaying.

3.5.1 Neuron as a Pattern Classifier

A single neuron with two inputs x_1 and x_2 and with weights w_1 and w_2 respectively can be implemented as a pattern classifier as shown in Figure 3.4. The discriminator surface L between the classified patterns can be represented as:

$$L : y = w_1 x_1 + w_2 x_2 = 0 \tag{3.6}$$

The neural output y above this boundary is +1 (for all the patterns belonging to class P_2) and the neural output y below this boundary is -1 (for all the patterns belonging to class P_1). A single neuron possesses the capability of classifying simple patterns. However, for complex problems such as power systems' applications, layers of neurons are used in series and parallel combinations to get the desired results.

3.5.2 MFNNs as Pattern Classifiers

Significant research has been done to test the ability of MFNNs and they have proven to perform well for pattern classification problems [60]. The pattern classification ability of MFNNs is dependent on various factors. Theories regarding the optimization of parameters of neural networks such as number of hidden layers, number of nodes (neurons) in each layer and number of training patterns have been proposed. Selection of these parameters affects the pattern classification ability of the neural networks. One theory [61] suggests that a four-layer network with two hidden layers is difficult to train

and is more prone to local minima as compared to a three layer network with one hidden layer. Another theory [68] suggests that a neural network with two hidden layers can form arbitrary disjoint decision regions and a one hidden layer neural network can form single convex decision regions. The design of a MFNN as pattern classifier is application dependent and should be modified accordingly. The detailed design of the ANN used in this project is discussed in chapter five. However, the general design procedure of a MFNN remains the same.

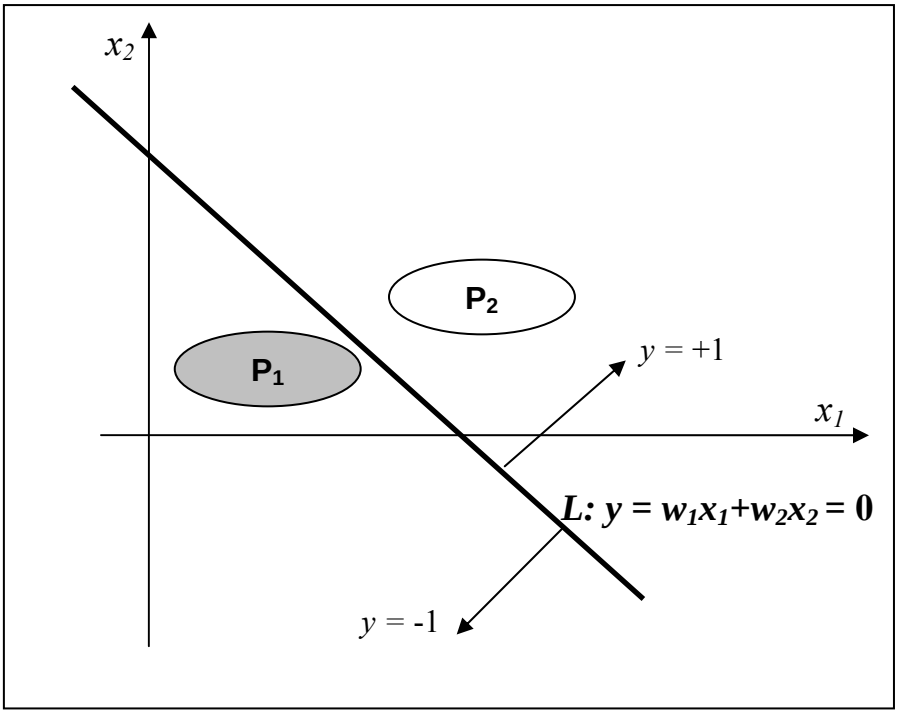

Figure 3.4: Single Neuron as a Pattern Classifier

3.6 Design of a Neural Network

A properly designed and trained neural network has the ability to provide reasonable results for a set of any possible inputs. To ensure generality, it is imperative that the input/output combinations used for training the network are representative of the external system/ environment. Figure 3.5 shows a flowchart for the design of a multi-layer feed forward network, as shown in reference [5]. The design of a neural network can be categorized into three main phases:

3.6.1ANN Selection and Input Pre-processing

Selection of appropriate input data is done and the data is given to the input layer of the ANN. The data is usually in the form of batch or individual inputs depending on the application. The desired output value for each set of input data is also established. Other network parameters such as the number of layers and the number of nodes in each layer are determined. Proper pre-processing of data is important to ensure that correct results

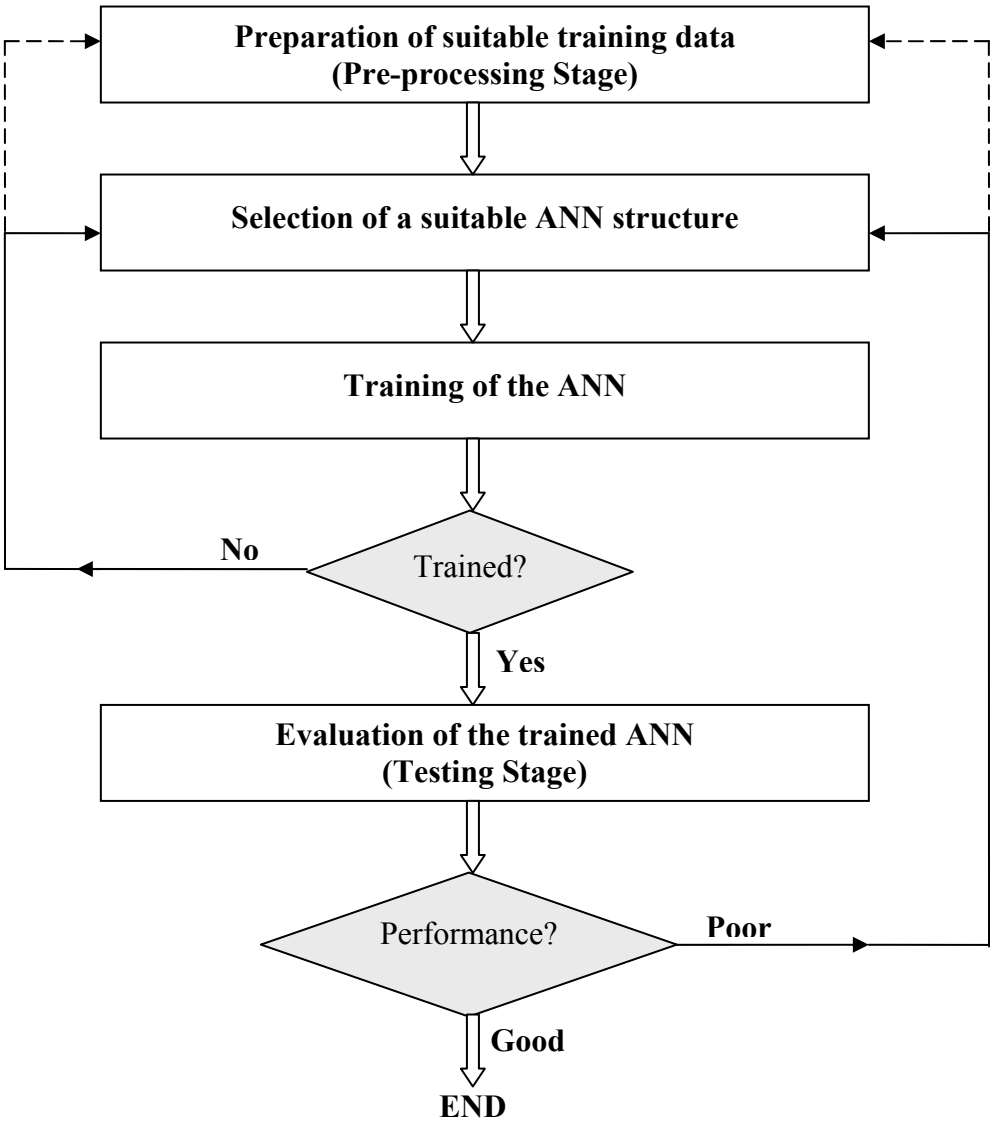

Figure 3.5: Flowchart: Design of a Neural Network [5]

are obtained from the ANN. These input parameters can be modified in the later stages depending on the results obtained in the training and testing phases.

3.6.2 Training and Feedback

The network is trained by giving the inputs and desired outputs. During the training, the desired targets and the actual outputs of the ANN are compared and the errors are back propagated to update the weights of the network and improve the performance index of the network. The training is stopped when the error of the network stops reducing significantly or reduces below the desired value.

3.6.3 Testing

The network is tested with input data different from the training data to ensure generality of the neural network. If the performance of the network is above an acceptable standard, the neural network is accepted. If the results are not acceptable, the parameters of the network such as the learning rate, inputs, configuration etc. are changed, usually using a trial and error method. This iterative process continues till satisfactory results are obtained. It is important to test the network extensively and for different situations in order to ensure accuracy and generalization.

3.7 Applications for Transmission Line Protection

Artificial neural networks have been used widely in last decade for various distance protection applications for the protection of transmission lines. These applications can be broadly classified into three categories.

- Fault Detection

Neural networks have been most commonly used for the detection of faults. Typical relays have been trained using current and voltage data to recognize a fault condition on a transmission line. Such relays only detect the presence of fault, irrespective of the type of fault. For example, a neural network trained to detect faults on phase A gives a +1 output in case of a single line to ground, phase to phase or three phase fault in all

situations where phase A is involved. Some relays combine this approach for A, B and C phases to further classify the faults into different categories. One such relay has been proposed recently [7], which combines the principle of fault detection and fault classification in a single ANN.

- Fault Classification

Classification of faults is another approach used for transmission line protection. In these relays, the neural networks are trained to recognize specific type of faults (single line to ground, phase to phase faults etc.). The input data is pre-processed (as previously shown in Table 2.2) to train specific ANNs and each trained ANN is used for only one type of fault that enables the classification of faults. This approach is closer to practical application of relays in power systems. ANN relays have also been used for directional discrimination of faults. One such relay was proposed in 1995 [6], where an ANN has been used to distinguish between forward and reverse faults.

- Fault Location

Neural networks have been used to estimate the location of faults on a transmission line. ANNs are trained to recognize faults belonging to a specific protection zone and the output of the ANN indicates if the fault belongs to the specified zone. For more precise measurement of fault location, current and voltage phasors need to be calculated.

3.8 Summary

This chapter presents the theory and principles of artificial neural networks. It also discusses the different configurations of neural networks and the learning processes used for training ANNs. The application of a single neuron and multi-layer neural networks as pattern classifiers are described. The neural network based applications of transmission line protection are discussed.

4. DISTANCE RELAY DESIGN METHODOLOGY

4.1 Introduction

The previous chapter presents the theory and principles of artificial neural networks and their applications as pattern classifiers. It also discusses protective relaying applications where ANNs have been used for fault detection, classification and location of faults. This chapter presents a new design methodology that was used for designing the proposed neural network based relays.

The last century has seen significant development of relays from electromechanical and solid state to state-of-the-art numerical relays. The same distance relay principles have been used in all these technologies. The security and dependability of relays has vastly improved with the advent of digital technology. There are, however, some inherent deficiencies in a distance relay phase comparison techniques that have not been addressed [76]. This chapter addresses some of these issues and discusses the modifications that were made to a conventional relay algorithm to eliminate some of these limitations.

4.2 Distance Relay Algorithm

In order to discuss the conventional distance relay algorithm, it is categorized into four main steps – mathematical representation, conversion in terms of phasors, implementation in electromechanical and solid-state relays and implementation in numerical relays.

4.2.1 Mathematical Representation

Figure 4.1 shows the ideal operating characteristics of a mho relay installed at a line terminal represented in the figure at the origin of the impedance diagram. The maximum reach of the relay is $\overline{Z}_r$. For a fault on the line, the impedance measured by the relay $\overline{Z}$ is inside the relay characteristic. By geometry, the angle of $\overline{Z}$ with respect to the angle of $\overline{Z}_r - \overline{Z}$ is less than ninety degrees when $\overline{Z}$ is in the operating zone of the relay. This

angle is more than ninety degrees if $\overline{Z}$ is outside the reach of the relay. This is mathematically expressed as:

$$-90° < \Phi < +90° \tag{4.1}$$

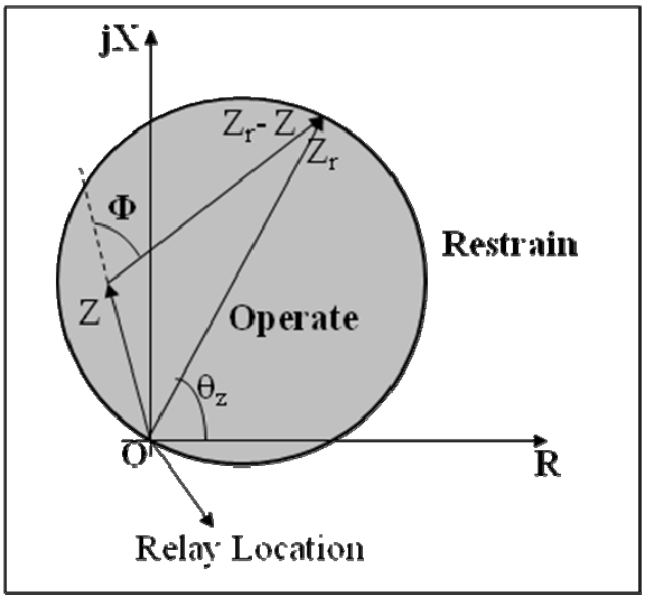

Figure 4.1: Ideal Operating Characteristics of a Mho Relay

When a fault occurs on a transmission line, the impedance seen by the relay cannot be measured directly. The current and voltage measured at relay location to calculate the positive sequence impedance. The current and voltage inputs vary depending on the type of relay as previously discussed in Chapter 2.

4.2.2 Phasor Representation

The impedances discussed in the previous section can be expressed in terms of phasors. Considering $\vec{I}_f$ to be the phasor of the current seen at the relay location, the angle between the phasors $\vec{I}_f\overline{Z}_r - \vec{I}_f\overline{Z}$ and $\vec{I}_f\overline{Z}$ is also equal to Φ. Because $\vec{I}_f\overline{Z}$ is the voltage ($\vec{V}_r$) at the relay location, it can be measured. The phasor of the current $\vec{I}_f$ can also be calculated. In the conventional approach, a phase comparator, therefore, measures the angle between the voltage at the relay location, $\vec{V}_r$ and $\vec{I}_f\overline{Z}_r - \vec{V}_r$.

The two inputs applied to the mho relay are therefore

$$Input_1 = \vec{V}_r \tag{4.2}$$

$$Input_2 = \vec{I}_f \overline{Z}_r - \vec{V}_r \tag{4.3}$$

The relay operates if the phase angle between the two phasors $Input_1$ and $Input_2$ lies between -90º and +90º. The individual phasors must, therefore, be determined accurately for correct operation of a relay.

4.2.3 Implementation in Analog Relays

In case of electromechanical and solid state relays, the voltage at relay location, $Input_1$ is used directly after scaling down to a relay appropriate level. For generating $Input_2$, the current $\vec{I}_f$ obtained from the power system is first processed by using $\overline{Z}_r$. In conventional designs, the phasor $\vec{I}_f \overline{Z}_r$ is obtained by either passing $\vec{I}_f$ through a replica impedance of the line using a magnetic transactor or by using a differentiator type operational amplifier circuit.

The significance of the input $\vec{I}_f \overline{Z}_r$ [77] is explained using Figure 4.2. For the purpose of addressing the problem, the current $\vec{I}_f$ is taken as a reference for a value of $1\angle 0°$ and is shown by a dotted line. The value of the relay reach $\overline{Z}_r$ is taken as $1\angle 90°$ and the input equivalent to $\vec{I}_f \overline{Z}_r$ is shown by a solid line. These values result in a pure sine waveform for the current $\vec{I}_f$ and a cosine waveform for voltage $\vec{I}_f \overline{Z}_r$. As a cosine waveform can be obtained from a sine waveform by the process of differentiation, thus the usual procedure to obtain a resultant input equivalent to $\vec{I}_f \overline{Z}_r$, is by use of a differentiator type circuit. It can further be observed in Figure 4.2 that the value of $\vec{I}_f \overline{Z}_r$ at the instant zero is equivalent to a future value of current $\vec{I}_f$. This implies that the value of $\vec{I}_f \overline{Z}_r$ has to be estimated before the actual value of current is obtained. This makes the algorithm dependent on approximate and not actual values of current. This may lead to an incorrect

zero crossing instant of the output $\vec{I}_f \overline{Z}_r$. Zero crossing detectors are used to calculate the phase difference between waveforms $\vec{I}_f \overline{Z}_r - \vec{V}_r$ and $\vec{V}_r$ in most solid state relays. This results in inaccurate phase difference calculations between the two inputs of a mho phase comparator.

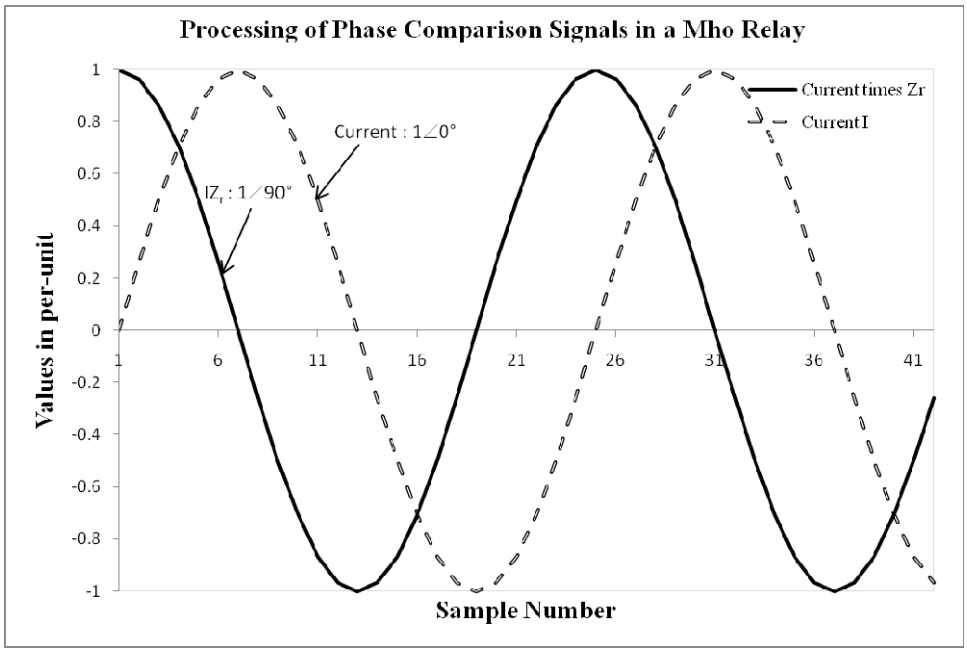

Figure 4.2: Phase Comparator Signal for Mho Relay

4.2.4 Numerical Phase Comparators

Numerical relays use instantaneous values of current. Instantaneous values of current flowing in a line are not used to predict equivalent future values to calculate $\vec{I}_f \overline{Z}_r$ unlike solid state relays. Numerical relays use an equivalent of replica impedance by implementing a phasor estimation algorithm. A numerical phase comparator uses fundamental frequency components of inputs to estimate current and voltage phasors $\vec{I}_f$ and $\vec{V}_r$ respectively. These phasors are then used to calculate the phase angle between $\vec{I}_f \overline{Z}_r - \vec{V}_r$ and $\vec{V}_r$. The typical data window size required to accurately estimate the phasor values is at least one cycle of samples after the occurrence of the fault. The fault detection time is, therefore, usually greater than one cycle and increases for remote bus faults. Various short-window and long-window phasor estimation techniques that are

discussed previously in Section 2.8 have been proposed and are used in traditional designs. The parameter estimation technique used and the system conditions primarily influences the accuracy and fault detection time. Alternative algorithms like neural networks have also been used for numerical distance relaying, however, none of those designs implement the characteristic of an admittance relay phase comparator.

4.3 Proposed Input Algorithm

This section presents an input processing algorithm that addresses the issues discussed in the previous section and attempts to eliminate these deficiencies. The inputs in the proposed design are handled in such a manner that the value of phase comparison inputs $\vec{I}_f \overline{Z}_r - \vec{V}_r$ and $\vec{V}_r$ depends on past instantaneous values of currents and voltages rather than estimated values. Moreover, the current and voltage samples are modified in such a way that it eliminates the need for calculating current and voltage phasors and the apparent impedance $\overline{Z}$.

4.3.1 Phasor Representation

Equations 4.4 and 4.5 show the mathematical modifications used in the proposed design. The current ($\vec{I}_f$) and voltage ($\vec{V}_r$) phasors are expressed in terms of their magnitudes and phase angles. The current and voltage are represented in the form of phasors only for describing the design using equations. The inputs shown in equation 4.2 and 4.3 can be modified by dividing both the terms by $1\angle\theta_z$. $Input_{1\text{mod}}$ and $Input_{2\text{mod}}$ were the two modified inputs [78] obtained.

$$Input_{1\text{mod}} = |V_r|\angle(\theta_v - \theta_z) \tag{4.4}$$

$$Input_{2\text{mod}} = |I_f||Z_r|\angle\theta_i - |V_r|\angle(\theta_v - \theta_z) \tag{4.5}$$

Mathematically, this modification does not change the angle between these two modified inputs. This condition can be represented as:

$$-90° \le ang(Input_{1\text{mod}}) - ang(Input_{2\text{mod}}) \le +90° \tag{4.6}$$

4.3.2 Implementation in Solid State Relays

$Input_{1\,\mathrm{mod}}$ is the voltage waveform at relay location that is delayed by an angle of θ_z. Therefore, it can be obtained by using a simple phase lag circuit. This implies that this input is dependent on the past values of the voltage. The first term of $Input_{2\,\mathrm{mod}}$ is independent of θ_z and can be obtained by multiplication of the current waveform $\vec{I}_f$ with a scalar quantity $|Z_r|$. The second term of $Input_{2\,\mathrm{mod}}$ has already been described. Figure 4.3 shows a block diagram of implementing this algorithm in solid – state relays.

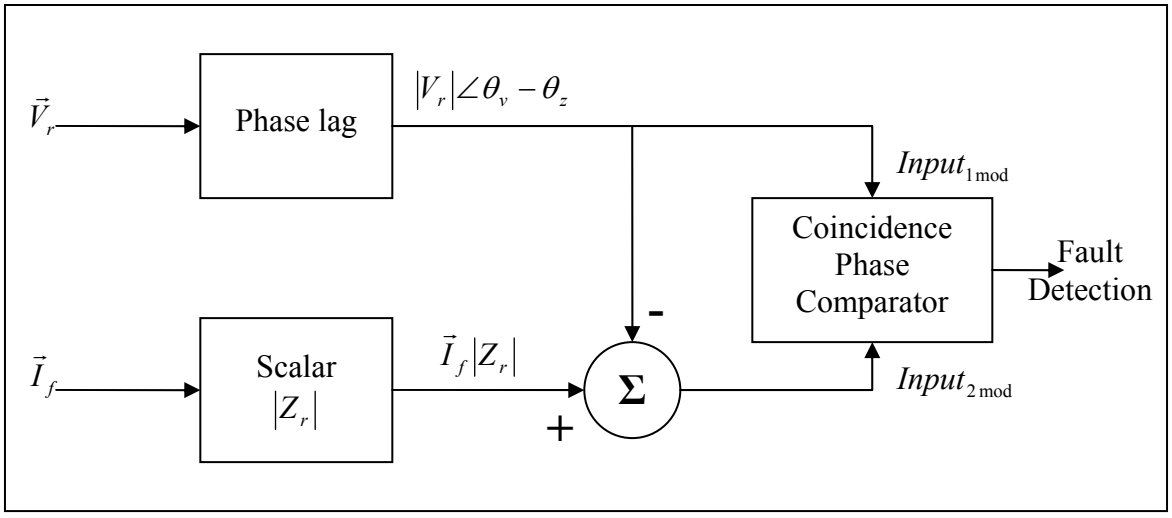

Figure 4.3: Implementation of Proposed Algorithm in Solid-state Relays

4.3.3 Implementation in Numerical Relays

The proposed methodology assumes the value of θ_z to be a multiple of the sampling angle θ_s, equal to $m\theta_s$. Although, any value of θ_z and θ_s can be considered, this assumption makes the design considerably easier to explain and implement. The first step is to pre-process the inputs to produce the necessary input equivalent to $|V_r|\angle\theta_v - \theta_z$. Since θ_z equals to $m\theta_s$; therefore the voltage input is delayed by m

samples to get the equivalent input. Thus, the first input is pre-processed using a standard delay procedure. The first input for any nth sample can be given as:

$$Input_{1\,\mathrm{mod}}[n] = V_r[n-m] \tag{4.6}$$

The second input is produced by using mathematical subtraction of values shown in equation 4.6. The parameters $|Z_r|$ and θ_z are known parameters and can be set according to the impedance reach of the relay. An input equivalent to $|I_f||Z_r|\angle\theta_i - |V_r|\angle(\theta_v - \theta_z)$ for an nth sample is, therefore, equal to:

$$Input_{2\,\mathrm{mod}}[n] = I_f[n]|Z_r| - Input_{1\,\mathrm{mod}}[n] \tag{4.7}$$

This further implies:

$$Input_{2\,\mathrm{mod}}[n] = I_f[n]|Z_r| - V_r[n-m] \tag{4.8}$$

Equations 4.6 and 4.8 can be applied to produce the modified inputs from the instantaneous values of currents and voltages obtained from a power system.

It should also be noted that the algorithm can be easily extended to design a relay for any sampling frequency or impedance value. The instantaneous values of voltage for samples other than multiples of sampling frequency can be obtained by simple interpolation techniques. For example, if the value of maximum sensitivity angle θ_z is 2.5 times θ_s, the "half-sample" instantaneous value of voltage can be calculated by taking an average of second and third voltage samples. This issue is addressed in more detail in Chapter 5.

Numerical relaying algorithms are usually implemented using input data windows and the fault detection time is the time calculated from the instant of fault

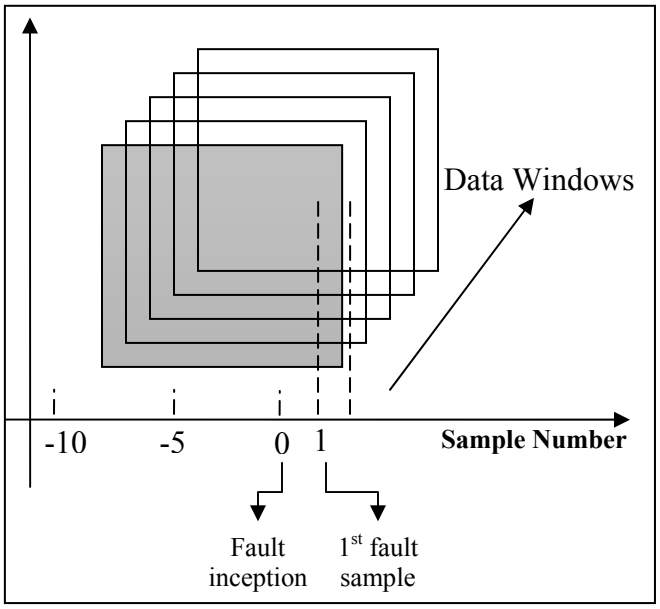

Figure 4.4: Input Samples' Data Windows

inception. It is, therefore, important to analyze the processed input samples at fault instant. Figure 4.4 illustrates the input data windows used in a numerical algorithm. It should be noted that the algorithm uses a data window that contains equal samples of both inputs. When an algorithm is implemented using data window of ***x*** samples, the first window after fault inception consists of ***x-1*** pre-fault samples and one fault sample. The conventional numerical algorithms calculate phasors accurately when data window is full of ***x*** fault samples. This translates to a time of ***x*** times the sampling interval. The proposed algorithm has been implemented similarly [79]; fault detection time is noted from the instant of fault occurrence.

As per the proposed algorithm, the first fault voltage sample is not used in the first fault window. As per equations 4.7 and 4.8, the first fault sample (or the last sample in the first fault window) for the modified inputs can be described as:

$$Input_{1\,\mathrm{mod}}[1] = V_r[1-m] \tag{4.9}$$

$$Input_{2\,\mathrm{mod}}[1] = I_f[1]\,|\,Z_r\,| - V_r[1-m] \tag{4.10}$$

It can be observed in equation 4.9 that the first fault sample for $Input_{1\,\mathrm{mod}}$ is actually a pre-fault voltage sample. Similarly, the second window uses the 1st and 2nd fault current samples, but all pre-fault voltage samples. Understandably, the $(m+1)^{th}$ window after the fault inception will have the 1st fault voltage sample as the last sample of $Input_{1\,\mathrm{mod}}$ data window. This algorithm has been combined with a neural network based approach discussed in the next chapter. Data windows containing pre-fault samples along with fault samples were used for training and testing an ANN relay.

4.4 Discussion

The traditional analog relays use hardware modules to estimate the values of currents and voltages. The result of calculating the apparent impedance from the estimated values of current and voltage are noisy and can lead to incorrect operation of a relay. The modified algorithm proposed here uses past values of currents and voltages to detect the fault.

Since no estimation is required and the values used in the algorithm are obtained directly from the system, the relay operation is more accurate.

The conventional numerical algorithms use fault samples to estimate the current and voltage phasors. Current phasor estimation gets affected by dc component present immediately after the inception of fault. This problem is counteracted by either modifying the numerical algorithm or delaying till this transient dc component has subsided. Most numerical algorithms are not able to accurately filter out the dc component; the second approach leads to a longer fault detection time. Therefore, the conventional phasor algorithms take more than one period of fundamental frequency to accurately determine the phasors. On the other hand, the presence of dc current for a long duration can lead to saturation of CTs. The conventional numerical algorithms, therefore, face a challenge to correctly determine current phasors in the presence of a decaying dc component and CT saturation. Similarly, a voltage transformer gets affected by the presence of high frequency transients that affect voltage phasors' calculations.

These factors influence the correct estimation of impedance seen by a distance relay. Incorrect estimation of phasors (and thus impedance) can lead to under-reach or over-reach of the relay; the integrity of the relay boundaries may not be preserved in such cases. The proposed algorithm does not use any phasor ($\vec{I}_f$ and $\vec{V}_r$) or impedance ($\overline{Z}$) values to detect the fault. Instantaneous current and voltage values obtained directly from a power system are used to process inputs. The algorithm is dependent only on the phase difference between the processed inputs. This algorithm was implemented using a neural network. The neural network was trained to recognize the phase difference between the processed inputs. This eliminates the need of calculating phasors. The processed inputs given to the neural network have a direct relationship with the outputs expected from a relay, which helps to use a data window lesser than one full cycle to accurately detect faults, making the algorithm faster than traditional designs.

A neural network was trained offline using a desired value of impedance reach. Once trained, the neural network was implemented on a transmission line with the same

impedance reach, in a different power system. This approach ensures generality in case of changes in power system network configurations as the relay is trained to "see" only the phase difference between processed inputs. The removal of deficiencies that exist in the conventional algorithms ensures the integrity of the relay characteristics' boundaries. The details about the configuration, training and testing of the neural network design are presented in the next chapter.

4.5 Validity of the Algorithm

As per the proposed algorithm, the angle between $Input_{1\,\mathrm{mod}}$ and $Input_{2\,\mathrm{mod}}$ should be in the [-90º, 90º] range for all faults lying within the relay protection zone. This section presents results to prove this condition. The algorithm was tested using a full cycle DFT algorithm that is described earlier in Chapter 2. It should be noted that the use of a phasor algorithm is solely for proving the validity of this proposed algorithm. In this project, neural networks were used to implement relay characteristics; no phasor calculations were involved in that process.

4.5.1 The Discrete Fourier Transform Technique

DFT technique uses sine and cosine functions as reference orthogonal waveforms. The sine and cosine weights are produced depending on the number of samples in a cycle. Each sample in the data window is multiplied with its respective sine and cosine weights and the weighted product is saved. The sum of weighted products is used to calculate the magnitude and phase angle of any input. In this case, one cycle of samples for the two inputs $Input_{1\,\mathrm{mod}}$ and $Input_{2\,\mathrm{mod}}$ was produced using the proposed algorithm and DFT was applied to these samples. The sine and cosine weights used are given in Appendix A.

4.5.2 Application of the DFT technique

The characteristic of an admittance relay was considered to test the algorithm using DFT technique. A *concentric circles approach* [80] was applied. Figure 4.5 shows this approach. The centre of the relay characteristics' circle was chosen as the center for all

circles and input points on the circumference of these circles refer to different values of impedance $\overline{Z}$. The current waveform was kept as a reference; always equal to $1\angle 0^{\circ}$ p.u and samples from this waveform were produced. The corresponding voltage waveform was then generated depending on the value of $\overline{Z}$ to obtain voltage samples. These current and voltage samples were used to obtain processed inputs. This approach and the processing of inputs is described in detail in the next chapter, in Section 5.2.1.1.

The impedance reach of the relay $\overline{Z}_r$ was chosen as $0.5\angle 75^{\circ}$ p.u. The first zone of protection was assumed as 80% of the total line impedance. The inputs were generated using a sampling rate of twenty-four samples/cycle (a sampling frequency of 1.44 kHz). A sampling angle θ_s of 15º implied that θ_z was five times θ_s. Current and voltage samples for different impedance values inside and outside the relay characteristic were used to produce $Input_{1\,\mathrm{mod}}$ and $Input_{2\,\mathrm{mod}}$. The phase angle between these two processed inputs was determined using a full-cycle DFT algorithm. The phasors for various impedance values on the circumference of relay characteristics are shown in Appendix A.

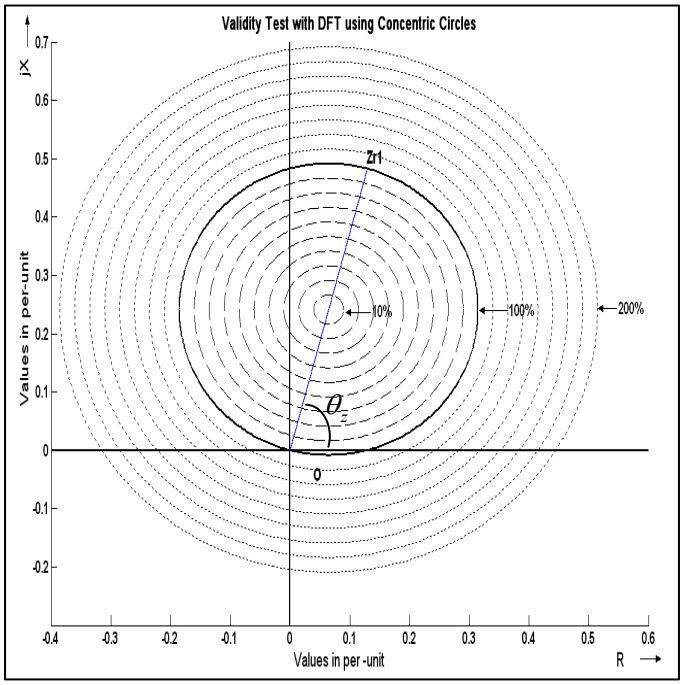

Figure 4.5: Algorithm Testing at Different Percentages of the Line

4.5.3 Validation Results

Twelve impedance points were considered on the circumference of each of these circles and results for six of these points are presented. Table 4.1 shows the phase angle difference between the two processed inputs for these different values of $\overline{Z}$. The radii of the circles is expressed as a percentage of relay characteristic radius. All these points with different values of $\overline{Z}$ are shown on the relay characteristics in Appendix A.

The results prove that the phase angle between the processed inputs is within the [-90°, 90°] range for inputs inside the relay boundaries. The phase angle for inputs on the relay boundary is exactly equal to either -90° or +90° depending on the location of input points on the relay characteristic. For all inputs outside the relay boundary, the phase angle between the two inputs is either less than -90° or more than +90°. The results prove that the proposed algorithm represents phase comparator characteristic of an admittance relay.

Table 4.1: Phase Angle Difference between Processed Inputs

	% of Relay Characteristic Radius	**Phase Angle (in degrees) between Processed Inputs**					
Inside the Relay Boundaries	**10%**	-8.1297	2.9931	11.0417	8.1297	-2.9931	-11.042
	20%	-16.416	6.1551	21.9233	16.4164	-6.1551	-21.923
	30%	-24.996	9.6842	32.492	24.9961	-9.6842	-32.492
	40%	-33.958	13.847	42.6119	33.9577	-13.847	-42.612
	50%	-43.314	19.0391	52.1722	43.3139	-19.039	-52.172
	60%	-52.975	25.8866	61.0948	52.9747	-25.887	-61.095
	70%	-62.744	35.3932	69.3367	62.7435	-35.393	-69.337
	80%	-72.349	48.9985	76.8875	72.349	-48.999	-76.888
	90%	-81.51	67.8126	83.7635	81.5097	-67.813	-83.764
	100%	-90	90	90	90	-90	-90
Outside the Relay Boundaries	**110%**	-97.688	110.244	95.6437	97.6881	-110.24	-95.644
	120%	-104.54	125.312	100.747	104.535	-125.31	-100.75
	130%	-110.57	135.718	105.363	110.572	-135.72	-105.36
	140%	-115.87	142.951	109.542	115.868	-142.95	-109.54
	150%	-120.51	148.153	113.334	120.509	-148.15	-113.33
	160%	-124.58	152.036	116.78	124.584	-152.04	-116.78

	170%	-128.17	155.033	119.92	128.172	-155.03	-119.92
	180%	-131.35	157.415	122.789	131.346	-157.41	-122.79
	190%	-134.17	159.352	125.416	134.167	-159.35	-125.42
	200%	223.314	160.961	127.828	-223.31	-160.96	-127.83

4.6 Summary

The design and implementation of conventional distance relay algorithms in electromechanical, solid-state and numerical relays is discussed in this chapter. This chapter also discusses some existing limitations of conventional distance relay phase comparator algorithms. A new algorithm that addresses these limitations is introduced. The implementation of the algorithm in solid-state and numerical relays is discussed.

The proposed algorithm was validated using a full cycle DFT. The obtained results prove that the algorithm implements the generic characteristic of an admittance relay. Given that the characteristics of all distance relays are similar; the proposed design can be extended for the design of other protective relays in a similar manner. This is undertaken in the next chapter.

5. IMPLEMENTATION OF THE ANN BASED RELAYS

5.1 Introduction

The design and implementation of conventional relay algorithms is discussed in the previous chapter. An algorithm that addresses some of the deficiencies that exist in current phase comparator designs is proposed. This chapter discusses the implementation of the proposed algorithm for different types of relays. The pre-processing technique discussed in the previous chapter is combined with a neural network approach to eliminate the use of input phasors.

This chapter also discusses two different approaches to train the neural network. The pre-processing of inputs for different relays characteristics is presented and training of the ANNs for these characteristics is discussed. The polarization techniques that were included in the design for directional discrimination of close-in faults are discussed.

5.2 Proposed Relay Implementation

This section discusses the training and testing of an ANN to implement the admittance relay phase comparator characteristic discussed in the previous chapter. The proposed algorithm was applied to design other relays; these designs are discussed in this section. Different relay characteristics were combined for the design of a quadrilateral relay. The concept is briefly discussed in Chapter 2. The details of the quadrilateral design using the proposed algorithm are also presented.

5.2.1 Admittance Relay Design

Two different approaches were considered for training the neural network. This first approach uses pure sinusoidal inputs generated using MATLAB for different $\overline{Z}$ values using the concept of *concentric circles* discussed in Chapter 4. The second approach is a fault equivalent circuit approach that generates current and voltage values obtained from

a circuit simulated using PSCAD/EMTDC. The $\overline{Z}$ values are represented in terms of resistance R and inductance $L = \left(\frac{X}{2\pi f}\right)$. These approaches are discussed in the next two sections.

5.2.1.1 Sinusoidal Approach using MATLAB

This approach is described briefly in the Chapter 4. The circles were generated by choosing the centre of the relay characteristics' circle as the center for all the circles. The diameter of the considered characteristic is 0.5 p.u., resulting in a radius of 0.25 p.u. Uniformly spaced impedance points on the circumference of these circles were considered to generate different patterns in MATLAB. These patterns, in the form of data windows, were used for training. This concept is explained by means of an example.

Figure 5.1 shows a point plotted on the impedance plane. This is one of the impedance points on 0.1 p.u. circle with impedance equal to 0.3476∠70.73° (0.1147+ j0.3281). The currents and voltages for this point are shown in Figure 5.2. It should be noted that the waveforms are plotted for explanation purposes; the algorithm uses discrete values of these waveforms. It is mentioned before that the current was taken as a reference with a value of 1∠0° p.u. This is shown in the first graph of Figure 5.2 for a sampling rate of 24 samples/cycle. This graph also shows the waveform produced using samples of $I[n]|Z_r|$ with $|Z_r|$ of 0.5 p.u.

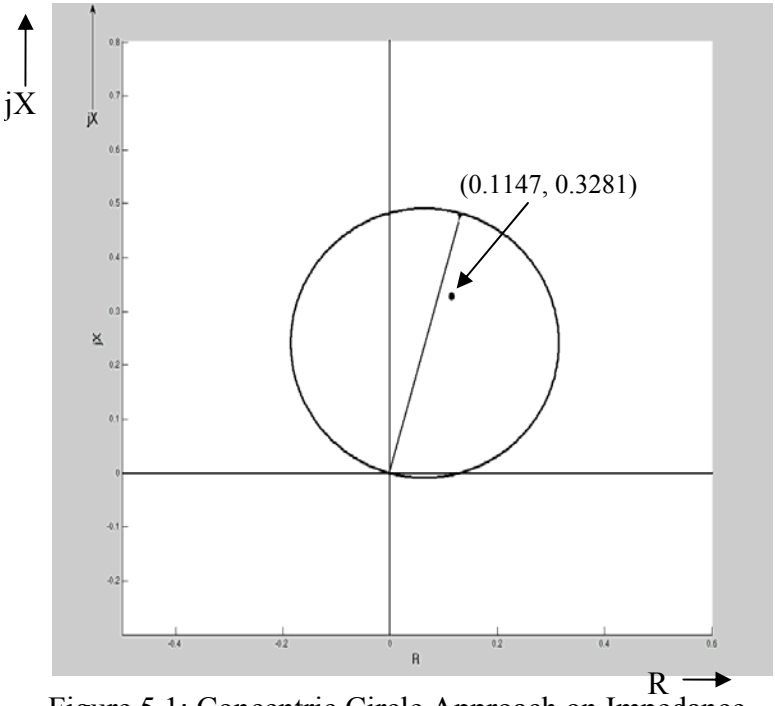

Figure 5.1: Concentric Circle Approach on Impedance Plane

The second graph of Figure 5.2 shows the voltage seen at relay location, produced using samples of $I[n]Z$. Since I is equal to $1\angle 0°$ p.u, the voltage samples correspond to the apparent impedance Z. $Input_{1\,\mathrm{mod}}$ waveform was obtained by delaying the voltage samples by five samples to account for 75° impedance reach angle. This delayed voltage waveform is shown in the second graph. The three waveforms for samples of $I[n]|Z_r|$, $Input_{1\,\mathrm{mod}}$ and $Input_{2\,\mathrm{mod}}$ are shown in the third graph.

The modified inputs $Input_{1\,\mathrm{mod}}$ and $Input_{2\,\mathrm{mod}}$ were similarly generated for each impedance point that was used in training. The *Concentric Circles'* approach ensured a uniform selection of different impedance magnitudes and angles as every input point corresponded to different impedance value. Different radii were taken into account to ensure that patterns from inside as well as close to boundary of the relay characteristic were given as inputs to the ANN. The radii of circles were changed on an iterative basis during training of the neural network to ensure

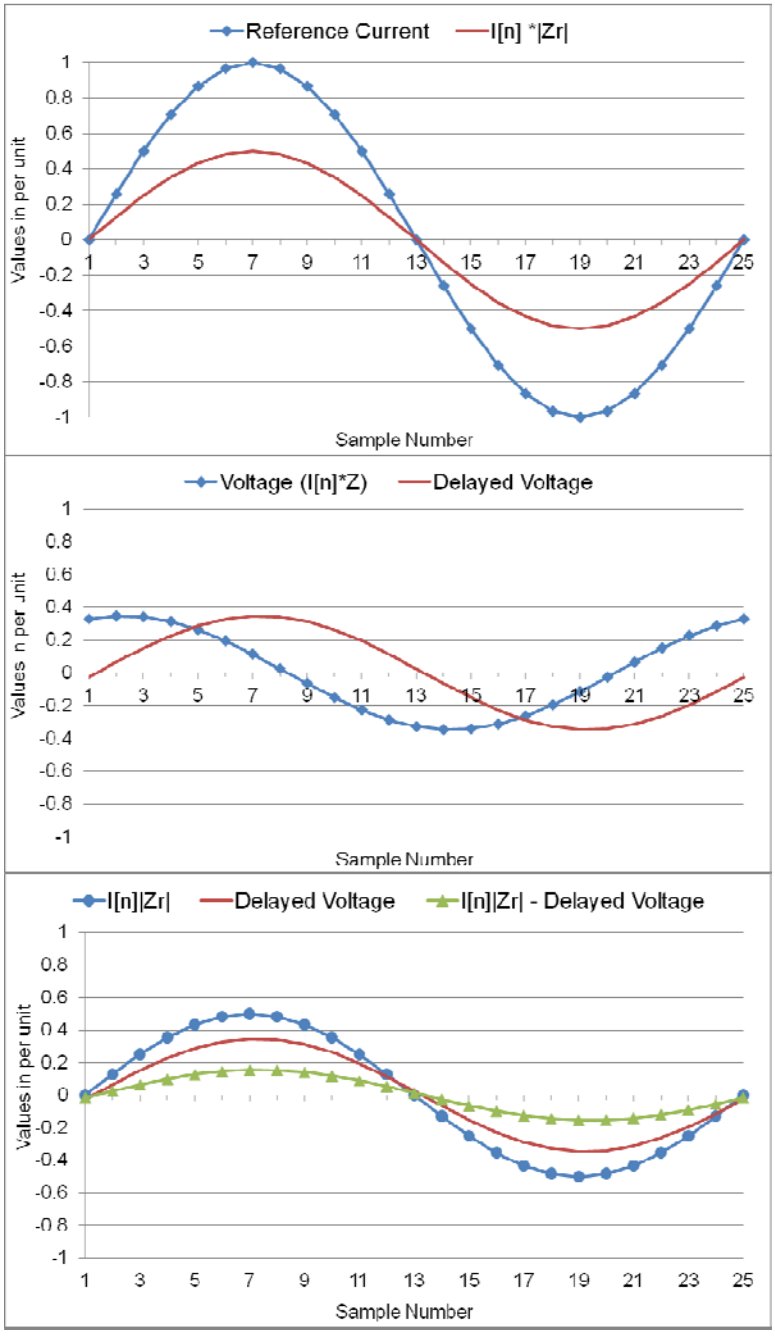

Figure 5.2: Signals Corresponding to a Specific Impedance

that the trained ANN is able to maintain the integrity of the relay boundaries.

Equal patterns were generated inside and outside the relay boundaries to avoid skewed training. A total of twenty-eight circles were generated, fourteen each inside and outside the relay boundaries. Twelve points on the circumference of each circle were produced, resulting in a total of 336 different patterns. The neural network seemed to perform well when trained with 168 fault and 168 non-fault patterns. Five cycles of data was produced at a sampling rate of twenty-four samples/cycle and given to the ANN in form of input data windows. Therefore, each pattern comprised of 4032 samples and (4032 – (n-1)) data windows, where, n is the size of the data window. The procedure of training the ANN using the generated patterns is covered in Section 5.2.1.3.

5.2.1.2 Fault Equivalent Circuit Approach using EMTDC

In this method, currents (I_a, I_b and I_c) and voltages (V_a, V_b and V_c) were produced using a simple fault equivalent circuit simulated on PSCAD shown in Figure 5.3. For a relay installed on a point shown by A at bus 1, the impedance seen during a fault is equal to the equivalent impedance of the series combination of resistance and reactance connected to the transmission line T. The values of R and L were thus, set according to the same impedance values as used in the previous approach. As in the previous case, a total of 336 different cases were run on the fault equivalent circuit and values of currents flowing in the line and voltages of three phases were

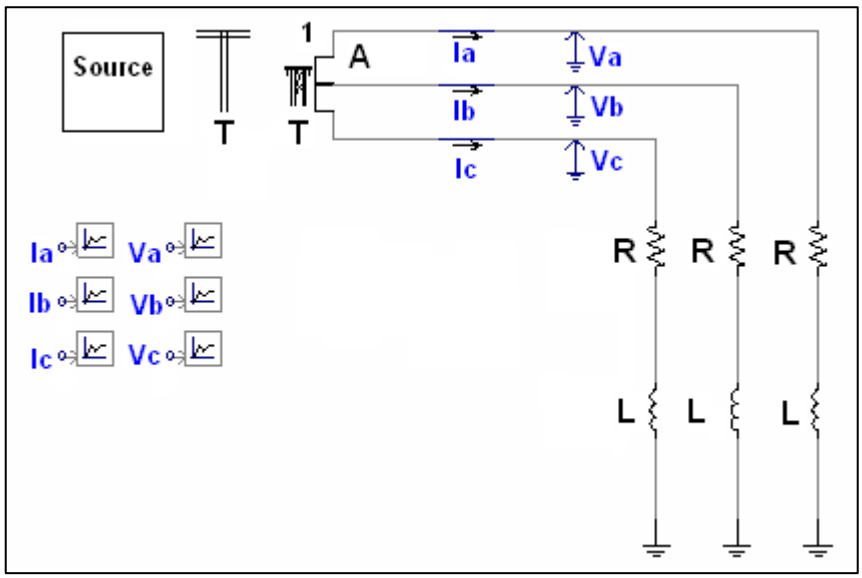

Figure 5.3: Fault Equivalent Circuit Simulated in PSCAD

recorded at point A. The circuit diagram shown in Figure 5.3 shows an inductance L corresponding to a positive reactance X. Appropriate capacitances were calculated for reactance values lying in second quadrant of the relay characteristic. The impedance was modeled as a series combination of a resistance and a capacitance $C = 2\pi X$ in those cases. The current and voltage samples are used to pre-process the inputs in the same manner as the first approach.

5.2.1.3 Training of the Neural Network

Multi-layer feed forward networks (MFNNs) have proven to perform well for pattern classification problems [60]. The detection of faults was identified as a pattern classification problem; therefore a three-layer feed forward neural network was used. The selection of one hidden layer was influenced by the fact that a four-layer network with two hidden layers is difficult to train and is more prone to local minima [61]. Increase in number of hidden layers also increases number of weights and thus the complexity of the network, leading to an increase in the computation time. The choice of number of input, hidden and output nodes (or neurons) was based on specific criteria. The number of hidden layer neurons was always kept equal to 2j+1 where j was the number of input neurons. This criterion always results in an odd number of hidden neurons that has been considered better than even number of neurons in a hidden layer. The ANN was required to give only one output to detect if there is a fault or not, so the number of output neuron(s) was always fixed equal to one.

The change in number of input neurons leads to different configurations of ANNs. The starting number of input neurons was taken as ten and was increased till desired results were obtained by testing the neural network. Some of the ANN configurations that were tested are 10-31-1, 12-25-1, 15-31-1, 16-33-1, 17-35-1 and 18-37-1. The fault and non-fault patterns were given to the ANN and it was trained to give a +1 or -1 output respectively. Tangent Sigmoid neurons were used in all three layers of the ANN; thus the output given by the output neuron was always between +1 and -1 values. The entire training process of the neural network was carried offline prior to testing the relay on a

17–bus power system simulated in PSCAD. The algorithm previously described in Figure 3.5 was followed to design the ANN iteratively. The block diagram for the implementation of the algorithm using the MATLAB approach is also been given in Appendix C.

Another important parameter to be considered is the learning algorithm used for neural network training. Standard back-propagation algorithm has proven to be successful in similar applications; however, it has some disadvantages that have been discussed in Chapter 3. To overcome the inherent problems associated with gradient descent back-propagation algorithms, resilient back-propagation learning algorithm [64] was used. Mean squared error performance function, that measures the mean of squared errors between the desired and the actual output, was used to update the weights of all the layers after each epoch.

Different sizes of the data windows were considered, the smallest being close to one-quarter of a cycle (i.e. six samples). The results obtained by using these sizes were compared and data window of one sample more than half-cycle, that is, a fixed window size of 13 samples was chosen. Each data window comprised of thirteen samples each of $Input_{1\,\mathrm{mod}}$ and $Input_{2\,\mathrm{mod}}$, resulting in a window size of twenty-six samples. The training of the neural network was a combination of batch and incremental training. All the samples of a data window (thirteen each of the two inputs) were given together in a batch. The weights were updated before each data window was given to the neural network, depending on the back-propagated errors between output from previous iteration and the desired output. As the next sample came in, the data window was updated to include the new sample and the new data window was given as a new input. The same procedure was followed till the mean square error stopped reducing by less than 10^{-6} or else the maximum number of epochs (20,000) was reached.

This procedure was followed for all different configurations of ANNs. Since this is an extensive iterative process, discussion of all the results obtained after the training of each configuration is not feasible. After the comparison of the results obtained by each

configuration mentioned previously, the configuration with 18 input neurons, 37 hidden neurons and one output neuron was selected. Figure 5.4 shows a graphical representation of the selected neural network. The MFNN is a fully-connected network where all the input nodes are connected to all the hidden nodes and all hidden nodes are connected to the output node. Since the input data window has a size of twenty-six samples, an ANN configuration of 18-37-1 resulted in 26x18, 18x37 and 37x1 order matrices for input layer, input-hidden layer and hidden-output layer weights respectively.

The next step was to compare the training results from the two training approaches discussed earlier. The sinusoidal inputs' approach were chosen over the fault equivalent circuit approach as this enables offline training without using any power system simulation data, therefore, is a much faster process. The iterations in the training process using a fault equivalent circuit can become a cumbersome process as there might be a need to run new cases every time after training the ANN. The first approach also ensured generality of the neural network as the network in this case had been trained on a

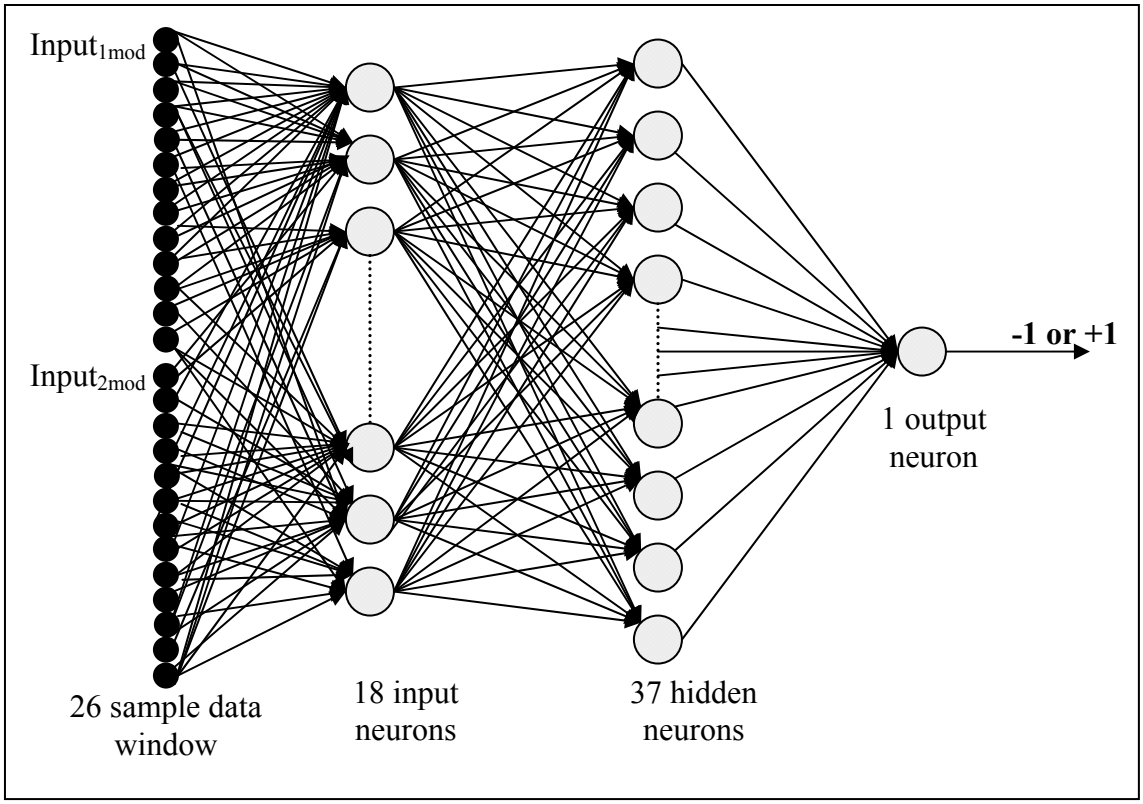

Figure 5.4: Schematic Representation of Proposed 18-37-1 Neural Network

different system and tested on a PSCAD based system. All the other designs that are discussed in subsequent sections use MATLAB generated pure sinusoidal inputs for training the ANN.

Figure 5.5 shows the block diagram of the proposed relay design. It illustrates the integration of preprocessing algorithm with trained ANN. Processing of one data window of thirteen samples is shown. The process can be explained by the following steps at time instant *n*:

1. The voltage measured at relay location was sampled and quantized using an analog sub-system[1] to obtain voltage samples for each phase. Voltage from one phase was used for ground relay. Voltages from two phases were used to calculate line voltage for a phase relay, as required. Thirteen voltage samples were used for one data window. The voltage samples were delayed by 5 samples to account for the impedance reach angle. This resulted in the next data window for $Input_{1\,\mathrm{mod}}$.

2. The current measured at relay location was sampled and quantized using an analog sub-system to obtain current samples for each phase. Zero sequence compensation was applied to current samples for ground relays. Line currents were calculated for phase relays. Each current sample was multiplied by the magnitude of impedance reach (0.5 p.u. in this case).

3. The samples obtained from Step 1 were mathematically subtracted from samples obtained from Step 2. The resulting samples formed the next data window for $Input_{2\,\mathrm{mod}}$.

4. The two 13-sample data windows were combined and given as one 26-sample data window to the trained neural network. The neural network gave a +1 or -1 output indicating a fault or non-fault condition respectively.

[1] Refer to Chapter 2 for details of an analog sub-system.

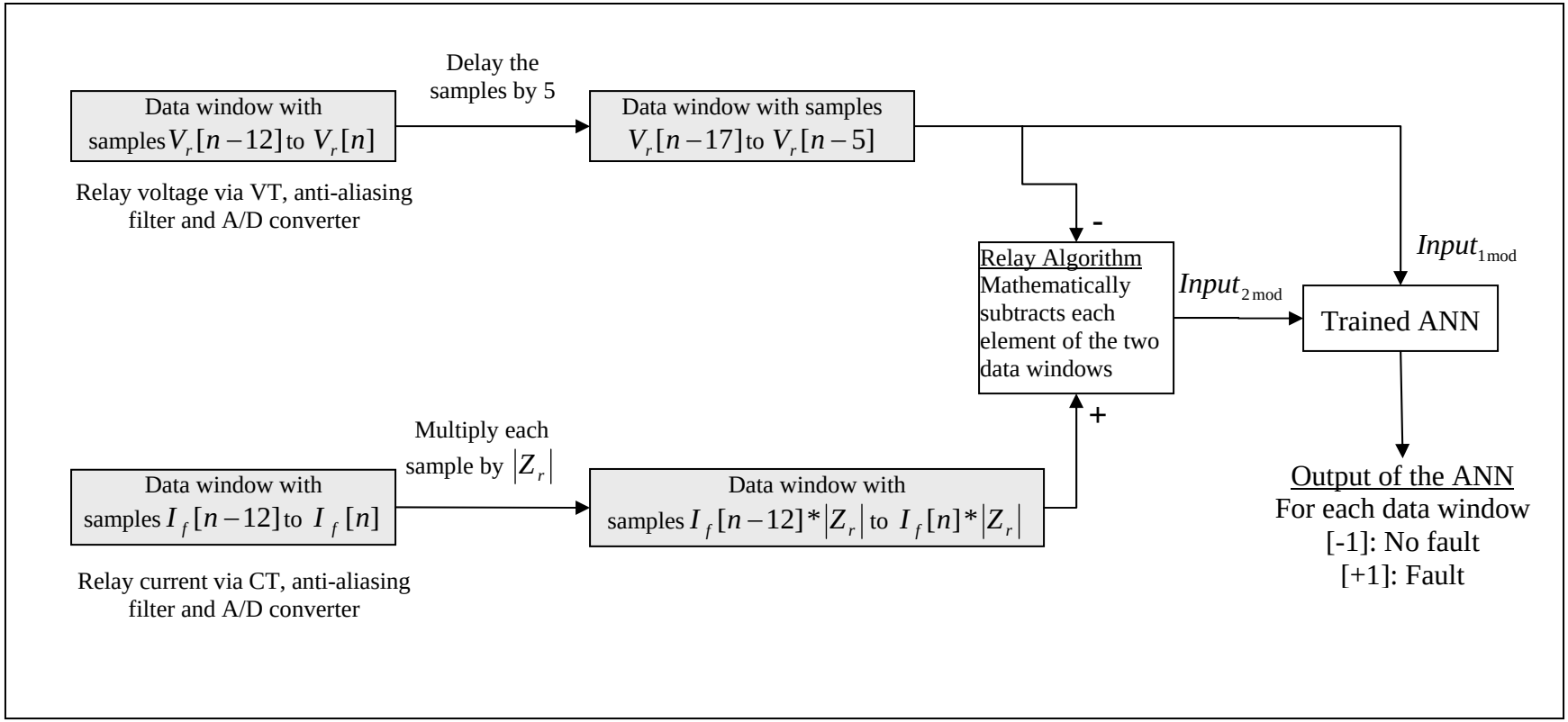

Figure 5.5: Relay Design

5.2.1.4 Discussion: Different Impedance Reach

It may be argued that the relay was trained for a particular impedance reach and ANN training is needed each time the impedance reach is changed. It should be noted that the processing of the inputs has been done in such a way that this relay can be used as a universal relay without any re-training. The impedance reach angle of the relay can be accounted for by interpolation, as mentioned before. The impedance magnitude can be expressed as a percentage (or fraction) of the impedance reach for which the ANN was trained (0.5 p.u. in this case). This is explained by means of an example.

In this project, the ANN has been trained using a transmission line impedance of $0.5\angle 75°$p.u. This reach is equal to 80% impedance of a transmission line. Assume that the same ANN relay has to be implemented for protecting a transmission line with an impedance reach equal to $0.8\angle$ 80° p.u. Without re-training the ANN, adjustments can be made so that the same ANN can be used. This is explained by the following steps.

1. The impedance for which the ANN was trained for $Z_r = 0.5\angle 75°$ p.u. therefore, the relationship between the new impedance reach and Z_r can be established as:

$$|Z_{r1}| = 0.625 * |Z'_{r1}| \text{ and } \theta'_z = 80° \Rightarrow \frac{\theta'_z}{15°} = \frac{16}{3} = 5\frac{1}{3}$$

$$\text{or } |Z_{r1}| = a * |Z'_{r1}| \text{ where a} = 0.625$$

2. As per the proposed algorithm,

$$Input_{1\,\mathrm{mod}}[n] = V_r[n-5]$$

The new modified input can be represented in phasor form as:

$$Input_{1\,\mathrm{mod}} = |V_r|\angle(\theta_v - \theta'_z)$$

In terms of discrete samples, this can be obtained by interpolating the values between voltage samples that have been delayed by 5 and 6 samples.

$$Input_{1\,\mathrm{mod}}[n] = V_r[n-5] + 1/3\left(V_r[n-6] - V_r[n-5]\right)$$

3. The second input can be represented in phasor form for the new impedance reach as:

$$Input_{2\,\mathrm{mod}} = \left|I_f\right\|Z_r^{'}\left|\angle\theta_i - \right|V_r\left|\angle(\theta_v - \theta_z^{'})\right.$$

Multiplying the above equation by the factor a,

$$Input_{2\,\mathrm{mod}} = a * \left|I_f\right\|Z_r^{'}\left|\angle\theta_i - a * \right|V_r\left|\angle(\theta_v - \theta_z^{'})\right.$$

In discrete samples, this equation can be written as

$$Input_{2\,\mathrm{mod}}[n] = I_f[n]\left|Z_r\right| - a * \left(V_r[n-5] + \tfrac{1}{3}\left(V_r[n-6] - V_r[n-5]\right)\right)$$

4. To keep the relationship the same between the two equations, the first input should be multiplied by the factor "*a"* as well. This implies that the first input is equal to:

$$Input_{1\,\mathrm{mod}}[n] = a * \left(V_r[n-5] + \tfrac{1}{3}\left(V_r[n-6] - V_r[n-5]\right)\right)$$

Therefore, for this impedance reach, the two modified inputs will be:

$$Input_{1\,\mathrm{mod}}[n] = a * \left(V_r[n-5] + \tfrac{1}{3}\left(V_r[n-5] + V_r[n-6]\right)\right)$$

$$Input_{2\,\mathrm{mod}}[n] = I_f[n]\left|Z_r\right| - Input_{1\,\mathrm{mod}}[n] \text{ where a = 0.625}$$

The above equations show how the inputs can be modified for any impedance reach value and the same trained ANN can be used for fault detection. Higher sampling rate can be used instead of interpolation as well to account for the angle delay in both inputs. For example, if a sampling angle of 10° (36 samples/cycle) is used instead of 15°, the voltage samples can be delayed by 8 samples instead of $5\,\frac{1}{3}$ samples to avoid retraining.

The next section discusses the extension of the proposed algorithm for other relays. A quadrilateral relay was designed to include a reactance relay characteristic, blinder characteristics and a directional relay characteristic. Conventional phase comparison characteristics of these relays are given in Chapter 2.

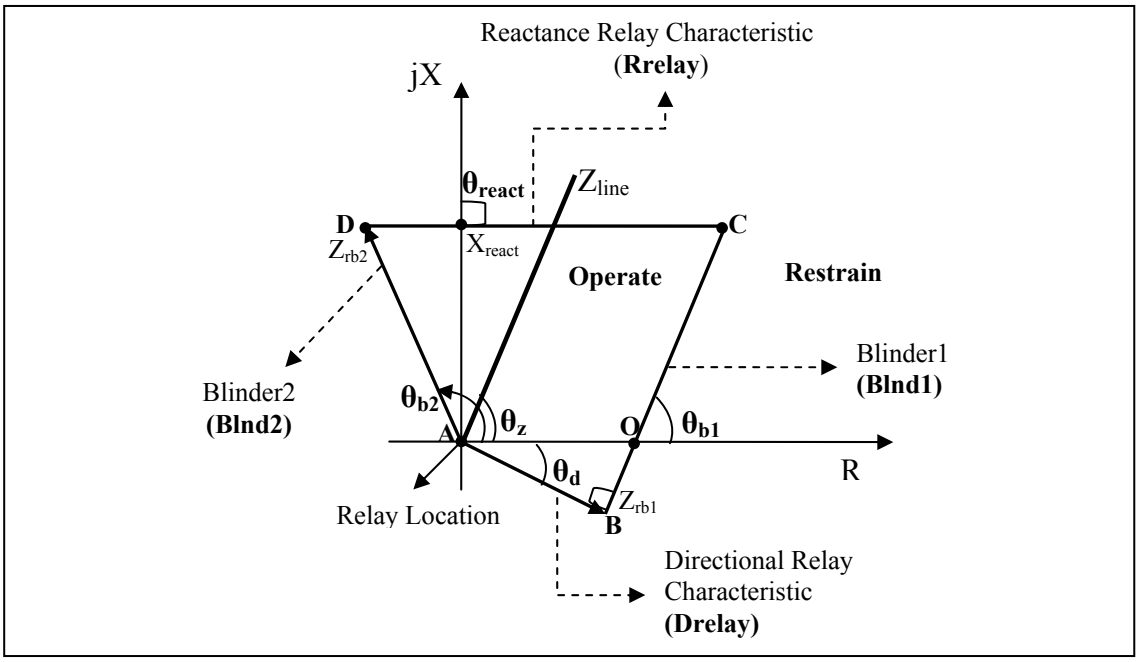

Figure 5.6: Quadrilateral Relay Design

5.2.2 Reactance Relay Design

The reactance relay design is a part of quadrilateral relay design shown in Figure 5.6. A reactance relay possesses a straight line characteristic parallel to the real axis on the impedance plane. The inputs used for fault detection using a reactance relay are dependent only on the reactance values; the reactance characteristics are independent of fault resistance. The impedance reach, therefore, is represented as $\overline{X}_{react}$. For any impedance $\overline{Z}$ inside the boundaries of the relay reach, the angle Φ between $\overline{X}_{react}$ and $\overline{X}_{react} - \overline{Z}$ is between -90º and +90º. Applying the previously discussed phase comparison principle to a reactance relay, the two inputs can be written as:

$$Input_1 = \vec{I}_f \overline{X}_{react} \tag{5.1}$$

$$Input_2 = \vec{I}_f \overline{X}_{react} - \vec{V}_r \tag{5.2}$$

Considering $\left|X_{react}\right|$ as the magnitude of the relay reach and θ_{react} as the reach angle (equal to 90º = $6\theta_s$ in this design), the proposed algorithm can be applied to obtain the processed inputs by adjusting θ_{react} as:

$$Input_{1\,\mathrm{mod}} = I_f \angle \theta_i \left| X_{react} \right| \tag{5.3}$$

$$Input_{2\,\mathrm{mod}} = I_f \angle \theta_i \left| X_{react} \right| - V_r \angle \left(\theta_v - \theta_{react} \right) \tag{5.4}$$

The sampling angle is equal to 15º, therefore, the voltage V_r is delayed by six samples in this case. The modified inputs are represented in the form of discrete samples in equations 5.5 and 5.6. For any nth sample:

$$Input_{1\,\mathrm{mod}}[n] = I_f[n] \left| X_{react} \right| \tag{5.5}$$

$$Input_{2\,\mathrm{mod}}[n] = I_f[n] \left| X_{react} \right| - V_r[n-6] \tag{5.6}$$

According to the above equations, the seventh data window of $Input_{2\,\mathrm{mod}}$ after fault inception uses the first fault sample of V_r.

Quadrilateral relay was designed and tested with a different impedance reach, equal to $0.85\angle 75º$ p.u. By geometry, this results in a value of $0.8210\angle 90º$ p.u. for $\overline{X}_{react}$. Parallel lines were plotted on the reactance relay characteristic to obtain different impedance points. The parallel lines were placed at lateral distance increments of ± 0.01 p.u. from the relay characteristic. Four lines each inside and outside the reach of the relay were chosen, with ten linearly spaced impedance values on each line. The impedance points on the reactance characteristic were considered as patterns belonging to the fault category. This resulted in a total of 80 patterns.

The value of I_f was kept as $1\angle 0°$ p.u and fault and non-fault samples were generated using different values of impedance $\overline{X}_{react}$. Similar to the admittance relay design, a data window of twenty-six samples (thirteen of each input) was given to train an ANN. Training of different ANN configurations was performed and results showed that a 12-25-1 ANN was able to accurately implement the desired reactance characteristic.

5.2.3 Blinders' Design

Blinder possesses another type of straight line characteristics that are versatile and flexible. Two types of blinders were used in this design to limit the quadrilateral characteristics on the right and left side as shown in Figure 5.6.

5.2.3.1 Blinder 1 / Positive Resistance Side (Blnd1)

The right blinder was used in the design to include a desired value of fault resistance and to separate the operating region of relay from system loads. Considering $\overline{Z}_{rb1}$ as the impedance reach of this blinder, for faults lying within the relay reach, the angle Φ between $\overline{Z}_{rb1}$ and $\overline{Z}_{rb1} - \overline{Z}$ lies between -90º and +90º. The phase comparator inputs in this case can be represented in phasor form as:

$$Input_1 = \vec{I}_f \overline{Z}_{rb1} \tag{5.7}$$

$$Input_2 = \vec{I}_f \overline{Z}_{rb1} - \vec{V}_r \tag{5.8}$$

These inputs were modified using the proposed algorithm as:

$$Input_{1\,\mathrm{mod}} = I_f \angle\theta_i \left| Z_{rb1} \right| \tag{5.9}$$

$$Input_{2\,\mathrm{mod}} = I_f \angle\theta_i \left| Z_{rb1} \right| - V_r \angle\left(\theta_v - \theta_{b1}\right) \tag{5.10}$$

The angle θ_{b1} was considered as 75º. Therefore, in terms of discrete samples, the pre-processed inputs for any nth sample can be calculated as:

$$Input_{1\,\mathrm{mod}}[n] = I_f[n] \left| Z_{rb1} \right| \tag{5.11}$$

$$Input_{2\,\mathrm{mod}}[n] = I_f[n] \left| Z_{rb1} \right| - V_r[n-5] \tag{5.12}$$

In the algorithm, the value of fault resistance is a user-defined value and was taken as 0.55 p.u. This is represented by AO in Figure 5.6. By geometry, the value of $\left|Z_{rb1}\right|$ is equal to 0.5321 p.u. Similar to the reactance relay design, parallel lines were plotted at a lateral distance of ± 0.01 p.u. and ten linearly spaced impedance points were taken on these lines. A 12-25-1 neural network was chosen in the final design and a total of 80 patterns were used to train the ANN.

5.2.3.2 Blinder 2 / Negative Resistance Side (Blnd2)

Considering $\overline{Z}_{rb2}$ as the impedance reach of the left blinder, for all the faults lying within the reach, the angle Φ between $\overline{Z}_{rb2}$ and $\overline{Z}_{rb2} - \overline{Z}$ lies between -90º and +90º. Therefore, the two inputs for phase comparison in this case can be represented in phasor form as:

$$Input_1 = \vec{I}_f \overline{Z}_{rb2} \tag{5.13}$$

$$Input_2 = \vec{I}_f \overline{Z}_{rb2} - \vec{V}_r \tag{5.14}$$

These inputs can be modified by using the proposed algorithm as:

$$Input_{1\,\mathrm{mod}} = I_f \angle \theta_i \left| Z_{rb2} \right| \tag{5.15}$$

$$Input_{2\,\mathrm{mod}} = I_f \angle \theta_i \left| Z_{rb2} \right| - V_r \angle \left(\theta_v - \theta_{b2} \right) \tag{5.16}$$

The terms $\left|Z_{rb2}\right|$ and θ_{b2} are impedance reach magnitude and angle respectively, as shown on the relay characteristic in Figure 5.4. A reach angle of 105º was chosen for this characteristic. Therefore, the processed inputs can be represented for an n^{th} sample as:

$$Input_{1\,\mathrm{mod}}[n] = I_f[n] \left| Z_{rb2} \right| \tag{5.17}$$

$$Input_{2\,\mathrm{mod}}[n] = I_f[n] \left| Z_{rb2} \right| - V_r[n-7] \tag{5.18}$$

Considering the reactance relay reach as 0.8210 p.u. and θ_{b2} as 105º, the value of $\left|Z_{rb2}\right|$ was calculated as 0.85 p.u. Parallel lines were plotted at a lateral distance of ± 0.01 p.u. to obtain impedance points, as in the case of previous designs. Linearly spaced impedance points were taken on these lines, resulting in thirty patterns inside the relay reach, ten patterns on the relay characteristics and forty non- fault patterns. A pattern corresponding to impedance on blinder characteristic was considered as a fault pattern. A 12-25-1 neural network was chosen for implementing the blinder characteristic. The patterns were given in a combination of batch and incremental training and resilient back-propagation was used to train the network like previous designs.

5.2.4 Directional Relay Design

Directional relays compare the currents and voltages of a transmission line and deliver a trip signal depending on phase angle between the two inputs. This phase comparison technique was used to design the directional feature of quadrilateral relay characteristic. This enables the relay to differentiate between the reverse and forward faults on the transmission line.

In Figure 5.6, AB represents the directional characteristics of the relay. As known previously, the value of $\overline{Z}_r$ is $0.85\angle 75^\circ$ p.u. The value of θ_d was considered as 15º in this design. It can be seen in the characteristic that for all forward faults on the line, the angle between $\overline{Z}_r$ and $\overline{Z}$ lies between -90º and +90º. The two inputs of a directional phase comparator can therefore be represented in the form of phasors as:

$$Input_1 = \vec{I}_f \overline{Z}_r \tag{5.19}$$

$$Input_2 = \vec{V}_r \tag{5.20}$$

The inputs were modified using the proposed algorithm by subtracting the phase angle θ_z from both the equations.

$$Input_{1\,\mathrm{mod}} = I_f \angle \theta_i \left| Z_r \right| \tag{5.21}$$

$$Input_{2\,\mathrm{mod}} = V_r \angle \left(\theta_v - \theta_z \right) \tag{5.22}$$

$Input_{1\,\mathrm{mod}}$ is scalar multiplication of current samples and impedance reach; $Input_{2\,\mathrm{mod}}$ was obtained by delaying voltage $\vec{V}_r$ by θ_z. Equations 5.23 and 5.24 show the processed inputs in discrete form for any nth sample. The voltage was delayed by five samples as θ_z is five times θ_s.

$$Input_{1\,\mathrm{mod}}[n] = I_f[n] \left| Z_r \right| \tag{5.23}$$

$$Input_{2\,\mathrm{mod}}[n] = V_r[n-5] \tag{5.24}$$

Inputs were obtained corresponding to impedance points on seven parallel lines at a lateral distance of ± 0.01 p.u. with respect to the directional relay characteristic. Linearly spaced impedance points on these lines represented eighty different input patterns. The patterns were given in a combination of batch and incremental training and resilient back-propagation was used to train the network, as done in all previous designs.

The input data window size was kept the same for all the designs including blinders, equal to thirteen samples each of both the inputs. This resulted in weight matrices of the order of 26x12, 12x25 and 25x1.

5.2.5 Quadrilateral Relay Design

The four characteristics were combined to obtain the desired quadrilateral relay design. Figure 5.7 shows the block diagram of this process. The four neural networks were trained offline as described in the preceding sections. Some of the values used in this design were user-designed values that can be varied when the program is run. Other required values were calculated. The calculations of the fixed and variable values in this design are given in Appendix B.

In Figure 5.7, four sub-systems are shown. Each of the sub-system shown comprises of the following:

(a) Data Generation: Training the ANN using sinusoidal inputs from MATLAB
(b) Input Pre-processing: Implementation of reactance, directional and blinder phase comparators
(c) Neural Network Training Algorithm

The weights and other parameters of the system were fixed after training and then tested on a 17-bus power system simulated in PSCAD for different fault resistances. The results of the testing the relay using this system are presented in the next chapter.

The outputs from these sub-systems were used as inputs to an AND logic gate. This logic gate can be a simple logic gate implemented in MATLAB or in the form of a simple neural network (with a 4-1 configuration) which represents the same principle. An AND logic gate requires inputs between [0, 1] range whereas the outputs of the four ANNs are in [-1, 1] range because of tan-sigmoid output neurons. All the negative outputs, therefore, need to be converted to a value of zero for an AND gate to see them as non-fault values. The neural network, on the other hand, takes inputs within [-1, 1] range and gives an output belonging to the same range. Since it is a simple ANN, the computation time is very small. Both these approaches were tested and it was observed that both performed well. The ANN approach was selected. The patterns used for training the AND neural network are given in Appendix B.

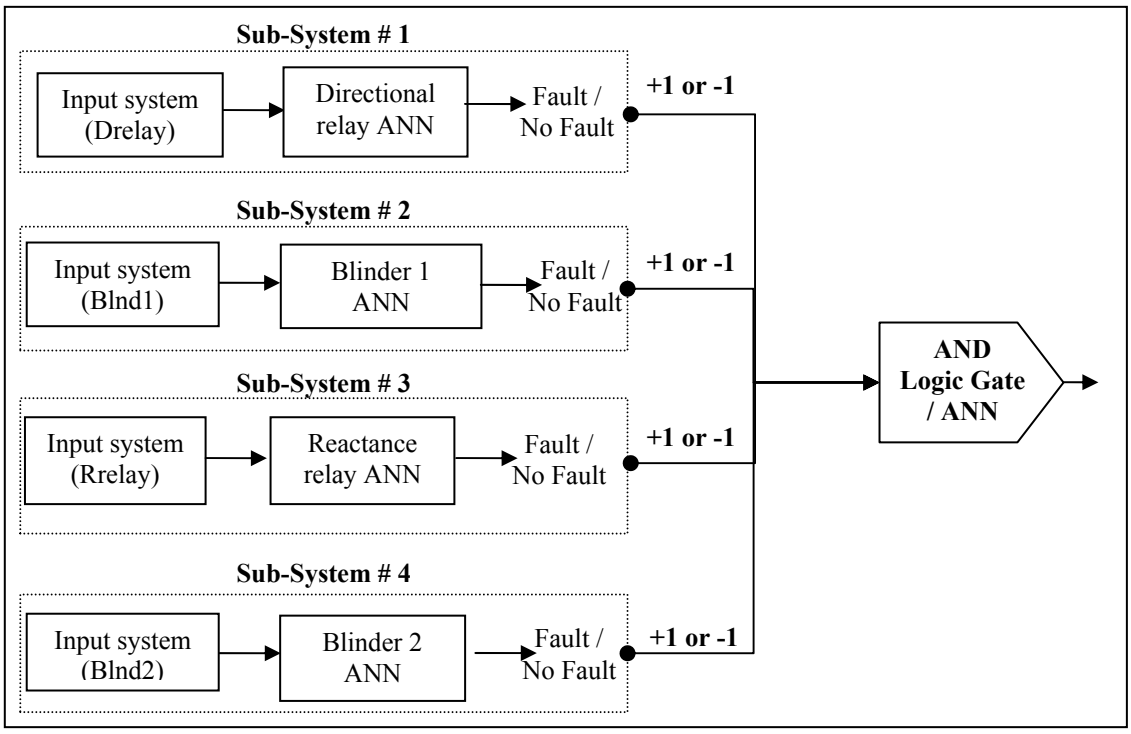

Figure 5.7: Block Diagram for the Implementation of a Quadrilateral Relay

5.3 Design for Different Faults

As discussed in Chapter 3, there are two main approaches for fault detection. The first method is based on the type of phase. It uses three or four different relays, one for each phase (A, B and C) and one for ground in some cases. The second approach is based on the type of fault. This approach is used the most, practically. It uses seven different elements, three for single line to ground faults, three for two phase faults and one for a three phase fault. The proposed technique uses the second approach based on the type of fault. The input processing for different types of faults was varied. These inputs are listed in Sections 5.3.1 and 5.3.2 depending on the values of the impedance reach chosen in the relay designs.

5.3.1 Single Phase Faults

The processed inputs for phase A to ground faults for different relay designs are shown in Table 5.1. The current I_a is the Phase-A fault current and V_a is the phase voltage

measured between phase A and ground. The inputs for other phases were obtained in a similar way. Zero sequence compensation was added to the phase current for single line to ground faults. The phase angle of zero sequence compensation current I_{comp}, is not a multiple of the sampling angle, 15°. The phase angle of the I_{comp} was adjusted by interpolation technique as described in previous sections.

Table 5.1: Processed Inputs for Single line to ground faults

Relay Characteristics'	Impedance Reach Angle	$Input_{1\,\mathrm{mod}}[n]$	$Input_{2\,\mathrm{mod}}[n]$
Admittance	75º	$V_a[n-5]$	$\left(I_a[n]+I_{comp}[n]\right)\lvert Z_r\rvert - V_a[n-5]$
Reactance	90º	$\left(I_a[n]+I_{comp}[n]\right)\lvert X_{react}\rvert$	$\left(I_a[n]+I_{comp}[n]\right)\lvert X_{react}\rvert - V_a[n-6]$
Blinder 1	75º	$\left(I_a[n]+I_{comp}[n]\right)\lvert Z_{rb1}\rvert$	$\left(I_a[n]+I_{comp}[n]\right)\lvert Z_{rb1}\rvert - V_a[n-5]$
Blinder 2	105º	$\left(I_a[n]+I_{comp}[n]\right)\lvert Z_{rb2}\rvert$	$\left(I_a[n]+I_{comp}[n]\right)\lvert Z_{rb2}\rvert - V_a[n-7]$
Directional	75º	$\left(I_a[n]+I_{comp}[n]\right)\lvert Z_r\rvert$	$V_a[n-5]$

Table 5.2: Processed Inputs for faults on two or more phases

Relay Characteristics'	$Input_{1\,\mathrm{mod}}$	$Input_{2\,\mathrm{mod}}$
Admittance	$V_a[n-5]-V_b[n-5]$	$(I_a[n]-I_b[n])\lvert Z_r\rvert - (V_a[n-5]-V_b[n-5])$
Reactance	$(I_a[n]-I_b[n])\lvert X_{react}\rvert$	$(I_a[n]-I_b[n])\lvert X_{react}\rvert - (V_a[n-6]-V_b[n-6])$
Blinder 1	$(I_a[n]-I_b[n])\lvert Z_{rb1}\rvert$	$(I_a[n]-I_b[n])\lvert Z_{rb1}\rvert - (V_a[n-5]-V_b[n-5])$
Blinder 2	$(I_a[n]-I_b[n])\lvert Z_{rb2}\rvert$	$(I_a[n]-I_b[n])\lvert Z_{rb2}\rvert - (V_a[n-7]-V_b[n-7])$
Directional	$(I_a[n]-I_b[n])\lvert Z_r\rvert$	$V_a[n-5]-V_b[n-5]$

5.3.2 Two and Three Phase Faults

Table 5.2 shows the processed inputs for faults on two or more phases using the proposed design. The impedance reach in each case remains the same. The inputs are shown for a two phase fault between A and B phases. For a three phase fault relay, any combination of the phases can be used; all the two phase relays will see a fault in case of a three phase fault.

5.4 Polarization Techniques

For faults on or very close to relay location, the voltage drops to a very low value. Polarization is employed to increase the voltage to an acceptable level so that close-in faults can be detected. The different types of polarization techniques are discussed in Chapter 2. This section presents the polarization techniques that were used along with the proposed design for improving the performance of the proposed relay for close-in faults.

Each polarization technique has some demerits. The design, therefore, proposes a technique to combine more than one polarization techniques. The aim was to eliminate the limitations by combining user-specified percentages of different polarizations. The type of polarization used was changed for different faults. Sections 5.4.1 to 5.4.2 discuss the polarization techniques that were applied to the designed admittance relay. Polarization for other relays can be applied in a similar way.

5.4.1 Single Line to Ground Faults

The algorithm combines three types of polarizations for single line to ground fault in addition to self polarizing input of a mho relay. These three options are listed below. The algorithm uses user-defined weights for different types of polarizations. The relay was tested with these options and results are presented in Chapter 6.

a. Self Polarization: An admittance relay is a self-polarized relay. The algorithm has the option to include or eliminate the standard inputs in the design. When included in the design, the three polarization inputs for the three phases are given in Table 5.3.

Table 5.3: Self Polarizing Inputs for Single Line to Ground Faults

Type of Fault	Self Polarizing Input ($Input_{1\,\mathrm{mod}}[n]$)	Operating Input ($Input_{2\,\mathrm{mod}}[n]$)
A-G	$V_a[n-5]$	$I_a[n]\lvert Z_r\rvert - V_a[n-5]$
B-G	$V_b[n-5]$	$I_b[n]\lvert Z_r\rvert - V_b[n-5]$
C-G	$V_c[n-5]$	$I_c[n]\lvert Z_r\rvert - V_c[n-5]$

b. Cross Polarization: The line voltage between the other two healthy phases was used as the cross-polarizing input. Table 5.4 list the cross- polarizing inputs for single line to ground faults using the proposed algorithm. Since phase angle difference between line voltage V_{bc} and voltage V_a is equal to 90º, it was adjusted by delaying the input by six (6) samples. Addition of five (5) samples due to the proposed algorithm resulted in a total delay of eleven (11) samples for the cross polarizing voltage.

   Cross-polarization is always implemented using a factor or a multiplier to ensure that impedance reach of a relay characteristic remains within the desired boundaries. Factors between 0.1 and 0.2 are typically used [38]. In this algorithm, the percentage of cross-polarization was user-defined and the tests were conducted by varying the cross-polarizing input for two levels, 10% and 20% i.e. a factor of 0.1 and 0.2 respectively.

c. Memory Polarization: The algorithm has the ability to use voltage inputs saved in the relay memory before the inception of fault. A factor of 0.75 and 1.0 was tested for memory polarization. Another aspect that was considered for applying this polarization was the amount of memory (number of prior cycles). The selected number of cycles should be enough so that the fault is cleared before the expiration of the memory samples. On the other hand, the number of cycles should not be too large as it may lead to unavailability of fault data, especially in cases such as fault occurrence at the instant of circuit breaker closing. These numbers of cycles were kept user-defined in the program; however, all the tests were conducted using a

memory polarization of two (2) cycles. This implied delaying the voltage samples by another forty-eight (48) samples. These inputs are shown in Table 5.5.

Table 5.4: Cross Polarizing Inputs for Single Line to Ground Faults

Type of Fault	Cross Polarizing Input ($Input_{1\,\mathrm{mod}}[n]$)	Operating Input ($Input_{2\,\mathrm{mod}}[n]$)
A-G	$jV_{bc}[n-5] = V_{bc}[n-11]$	$I_a[n]\lvert Z_r\rvert - V_a[n-5]$
B-G	$jV_{ca}[n-5] = V_{ca}[n-11]$	$I_b[n]\lvert Z_r\rvert - V_b[n-5]$
C-G	$jV_{ab}[n-5] = V_{ab}[n-11]$	$I_c[n]\lvert Z_r\rvert - V_c[n-5]$

Table 5.5: Memory Polarizing Inputs for Single Line to Ground Faults

Type of Fault	Memory Polarizing Input ($Input_{1\,\mathrm{mod}}[n]$)	Operating Input ($Input_{2\,\mathrm{mod}}[n]$)
A-G	$V_{amem} = V_a[n-53]$	$I_a[n]\lvert Z_r\rvert - V_a[n-5]$
B-G	$V_{bmem} = V_b[n-53]$	$I_b[n]\lvert Z_r\rvert - V_b[n-5]$
C-G	$V_{cmem} = V_c[n-53]$	$I_c[n]\lvert Z_r\rvert - V_c[n-5]$

d. Positive Sequence Memory Polarization: Positive sequence memory polarization has been considered reliable for cases of zero or low voltage faults [65]. Positive sequence voltages during faults can be calculated by analysis of a power system by using symmetrical components. Appendix E shows the analysis to determine the positive sequence voltage during single line to ground faults. Table 5.6 shows the positive sequence memory polarization voltages used for single line to ground faults. Two (2) cycles of memory were used in this case as well.

5.4.2 Two and Three Phase Faults

a. Self Polarization: Self polarizing inputs for faults on two or more phases use line voltages and currents as listed in Table 5.7. Before applying these inputs to the ANN,

these were scaled down to the same level as phase values using a factor of $1/\sqrt{3}$ or 0.5774.

Table 5.6: Positive Sequence Memory Polarizing Inputs for Line to Ground Faults

Type of Fault	Positive Sequence Memory Polarizing Input ($Input_{1\,\mathrm{mod}}[n]$)	Operating Input ($Input_{2\,\mathrm{mod}}[n]$)
A-G	$V_{a1mem} = V_{a1}[n-53]$	$I_a[n]\lvert Z_r\rvert - V_a[n-5]$
B-G	$V_{b1mem} = V_{b1}[n-53]$	$I_b[n]\lvert Z_r\rvert - V_b[n-5]$
C-G	$V_{c1mem} = V_{c1}[n-53]$	$I_c[n]\lvert Z_r\rvert - V_c[n-5]$

Table 5.7: Self Polarizing Inputs for Two and Three Phase Faults

Type of Fault	Self Polarizing Input ($Input_{1\,\mathrm{mod}}[n]$)	Operating Input ($Input_{2\,\mathrm{mod}}[n]$)
A-B, AB-G and ABC-G	$V_{ab}[n-5]$	$I_{ab}[n]\lvert Z_r\rvert - V_{ab}[n-5]$
B-C, BC-G and ABC-G	$V_{bc}[n-5]$	$I_{bc}[n]\lvert Z_r\rvert - V_{bc}[n-5]$
C-A, CA-G and ABC-G	$V_{ca}[n-5]$	$I_{ca}[n]\lvert Z_r\rvert - V_{ca}[n-5]$

b. Cross Polarization: The cross polarization inputs for faults on two phases are given in Table 5.8. The samples of the polarizing voltage were adjusted to bring them in phase with the reference voltage. A percentage of voltage was used, as in previous cases. The polarizing voltage $-jV_c$ (for an AB or AB-G fault) was delayed by five samples and advanced by six (6) samples, resulting in an adjustment of one sample. One sample is equivalent to a time lag of 0.694 ms. This delay was eliminated by using memory cross–polarizing voltages. Moreover, cross-polarization cannot be applied for three phase faults as there are no healthy phases during a three-phase fault. Only memory cross-polarizing voltages were therefore used. This is discussed in the next section.

Table 5.8: Cross Polarizing Inputs for Two and Three Phase Faults

Type of Fault	Cross Polarizing Input ($Input_{1\,\mathrm{mod}}[n]$)	Operating Input ($Input_{2\,\mathrm{mod}}[n]$)
A-B and AB-G	$-jV_c[n-5] = V_c[n+1]$	$I_{ab}[n]\lvert Z_r\rvert - V_{ab}[n-5]$
B-C and BC-G	$-jV_a[n-5] = V_a[n+1]$	$I_{bc}[n]\lvert Z_r\rvert - V_{bc}[n-5]$
C-A and CA-G	$-jV_b[n-5] = V_b[n+1]$	$I_{ca}[n]\lvert Z_r\rvert - V_{ca}[n-5]$

c. Memory Polarization: Two types of memory polarization were considered for faults on two or more phases. The first type is using self- polarization voltages. Table 5.9 gives the memory self-polarization voltages for two phase and three phase faults using a memory of two (2) cycles.

Table 5.10 gives the memory cross-polarizing voltages for faults on two or three phases. This is one of the most reliable polarizations for phase to phase and three phase low voltage faults. It can be noted that cross voltage was delayed by forty - seven (47) samples to account for three parameters - delay of five samples as proposed in the algorithm, advancement of six samples to adjust the phase of polarizing voltage and delay of forty eight samples for memory of two cycles.

Table 5.9: Memory Self Polarizing Inputs for Two and Three Phase Faults

Type of Fault	Memory Self Polarizing Input ($Input_{1\,\mathrm{mod}}[n]$)	Operating Input ($Input_{2\,\mathrm{mod}}[n]$)
A-B, AB-G and ABC-G	$V_{abmem} = V_{ab}[n-53]$	$I_{ab}[n]\lvert Z_r\rvert - V_{ab}[n-5]$
B-C, BC-G and ABC-G	$V_{bcmem} = V_{bc}[n-53]$	$I_{bc}[n]\lvert Z_r\rvert - V_{bc}[n-5]$
C-A, CA-G and ABC-G	$V_{camem} = V_{ca}[n-53]$	$I_{ca}[n]\lvert Z_r\rvert - V_{ca}[n-5]$

Table 5.10: Memory Cross Polarizing Inputs for Two and Three Phase Faults

Type of Fault	Memory Cross Polarizing Input ($Input_{1\,\mathrm{mod}}[n]$)	Operating Input ($Input_{2\,\mathrm{mod}}[n]$)
A-B, AB-G and ABC-G	$-jV_{cmem}[n-5] = V_c[n-47]$	$I_{ab}[n]\lvert Z_r\rvert - V_{ab}[n-5]$
B-C, BC-G and ABC-G	$-jV_{amem}[n-5] = V_a[n-47]$	$I_{bc}[n]\lvert Z_r\rvert - V_{bc}[n-5]$
C-A, CA-G and ABC-G	$-jV_{bmem}[n-5] = V_b[n-47]$	$I_{ca}[n]\lvert Z_r\rvert - V_{ca}[n-5]$

d. Positive Sequence Memory Polarization: Positive Sequence Memory Polarization using cross polarizing voltages has the maximum expansion (back to the source) for resistive coverage in the case of low voltage two and three phase faults [65]. The calculation for positive sequence voltage during two and three phase faults is shown in Appendix E. These inputs are shown in Table 5.11

Table 5.11: Positive Sequence Memory Polarizing for Two and Three Phase Faults

Type of Fault	Positive Sequence Memory Polarizing Input ($Input_{1\,\mathrm{mod}}[n]$)	Operating Input ($Input_{2\,\mathrm{mod}}[n]$)
A-B, AB-G and ABC-G	$-jV_{c1mem}[n-5] = V_{c1}[n-47]$	$I_{ab}[n]\lvert Z_r\rvert - V_{ab}[n-5]$
B-C, BC-G and ABC-G	$-jV_{a1mem}[n-5] = V_{a1}[n-47]$	$I_{bc}[n]\lvert Z_r\rvert - V_{bc}[n-5]$
C-A, CA-G and ABC-G	$-jV_{b1mem}[n-5] = V_{b1}[n-47]$	$I_{ca}[n]\lvert Z_r\rvert - V_{ca}[n-5]$

5.5 Noise Effect on the Performance of the ANN

The relays always work along with other electronic equipment in a power system. These components may introduce noise (known as white noise) in the relay inputs. If the strength of the noise present in the system is substantially high, it can lead to inaccuracies in the inputs, thus leading to mis–operation of relays. The algorithm was tested by adding a white Gaussian noise to the pre-processed inputs. The aim of this test was to calculate fault detection error using the proposed algorithm for different levels of noise. Three different signal-to-noise (SNR) ratios of 30 dB, 20 dB and 10 dB white Gaussian

noise were used. Some of the processed waveforms produced by using these SNRs are shown in Appendix F.

The results and error percentages obtained without any input filtering are listed in Table 5.12. The outer diameter d_{outer} is the diameter of the concentric circle (value in per–unit) when the ANN started performing correctly. Similarly, the inner diameter d_{inner} is the inner circle diameter when the ANN started detecting the fault inside the relay boundaries. The difference between these values gave the value of band around the relay characteristics where the ANN was not able to perform well without any filter. The error percentage is calculated by dividing this value by the diameter of relay characteristics. It is worth mentioning that a 10 dB SNR ratio implies that the noise is equal to 10% value of signal. It should be noted that the ANN performs accurately (with an error percentage of less than 0.1%) when the noise is filtered out from the inputs.

Table 5.12: Performance of ANN for Noisy Signals

Signal to Noise Ratio (in dB)	Inner Diameter (d_{inner}) in p.u.	Outer Diameter (d_{outer}) in p.u.	Inner Band Error $\left(\frac{0.5 - d_{inner}}{0.5 p.u.}\right) * 100$	Outer Band Error $\left(\frac{d_{outer} - 0.5}{0.5 p.u.}\right) * 100$	Total Error
30.0	0.4840	0.5180	3.20%	3.60%	6.80%
20.0	0.4720	0.5220	5.60%	4.40%	10.0%
10.0	0.4200	0.5500	16.0%	10.0%	26.0%

5.6 Summary

This chapter discusses the implementation of the proposed algorithm using neural networks. Two different approaches for training the ANN are presented and design of the chosen neural network is discussed. The proposed algorithm was extended for designing different relays; mathematical modifications involved in this process are

presented. The polarization techniques used for detecting close-in faults are discussed. This chapter also discusses the influence of noise on relaying inputs.

The designed ANNs were tested for admittance and quadrilateral relay characteristics by applying different faults at various locations on a transmission line. The polarization techniques presented in this chapter were used to improve the reliability of the relay for faults close to relay location. The results obtained from all these tests are presented in the next chapter.

6. RESULTS

6.1 Introduction

Implementation of the proposed algorithm for designing different relays is presented in Chapter 5. Different polarization techniques for detecting faults close-in faults are discussed in that chapter. ANN based relays were trained in MATLAB and tested on a 17-bus power system simulated in PSCAD. Results from these tests are presented in this chapter. A comparative analysis of these results with a conventional full-cycle DFT algorithm is presented as well. This chapter also presents results for faults close to the origin in an impedance plane.

6.2 The PSCAD/EMTDC Test System

The neural network was trained to differentiate between fault and non-fault patterns using sinusoidal inputs generated in MATLAB. It was important to test the designed relays on a system different than the one they were trained on. The generalization capability of the designed relays was, therefore, tested using a 17-bus power system simulated in PSCAD/EMTDC™.

6.2.1 Test System

The system model is shown in Figure 6.1. This power system was originally modeled by the Power System Protection Group at the University of Saskatchewan. The parameters of different equipment are given in Appendix D. The impedance of the transmission line L_5 was set as to $0.625\angle 75°$ p.u. This impedance was changed for quadrilateral relay tests to $0.85\angle 75°$. The calculated transmission line parameters for both types of relays are shown in Appendix D. The relays were tested by applying single line to ground, phase to phase, double line to ground and three phase faults at different locations of the line L_5. The relay was tested for the following conditions:

™ Trademark of Manitoba Hydro HVDC Research Center

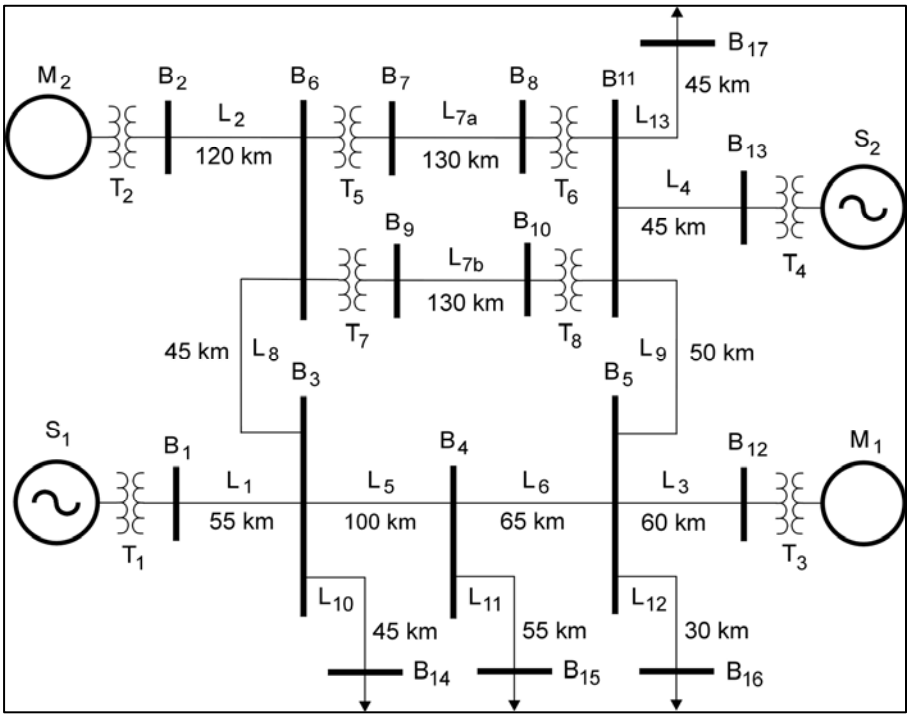

Figure 6.1: Seventeen – bus Power System Simulated in PSCAD

(a) Fault Location: The fault locations were considered at every 5% of the line length for single line to ground faults. The length of the line L_5 is 100 km, therefore, single line to ground faults were applied at every 5 km. The ANN was tested more thoroughly for faults located close to the relay boundary (i.e. 80% length of L_5) by applying faults at every 2-2.5% of the line. This also helped in testing the capability of relay for remote faults. For two and three phase faults, the relay was tested at different fault locations for both close-in and remote faults; the fault locations were kept 5% line length apart for faults close to relay boundaries. The relay was tested for one mid-line fault location for two and three phase faults.

(b) Fault Inception time: In practice, a fault can occur at any time and a reliable protective relay should work well for different fault inception instants. The trained ANN was tested for two fault inception angles, 0º and 90º respectively.

(c) Fault resistance: A relay should be able to perform correctly in cases when fault resistance is present. Both admittance and quadrilateral relay were tested in the presence of fault resistance. It was further evaluated if the apparent impedance in the presence of

fault resistance lies inside the relay protection zone. The test results obtained from these cases are presented in Section 6.3.

6.2.1 Application of Faults using PSCAD

Figure 6.2 shows a block diagram describing ANN relay testing by integrating the PSCAD/EMTDC test system with the neural network trained in MATLAB. Following are the details of various components that were incorporated in this relay design:

(a) Fault Application: Different types of faults were applied at different locations on the transmission line L_5. The procedure of fault application in PSCAD is shown in Figure 6.3. The transmission line L_5 was divided into two parts and the faults were applied by choosing appropriate length for each of these portions. The case shown in Figure 6.3 is for an A-G fault at 5% of line length. Fifteen (15) cycles of currents and voltages were recorded for relay testing. The first five cycles of data were pre-fault currents and voltages. The fault was applied in the sixth cycle; fault instant was dependent on the inception angle used for that particular case. Fault was removed at the end of tenth cycle, resulting in five cycles of post-fault data. The currents and voltages were passed through a low-pass filter to prevent anti-aliasing.

(b) A/D Conversion: The currents and voltages then were sampled and quantized in EMTDC program using a calculation time-step of 46.296μs. It is recommended to use a calculation step of equal or less than 50 μs considering the transmission line traveling wave time. The choice of selected time step is attributed to the fact that this time interval was divisible by the original sampling time. The samples equivalent to a sampling time of 694.44 μs ($= 1/1440Hz$) that was used to train the ANN were obtained by picking up every 15^{th} sample (as 46.296 μs times 15 = 694.44μs). The data samples were then exported to MATLAB.

(c) Pre-processing of Inputs and Testing: The current and voltage samples were processed as per the proposed algorithm. Each fault data window consists of thirteen

(13) samples each of the processed inputs, resulting in a data window size of twenty-six (26) samples. The sample number at which a fault was detected by the neural network was noted. The time taken by the ANN to detect a fault was calculated as:

$$Time_{fault} = (SampleNumber * 0.6944)ms \tag{6.1}$$

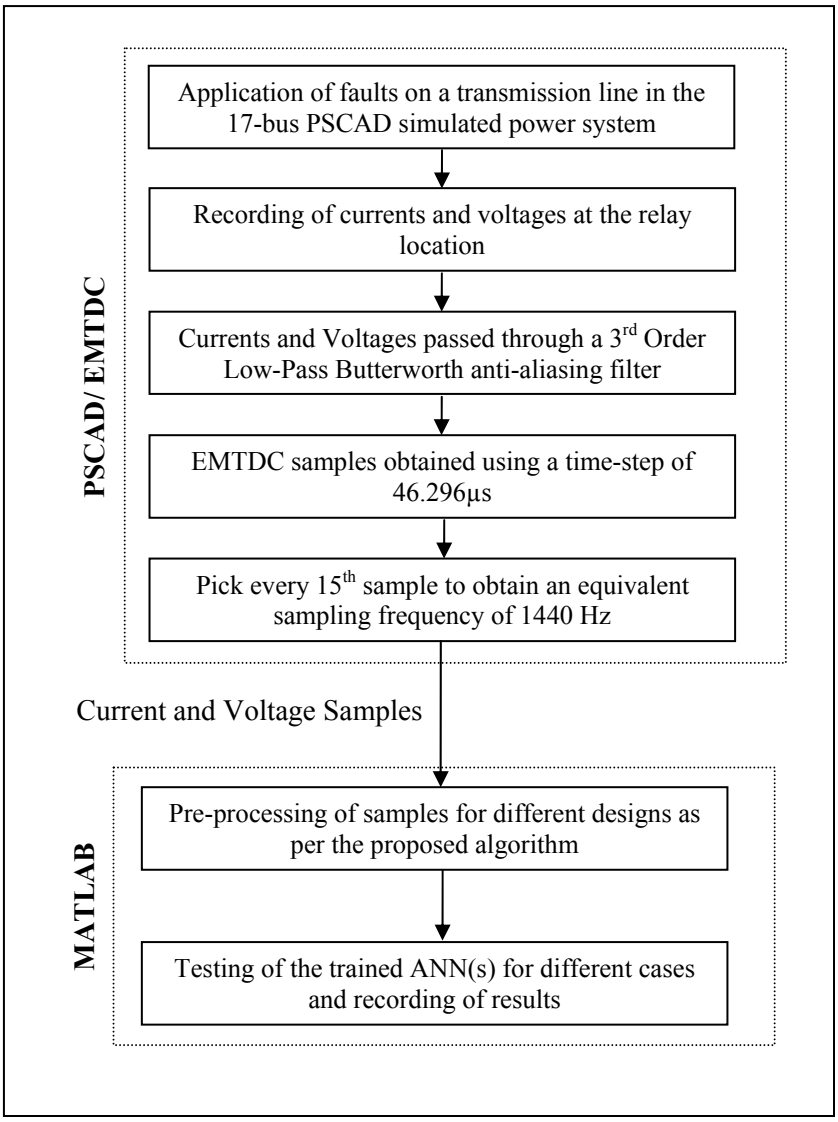

Figure 6.2: Testing of Neural Network Relay on a PSCAD/EMTDC System

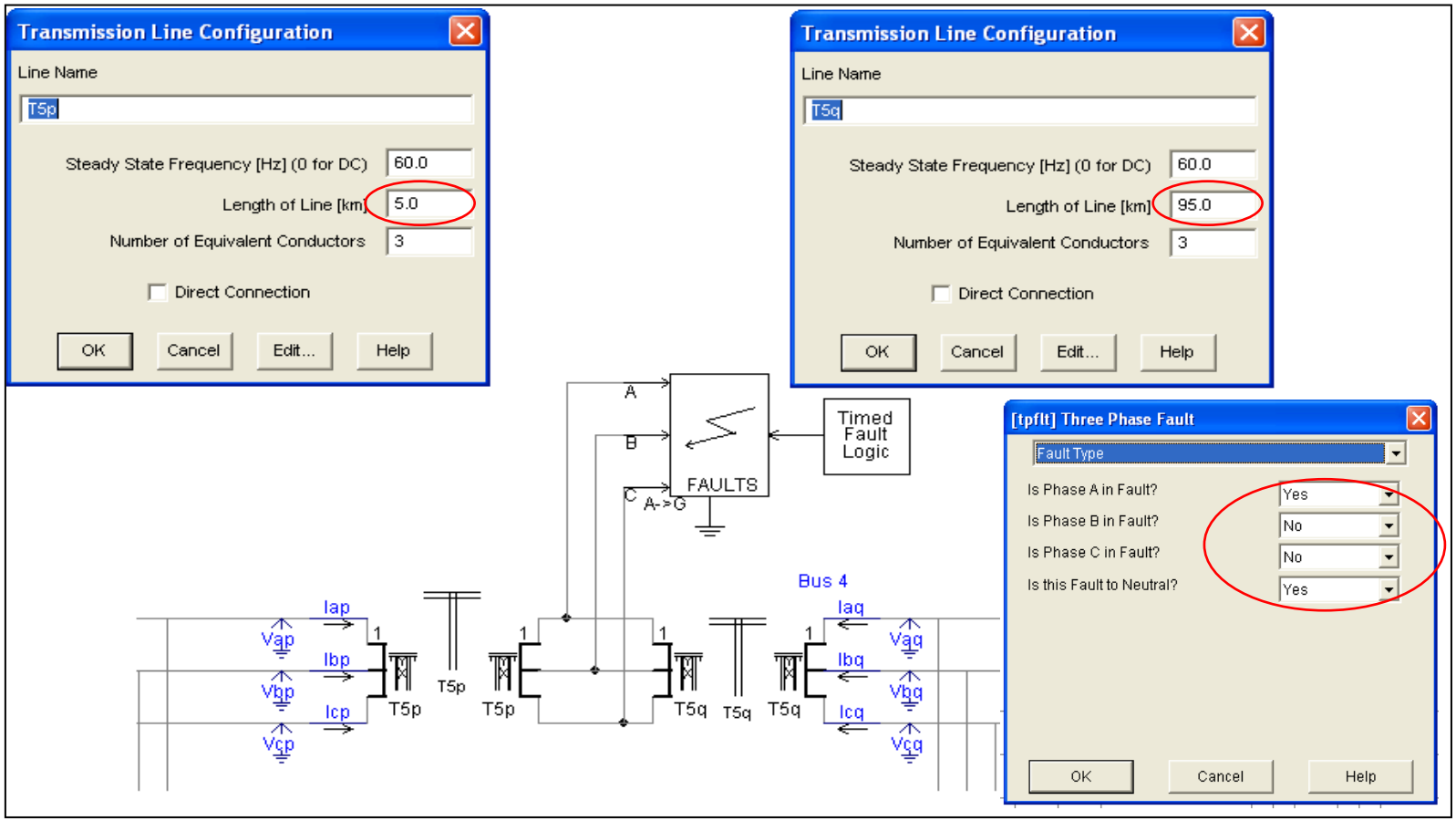

Figure 6.3: Application of Faults at Different Locations of L_5

(The example shows an A-G fault applied at 5% of the transmission line)

6.3 Admittance Relay Results

This section presents the test results obtained by applying processed fault and non-fault data to the designed admittance relay. The following sections show currents' and voltages' waveforms, pre-processed inputs' waveforms and the fault detection results of the ANN for different faults. As mentioned previously, each pattern comprised of five cycles each of pre-fault data, fault data and post-fault data. These patterns were applied to the ANN as data windows. It was observed that the trained ANN performed accurately (gave a -1 output) for all pre-fault and post-fault patterns. These results, therefore, are not shown. Due to size limitation of this dissertation, only selective cases are included in the main body of the dissertation. All the other results are included separately in Appendix G.

6.3.1 Relay Performance for Single Line to Ground Faults

Sections 6.3.1.1 and 6.3.1.2 present ANN results for single line to ground faults at two different locations. Given that single line to ground faults are the most commonly occurring faults on a transmission line, the ANN relay was tested most thoroughly for these faults. The test results for faults at other locations are given in Appendix G. These include faults at every 5% length of the selected transmission line L_5 for both 0° and 90° fault inception angles.

6.3.1.1 Close-in Single Line to Ground Fault

Figures 6.4 shows the currents and voltages before, during and after a single line to ground (SLG) fault was applied at 0% length of L_5. These waveforms were generated from current and voltage samples obtained from the PSCAD test system. Fault inception can be seen by an increase in current of phase A with a sudden voltage drop at the same instant. There is no significant change in the current and voltage of phase B and C.

Figure 6.5 shows the two inputs $Input_1$ and $Input_2$ that were given to the neural relay. It should be noted that these inputs are referred as $Input_{1\text{mod}}$ and $Input_{2\text{mod}}$ respectively in the previous chapters. $Input_1$ that has been delayed by five samples is plotted on the

secondary Y-axis in Figure 6.4. The processed inputs' waveforms show that phase angle difference between these inputs satisfies the criteria of a phase comparator.

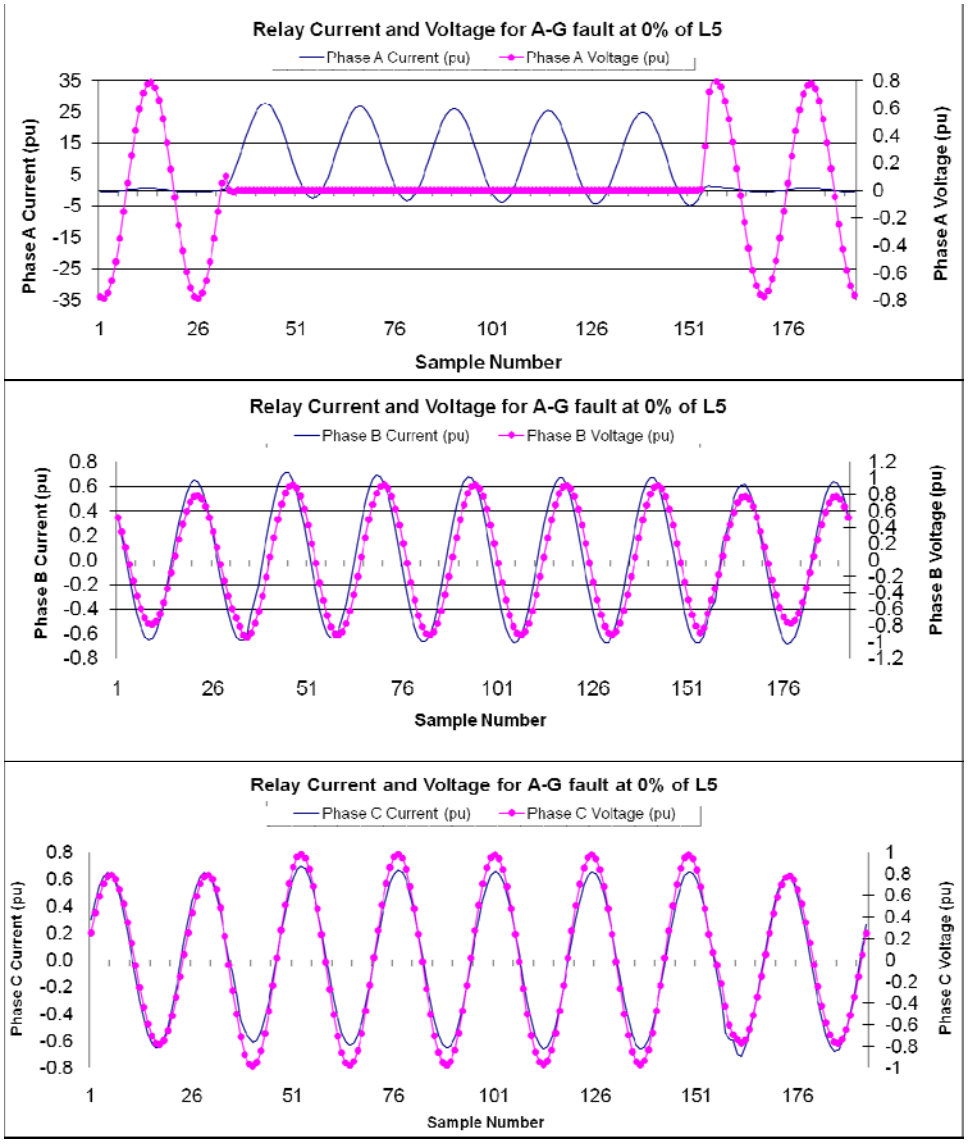

Figure 6.4: Conventional Relay Inputs for a SLG Fault at 0% of L_5

Figure 6.6 shows the output of A-G, B-G and C-G ANNs for a Phase A to ground fault at 0% line length, for a fault inception angle of 0º with respect to Phase A. The fault location 0% length of the transmission line implies a fault right in front of the relay location (translates to a fault at the origin of relay characteristic). It can be seen that the A-G relay was able to detect a fault in less than one cycle. No fault was detected by Phase B and C relays. It should be noted that the ANNs produced similar results when tested for B-G and C-G faults. The results obtained for 90° fault inception were better where the relay detected a fault in about 10.4*ms* (about half of a cycle) of a cycle. One other case where a mid-line fault was applied at 40% of the transmission line is discussed in the next section.

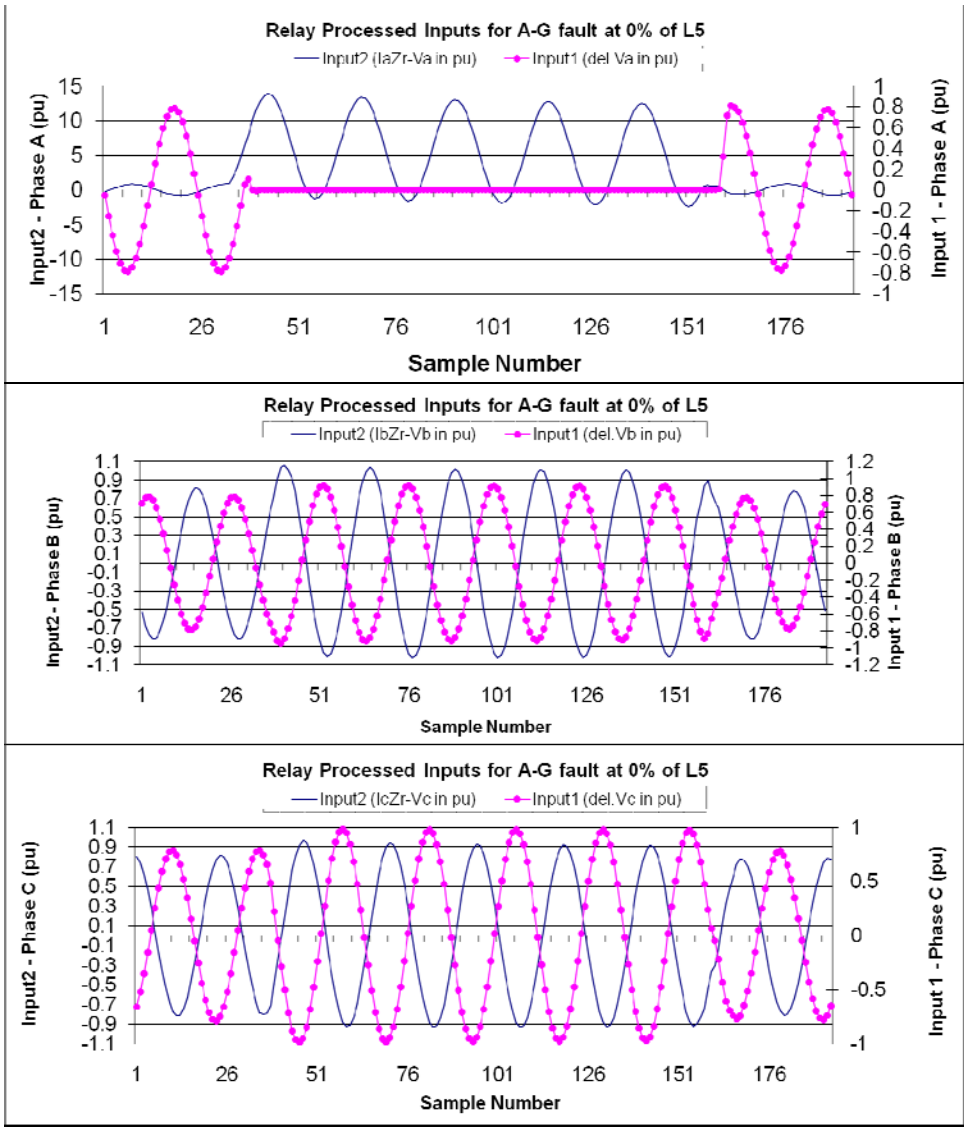

Figure 6.5: Relay Processed Inputs for a SLG Fault at 0% of L_5

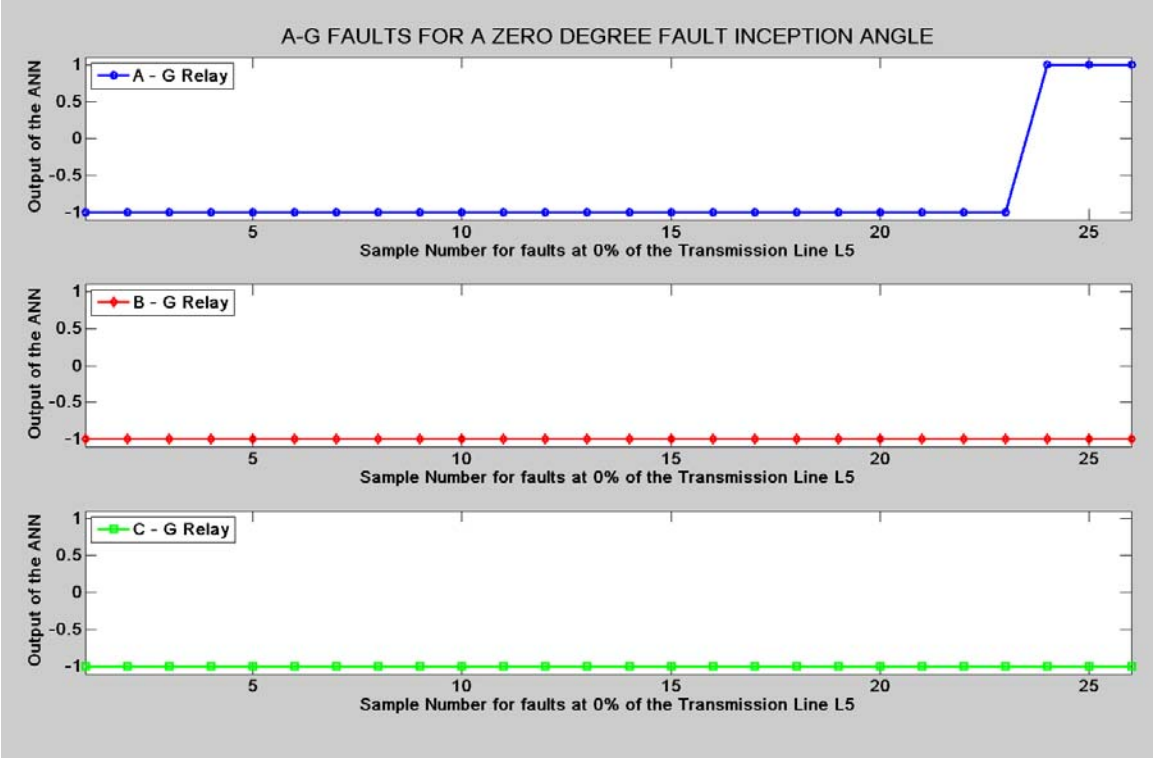

Figure 6.6: Relay Outputs for A-G Fault at 0% length of L_5

The output of the ANN for other faults is shown in Figures G.1 to G.22 in Appendix G. The results from all these fault cases for a fault inception angle of 90° are shown in Figures G.23 to G.46 of Appendix G.

6.3.1.2 Mid-line Single Line to Ground Fault

Figure 6.7 shows the current and voltage waveforms for an A-G fault applied at 45% of the transmission line. As expected, the change in current and voltage values is lesser than in the previous case. The current and voltage samples were pre-processed to obtain relay inputs; the waveforms are shown in Figure 6.8. The processed inputs show that the phase difference between inputs to be less than 90° for the A-G relay. The phase difference between inputs is greater than 90° for B-G and C-G relays.

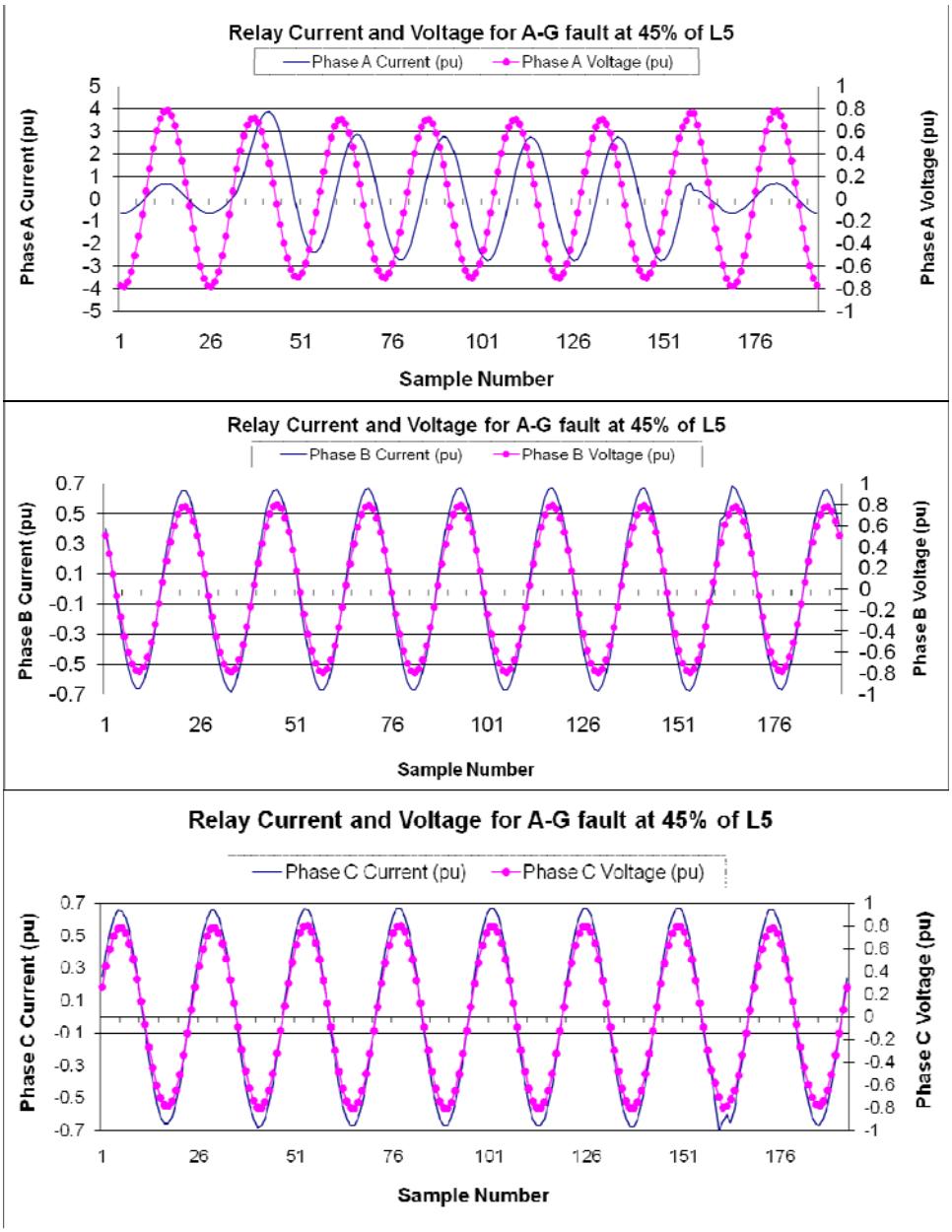

Figure 6.7: Current and Voltage at Relay Location for an A-G Fault at 45% of L_5

Figure 6.9 shows the ANN results for this fault location. The ANN employed for phase A detected the fault in three-quarters (12.5*ms*) of a cycle. No fault was detected by Phase B and C relays. The results for this fault location did not vary for a 90° fault inception angle and can be seen in Appendix G.

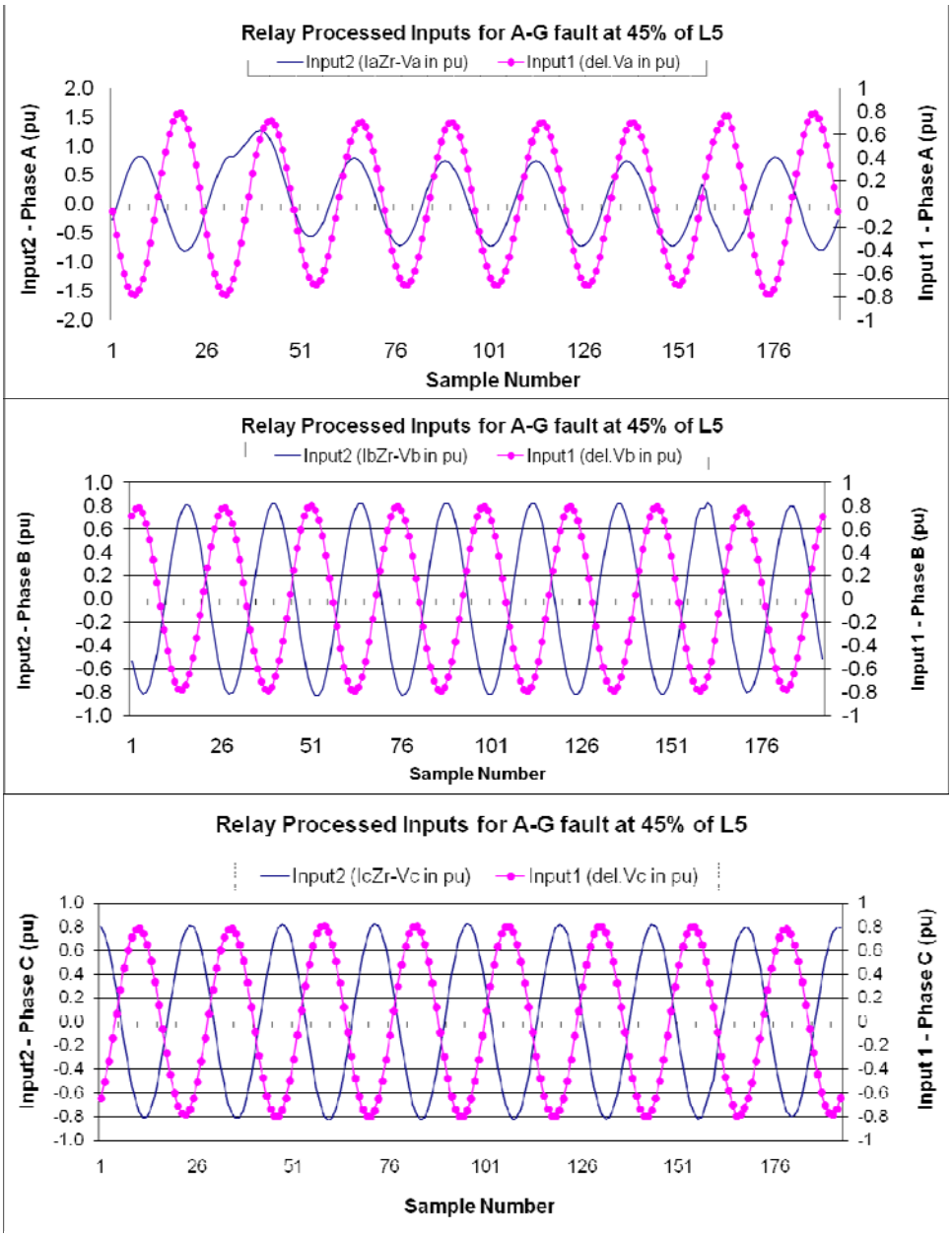

Figure 6.8: Relay Processed Inputs for a A-G Fault at 45% of L_5

6.3.1.3 Discussion

The single line to ground fault results presented in the previous two sections and in Appendix G show that the fault detection time decreased as the applied fault was located away from the relay location. The fault was detected in less than one cycle in all the cases and in about half a cycle for faults at 70% and beyond of the transmission line. It can also be observed that no fault was detected when a fault was beyond 85% length of

the transmission line, thus, complying with the requirements of zone-1 distance protection of transmission lines. The input waveforms show that DC offset was present in the test inputs obtained from PSCAD. No filter was applied to filter this DC offset; it was observed that this had a minimal effect on the neural network results.

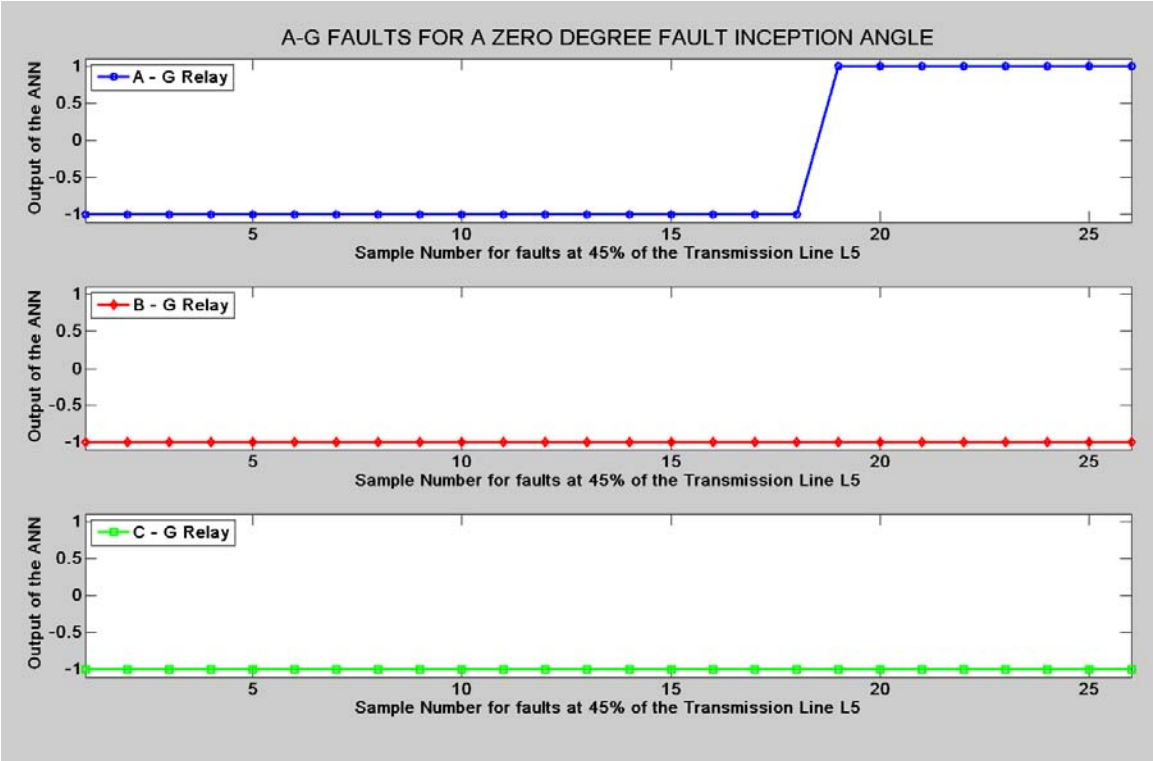

Figure 6.9: Relay Outputs for A-G Fault at 45% length of L_5

The results did not vary significantly for a fault inception angle of 90º with respect to Phase A. The neural network was trained for an impedance reach equal to 80% length of the transmission line. The relay was able to detect fault up to 75% of the transmission line, even though it was trained on a different system. The relay was able to perform well for all faults within the defined operating boundary of relay characteristic. Further, the relay took less than one cycle to correctly detect a fault in all cases.

6.3.2 Relay Performance for Two Phase Faults

The proposed algorithm for ground faults was extended for two and three phase faults as described in the last chapter. This section shows the relay processed inputs and results for line to line and double line to ground faults.

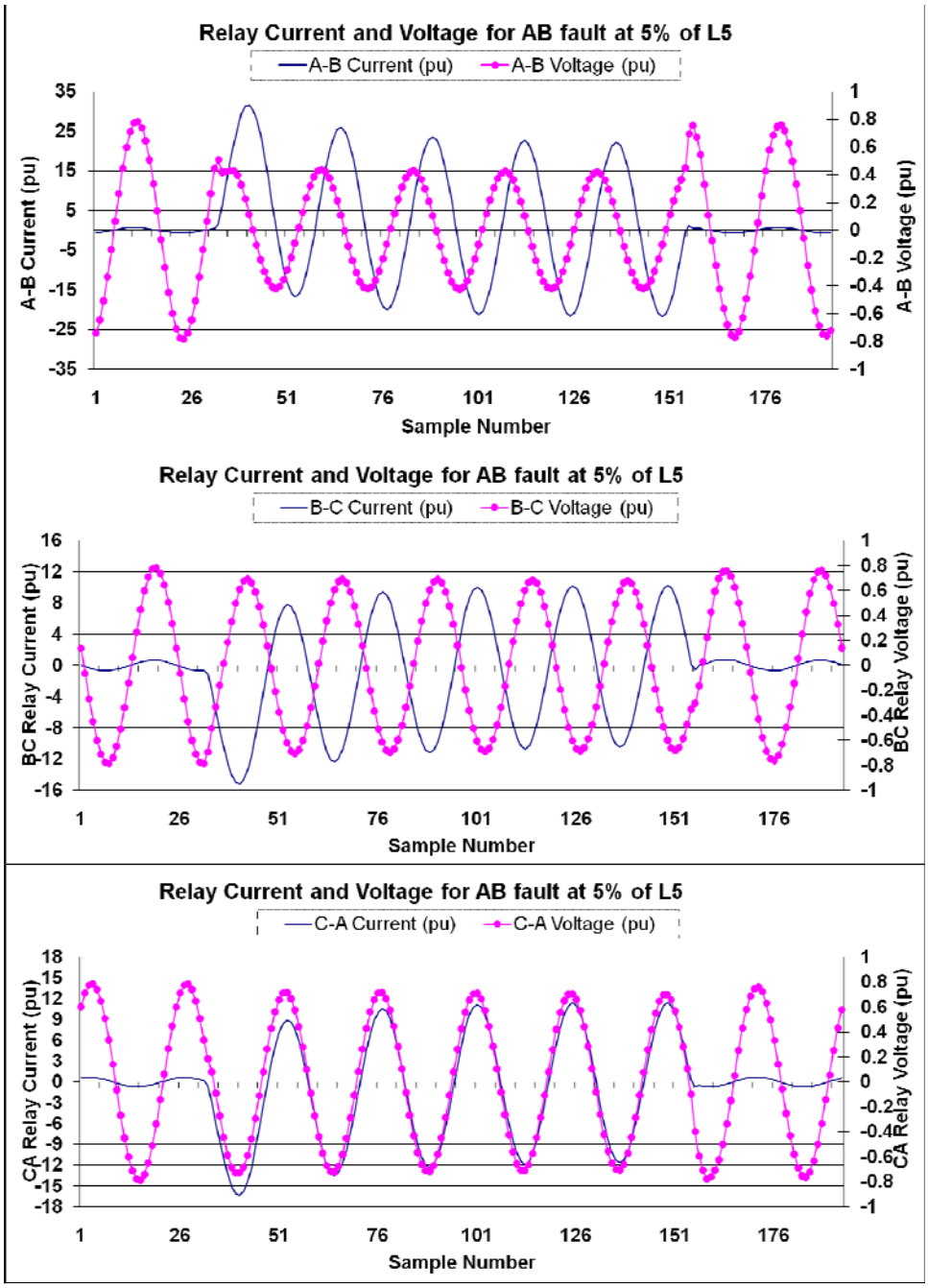

Figure 6.10: Relay Inputs for A-B Fault at 5% Fault Location of L_5

The inputs were modified as per equations given in the last chapter and the same 18-37-1 neural network was used to test the relay for line to line and double line to ground faults. For applying the same trained ANN for faults on two or more phases, line voltages ($V_a - V_b, V_b - V_c, V_c - V_a$) and currents ($I_a - I_b, I_b - I_c, I_c - I_a$) were divided by a factor of square root of three (√3) to reduce them to phase voltage and current levels. This also

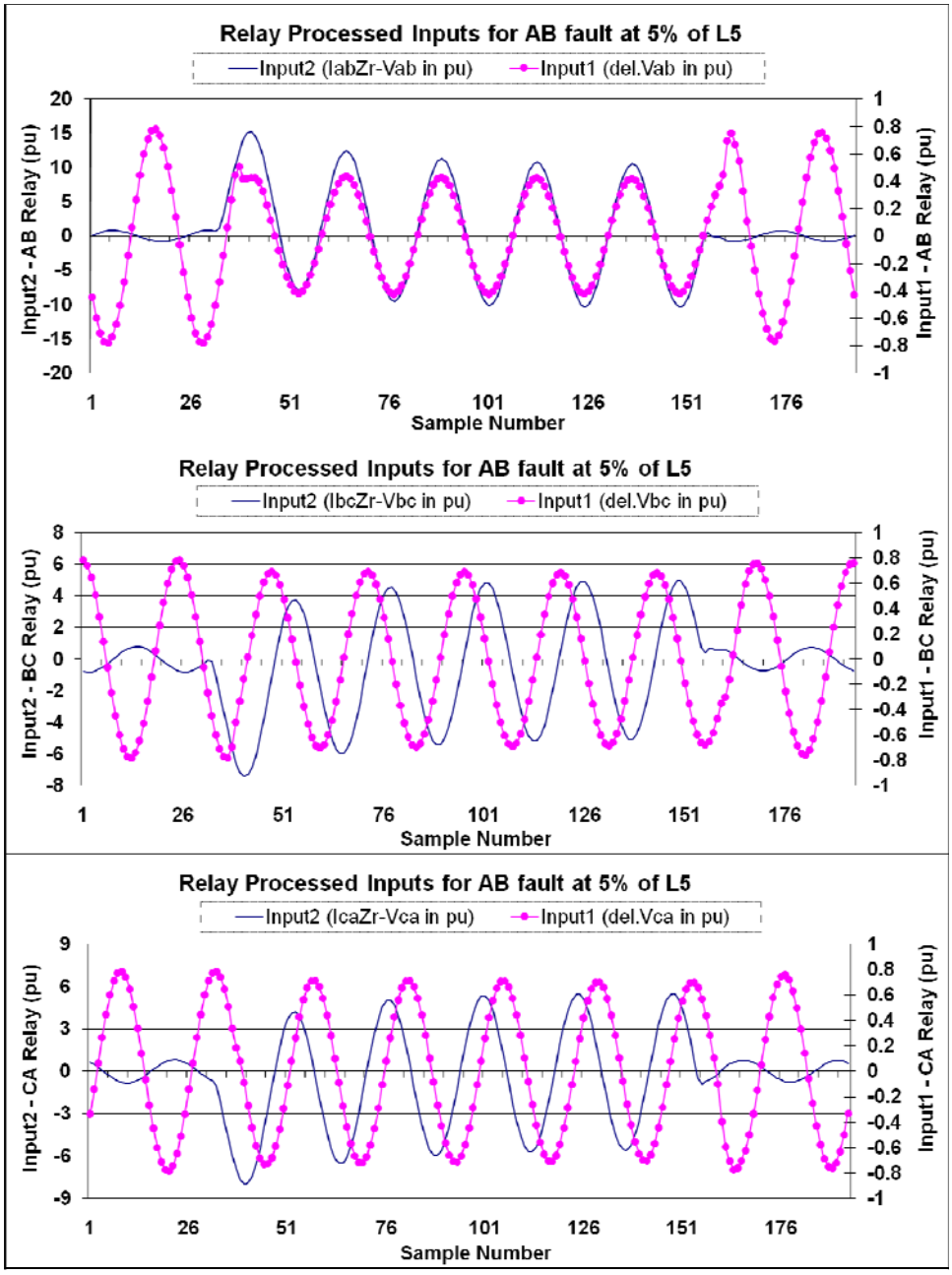

Figure 6.11: Processed Relay Inputs for A-B Fault at 5% Location of L_5

ensured that the normal line current and voltage values were between [-1, 1] per-unit range. The line current and voltage waveforms shown in the subsequent sections are scaled down by this factor.

6.3.2.1 Close-in Line to Line Fault

Figure 6.10 shows the scaled line currents and voltages for an A-B fault applied at 5% length of the transmission line L_5. Relay inputs obtained by applying the proposed algorithm are shown in Figure 6.11. The phase differences between the relay inputs during the fault in less than 90° and is evident from these waveforms. The outputs of the A-B, B-C and C-A phase relays are shown in Figure 6.12. The result shows that the A-B relay picks up the fault at 6^{th} sample after the data window is full of fault samples, resulting in a fault detection time of 13.19*ms*. It can also be observed that the other two phase relays also pick up the fault, though it is much later than A-B relay. The B-C and C-A relay pick up the fault in 22.22 ms and 20.14ms respectively i.e. the second cycle

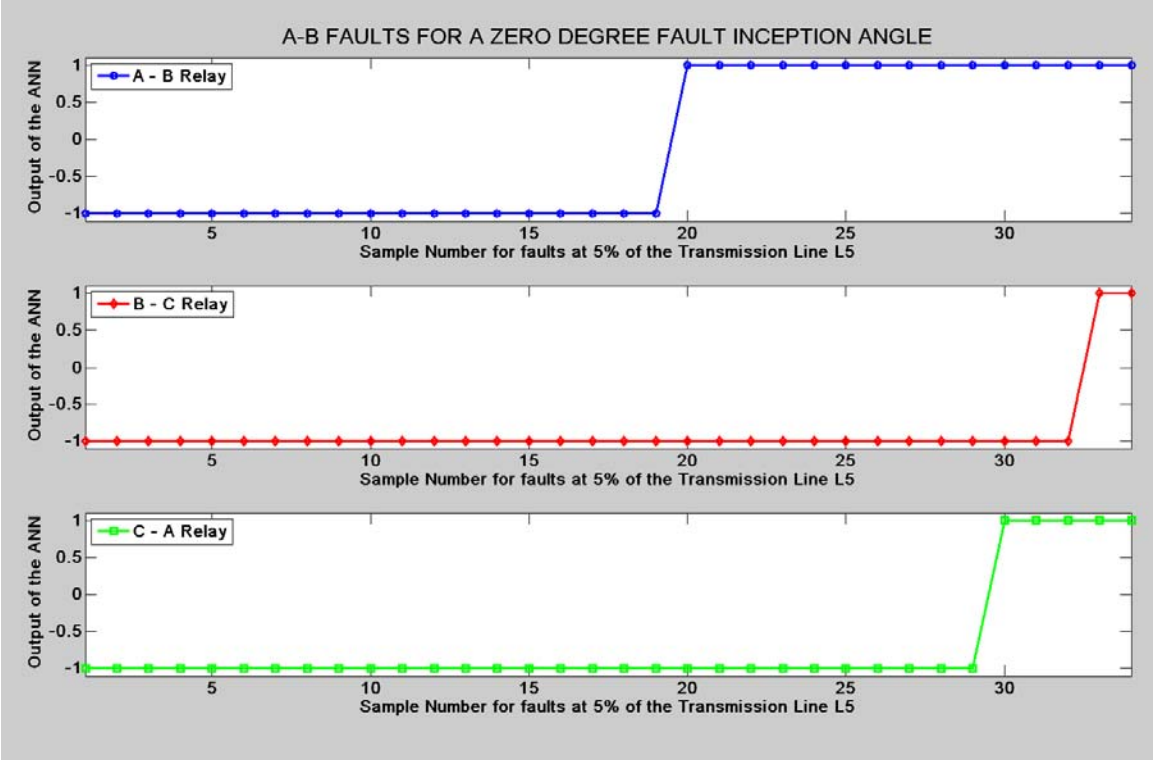

Figure 6.12: Relay Outputs for A-B Fault at 5% length of L_5

after fault inception. This can be attributed to the fact that the voltages drop on both A and B phases affects the self-polarizing voltages (i.e. V_{ab}, V_{bc} and V_{ca}) of all relays and results in tripping. Impedance zones of the three phase relays also contribute to these results. This issue is discussed later in this chapter.

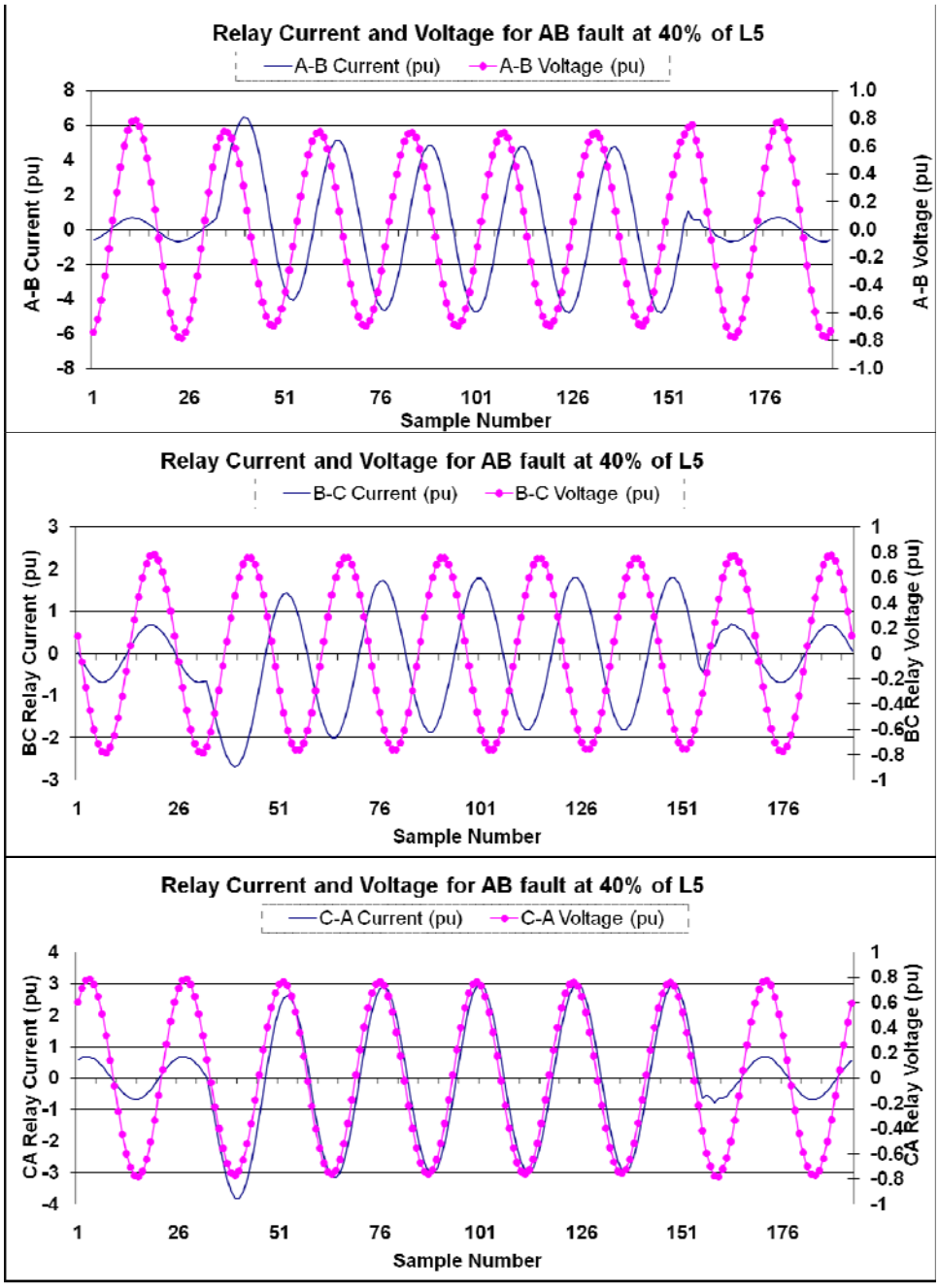

Figure 6.13: Relay Inputs for A-B Fault at 40% Fault Location of L_5

6.3.2.2 Mid-line Line to Line Fault

Figure 6.13 shows the currents and voltages at the relay location for a fault at 40% of the transmission line. It can be noticed that the phase angle difference between the processed relay inputs lies within the [-90°, 90°] range; and is close to zero degrees for A-B relay. The self-polarizing voltage of the B-C and C-A relay does drop as significantly as in case

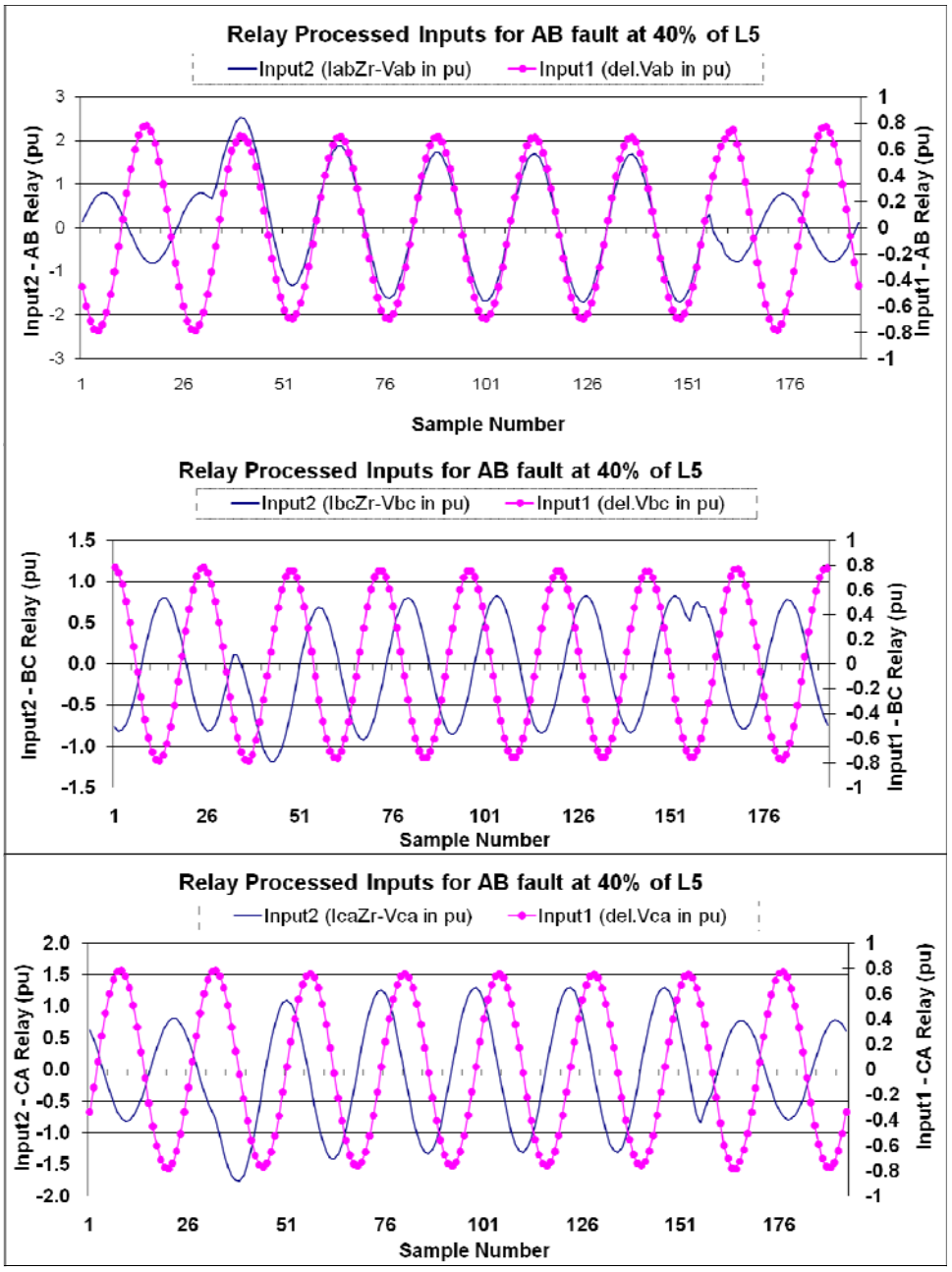

Figure 6.14: Processed Relay Inputs for A-B Fault at 40% Location of L_5

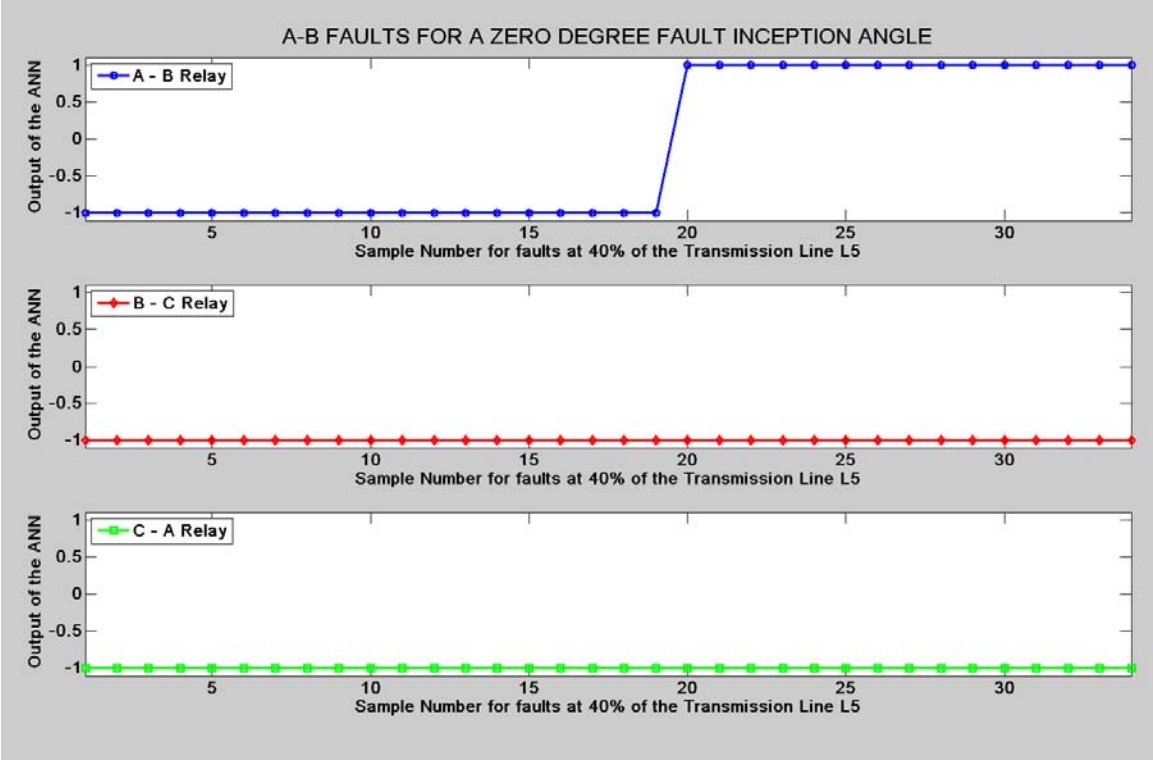

Figure 6.15: Relay Output for A-B Fault at 40% length of L_5

on a close-in fault. The output of the three relays is shown in Figure 6.15. It can be seen that the A-B relay detected this fault after the 6th sample, indicating a detection time of 13.19*ms*. The B-C and C-A relays do not detect a fault in this case. This further confirms the fact that B-C and C-A relays trip only for A-B close-in fault.

Tests for other fault locations, which included faults at 0%, 10%, 75%, 80%, 85% and 100% line length were conducted. The results for all these cases are provided in Appendix G in Figures G. 47 to G.52. The A-B ANN is able to detect a fault in about half a cycle (~8.33*ms*) for faults close to relay boundaries (at 75% and 80% of the transmission line). This shows that the relay works well close to relay operating boundary and detects a fault in lesser time than conventional algorithms. The results also show that B-C and C-A relays trip only for close-in A-B fault at 0% and 5% fault location; these relays do not operate for faults at 10% or further away on the transmission line. The drop in the self-polarizing voltage causes these relays to operate. This can be corrected by usage of a memory polarization scheme. This is discussed later in this chapter.

6.3.2.3 Close-in Double Line to Ground Fault

For close-in double line to ground faults, the ANN was tested for faults at relay location, 5km and 10km away from the relay location. The line currents and voltages for an AB-G fault at 5% length of the transmission line are shown in Figure 6.16. The relay inputs were processed in the same manner as in case of line to line faults and are shown in

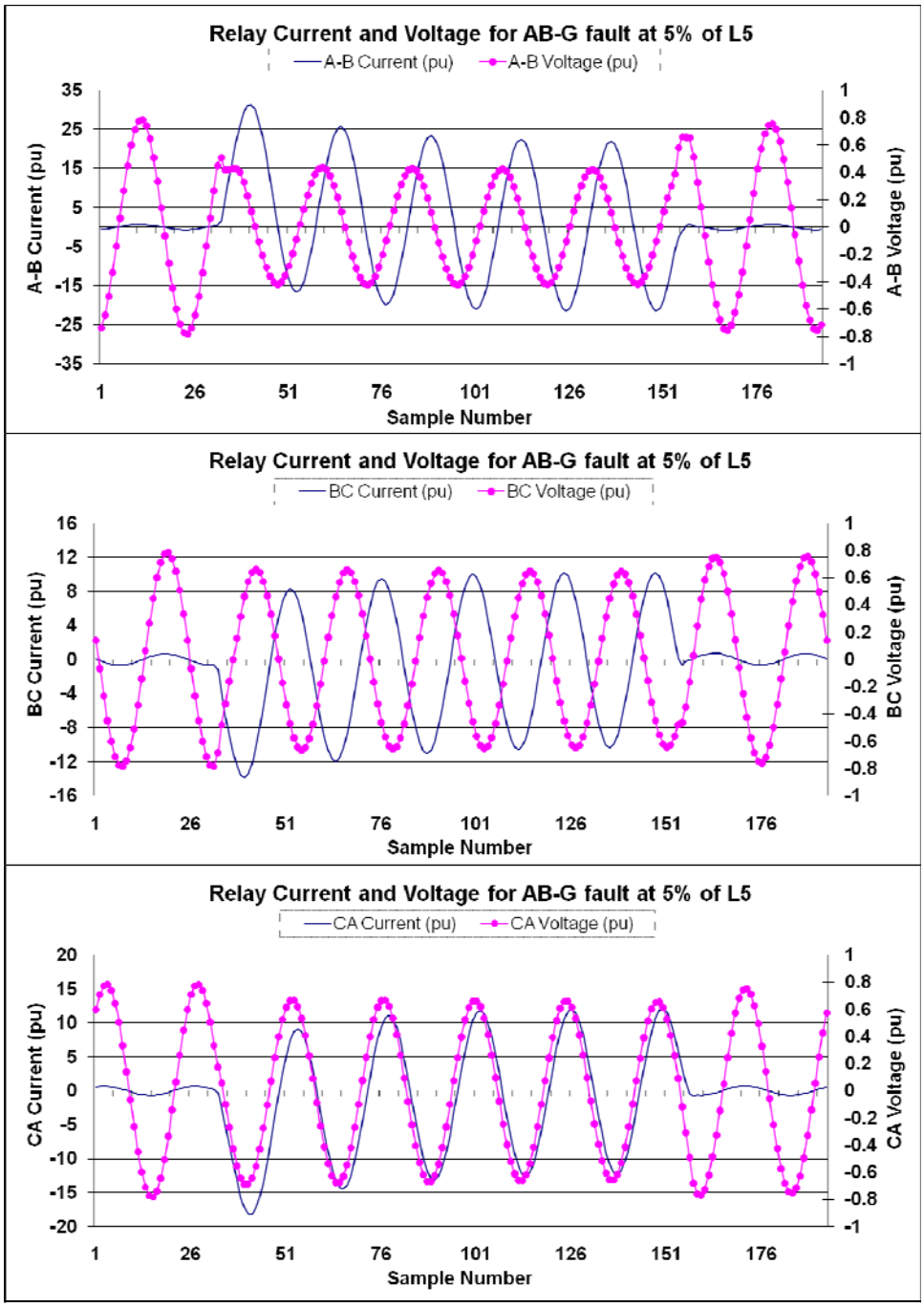

Figure 6.16: Relay Inputs for AB-G Fault at 5% Fault Location of L_5

Figure 6.17. The pre-processing of inputs leads to a clear distinction of phase angle differences between the inputs of A-B relay, bringing it close to zero degrees. Figure 6.18 shows the output of the three relays. Relay A-B picked up the fault at 7th sample after fault inception, resulting in a fault detection time of 13.19*ms*. As in the case of close-in AB fault, B-C and C-A relays also pick up this fault at 22.91*ms* and 20.80*ms* respectively. The results obtained for A-B fault at 0% fault location were similar. The

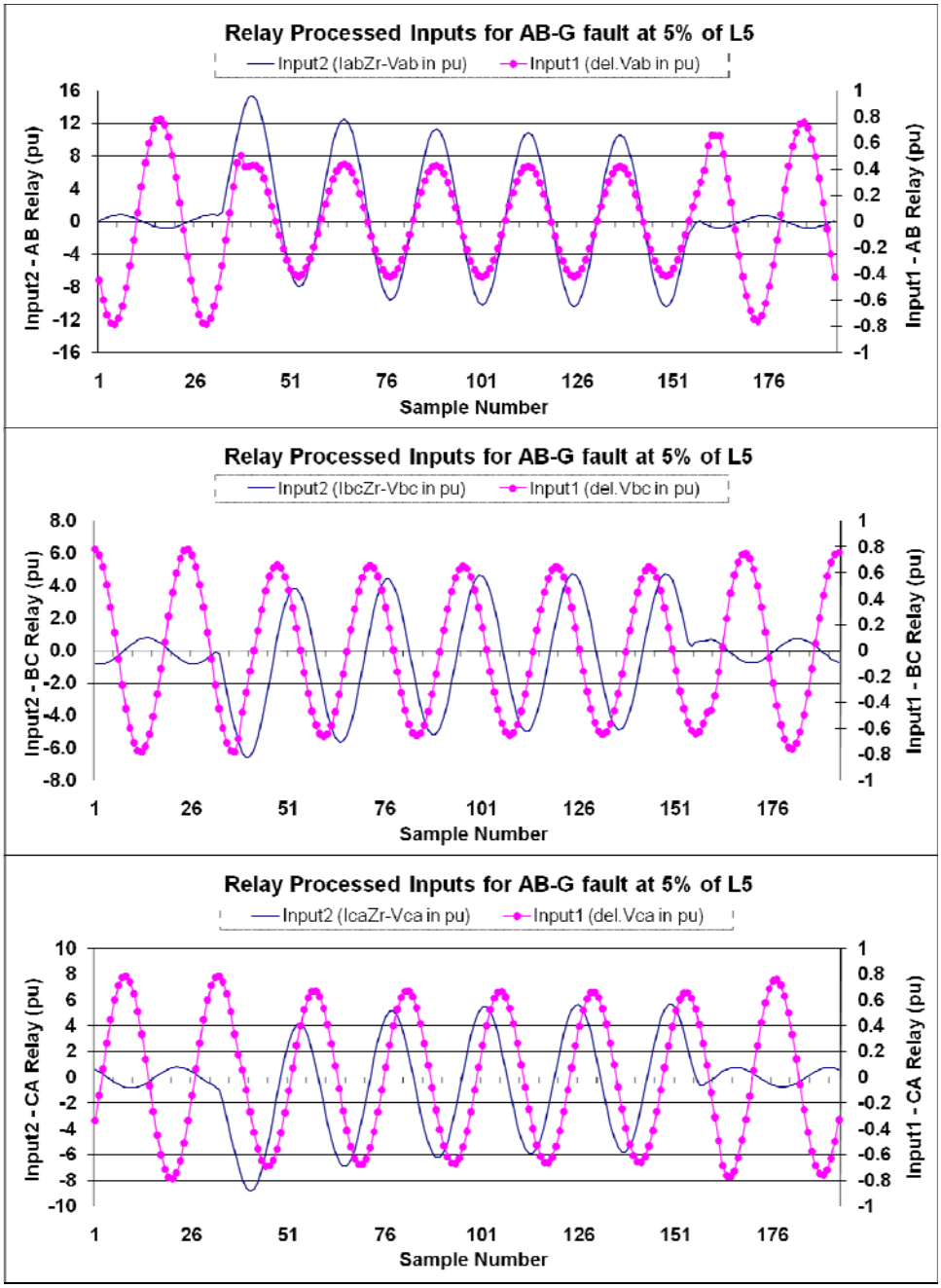

Figure 6.17: Processed Relay Output for AB-G Fault at 5% Location of L_5

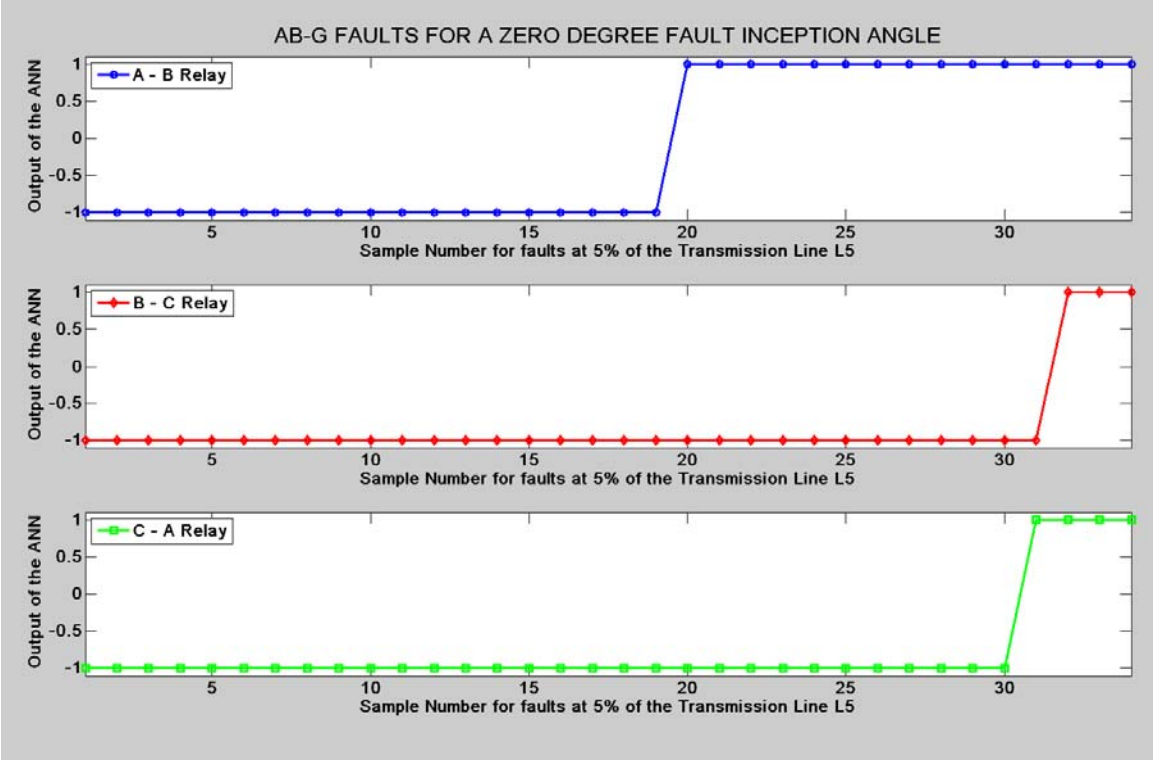

Figure 6.18: Relay Output for AB-G Fault at 5% length of L_5

B-C and C-A relays did not operate for an A-B fault at 10% of the transmission line.

6.3.2.4 Mid-line Double Line to Ground Fault

Figure 6.19 shows the line currents and voltages as seen on the relay location before, during and after AB-G fault inception at 40% transmission line length. The processed inputs for the three relays are shown in Figure 6.20. The phase comparison of the processed inputs indicates an A-B fault, which is not evident by comparing the line currents and voltages. The output of the ANNs shown in Figure 6.21 indicates that the A-B relay picked up a fault after a time of 12.50*ms* in this case. The ANN output was -1 for all patterns before the occurrence and after the removal of the fault. The B-C and C-A relays did not operate in this case.

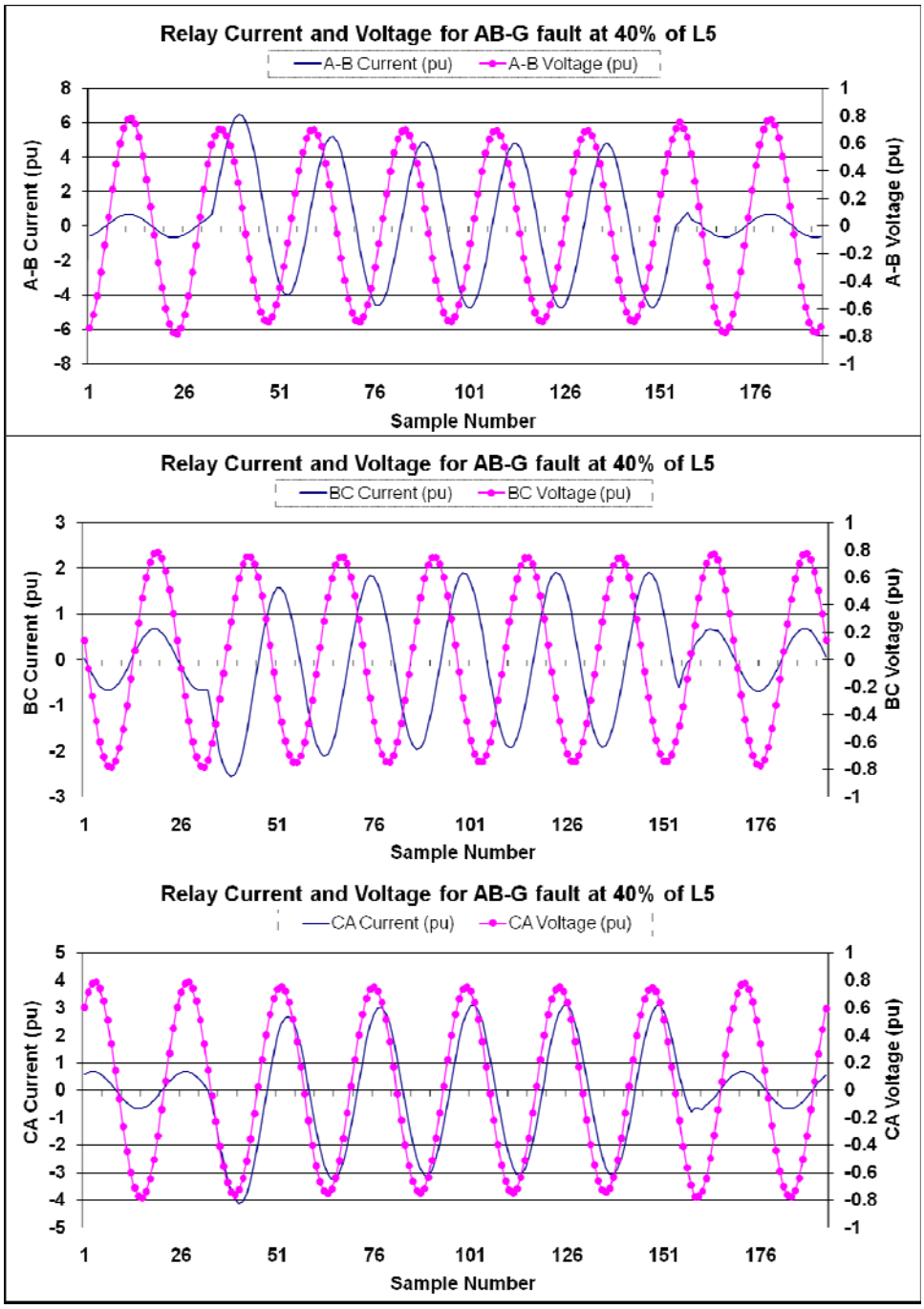

Figure 6.19: Relay Inputs for AB-G Fault 40% Fault Location of L_5

6.3.2.5 Discussion

The results presented in this section show that all the phase relays pick up close-in faults on any phase. This applies to both line to line and double line to ground faults. The B-C and C-A relays do not trip for faults beyond 10% of the transmission line. This translates

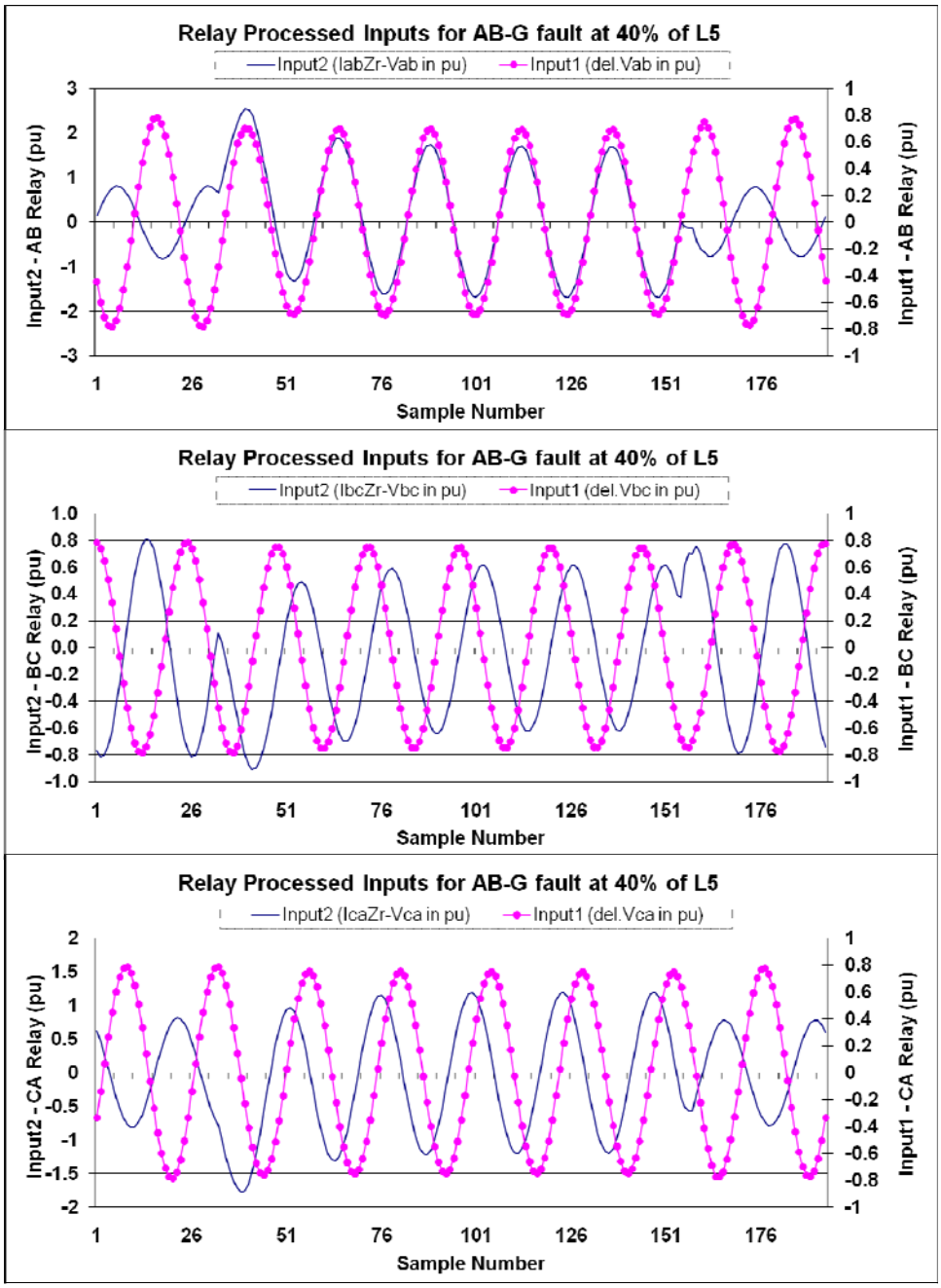

Figure 6.20: Processed Relay Inputs for AB-G Fault 40% Fault Location of L_5

to the impedance zones of different phase relays, shown in Figure 6.22. It can be seen that the impedance zones of all the phase relays lie very close to each other when impedance is low i.e. fault is close to the relay location. The impedance zones are separated out as the faults move away from the relay location. In the conducted tests, B-C and C-A relays did not detect an A-B fault away from the relay location. This testifies

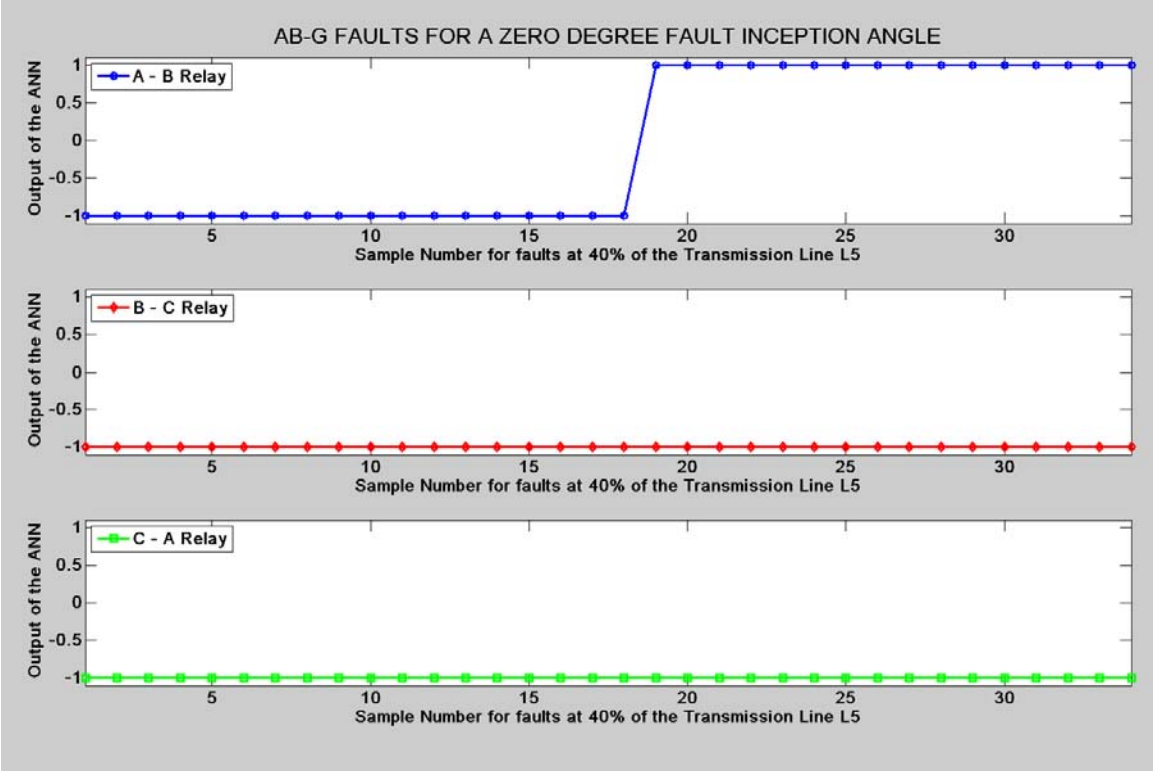

Figure 6.21: Relay Output for AB-G Fault at 40% Length of L_5

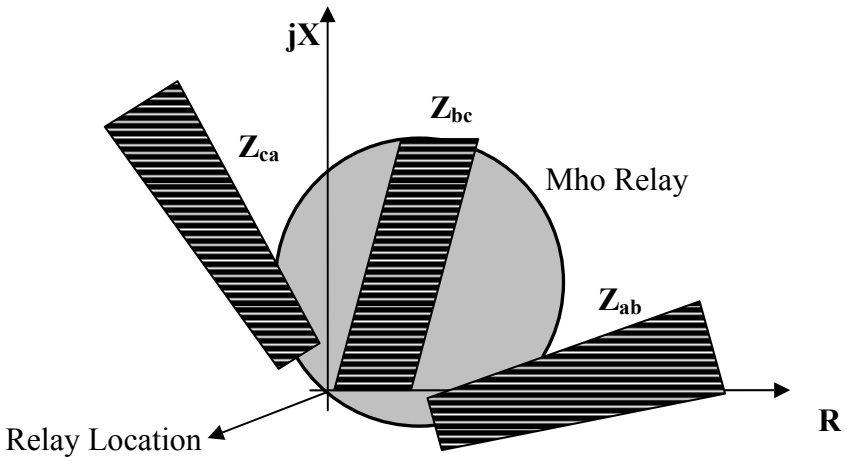

Figure 6.22: Impedance Zones of Phase Relays

the fact that the ANN relay gave output in accordance with typical distance relay characteristics.

Memory polarization and positive sequence polarization schemes are helpful in such situations. The usage of pre-fault voltages expands the characteristics of the relay as the

strength of pre-fault voltages is more than fault voltage for close-in faults. So it translates to a fault away from the relay location. This helps in correct fault detection by phase relays for faults on only two phases. The previous chapter discussed self memory and positive sequence memory polarization techniques. These were applied for two phase and three faults to assess the performance of relays during close-in faults. The used technique and results are presented in Section 6.4.

6.3.3 Extension of Admittance Relay Algorithm for Three Phase faults

The percentage of occurrence of three phase (symmetrical) faults is much lesser as compared to unsymmetrical faults in power systems; however, these types of faults are the most severe in nature. Further, persistent single line to ground and phase to phase faults get converted into three phase faults. Therefore, the admittance relay design was extended for three phase faults. As in the case of two phase faults, the tests for three phase faults were conducted for eight different fault locations.

The inputs used for three phase faults were line voltages and currents; therefore, the adjustment of the inputs for phase voltages and currents was done by square root of 3. Any one set of line voltages and currents (i.e. A-B, B-C or C-A) can be used for three phase faults. The results presented in the next section show the processed inputs and the results for all three ANNs used as A-B, B-C and C-A phase relays.

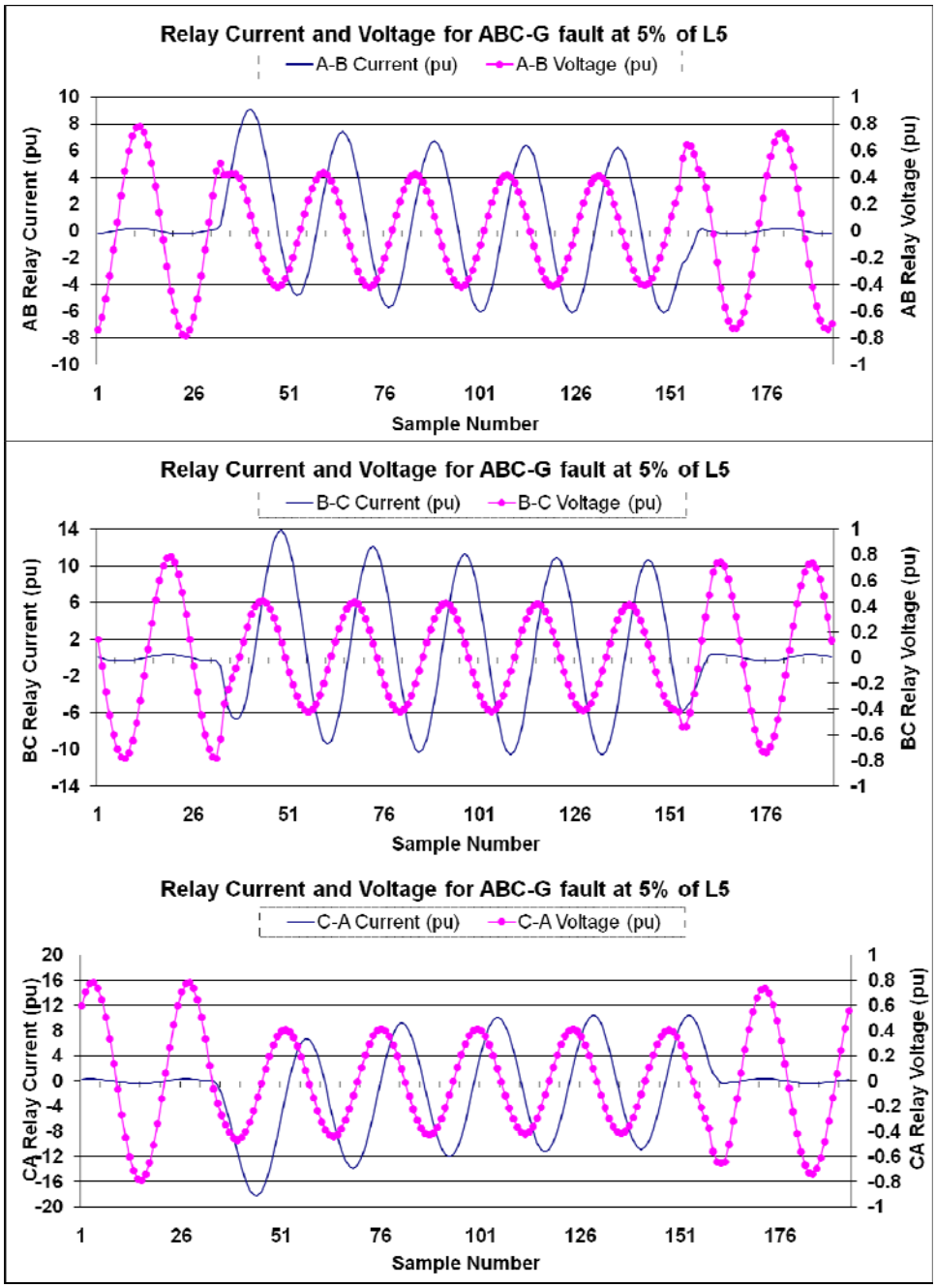

Figure 6.23: Relay Inputs for a Three Phase to Ground Fault at 5% Fault Location of L_5

6.3.3.1 Close-in Three Phase to Ground Fault

Figures 6.23 show the line voltages and currents for an ABC-G fault at 5% length of transmission line. Figure 6.24 shows the processed relay inputs obtained by applying the proposed algorithm. It can be seen that the pre-processing results in an almost 0° phase angle difference between the modified inputs for all three relays.

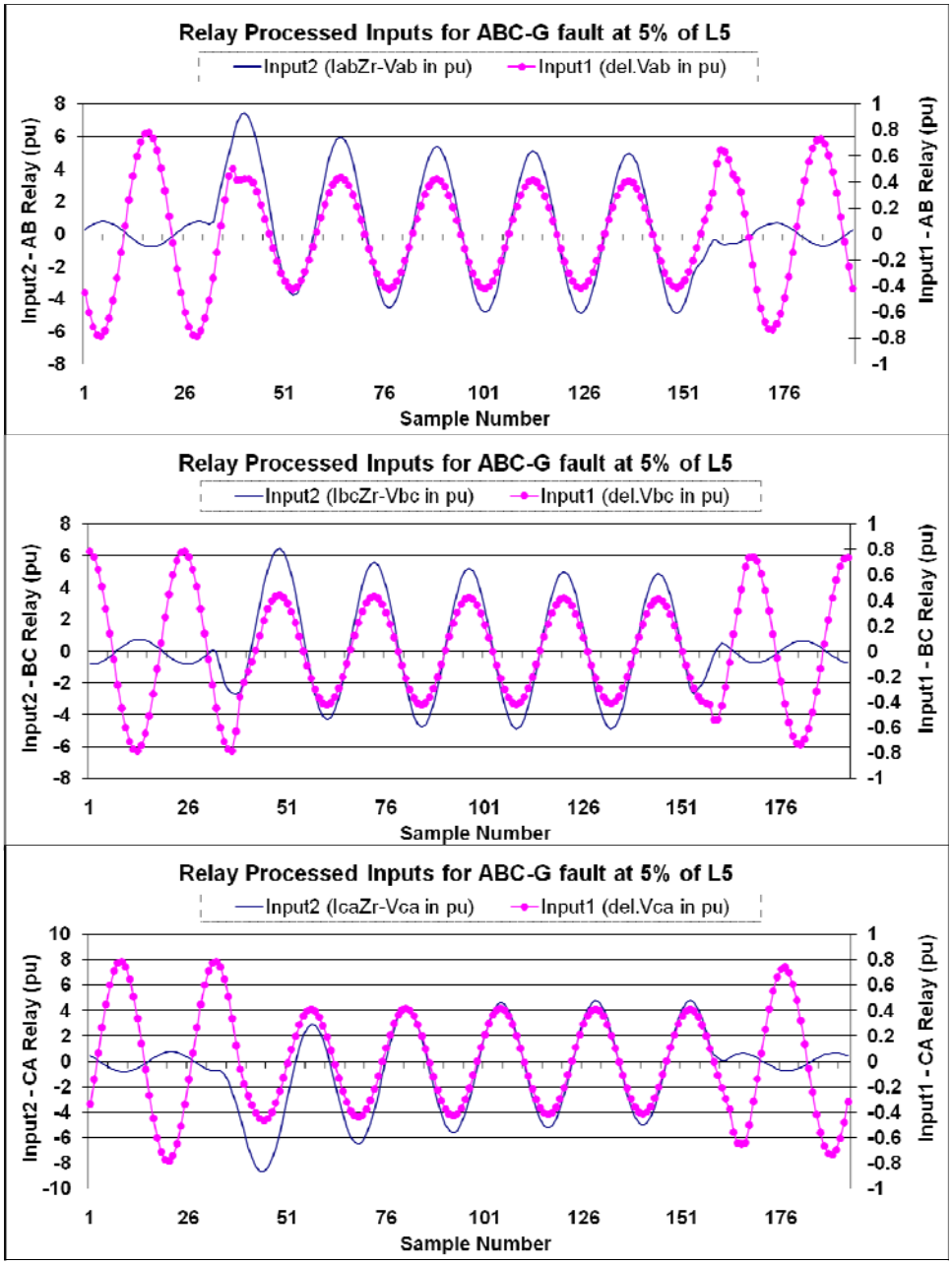

Figure 6.24: Processed Relay Inputs for ABC-G at 5% Fault Location of L_5

The output of the three ANNs for this case is shown in Figure 6.25. Both A-B and B-C relays detect a fault at 7th sample after one data window is full of fault samples, resulting in a fault detection time of about 13.2*ms*. The C-A relay detects a fault in 9.03*ms*. The other close-in fault locations for which the relay was tested are 0% and 10% length of the

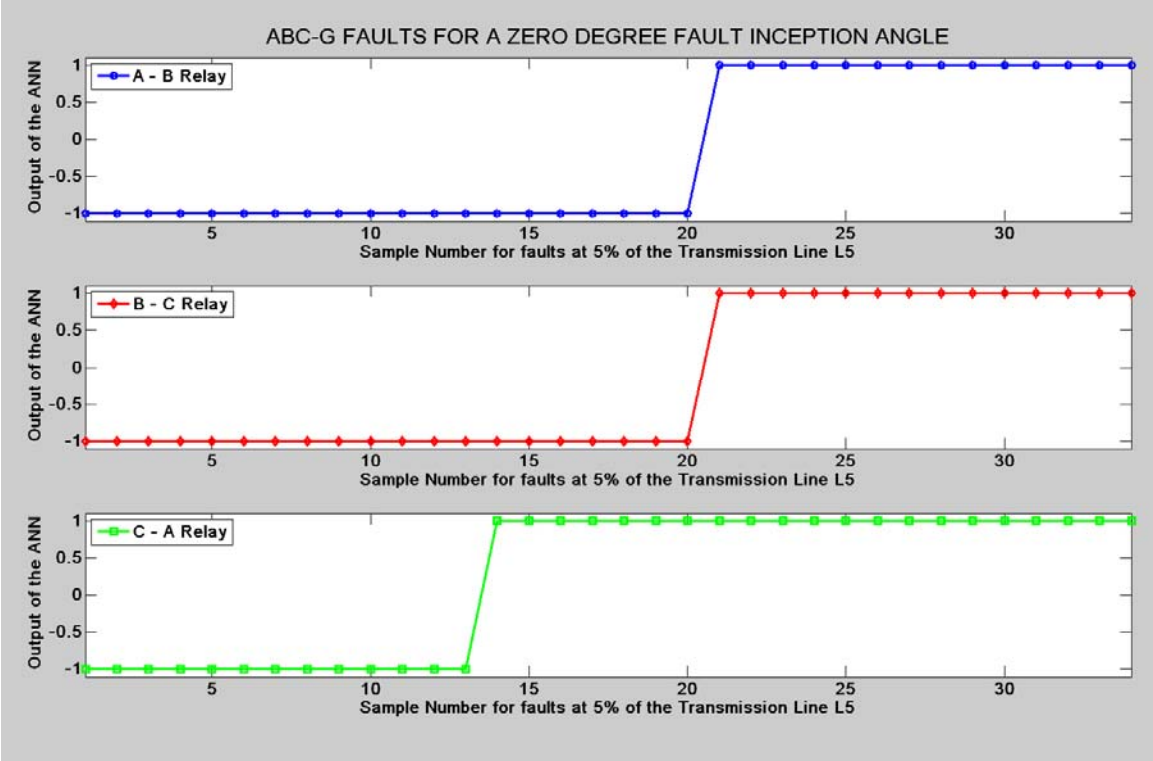

Figure 6.25: Relay Output for ABC-G Fault at 5% length of L_5

transmission line. The relays yielded similar results for other locations and can be seen in Appendix G.

6.3.3.2 Mid-line Three Phase to Ground Fault

Figure 6.26 shows the line currents and voltages as seen at the relay location for an ABC-G fault at 40km away from the relay. The phase angle difference processed between the fault and non-fault patterns is clearly evident when the inputs are processed, as shown in Figure 6.27. Outputs of ANNs for this fault location are shown in Figure 6.28. The A-B relay detects a fault after 13 samples, resulting in a fault detection time of about 9.03*ms*. It can be seen that the B-C relay detects a fault 2 samples before the data window is full of 13 fault samples, which is equal to 7.64*ms* detection time.

The other percentages at which the relay was tested are 75%, 80%, 85% and 100% of length of transmission line. Output of ANNs for these fault locations are shown in Figures G.60 to Figure G.66 in Appendix G.

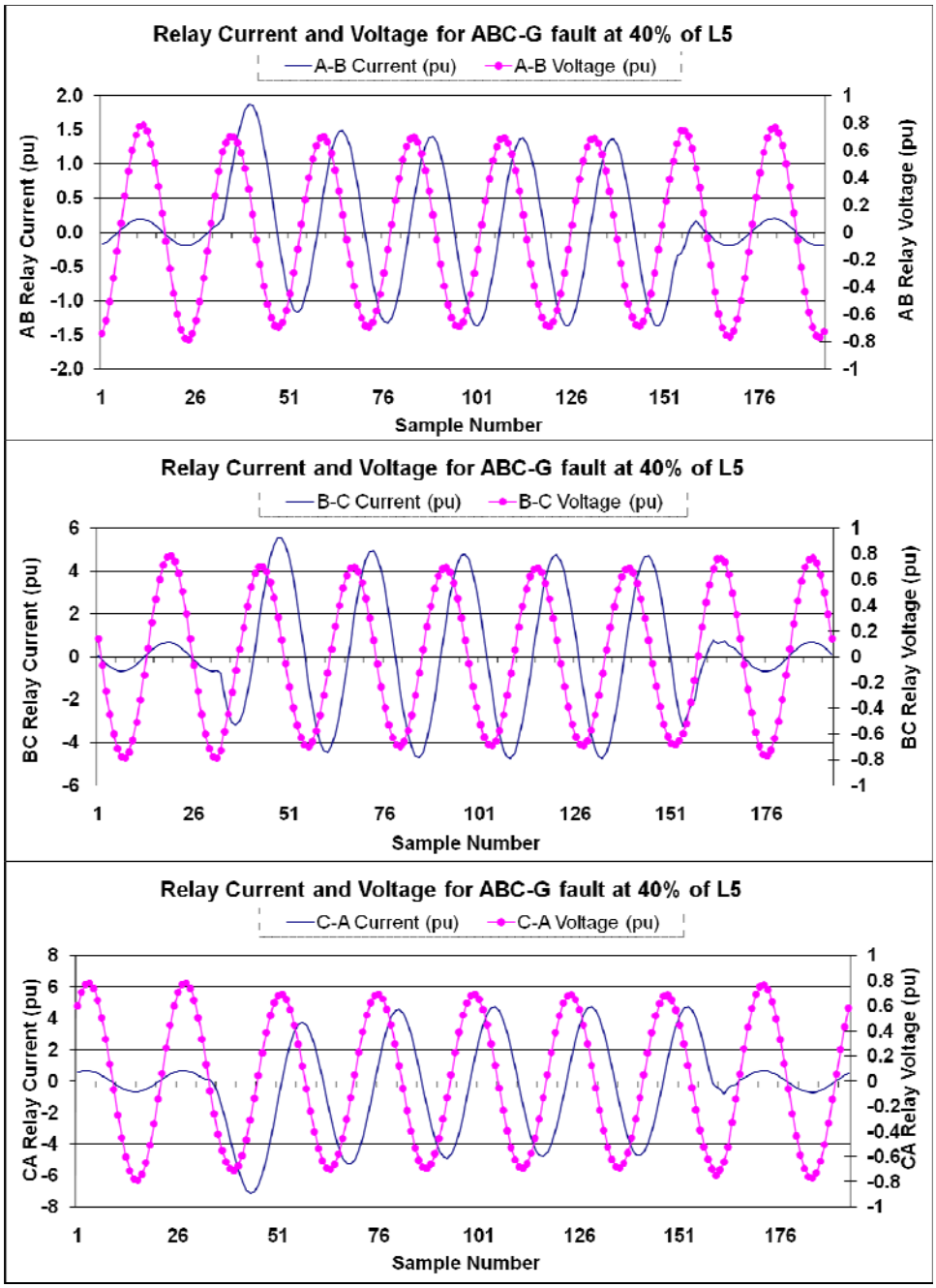

Figure 6.26: Relay Inputs for a ABC-G Fault at 40% Fault Location of L_5

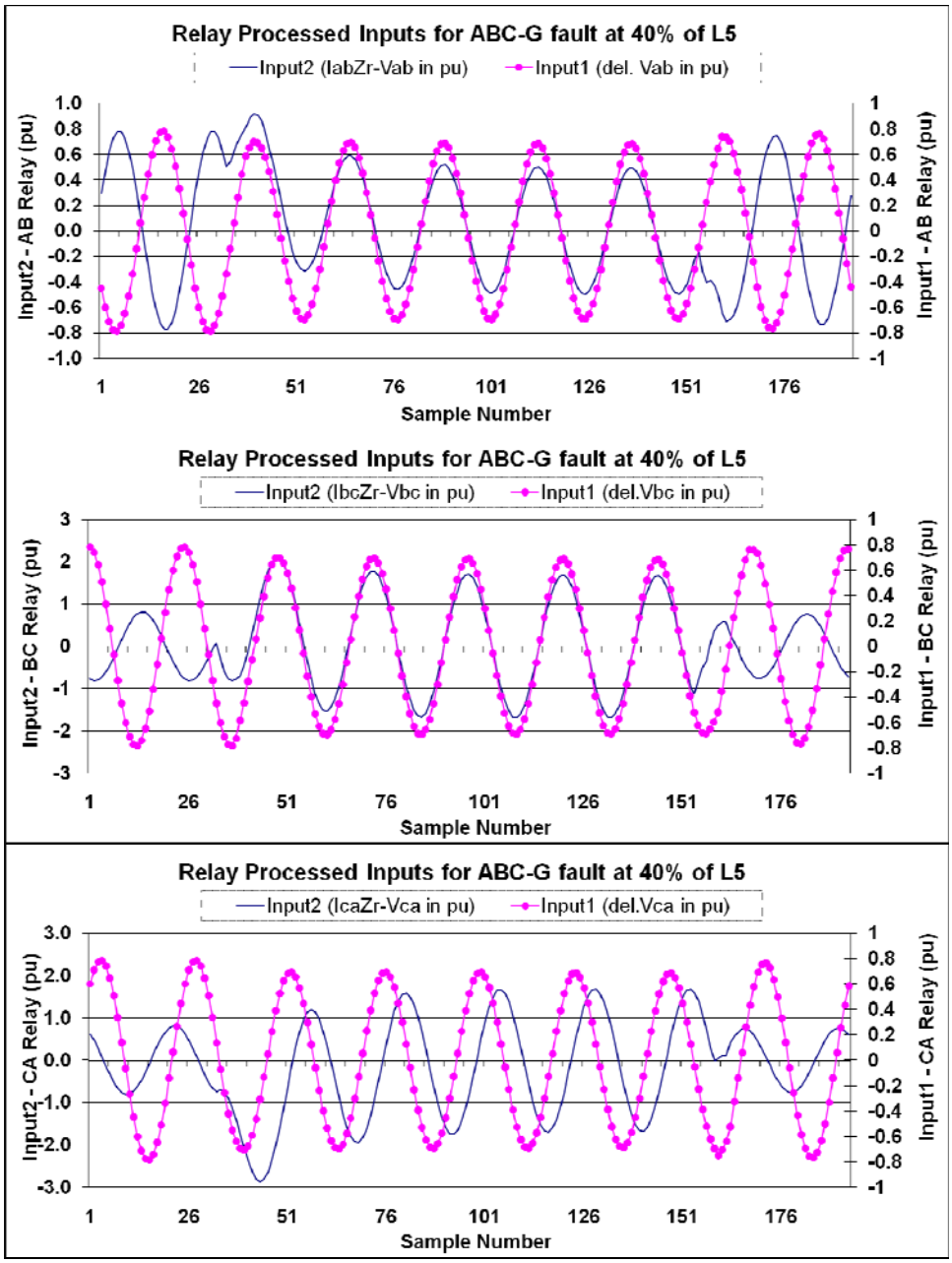

Figure 6.27: Processed Relay Inputs for ABC-G Fault at 40% Fault Location of L_5

6.3.3.3 Discussion

The results for ABC-G faults show that the relay was able to detect faults in less than one cycle for close-in faults, i.e. faults at 0% and 5% of the transmission line. For faults away from the relay location, the ANN was able to detect a fault in less than half-cycle, before a data window was full of thirteen fault samples. No faults were detected for

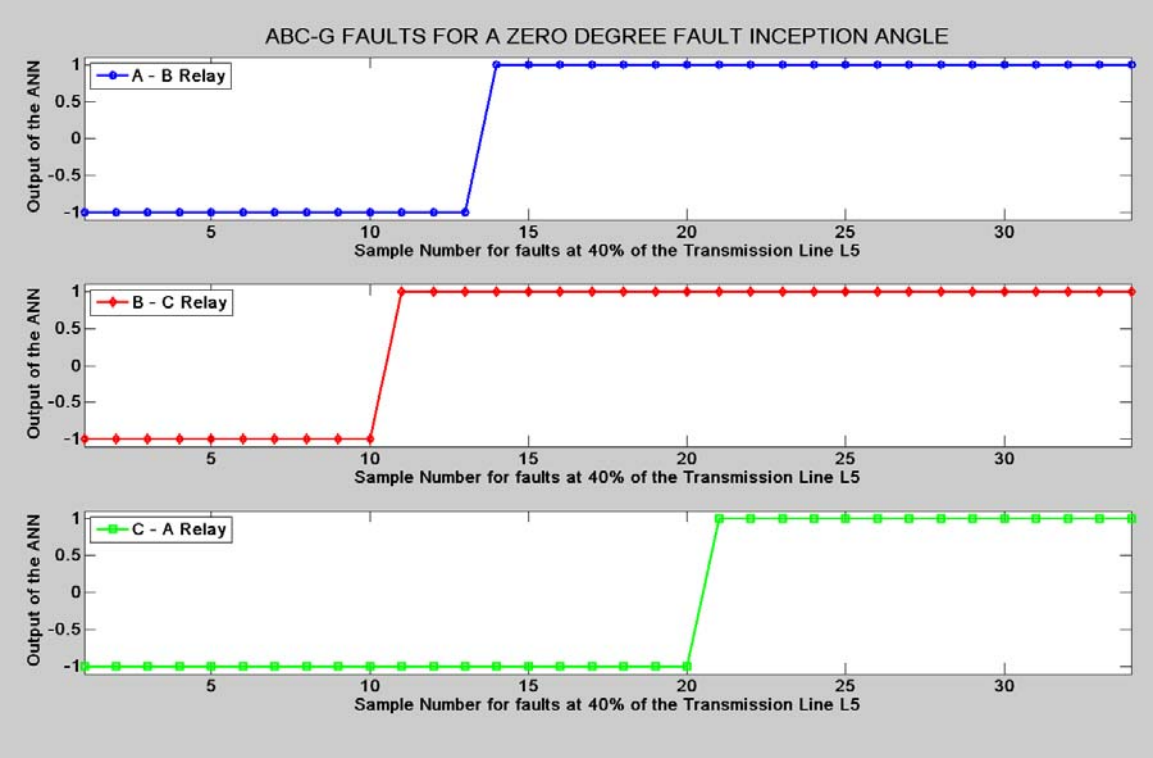

Figure 6.28: Relay Output for ABC-G Fault at 40% length of L_5

locations beyond 80% of the transmission line, thus, clearly defining the operating relay boundary. The results presented for symmetrical and unsymmetrical faults in the last few sections prove consistency of the designed ANN as a phase comparator. Relays were able to detect their respective faults in less than one cycle in all the cases, which is lesser than time taken by any conventional algorithm.

6.4 Polarization Results

The capability of the proposed algorithm to include different types of polarization techniques was tested. Polarizing inputs are important for cases when the available self - polarizing voltage is low or not available. A methodology was developed that used a sum of different polarizing voltages (in different percentage) which work individually as well as in conjunction with other polarization voltages. The proposed algorithm was then tested for these different polarization combinations. The aim for combining different polarizations in one application was to eliminate the limitations of individual methods.

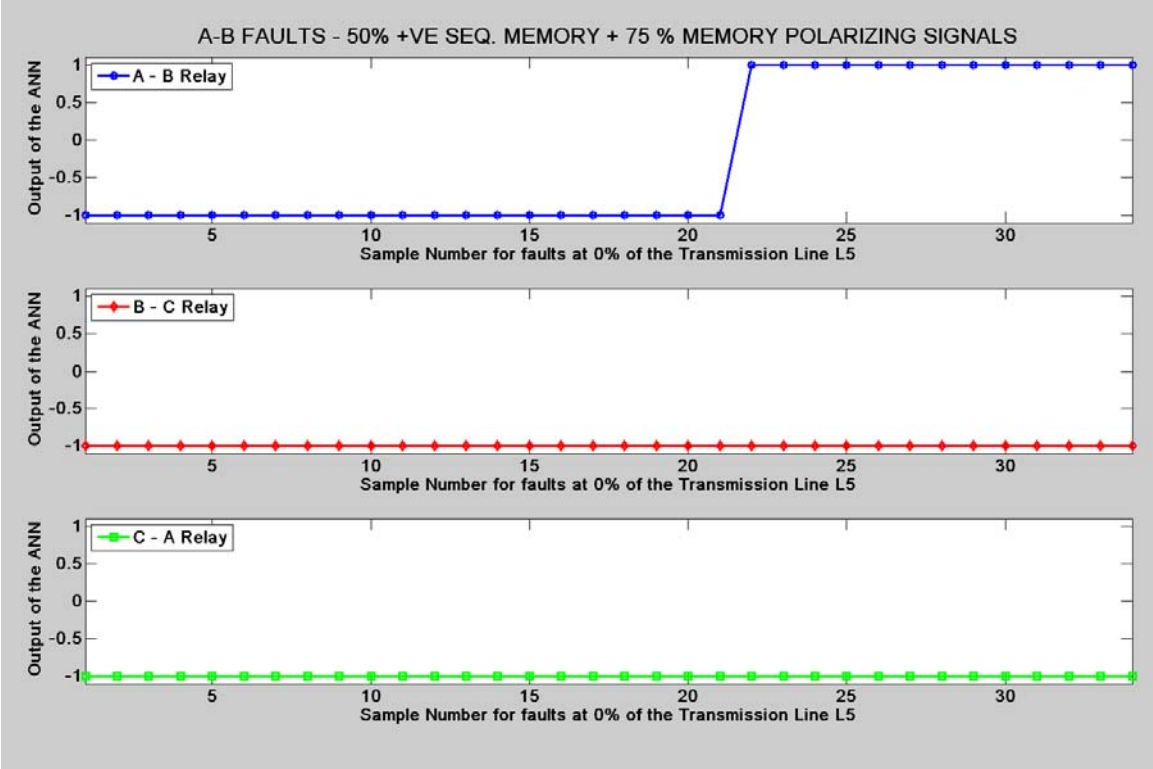

Figure 6.29: A-B fault - 75% Self and 50% Positive Sequence Memory Polarization

The algorithm was tested for reliability and consistency by using a combination of different polarizations; however, due to space constraints, only selective polarization results for two and three phase faults are included in the main body of the thesis. The next few sections list the results for different types of polarizations that were used to test the ANN. The obtained results for each of these cases are given in Appendix G.

6.4.1 Line to Line Faults

Different polarization techniques were tested for line to line faults. This included cross memory polarization, self memory polarization, positive sequence memory polarization and their combinations. Figures G.218 to G.221 present the results for line to line faults using positive sequence memory polarization. The results presented are for 100% positive sequence polarization, however, it was observed during testing that 75% polarizing voltage and 50% polarizing voltage also worked well for detecting faults

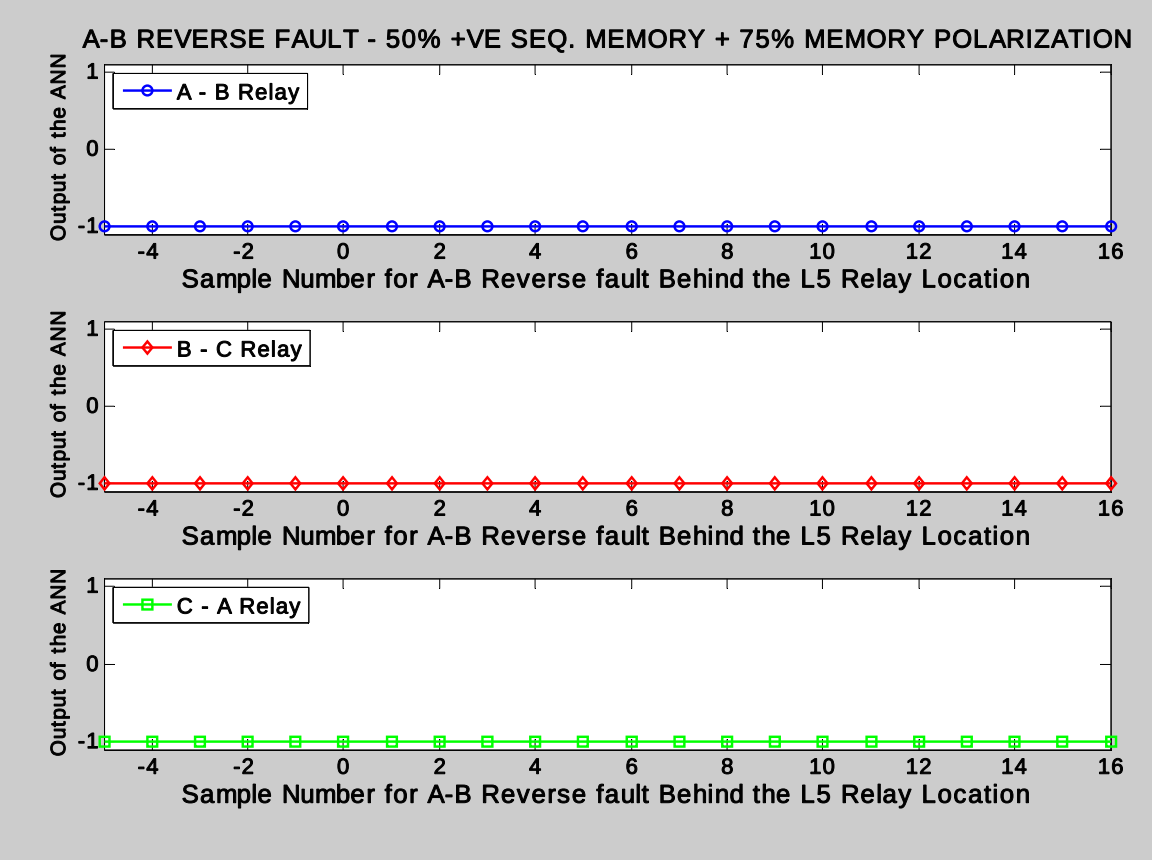

Figure 6.30: A-B Reverse Fault-75% Self and 50% Positive Seq. Memory Polarization

The ANN worked well with 75% self-memory as well as 50% positive sequence memory polarizing voltage. Therefore, these two voltages were added to test if a combination was able to detect all types of faults while maintaining the integrity of the relay boundaries. This helps to increase the reliability of a relay and also ensures that it works correctly even if one of the polarizing voltages is not available. Figures 6.29 shows the output of phase relays for an A-B faults at 0% transmission line length, implying a forward fault on the bus. This fault case is previously presented in Section 6.3.2, where it is noted that B-C and C-A relays detect a close-in A-B fault due to lack of substantial polarizing voltage.

It was observed that the B-C and C-A relay did not operate when memory polarized voltages were used. There was no change in the fault detection time of A-B relay. It can be seen in Figure 6.29 that other phase relays did not operate for A-B faults.

It is well understood that addition of polarization expands the relay operating boundaries in the reverse direction, with maximum expansion for positive sequence memory polarizing voltage. One of the issues that may arise with usage of polarization is its effect on the inherent directional capability of an admittance relay. Usually, to maintain the directional discrimination nature of a memory polarized relay, a directional element or a phase comparator is used to avoid relay tripping for reverse faults. This implies that a reliable phase comparison technique using polarization should not operate for reverse faults. Keeping this issue in mind, the proposed algorithm was tested for reverse faults using polarizing voltage. A fault was applied on transmission line L_1 shown in Figure 6.1. This condition should appear as a fault in reverse direction to a relay installed to see faults at L_5. Figure 6.30 shows the output of A-B, B-C and C-A relays for A-B reverse fault. It can be seen that none of the relays operate in this case, implying that the proposed algorithm maintained directional security of the relay.

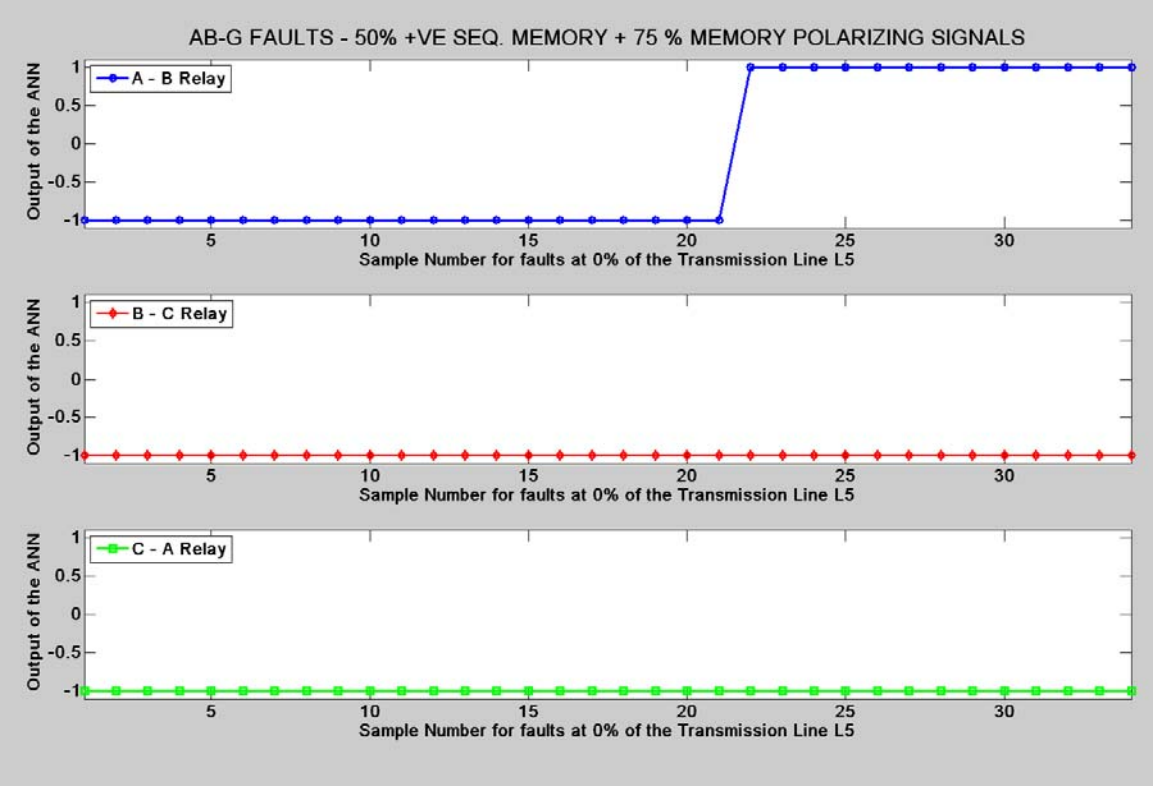

Figure 6.31: AB-G Forward Fault-75% Self and 50% Positive Seq. Memory Polarization

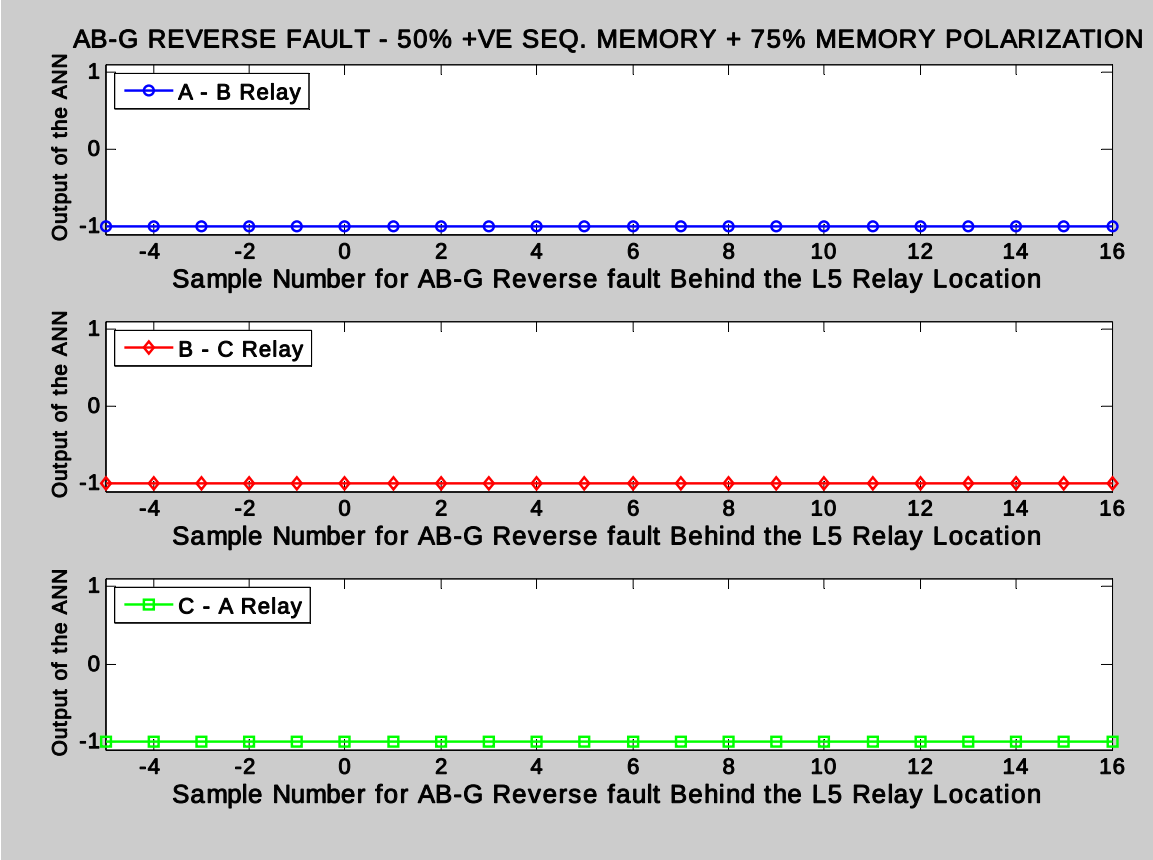

Figure 6.32: AB-G Reverse Fault-75% Self and 50% Positive Seq. Memory Polarization

6.4.2 Double Line to Ground Faults

The polarization schemes used for line to line faults were used for double line to ground faults as well. The ANN performed well for all these cases and showed good consistency. The results for all fault locations for cross polarization, self & positive memory polarization and their combinations were tested. One of the fault cases is discussed in this section.

As in case of line to line faults, 50% positive sequence memory and 75% self memory polarization voltages were added to test if a combination was able to detect all types of faults while maintaining the integrity of relay boundary. Figure 6.31 shows the outputs of three phase relays for an AB-G ground fault at 0 km of transmission line using 50% positive sequence memory and 75% self memory polarization voltages. The output and fault detection time of A-B relay did not change when this combination of memory

polarization was used. B-C and C-A relays did not operate in this case unlike when self-polarizing voltages were used. The other results show that the ANN was able to detect faults in less than one cycle for all the cases and did not operate for faults the relay protection zone. The other results for this combination of polarization are given in Appendix G, Figures G.222 to G.229.

The directional discrimination capability of the ANNs was tested by applying an AB-G reverse fault behind the relay location. The results obtained are shown in Figure 6.32. It was noticed that none of the relays operated for a double line to ground fault, thus, preserving the directional security of the proposed algorithm.

6.4.3 Three Phase to Ground Faults

Figure 6.33 shows the outputs of phase relays for an ABC-G fault at 0% length of the transmission line using 50% positive sequence memory and 75% self memory polarization voltages. It can be seen that the ANN took a total of 21 samples, or 14.58 ms to detect a fault. The ANN worked well for individual tests using these polarization voltages as well. Figure G.230 to G.236 present the results for other fault locations for ABC-G faults using this polarization scheme. It can be seen that all the three relays pick up a fault for a symmetrical three phase fault.

Figure 6.34 shows the results for an ABC-G reverse fault on transmission line L_1. None of the relays detected a fault when a reverse fault occurred and thus were able to discriminate between forward and reverse faults when polarizing voltage was used.

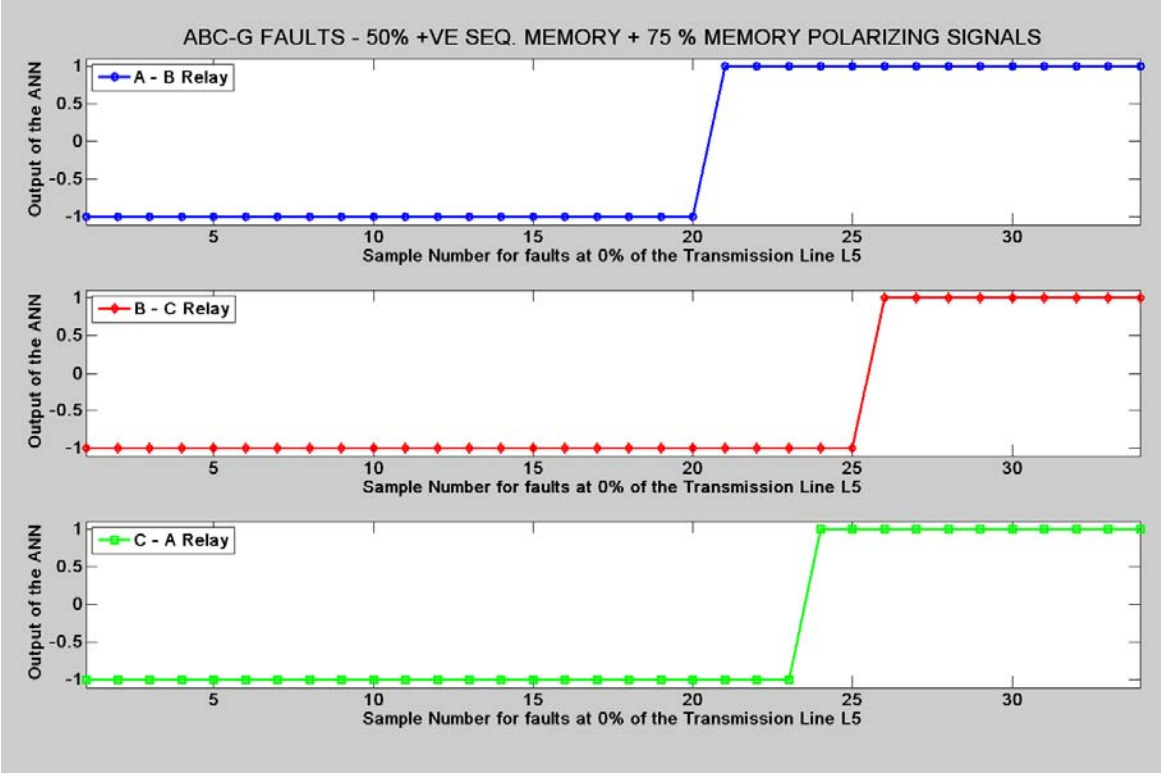

Figure 6.33: ABC-G Forward Fault-75% Self and 50% Positive Seq. Memory Polarization

6.4.4 Single Line to Ground Faults

The ground relays (A-G, B-G and C-G) relays performed well with self-polarizing voltages. These relays were tested using some of the polarization techniques to ensure reliability and consistency of the proposed algorithm for different types of faults. The results that are given in Appendix G can be summarized as:

- Cross Polarization

Both 10% and 20% cross polarization performed well for close-in faults. The results with 10% cross polarization for SLG faults are presented in Appendix G in Figure G.120 to G.128. It was observed that a small percent of cross polarization was enough to detect close-in faults. For faults farther away from the relay location, the percentage of polarizing voltage had to be increased.

- Self Memory Polarization

The results using 100% memory polarization and 75% memory polarization are shown in Figures G.129 to G.152 and Figures G.153 to G.176 respectively. It was observed during

the tests that a memory polarization less than 50% of the original voltage did not work well for remote faults.

- 75% Self Memory and 10% Cross Polarization

Figures G.177 to G.200 show the results when these two voltages were added for detecting single line to ground faults.

- Positive Sequence Memory Polarization

Figure G.201 to Figure G.213 show the results of positive sequence memory polarization for SLG faults on the transmission line L_5. It was observed that the positive sequence polarization technique also performed well when combined with other polarization techniques. Due to space constraints, those results are not included in the thesis.

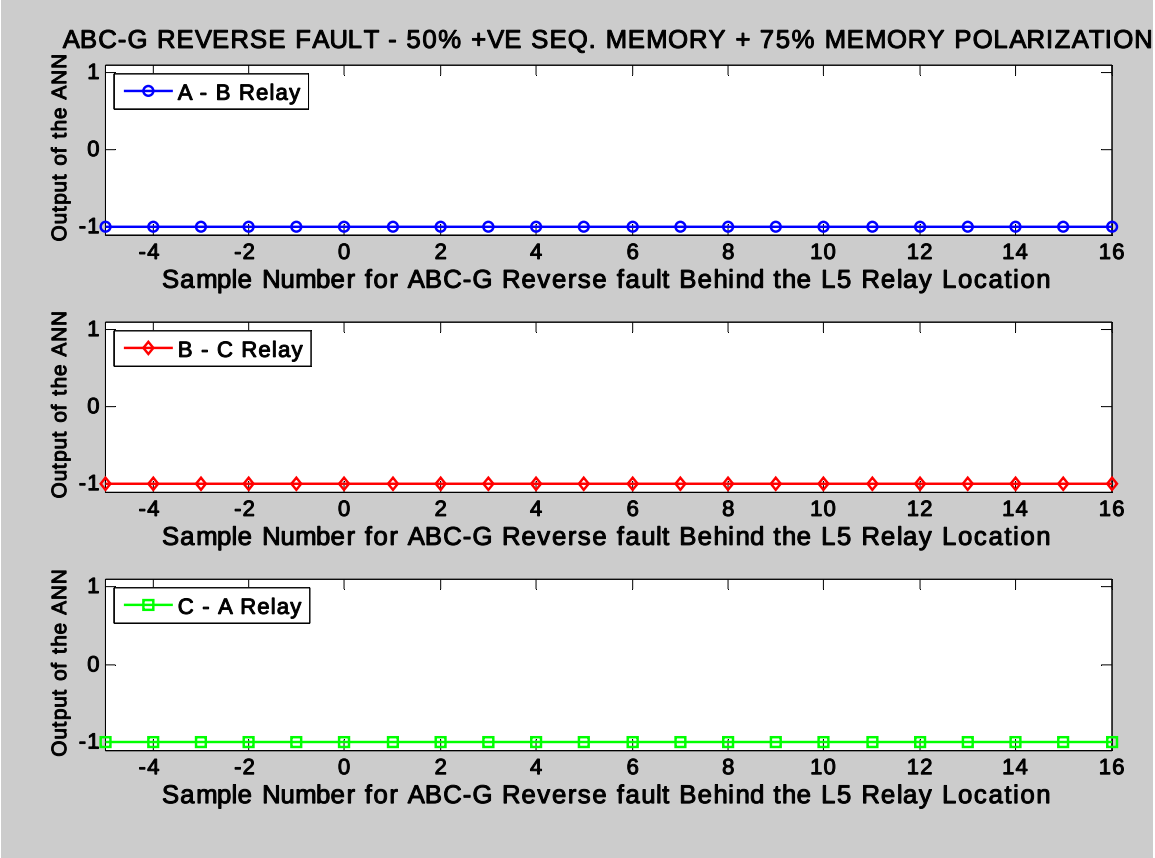

Figure 6.34: ABC-G Reverse Fault-75% Self and 50% Positive Seq. Memory Polarization

6.4.4 Discussion

Different polarization techniques and their combinations were used to test the designed relays. Addition of two or more polarizing voltages helped to eliminate some of the deficiencies of individual polarization techniques. It was observed that techniques that performed well individually worked equally well when they were added. The presented polarizing technique also helped in avoiding unwanted tripping of phase-phase relays for double line and double line to ground close-in faults.

The memory polarized relays were further tested for reverse faults to ensure their directional discrimination capability. None of the relays operated for a reverse fault, which suggests that the proposed algorithm is able to discriminate between forward and reverse faults. Due to time and space restrictions, only few combinations of polarizations were tested. Other percentages of polarization voltages can be tested as future work to achieve a combination that performs well in all circumstances.

6.5 Performance in the Presence of Fault Resistance

The designed admittance relay was tested for high resistance single line to ground fault. A-G fault at 75% length of the transmission line with a fault resistance of fifty (50) ohms was simulated in PSCAD. The current and voltage at relay location were processed as previously described and the designed ANN was tested by applying the processed inputs. The outputs of three ground relays obtained in this case are shown in Figure 6.34. It can be seen that the A-G relay did not pick up this high resistance fault and the output of all three A-G, B-G and C-G relays remained -1 after the fault inception. The analysis of this result was therefore, conducted.

Addition of a 50Ω fault resistance translates to an impedance point outside the designed relay admittance characteristic. Therefore, the relay performs accurately if *only* the relay characteristic is taken into account. However, if this relay is implemented at a site where chances of a high fault resistance are likely, the relay may not be able to detect a ground fault. This condition applies in any conventional relay as well.

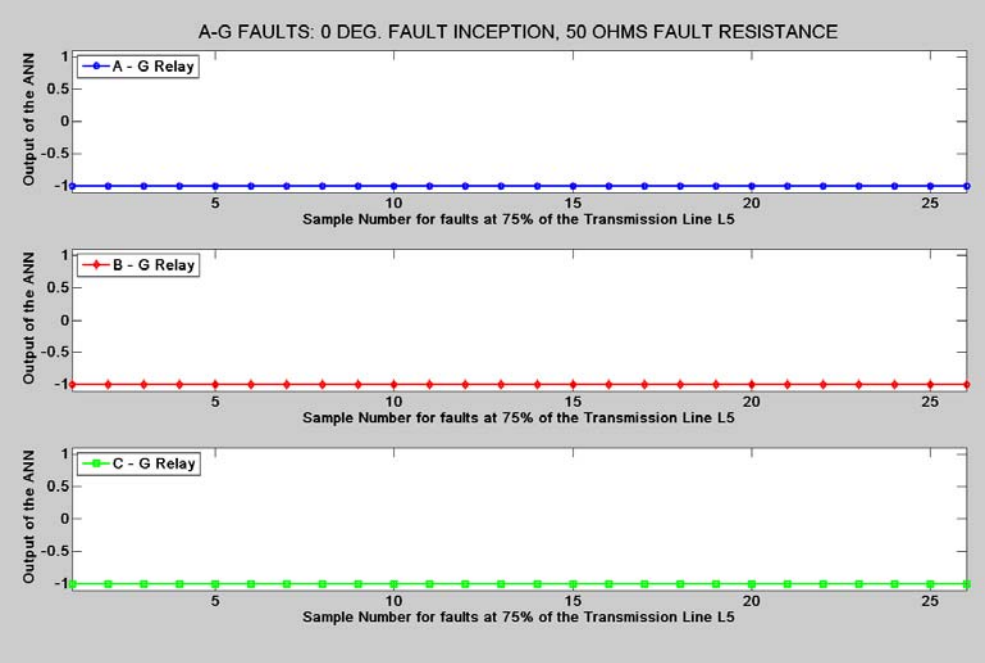

Figure 6.35: Relay Output for A-G Fault at 75% length of L_5, Fault Resistance of 75Ω

To improve resistive coverage for such a relay, one option may be to increase the diameter of the relay characteristic. However, this will also increase the impedance reach of the relay. A blinder can be used in addition to this relay to reduce the impedance reach to a desired value as shown in Figure 6.36. One major limitation of such a method is that the relay characteristic may interfere with the load impedance zone and may cause incorrect tripping of a relay under heavy load conditions. This option was, therefore, considered impractical.

Another option for such locations is using a quadrilateral relay that can be designed using different set of blinders as described in the Chapter 5. This was the main motivation to design a quadrilateral relay using the proposed algorithm. The next section presents various cases for which the designed quadrilateral relay was tested. Only one fault case of an A-G fault in the presence of a 50Ω fault resistance is discussed in detail. All the other test results can be found in Appendix G; the corresponding figures are referred to in each section.

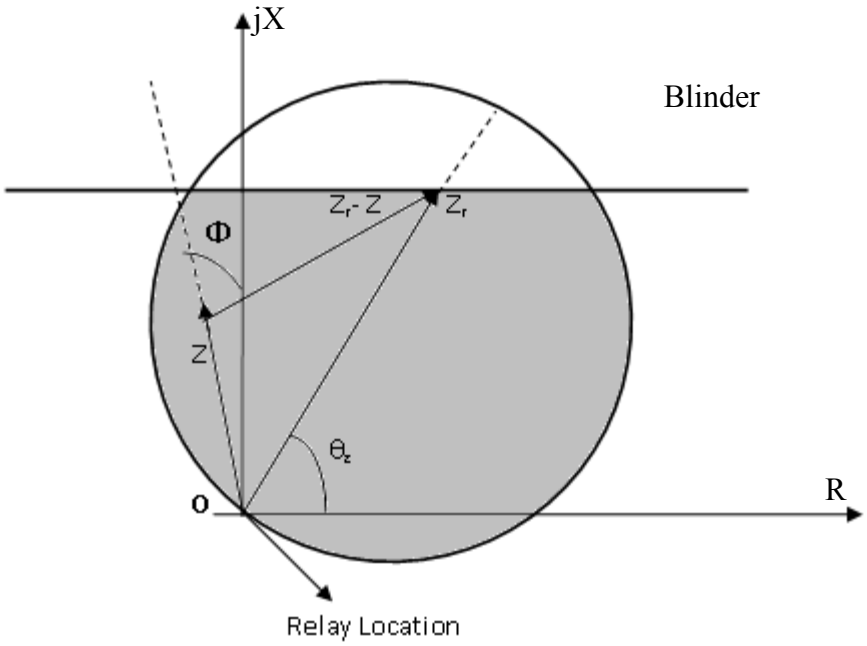

Figure 6.36: Addition of Blinder Characteristic to an Admittance Relay

6.5.1 Quadrilateral Relay Performance for Single Line to Ground Faults

The Quadrilateral relay algorithm was tested for seven fault locations on the transmission line. This included faults applied at 0%, 5%, 20%, 75%, 80%, 85% and 95% length of L_5. Other parameters that were considered for testing the quadrilateral relay are:

- Fault Inception Angle: Fault inception angles of 0° and 90° were considered.
- Fault Resistance: Fault resistances of 0Ω, 15Ω and 50Ω were considered.
- Different Types of Faults: The relay was tested for single line to ground, phase to phase, two phase to ground and three phase faults.

Single line to ground fault tests were conducted for two different fault inception angles and fault resistances of 0Ω, 15Ω and 50Ω. A fault inception angle of 0° and fault resistance of 0Ω were considered for two phase and three phase faults. It should be noted that the purpose of testing the relay for two and three phase faults was to test the reliability of the quadrilateral relay for these different faults. Variation in fault inception angle and fault resistances was not considered for these fault types.

The currents and voltages before, during and after applying a fault were processed for the four different relay characteristics and applied to the individual trained ANNs as explained in Chapter 5. The output of these four ANNs was applied to the "AND" 4-1 ANN and the output was noted. Figure 6.37 shows the output of the three ground relays when the designed quadrilateral relay was tested for a single line to ground fault at 75% length of transmission line, for a 0° fault inception angle and 50Ω fault resistance. The result show that the A-G relay implementing a quadrilateral characteristic was able to detect a fault in about 7.64ms, before one data window was full of 13 fault samples. B-G and C-G relays did not pick up a fault in this case and their output remained -1.

The other results for a 50 Ω fault resistance, both for 0° and 90° fault inception angles are shown in Figures G.95 to G.107. The result presented here shows that addition of fault resistance of 50Ω does not affect the performance of a quadrilateral relay. This is because a desired value of fault resistance can be accounted for when designing a quadrilateral relay while blocking off the load impedance zone using a blinder. Analysis of currents and voltages during this fault case showed that the impedance point lies inside the quadrilateral relay boundary, therefore, the relay operated correctly.

The results show that in almost all cases, the fault is detected before the data window (thirteen samples) is full of all fault samples, resulting in a fault detection time of about half cycle. No faults are detected by B-G and C-G relays. Further, the A-G relay does not detect any fault outside its protection zone, thus maintaining the integrity of the relay boundaries.

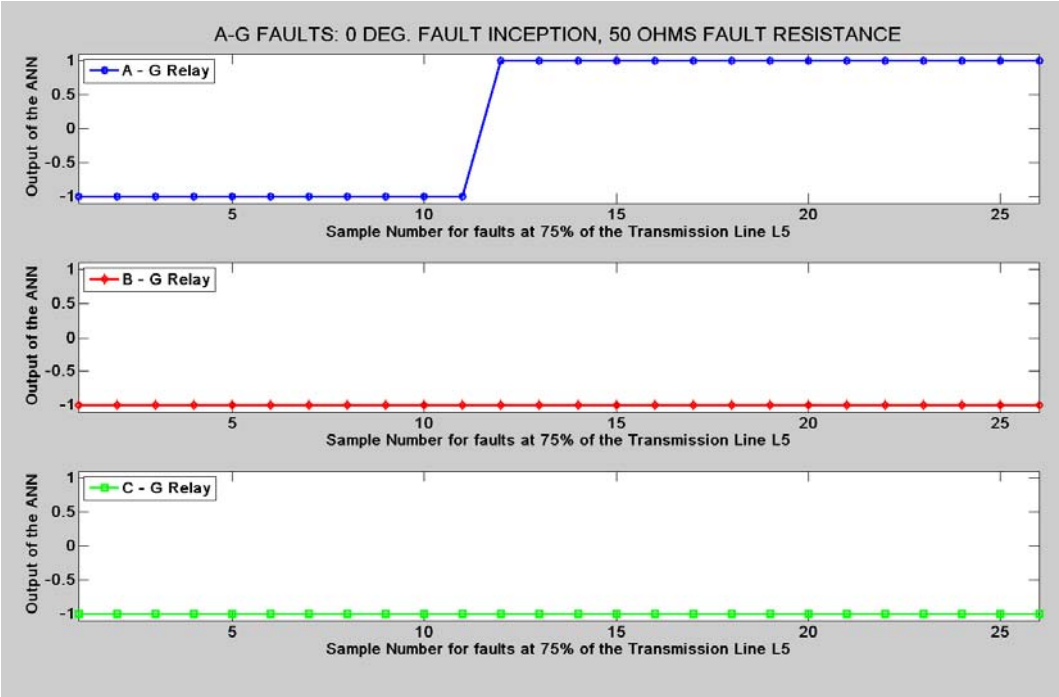

Figure 6.37: Quadrilateral Relay for A-G Fault at 75% Length of L_5

6.5.1.1 Performance for Different Fault Resistances

(a) No fault resistance: The A-G relay was able to detect line to ground faults for five different fault locations for a fault inception angle of 0º and zero ohms fault resistance. The B-G and C-G relays did not detect an A-G fault in any of these cases. The relay detected a fault in less than one cycle in all cases and in less than half a cycle for remote faults. The A-G relay did not detect a fault outside the relay boundaries, thus operating only within the specified protective zone.

The results for single line to ground faults without any fault resistance for a 90° fault inception angle show that the relay detected faults close to the relay location (0% and 5%) is less than quarter of a cycle. Remote faults were detected in less than one cycle, as in other cases. The relay did not detect a fault for faults located at 80% or beyond on the transmission line. The results show that the designed relay did not get affected by fault inception angle and was able to perform consistently. The B-G and C-G relays did not detect any fault in all these cases.

(b) Performance for fifteen ohms fault resistance: Figures G.81 to G.87 show the results for single line to ground faults for a fault inception angle of 0º when a fault resistance of 15Ω was added to the fault circuit. The test results for an A-G fault with a 15Ω fault resistance and 90° fault inception angle are results are shown in Figures G.88 to G.94.

The results of the quadrilateral relay do not get affected by 15Ω fault resistance. On the contrary, addition of 15Ω fault resistance translates to a fault well within the relay boundary. The results show a decrease in fault detection time. The relay detected a fault in less than half cycle of fundamental frequency in almost all the cases. The integrity of relay boundary is preserved as no faults outside the protection zone were detected.

6.5.2 Extension of Quadrilateral Relay Algorithm for Two and Three Phase faults

The quadrilateral relay algorithm was tested for line to line, double phase to ground and three phase to ground faults using the same processing method as in the case of an admittance relay. These tests were conducted only for zero ohms fault resistance. Line to Line (A-B) and Double line to ground fault (AB-G) detection results for faults on these different locations of transmission line L_5 are shown in Figures G.108 to G.111 and G.112 to G.115 respectively. It can be seen in all tests that the output of the relay becomes +1 in less than one cycle after applying a fault.

Figures G.116 to G.119 show the test results for cases when a symmetrical three phase to ground fault (ABC-G) was applied at different locations of transmission line L_5. The results show that the ANN detected a fault in less than one cycle in all these cases. The ANN did not detect a fault beyond 85% of the transmission line. These results prove reliability of the design for two and three phase faults.

6.6 Consistency Tests for Faults Close to the Relay Location

The ANN performed well for all the patterns using which it was trained in MATLAB. It also gave accurate results for other values of impedance points inside the relay protection zone, both close and away from the relay boundary. This section presents the results

obtained by testing the trained ANN relay very close to its location. Ten concentric circles at an interval of 0.01 p.u. were plotted around the origin of the admittance relay characteristic as shown in Figure 6.38. For a 360º span of a circle, impedance points were taken at each 15º, resulting in twenty-four impedance points on each circle. Currents and voltages produced for these points were processed as applied to the ANN. The ANN performed accurately for each of these points i.e. it gave a positive output for all fault patterns and negative output for all non-fault patterns.

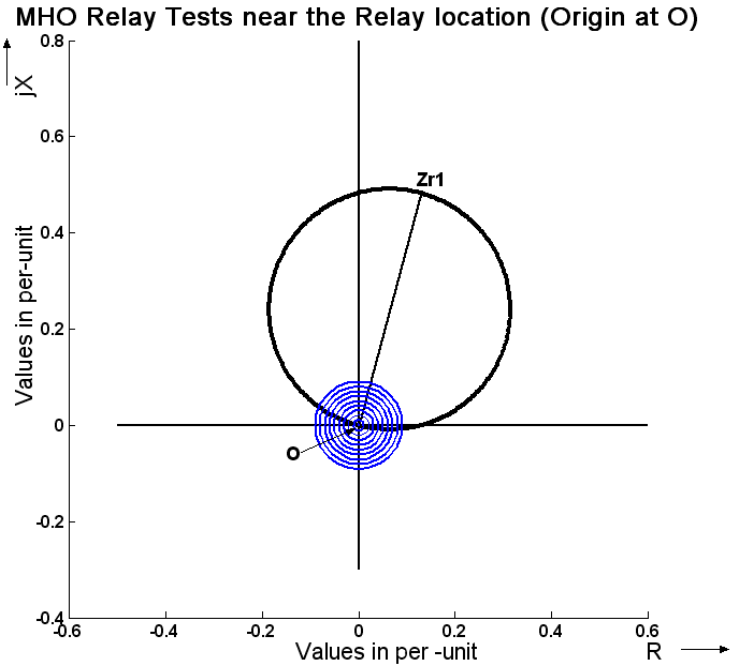

Figure 6.38: Consistency Tests for Close-in Faults

The angle between the processed inputs was calculated for each of these impedance points to distinguish fault and non-fault patterns. The performance of the ANN was evaluated further by "micro-testing" the ANN only for impedance points where the angle between the processed inputs changed from the [-90º, 90º] range to angles belonging to non-fault range (i.e. less than -90º or more than +90º). Since the impedance points had been taken all around the origin, this also tested the accuracy of the ANN for faults behind the relay (in the reverse direction).

Table 6.1(a) and 6.1(b) show the results for each of these ten radii, the angle between the processed inputs and the expected and obtained outputs.

Table 6.1(a): Consistency Tests' Results: Part 1

Radius (in p.u.)	Angle of Impedance Z	Angle between Processed Inputs	Expected Output	Obtained Output
0.01	171º	97.14º	-1	-0.0743
0.02	169º	96.28º	-1	-0.4100
0.03	165º	93.43º	-1	-0.2950
0.04	161º	90.59º	-1	-0.3092
0.05	161º	91.74º	-1	-0.1701
0.06	160º	91.89º	-1	-0.8456
0.07	159º	92.04º	-1	-0.8126
0.08	157º	91.20º	-1	-0.1705
0.09	156º	91.37º	-1	-0.8979
0.1	155º	91.53º	-1	-0.1620

The results shown are for impedance values closest value +90º or -90º for angle between the processed inputs where the ANN is able to perform correctly for each radius.

Table 6.1(b): Consistency Tests' Results: Part 2

Radius (in p.u.)	Angle of Impedance Z	Angle between Processed Inputs	Expected Output	Obtained Output
0.01	-12º	-88.15º	+1	0.1325
0.02	-14º	-91.29º	-1	-0.3995
0.03	-13º	-91.44º	-1	-0.4324
0.04	-9º	-88.59º	+1	0.8847
0.05	-8º	-88.74º	+1	0.9223

0.06	-8º	-89.89º	+1	0.7198
0.07	-7º	-90.05º	-1	-0.0902
0.08	-4º	-88.20º	+1	0.9779
0.09	-5º	-90.37º	-1	0.5856
0.1	-3º	-89.54º	+1	0.7200

6.7 Comparison of the ANN Results with a Conventional DFT Algorithm

This section presents a comparison of results obtained by the proposed algorithm and a conventional numerical algorithm. A DFT algorithm was applied to currents and voltages obtained by applying faults in PSCAD. Three phase faults were considered for comparison. This section presents the results obtained in the form of an impedance trajectory for faults on 5% (within the relay protection zone) and 40% (mid-line fault) of the transmission line. Since a three-phase fault was considered, the apparent impedance seen at the relay location by the A-B phase relay can be given as:

$$Z_{apparent} = \frac{\vec{V}_a - \vec{V}_b}{\vec{I}_a - \vec{I}_b} \tag{6.2}$$

The voltage phasors $\vec{V}_a$ and $\vec{V}_b$ and the current phasors $\vec{I}_a$ and $\vec{I}_b$ were calculated using a full cycle DFT algorithm and the apparent impedance was calculated using equation 6.2.

Figure 6.39 shows trajectory of the impedance as seen at the relay location, for a three-phase to ground fault applied at 5% of the transmission line. The first sample indicates the instant after the data window is full of one cycle (24) of fault samples. It can be seen that the fault is detected at 2nd sample, which indicates that the algorithm took a total of 26 samples (= 18.0555 ms) to detect a fault. The time taken by the proposed algorithm is previously shown in Figure 6.24. The designed ANN took eight samples to detect the fault after one data window is full of fault samples (13), resulting in a total of 21 samples (= 14.5833 ms).

Figure 6.40 shows the apparent impedance trajectory for a three phase to ground fault at 40% length of the transmission line. The DFT algorithm took 18.0555 ms to detect a fault at 40% length of the transmission line. It can be seen in Figure 6.27 in that the proposed algorithm detected the fault at 1st sample after the fault inception, resulting in a fault detection time of 9.0277 ms. The fault detection time, therefore, for proposed algorithm is almost half the time taken by the conventional phasor estimation algorithm for the same fault. This is a significant reduction in time, especially in the case of distance relays, where fault detection time is of critical importance.

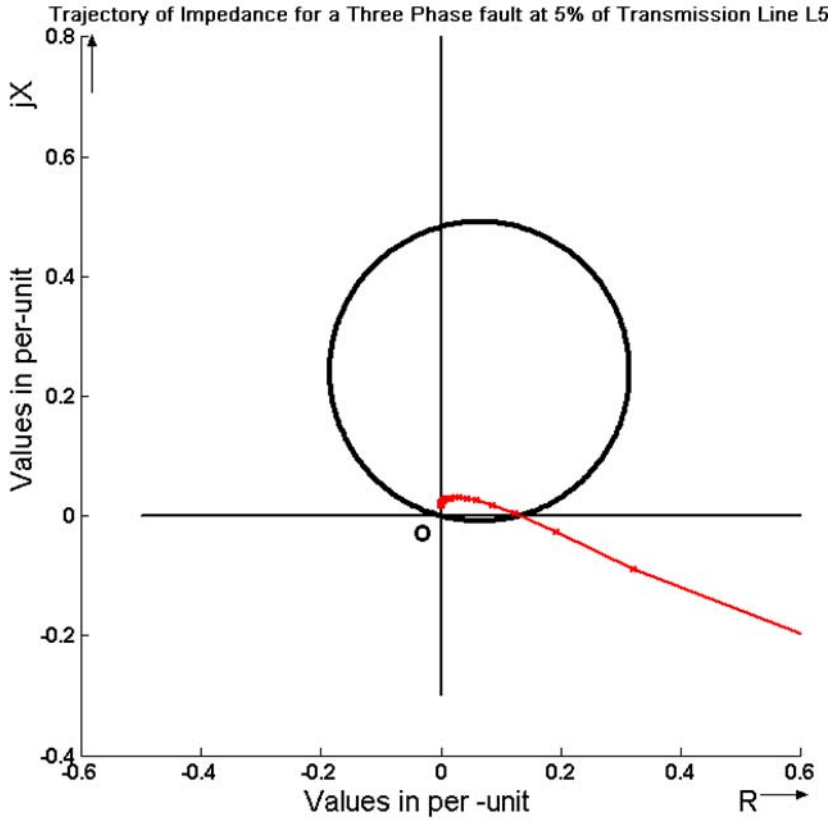

Figure 6.39: Trajectory of Impedance for a 3Φ fault at 5% of Transmission Line

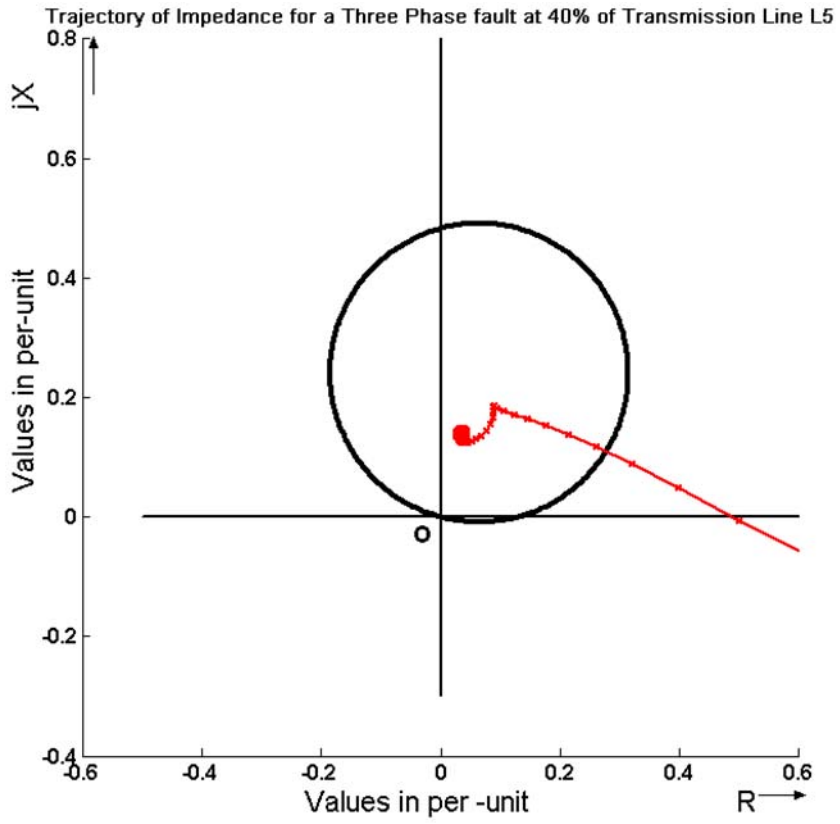

Figure 6.40: Trajectory of Impedance for a 3Φ fault at 40% of Transmission Line

6.8 Summary

This chapter presents the results obtained by testing the designed relays for different types of faults. Polarization techniques were inculcated into the proposed algorithm and results are presented in cases where polarization techniques were combined to detect two and three phase faults. Polarized relays were tested for reverse faults to ensure that the proposed algorithm maintains directional discrimination capability of a mho relay.

The performance of the designed admittance relay was evaluated in the presence of high fault resistance. A solution for such circumstances was provided by implementing the characteristic of a quadrilateral relay. The consistency of the algorithm for faults very close to relay location is presented. The proposed algorithm results are compared with the results obtained using a conventional DFT algorithm.

7. SUMMARY AND CONCLUSIONS

7.1 Summary

The occurrence of faults in a power system can cause extensive damage to the equipment. In addition, these occurrences can also cause injury to personnel and substantial losses to electrical utilities and the consumers. A protective relaying system should be able to minimize this damage due to faults and other abnormal operating conditions by isolating the faulted equipment as soon as possible. This is significant to ensure safe and reliable operation of an electrical power system.

Protective relays play a vital role in power system protection. The last decade has seen vast improvements in operation and reliability of relays. Artificial Intelligence techniques such as neural networks are gaining a lot of interest from researchers and industry because of their robustness and generalization capabilities. Some research has been done to combine the existing numerical relay algorithms with neural networks.

The literature review of the relays proposed till now showed that the ANN relays lack generalization as they have been trained and tested on the same power system. The ANN relay, therefore, will need to be re-trained before implementation on a different system. Further, neural network relays have not been based on any relay characteristic; therefore, no clear operating boundary has been defined. The ANN relays use phasor estimation techniques as pre-processing tools instead of fully utilizing the pattern recognition capabilities of a neural network.

There is also a need to address the inherent deficiencies that exist in the conventional relay algorithms. The conventional relay algorithms use processes to estimate the relay inputs which may results in inaccuracies. The accuracy of numerical algorithms depends on phasor estimation technique used. Most algorithms require atleast one cycle of fundamental frequency to estimate relay inputs. This time may increase depending on fault location and presence of other frequency components in fault current and voltage.

Chapter 1 overviews basics of power system protection and neural network applications in power systems. This chapter presents a literature review of the research that has been done in the area of neural network based protective relaying, in last fifteen (15) years. The existing deficiencies in the numerical relays are discussed. This chapter also outlines the objectives of this research project. It provides a summary and organization of the thesis.

Chapter 2 presents the principles of protective relaying in detail. Different types of relays used for transmission line protection are discussed. The amplitude and phase comparison characteristics of different distance relays are explained. The polarization techniques associated with the operation of distance relays are presented. This chapter also presents a typical configuration of a numerical relay and its components. The principles of numerical relaying algorithms are discussed using mathematical equations.

The theory and principles of artificial neural networks is presented in Chapter 3. Different types of neural networks and their structures are described. Learning paradigms that are used for the training of neural networks are explained. This chapter also discusses the principle of resilient back-propagation that was used in this project. Multi-layer feed forward networks that were used in this research, are described in detail. This chapter also explains the design process of a neural network.

The limitations existing in traditional distance relay algorithms are described in Chapter 4. A new methodology that addresses these issues is proposed. Implementation of the proposed methodology in electromechanical, solid-state and numerical relays is also described. A full cycle DFT algorithm was used to prove the validity of the proposed algorithm and selected results are presented in this chapter.

The results presented in chapter 4 proved that the algorithm implements the generic characteristic of an admittance relay. Given that the characteristics of all distance relays are similar; the proposed design can be extended to design other protective relays in a similar manner. This was undertaken in Chapter 5, which discusses the extension of

proposed algorithm for different type of relays. The mathematical modifications for designing other relays are described in this chapter. Specifically, the application of the proposed algorithm for designing directional relay, reactance relay and blinders is discussed. These characteristics have been combined to form a quadrilateral relay.

Chapter 5 also discusses two different approaches that can be used for training the ANN. The training process, configuration and parameters of the selected neural network are discussed. The proposed design also has a provision to include different polarization techniques in cases when the magnitude of self-polarizing voltage is low or during the occurrence close-in faults. Polarization techniques that can be used for different types of faults are described.

In practice, white noise is present in any power system, mainly due to the presence of electronic components. The robustness of the trained neural network was tested for noisy inputs. A white Gaussian noise of SNRs of 30 dB, 20 dB and 10 dB was added to the processed fault and non fault relaying inputs; results are presented in this chapter.

Chapter 6 presents the results obtained by testing the ANN based relays. The ANNs were trained to implement the characteristics of different relays; these were tested for fault patterns at various fault locations on a transmission line. The relays were tested for all types of shunt faults (Single line to ground, line to line, double line to ground and three line to ground). The waveforms of currents and voltages and the processed inputs during faults are shown. The results for different fault conditions are presented.

The proposed algorithm was further tested for reliability during very close-in faults, both in forward and reverse directions and the results are presented. This chapter also presents the results obtained by applying polarization techniques. A comparative analysis of the proposed algorithm with a conventional phasor estimation technique was performed and results are presented in this chapter.

7.2 Contributions of the Research

A new algorithm for designing generic distance relays is presented in this dissertation. The algorithm was tested for different types of relays, fault inception instants and fault resistances. Specifically, this research has addressed the following main issues.

1. Implementation of Admittance Relay Characteristic

The neural network in the proposed design was trained to recognize pre-processed fault and non-fault patterns for admittance relay characteristic. The presented algorithm enabled the trained ANN to detect fault patterns while maintaining the integrity of relay boundaries. The neural network was trained with an impedance reach equal to 80% impedance of a transmission line. Test results proved that this impedance reach was maintained even when the neural network was implemented on a different power system. It can be concluded that the designed ANN worked as an admittance relay phase comparator with clearly defined operating boundary.

2. Development of other Relays

The presented design was extended for developing other distance relays and directional relays. All relays were trained and tested based on their individual phase comparator characteristics. Test results proved that the design was extensible to other relays.

3. Generic Nature of the Algorithm

The dissertation also explains the process by which the trained ANN can be used as a universal relay without any re-training. The ANN is dependent only on the phase angles between modified inputs. The results, therefore, did not get affected by the system where it was implemented. The relay was trained using sinusoidal inputs generated in MATLAB and implemented in PSCAD without any re-training. This proves the generic nature of the relay. The algorithm can also be applied for any value of impedance reach. The mathematical modifications are explained by means of an example and can be easily integrated into any relay design. This is in line with a practical power system where it is not feasible to train a relay every time it is implemented in a different power sytem.

4. Removal of Phasors and Fault Detection Time

Traditional ANN relays use phasor estimation algorithm for producing inputs, making the use of ANN redundant. This process also introduces a delay in the fault detection process. In the proposed design, the capabilities of a neural network were used to eliminate phasors. Sampled and quantized values of current and voltage waveforms were modified to obtain inputs for the relay. Phasor estimation algorithms were not used for ANN training or testing. The elimination of phasors helped to reduce the fault detection time taken by a conventional ANN relay for input pre-processing. The results prove that the algorithm is able to detect faults in about half a cycle (of fundamental frequency) in some cases and in less than one cycle in all cases. This is a significant reduction in time in comparison to conventional relay designs where the nominal fault detection time is about 1 - 2 cycles of fundamental frequency.

5. Flexibility and Accuracy of the Algorithm

The relay performed well for different types of faults. The neural network as tested for different fault inception angles and different fault resistances for five different relay designs. The neural network showed encouraging results in all these cases, proving the flexibility and accuracy of the proposed design.

6. Detection of Close-in Faults

Polarization techniques were used to make the algorithm flexible and accurate for detecting close-in faults. A technique for combining percentages of different polarizing voltages was introduced. Polarized relays were also tested for reverse faults; the results showed that the proposed algorithm maintained directional discrimination capability of an admittance relay.

7. Deficiencies of Conventional Relay Algorithms

Conventional algorithms use estimated values of currents and voltages leading to noisy results. This algorithm eliminates these inherent deficiencies present in conventional designs of distance relays. Mathematical modifications that facilitate the use of past values of currents and voltages for detection of faults are proposed. The implementation

of this algorithm for solid-state and numerical relays is presented. All the patterns used in the algorithm were based on actual values of currents and voltages; none of the values were estimated in the design.

7. 3 Conclusion

The algorithm presented in this thesis implements the phase comparator characteristic of a distance relay with a clear operating boundary. The neural network relay design is flexible and can be used a generic phase comparator without any re-training. The issues associated with conventional relay algorithms are addressed. Implementation of the proposed algorithm shows a significant improvement in results in comparison to conventional relay designs. Thus, it can be concluded that the objectives set for this research work have been successfully achieved.

REFERENCES

1. Walter A. Elmore, Protective relaying theory and applications, Marcel Dekker, New York, Revised Edition, 2004.
2. A.R. Warrington, Protective Relays – their theory and practice, Chapman and Hall, Vol. I 1962
3. C. R. Mason, The Art and Science of Protective Relaying, John Wiley and Sons, New York, 1956.
4. M. S. Sachdev, *Class Notes and Instructional Material for Power System Relays and Protection.*
5. M. S. Sachdev (Course Coordinator), Advancements in microprocessor-based protection and communication, IEEE Tutorial Course Text. Piscataway, NJ, IEEE Press, 1997.
6. T. S. Sidhu, H. Singh, and M. S. Sachdev, "Design, Implementation and Testing of an Artificial Neural Network-Based Fault Direction Discriminator for Protecting Transmission Lines", *IEEE Transactions on Power Delivery*, Vol. 10, No. 2, Apr. 1995, pp. 1002-1011.
7. A.L.O Fernandez and N.K.I Ghonaim, "A Novel Approach using a FIRANN for Fault Detection and Direction Estimation for High Voltage Transmission Lines", *IEEE Transactions on Power Delivery*, Vol. 17, No. 4, 2002, pp 894-900.
8. R.K. Aggarwal, A Bennett , R.W. Dunn , A.T. Johns and Q. Y. Xuann, "A Novel Classification Technique for Double-circuit lines Based on Combined Unsupervised/Supervised Neural Network", *IEEE Transactions on Power Delivery*, Vol. 14, No. 4, 1999, pp 1250-1255.
9. B. Balamurugan, R. Venkatesan, "A Real-Time Hardware Fault Detector Using an Artificial Neural Network for Distance Protection", *IEEE Transactions on Power Delivery*, Vol.16, No. 1, Jan 2001, pp 75-82.
10. A.L.Orille-Fernandez, Jaime A. Valencia , N.K.I Ghonaim, "A FIRANN as a Differential Relay for Three Phase Power Transformer Protection", *IEEE Transactions on Power Delivery*, Vol.16, No. 2, April 2001, pp 215-218.
11. Abdel-Maxoud I. Talaab, Hatem A. Darwish, Tamer A. Kawady, "Development and Implementation of an ANN-Based Fault Diagnosis Scheme for Generator

Winding Protection", *IEEE Transactions on Power Delivery*, Vol.16, No. 2, April 2001, pp 208-214.

12. Howard Demuth, Mark Beale, *Neural Network Toolbox, User's Guide, Version 5* The Math Works Inc., 2006.
13. T.S. Sidhu, L. Mital, M.S. Sachdev, "A Comprehensive Analysis of an Artificial Neural Network Based Fault Direction Discriminator", *IEEE Transactions on Power Delivery*, Vol.19, No. 3, July 2004, pp 1042-1048.
14. A.M. Sharaf, L.A. Snider, K. Debnath, "A Neural Network Based Relaying Scheme for Distribution System High Impedance Fault Detection", *Proceedings of First New Zealand International Two-Stream Conference on Artificial Neural Networks and Expert Systems*, 1993.
15. R.K. Aggarwal, A.T. Johns, Y.H. Song, R.W. Dunn, D.S. Fitton, "Neural-network Based Adaptive Single-pole Auto Reclosure Technique for EHV Transmission Systems", *IEE Proceedings on Generation, Transmission and Distribution,* Vol.141, No. 2, March 1994, pp 155-160.
16. W. Qi, G.W. Swift, P. G. McLaren, A.V. Castro, "An Artificial Neural Network Application to Distance Protection", *Proceedings of International Conference on Intelligent Systems Applications to Power Systems (ISAP '96)*, February 1996, pp 226-230.
17. F. Zahra, B. Jeyasurya and J. E. Quaicoe, "High-speed Transmission Line Relaying using Artificial Neural Networks ", *Electric Power Systems Research*, Volume 53, Issue 3, March 2000, Pages 173-179.
18. S.A. Khaparde, N. Warke, S.H. Agarwal, "An Adaptive Approach in Distance Protection using an Artificial Neural Network", *Electric Power Systems Research* Volume 37, January 1996, Pages 39-44.
19. M. Sanaye-Pasand, H. Khorashadi-Zadeh, "Transmission Line Fault Detection & Phase Selection using ANN", *International Conference on Power Systems Transients – IPST,* 2003, New Orleans, USA
20. T. Dalstain, and B. Kulicke, " Neural Network-Approach to Fault Classification for High Speed Protective Relaying ", *IEEE Transactions on Power Delivery*, Vol. 10 , No. 2, Apr. 1995, pp. 1002-1011.
21. M. S. Sachdev , H. C. Wood and N.G. Johnson, "Kalman Filtering Applied to Power System Measurements for Relaying", *IEEE Transactions on Power Apparatus and Systems*, Vol. PAS-104, Dec. 1985, pp. 3565-3573.

22. M. Nagpal and M. S. Sachdev, “A Recursive Least Error Squares Algorithm for Power System Relaying and Measurement Applications”, *IEEE Transactions on Power Delivery,* Vol. 6, No. 3, July 1991.
23. A. G. Phadke and J. S. Thorp, Computer Relaying for Power Systems. New York: Wiley, 1988.
24. Tarlochan S. Sidhu, Daljit S. Ghotra, and Mohindar S. Sachdev, “An Adaptive Distance Relay and its Performance Comparison with a Fixed Data Window Distance Relay”, *IEEE Transactions on Power Delivery*, Vol. 17, No. 3, July 2002. pp 691-697
25. S. Ebron, S. D.L. Lubkeman, M. White, “A Neural Network Approach to the Detection of Incipient Faults on Power Distribution Feeders”, *IEEE Transactions on Power Delivery*, Vol.5, No. 2, April 1990, pp 905-914.
26. B. Kulicke, W. Bayer, K.H. Kriiger, D. Povh, “Studies for HVDC and SVC using the NETOMAC Digital Program System”, *IEEE PES/CSEE Joint Conference on High Voltage Transmission Systems*, Beijing, China, October 17-22, 1987.
27. H. Dommel, “EMTP Reference Manual,” Bonneville Power Administration 1986.
28. D. V. Coury and D. C. Jorge, “Artificial Neural Network Approach to Distance Protection of Transmission Lines”, *IEEE Transactions on Power Delivery*, Vol. 13, No. 1, January 1998, pp 102-108.
29. M. Sanaye-Pasand and O. P. Malik, “Implementation and Laboratory Test Results of an Elman Network-based Transmission Line Directional Relay,” *IEEE Transactions on Power Delivery*, Vol. 14, July 1999, pp. 782–788.
30. Slavko Vasilic and Mladen Kezunovic, "Fuzzy ART Neural Network Algorithm for Classifying the Power System Faults", *IEEE Transactions on Power Delivery*, Vol. 20, No. 2, April 2005, pp 306-1314.
31. H. Wang and W. W. L. Keertipala, “Fuzzy-neuro Approach to Fault Classification for Transmission Line Protection,” *IEEE Transactions on Power Delivery*, Vol. 13, No. 4, 1998, pp. 1093–1103.
32. P. K. Dash, A. K. Pradhan and G. Panda, “A Novel Fuzzy Neural Network Based Distance Relaying Scheme”, *IEEE Transactions on Power Delivery*, Vol. 15, No. 3, July 2000, pp 902-907.
33. A. H. Osman, Tamer Abdelazim and O. P. Malik, “Transmission Line Distance Relaying using On-Line Trained Neural Networks”, *IEEE Transactions on Power Delivery*, Vol. 20, No. 2, April 2005, pp 1257- 1264.

34. Simon Haykin, "Neural Networks: A Comprehensive Foundation", Second Edition, Prentice Hall, New Jersey, 1999.
35. L. Mital, "A Technique for Analysis of Artificial Neural Network Based Fault Direction Discriminator", *M.Sc. Thesis*, University of Saskatchewan, Canada, 2003.
36. PSCAD/EMTDC User's Manual, Manitoba HVDC Research Center, Winnipeg, Manitoba, Canada.
37. A. Osman, T. Abdelazim, and O. P. Malik, "Adaptive Distance Relaying Technique using On-line Trained Neural Network," *Proceedings of IEEE PES General Meeting*, Toronto, ON, Canada, Jul. 2003.
38. V. Cook, Analysis of Distance Protection, Research Studies Press Book, London, 1985.
39. Y.G. Paithankar, Transmission Network Protection – Theory and Practice, Marcel Dekker Inc., New York 1998.
40. H.Singh, "An Artificial Neural Network Based Fault Direction Discriminator for Protecting Transmission Lines", *M.Sc. Thesis*, University of Saskatchewan, Canada, 1994.
41. Qi Weiguo, "Application of Artificial Neural Networks to Distance Protection", *Ph.D. Dissertation*, University of Manitoba, Canada, 1997.
42. Ioni T. Fernando, "Protection of Transmission Lines Sharing the Same Right-of-ay", *Ph.D. Dissertation*, University of Manitoba, Canada, 1997.
43. Fatima Zahra, "Artificial Neural Network Approach to Transmission Line Relaying", *M. Eng Thesis*, Memorial University of Newfoundland, Canada, 1998.
44. A.R. Warrington, Protective Relays – their theory and practice, Chapman and Hall, Vol.2, 1977.
45. B. Ravindranath and M. Chander, Power System Protection and Switchgear, Wiley Eastern Limited, New Delhi, 1977.
46. Gerhard Ziegler, Numerical Distance Protection – Principles and Applications, Siemens AG, Berlin and Munich, Germany 1999.
47. A.G. Phadke *et. al,* "Synchronized Sampling and Phasor Measurements For Relaying and Control", *IEEE Transactions on Power Delivery*, Vol. 9, No. 1, January 1994, pp. 442-452.
48. Bart and Kosko, Fuzzy Thinking: The New Science of Fuzzy Logic, Hyperion, New York, 1993.

49. Timothy J. Ross, Fuzzy Logic with Engineering Applications, International Edition, Mc-Graw Hill, Inc., 1995.
50. Lofti Asker Zadeh**,** Fuzzy logic: Advanced Concepts and Structures, IEEE Educational Activities Board, Piscataway, New Jersey, 1992.
51. George Bojadziev and Maria Bojadziev, Advances in Fuzzy Systems – Applications and Theory Vol. 5 (Fuzzy Sets, Fuzzy Logic, Applications), World Scientific Publishing Co. Pte Ltd., 1995.
52. Biswarup Das and J. Vittal Reddy, "Fuzzy-Logic-Based Fault Classification Scheme for Digital Distance Protection", *IEEE Transactions on Power Delivery*, Vol. 20, No. 2, April 2005, pp 609-616.
53. A. Ferrero, S. Sangiovanni, and E. Zapitelli, "A Fuzzy Set Approach to Fault Type Identification in Digital Relaying," *IEEE Transactions on Power Delivery*, Vol. 10, January 1995, pp. 169–175.
54. A. A. Girgis and M. B. Johns, "A Hybrid Expert System for Faulted Section Identification, Fault Type Classification and Selection of Fault Location Algorithms," *IEEE Transactions on Power Delivery*, Vol. 4, April 1989, pp. 978–985.
55. C. A. Protopapas, K. P. Psatiras, and A. V. Machias, "An Expert System for Substation Fault Diagnosis and Alarm Processing," *IEEE Transactions on Power Delivery*, Vol. 6, Apr. 1991, pp. 648–655.
56. Héctor. O. Pascual, Jorge L. Dampé and José A. Rapallini, "Behaviour of Current Transformers (CT's) under severe saturation conditions", *Proceedings of the International Conference on Power Systems Transients*, Brazil, 2001.
57. IEEE Standard Dictionary of Electrical and Electronic Terms, John Wiley & Sons, Inc., 1972.
58. T.S. Madhava Rao, Power system Protection, Tata McGraw Hill, New Delhi, 1981.
59. Madan. M. Gupta, *Class Notes and Instructional Material for Neural Networks.*
60. E. Barnard, "Optimization for training neural nets," *IEEE Transactions on Neural Networks*, Vol. 2, March 1992, pp 232-240.
61. Jacques de Villiers and Etienne Barnard, "Backpropagation Neural Nets with One and Two Hidden Layers", *IEEE Transactions on Neural Networks*, Vol. 4, No. 1, January 1992 , pp 136-141.

62. Kishan Mehrotra, Chilukuri K. Mohan, Sanjay Ranka, Elements of Artificial Neural Networks – *Complex Adaptive Systems* (E-Book), Cambridge, Mass. MIT Press, 1997.
63. Anthony Adams, "Momentum in a Back Propagation Artificial Neural Network", *Proceedings of 4th Australian Joint Conference on Artificial Intelligence*, 1990.
64. M. Riedmiller, H. Braun, "A direct adaptive method for faster Backpropagation learning: the RPROP algorithm", *IEEE International Conference on Neural Networks*, 1993, pp 586 – 591.
65. E. O. Schweitzer III, Jeff Roberts, , "Distance Relay Element Design", Schweitzer Engineering Laboratories, Presented at Forty – Sixth Annual Conference for Protective Relay Engineers, Texas A&M University, Texas, April 12- 14, 1993.
66. David Mart, Damir Novosel, Fernando Calero, Eric Udren and LiFeng Yang, "Development of a Numerical Comparator for Protective Relaying: Part II", *IEEE Transactions on Power Delivery*, Vol. 11, No. 3, July 1996, pp 1274- 1284.
67. M. Kezunovic, Y.Q. Xia, Y. Guo C.W. Fromen, D.R. Sevcik, "An Advanced Method for Testing of Distance Relay Operating Characteristic", *IEEE Transactions on Power Delivery*, Vol. 11, No. 1, January 1996, pp 149-157.
68. Guang-Bin Huang, Yan-Qiu Chen, and Haroon A. Babri, "Classification Ability of Single Hidden Layer Feedforward Neural Networks", *IEEE Transactions On Neural Networks*, Vol. 11, No.3, May 2000, pp 799 - 801.
69. Fernando Calero, "Development of a Numerical Comparator for Protective Relaying: Part I", *IEEE Transactions on Power Delivery*, Vol. 11, No. 3, July 1996, pp1266-1273.
70. A. S. AlFuhaid and M. A. El-Sayed, "A Recursive Least-Squares Digital Distance Relaying Algorithm", *IEEE Transactions on Power Delivery*, Vol. 14, No. 4, October 1999, pp1257- 1262.
71. Khalil El-Arroudi, Géza Joós, Donald T. McGillis, and Reginald Brearley, "Comprehensive Transmission Distance Protection Settings Using an Intelligent-Based Analysis of Events and Consequences", IEEE Transactions on Power Delivery, Vol. 20, No. 3, July 2005, pp 1817-1824.
72. A. H. Osman, Tamer Abdelazim and O. P. Malik, "Transmission Line Distance Relaying Using On-Line Trained Neural Networks", *IEEE Transactions on Power Delivery*, Vol. 20, No. 2, April 2005, pp 1257- 1264.

73. M. M. Eissa and M. Masoud, "A Novel Digital Distance Relaying Technique for Transmission Line Protection", *IEEE Transactions on Power Delivery*, Vol. 16, No. 3, July 2001, pp 380-384.
74. Trinidad Segui, Pierre Bertrand, Matthieu Guillot, Pascal Hanchin, and Patrick Bastard, "Fundamental Basis for Distance Relaying with Parametrical Estimation", *IEEE Transactions on Power Delivery*, Vol. 16, No. 1, January 2001, pp 99-104.
75. IEEE Std. 242-2001, *the IEEE Buff Book*™, "IEEE Recommended Practice for Protection and Coordination of Industrial and Commercial Power Systems", Piscataway, NJ, IEEE Press, 2001.
76. Gaganpreet Chawla, Mohindar S. Sachdev and G. Ramakrishna, "Artificial Neural Network applications for Power Systems", *Proceedings of IEEE Canadian Conference on Electrical and Computer Engineering,* 2005, *Canada*.
77. Gaganpreet Chawla, Mohindar S. Sachdev and G. Ramakrishna, "An Improved Distance Protective Relaying Technique for Transmission Lines", *Proceedings of CIGRE Canada Conference on Power Systems,* October 2008, Winnipeg, Canada.
78. Gaganpreet Chawla, Mohindar S. Sachdev and G. Ramakrishna, "A Novel Algorithm for the Design of Distance Relays for the Protection of Transmission Lines", *Proceedings of International Conference on Advanced Power System Automation and Protection,* 2007, Korea.
79. Gaganpreet Chawla, Mohindar S. Sachdev and G. Ramakrishna, "Design, Implementation and Testing of an Artificial Neural Network based Admittance Relay", *Proceedings of IFAC Symposium on Power Systems and Power Systems Control, Calgary,* 2006, Canada.
80. Gaganpreet Chawla, Mohindar S. Sachdev and G. Ramakrishna, "An Improved ANN Based Admittance Relay Using Pre-Processed Inputs", *Proceedings of IEEE Conference & Exhibition on Control, Communication and Automation,* December 2008, Kanpur, India.

APPENDIX A: THE DISCRETE FOURIER TRANSFORM

The Discrete Fourier Transform has been used to test the validity of the proposed algorithm and some of the results have been presented in Chapter 4. The next two sections present the sine and cosine weights and the impedance points respectively used for the testing.

A.1 Sampled Sine and Cosine Waveforms

Figure A.1 show the sampled sine and cosine waveforms respectively. The sine and cosine weights used in the DFT test have been given in Table A.1 and A.2 respectively.

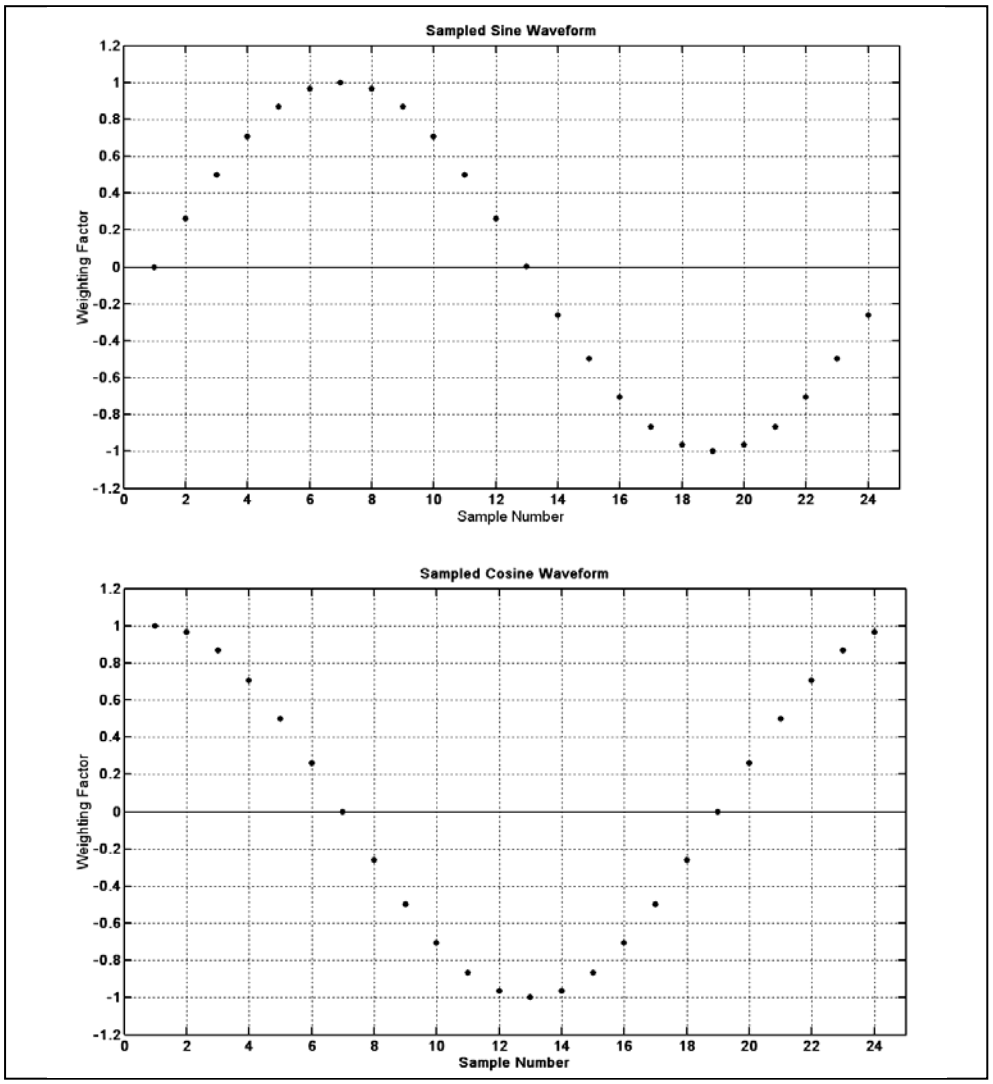

Figure A.1: Sine and Cosine Weights used for DFT testing

Table A.1: Sine Weights for Different Samples used for DFT Testing

Sample Number	Weighting Factor	Sample Number	Weighting Factor
1	0.0000	**13**	0.0000
2	0.2588	**14**	-0.2588
3	0.5000	**15**	-0.5000
4	0.7071	**16**	-0.7071
5	0.8660	**17**	-0.866
6	0.9659	**18**	-0.9659
7	1.0000	**19**	-1.0000
8	0.9659	**20**	-0.9659
9	0.8660	**21**	-0.8660
10	0.7071	**22**	-0.7071
11	0.5000	**23**	-0.5000
12	0.2588	**24**	-0.2588

Table A.2: Cosine Weights for Different Samples used for DFT Testing

Sample Number	Weighting Factor	Sample Number	Weighting Factor
1	1.0000	**13**	-1.0000
2	0.9659	**14**	-0.9659
3	0.8660	**15**	-0.8660
4	0.7071	**16**	-0.7071
5	0.5000	**17**	-0.5000
6	0.2588	**18**	-0.2588
7	0.0000	**19**	0.0000
8	-0.2588	**20**	0.2588
9	-0.5000	**21**	0.5000
10	-0.7071	**22**	0.7071
11	-0.8660	**23**	0.8660
12	-0.9659	**24**	0.9659

A.2 Impedance Points Used for Testing

Figure A. 3 shows the impedance points that have been used to test in the DFT test to ensure the validity of the algorithm. The phase angles between some of these points have been already presented in Chapter 4.

Table A.3: Impedance Values for points within the relay boundaries

Radius of the circle (% of impedance reach)	Impedance Values of the Different points used for testing (Inside and on the Relay Boundaries)					
0.025 (10%)	0.27∠71.22º	0.27∠76.35º	0.26 ∠80.38º	0.23∠79.35º	0.23 ∠73.36º	0.24∠69.34º
0.050 (20%)	0.29∠67.93º	0.30∠77.48º	0.27∠85.41º	0.22∠84.35º	0.20∠71.33º	0.24∠63.48º
0.075 (30%)	0.31∠65.07º	0.32∠78.44º	0.28∠90.05º	0.20∠90.07º	0.18∠68.76º	0.24∠57.56º
0.100 (40%)	0.33∠62.57º	0.35∠79.27º	0.29∠94.30º	0.19∠96.52º	0.16∠65.42º	0.24∠51.68º
0.125 (50%)	0.35∠60.36º	0.37∠79.99º	0.31∠98.15º	0.18∠103.67º	0.13∠60.95º	0.25∠45.98º
0.150 (60%)	0.37∠58.41º	0.40∠80.61º	0.32∠101.64º	0.18∠111.39º	0.11∠54.73º	0.26∠40.55º
0.175 (70%)	0.39∠56.68º	0.42∠81.17º	0.34∠104.78º	0.18∠119.42º	0.09∠45.78º	0.26∠35.45º
0.200 (80%)	0.42∠55.13º	0.45∠81.66º	0.36∠107.62º	0.18∠127.48º	0.08∠32.66º	0.28∠30.74º
0.225 (90%)	0.44∠53.75º	0.47∠82.10º	0.37∠110.19º	0.18∠135.26º	0.07∠14.29º	0.29∠26.42º
0.250 (100%)	0.46∠52.50º	0.49∠82.50º	0.40∠112.50º	0.19∠142.50º	0.06∠-7.50º	0.30∠22.50º

Table A.4: Impedance Values for points outside the relay boundaries

Radius of the circle (% of impedance reach)	Impedance Values of the Different points used for testing (Outside the Relay Boundaries)					
0.275 (110%)	0.48∠51.37º	0.52∠82.86º	0.42∠114.59º	0.20∠149.06º	0.073∠-27.38º	0.32∠18.95º
0.300 (120%)	0.51∠50.34º	0.54∠83.18º	0.44∠116.49º	0.22 ∠154.88º	0.09∠-42.13º	0.34∠15.74º
0.325 (130%)	0.53∠49.41º	0.57 ∠83.48º	0.46 ∠118.21º	0.23∠159.98º	0.11∠-52.23º	0.35∠12.85º
0.350 (140%)	0.55∠48.55º	0.59∠83.76º	0.48∠119.79º	0.25∠164.42º	0.13∠-59.19º	0.37∠10.25º
0.375 (150%)	0.58∠47.76º	0.62∠84.01º	0.51∠121.22º	0.26∠168.27º	0.15∠-64.14º	0.39∠7.89º
0.400 (160%)	0.61∠47.04º	0.64∠84.24º	0.52∠122.54º	0.28∠171.62º	0.17∠-67.79º	0.41∠5.76º
0.425 (170%)	0.63∠46.37º	0.67∠84.45º	0.55∠123.75º	0.30∠174.54º	0.19∠-70.58º	0.43∠3.83º
0.450 (180%)	0.65∠45.75º	0.69∠84.65º	0.57∠124.86º	0.32∠177.08º	0.22∠-72.76º	0.45∠2.08º
0.475 (190%)	0.67∠45.17º	0.72∠84.84º	0.59∠125.89º	0.357∠179.34º	0.24∠-74.51º	0.48∠0.48º
0.500 (200%)	0.70∠44.64º	0.74∠85.01º	0.61∠126.85º	0.37∠-178.67º	0.27∠-75.95º	0.50∠-0.98º

APPENDIX B: PARAMETERS OF THE RELAYS

B.1 Admittance relay

A neural network with a configuration of 18-37-1 has been chosen to implement the characteristics of an admittance relay. The following sections give the parameters of the trained neural network. There are three weight matrices – for weights between inputs and the input layer (18x26), input layer and the hidden layer (37x18) and finally, between the hidden layer and the output layer (1x37). Each of these layers has a matrix of biases of the order of 18x1, 37x1 and 1x1 respectively.

B.2 Quadrilateral relay

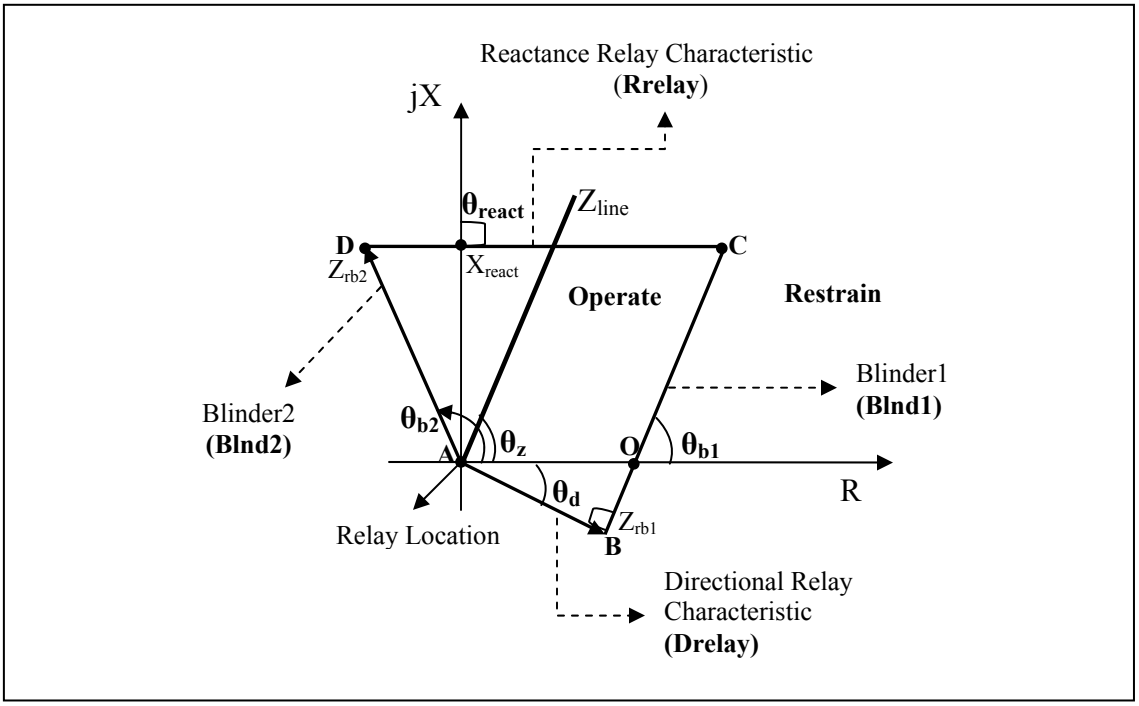

Figure B.1: Quadrilateral Relay Characteristics

Flexible Parameters (Values entered by the user and considered in the algorithm):
Value of A (origin) = $[0,0]$
Value of Fault Resistance AO = $0.55\,p.u.$

Value of θ_d = 15º
Value of θ_{b1} = 75º
Value of Z_r = 0.85 *p.u.*
Value of θ_{react} = 90º
Value of θ_{b2} = 15º

Calculated Points (Before the Training of the ANN and calculation of impedance points)
Value of B = [0.51316, - 0.1375]
Value of D = [-0.22, 0.82104]
Value of C = [0.77, 0.82104]
Length of AB = 0.53216 p.u.
Length of BC = 0.99235 p.u.
Length of CD = 0.98999 p.u.
Length of DA = 0.85 p.u.
Impedance Reach for Blinder 2 (Left Blinder) = 0.61345 p.u.
Impedance Reach for Blinder 1 (Right Blinder) = 0.53216 p.u.
Impedance Reach for Reactance Relay = 0.82104 p.u.

Coordinates of the Quadrilateral Characteristics:
X Coordinates [Ax Bx Cx Dx] = [0 0.5132 0.7700 -0.2200]
X Coordinates [Ay By Cy Dy] = [0 -0.1375 0.8210 0.8210]

B.1.1 Training Points

As mentioned in Chapter 5, the training points for all characteristics have been produced at lines separated by a lateral distance of ± 0.1 p.u. The training data for the 4-1 "AND" ANN for Quadrilateral Relay is given in Table B.5.

Table B.5: Training Patterns and Target Outputs for 4-1 AND ANN

Training Pattern	Target Output	Training Pattern	Target Output
$\begin{bmatrix}-1\\-1\\-1\\-1\end{bmatrix}$	$[-1]$	$\begin{bmatrix}+1\\-1\\-1\\+1\end{bmatrix}$	$[-1]$
$\begin{bmatrix}-1\\-1\\-1\\+1\end{bmatrix}$	$[-1]$	$\begin{bmatrix}+1\\-1\\+1\\-1\end{bmatrix}$	$[-1]$

$\begin{bmatrix}-1\\-1\\+1\\-1\end{bmatrix}$	$[-1]$	$\begin{bmatrix}-1\\+1\\-1\\+1\end{bmatrix}$	$[-1]$
$\begin{bmatrix}-1\\+1\\-1\\-1\end{bmatrix}$	$[-1]$	$\begin{bmatrix}-1\\+1\\+1\\+1\end{bmatrix}$	$[-1]$
$\begin{bmatrix}+1\\-1\\-1\\-1\end{bmatrix}$	$[-1]$	$\begin{bmatrix}+1\\+1\\+1\\-1\end{bmatrix}$	$[-1]$
$\begin{bmatrix}-1\\-1\\+1\\+1\end{bmatrix}$	$[-1]$	$\begin{bmatrix}+1\\-1\\+1\\+1\end{bmatrix}$	$[-1]$
$\begin{bmatrix}-1\\+1\\+1\\-1\end{bmatrix}$	$[-1]$	$\begin{bmatrix}+1\\+1\\-1\\+1\end{bmatrix}$	$[-1]$
$\begin{bmatrix}+1\\+1\\-1\\-1\end{bmatrix}$	$[-1]$	$\begin{bmatrix}+1\\+1\\+1\\+1\end{bmatrix}$	$[+1]$

APPENDIX C: TRAINING ANNs IN MATLAB

The algorithm has been trained and tested in MATLAB. Figure C.1 shows the block diagram of training ANNs in MATLAB. The MATLAB and MATLAB Neural Network toolbox commands used in the algorithm have been explained in Sections C.1 and C.2.

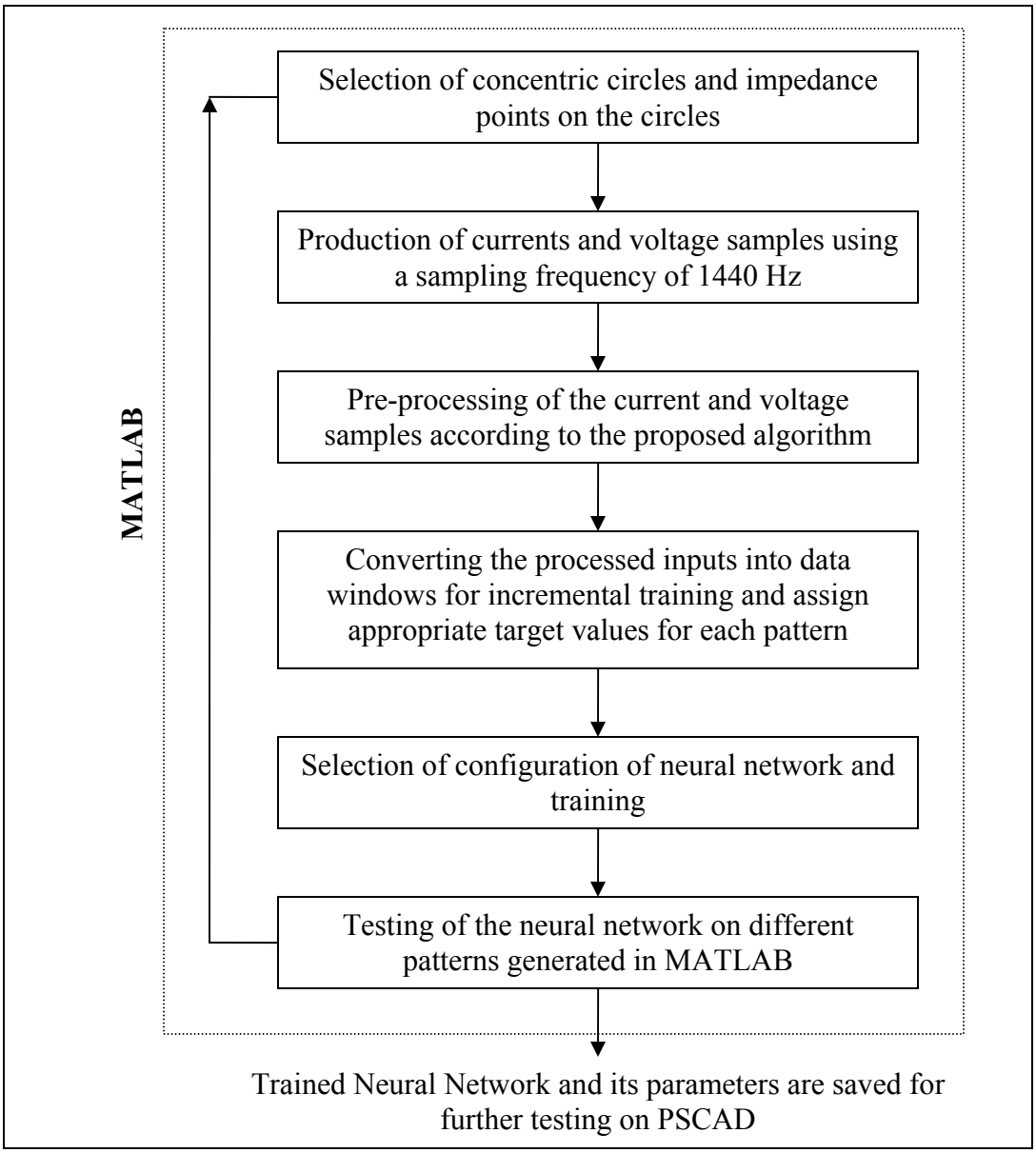

Figure C.1 Block Diagram of Implementation of the Algorithm in MATLAB

C.1 MATLAB Neural Network Toolbox

Various operators and commands have been used in MATLAB. The specific functions used from MATLAB Neural Network Toolbox and their description (as given in the MATLAB product help) have been given below.

Logsig	**Logarithmic sigmoid transfer function (limits between 0 and +1)**
Mse	**Mean squared error performance function**
Newff	**Create a feed-forward back propagation network**
Sim	**Simulate the Simulink Model (Trained neural network in this case)**
Tansig	**Hyperbolic tangent sigmoid transfer function (limits between -1 and +1)**
Train	**Train a neural network**
Trainrp	**RPROP back propagation - Specifies the back propagation algorithm as resilient back propagation**

Training Parameters

net.trainParam.delt_dec	**Value of decrease in learning rate (adaptive learning rate)**
net.trainParam.delt_inc	**Value of increase in learning rate (adaptive learning rate)**
net.trainParam.epochs	**Value of maximum number of epochs**
net.trainParam.goal	**Value of minimum performance error**
net.trainParam.lr	**Value of learning rate**
net.trainParam.show	**Value of epochs after which error is displayed**

APPENDIX D: TEST POWER SYSTEM DATA AND PARAMETERS

D.1 Per – unit Calculations

The impedance calculation for the transmission line L_5 for admittance and quadrilateral relay is shown below.

(a) Admittance relay

$$Z_{reach} = 0.5\angle 75° p.u = 0.1294 + j0.4830 p.u.$$

Since reach is considered as 80% of the impedance of transmission line L_5,

$$Z_{line} = 0.625\angle 75° p.u = 0.1618 + j0.6037 p.u.$$

Therefore, the resistance and reactance components of the transmission line L_5 can be set as:

$$R_{line} = 0.1618 p.u. \Rightarrow R_{line} = \frac{0.1618 p.u.}{10^5 m} = 1.618 * 10^{-6} \text{ per unit per m}$$

Similarly,

$$X_{line} = 0.6037 p.u. \Rightarrow X_{line} = \frac{0.6037 p.u.}{10^5 m} = 6.037 * 10^{-6} \text{ per unit per m}$$

(b) Quadrilateral relay

$$Z_{reach} = 0.85\angle 75° p.u = 0.2200 + j0.8210 p.u.$$

Since reach is considered as 80% of the impedance of transmission line L_5,

$$Z_{line} = 0.2750 + j1.0625 p.u.$$

Therefore, the resistance and reactance components of the transmission line L_5 can be set as:

$$R_{line} = 0.2750 p.u. \Rightarrow R_{line} = \frac{0.2750 p.u.}{10^5 m} = 2.750 * 10^{-6} \text{ per unit per m}$$

Similarly,

$$X_{line} = 1.0625 p.u. \Rightarrow X_{line} = \frac{1.0625 p.u.}{10^5 m} = 1.0625 * 10^{-5} \text{ per unit per m}$$

These values of resistance and reactance are set for applying different faults on the transmission line. The current and voltage values from the line are recorded. The base values used to convert the current and voltage values into per unit values are:

$$MVA_{base} = 500MVA$$
$$KV_{base} = 500KV$$
$$Z_{base} = \frac{(500KV)^2}{500MVA} = 500\Omega$$
$$I_{base} = \frac{500MVA}{500KV * \sqrt{3}} = 0.5774kA = 577.4A$$

D.2 Different Components and their parameters

All the components used for tests on Mho and Quadrilateral Relay are the same, except the impedance of the transmission line L_5 as shown in the previous section.

D.2.1 Transformers

Transformer	Voltage Ratio	MVA Rating
T_1	15 kV / 500kV	2500 MVA
T_2	15 kV / 500kV	1000 MVA
T_3	500 kV / 15kV	2000 MVA
T_4	500 kV / 15kV	600 MVA
T_5	500 kV / 735 kV	1000 MVA
T_6	735 kV / 500 kV	1000 MVA
T_7	500 kV / 735 kV	1000 MVA
T_8	735 kV / 500 kV	1000 MVA

D.2.2 Transmission Lines

Transmission Line	Length of the line	Number of Conductors
L_1	55 km	3
L_2	120 km	3
L_3	60 km	3
L_4	45 km	3
L_5	100 km	3
L_6	75 km	3
L_{7a}	130 km	3
L_{7b}	130 km	3
L_8	45 km	3
L_9	50 km	3
L_{10}	45 km	3
L_{11}	55 km	3
L_{12}	30 km	3
L_{13}	45 km	3

D.2.3 Loads

Fixed Load	MW Rating
$Load_1$ (Bus 14)	600 MW
$Load_2$ (Bus 15)	450 MW
$Load_3$ (Bus 16)	450 MW
$Load_4$ (Bus 17)	750 MW

D.2.4 Machines and Sources

Machine / Source	MW/MVA Rating	Voltage Rating
S_1 (Equivalent Voltage Source)	100 MVA	15 kV
S_1 (Synchronous Generator)	1600 MW	15 kV
M_1 (Motor)	600 MW	15 kV
M_2 (Motor)	500 MW	15 kV

APPENDIX E: POSITIVE SEQUENCE VOLTAGES FOR FAULTS ON TRANSMISSION LINES

For transmission lines, the positive sequence impedance Z_1 is equal to negative sequence impedance Z_2. Therefore, the positive sequence voltage V_{a1} (or V_{b1} and V_{c1}) used for positive sequence memory polarization in different faults has been calculated by short circuit calculations.

E.1 Single Line to Ground fault

The Connections of the three sequence networks have been shown in Figure E.1. The following equations represent a single line to ground fault (A-G).

$$I_b = 0$$

$$I_c = 0$$

$$V_a = 0$$

For a A-G fault,

$$I_{a1} = I_{a2} = I_{a0} = \frac{V_a}{Z_1 + Z_2 + Z_0}$$

In the equation, V_a is the voltage seen by the relay during fault.

In case of transmission line,

$$Z_1 = Z_2$$

Therefore,

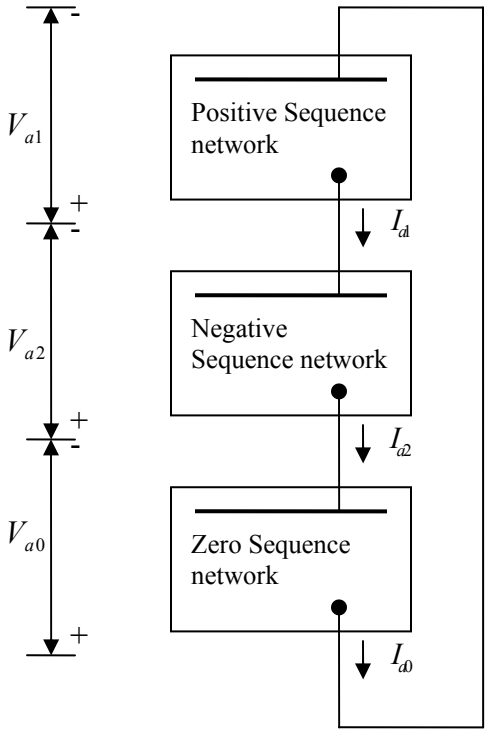

Figure E.1: Sequence Networks for Single Line to Ground Faults

$$I_{a1} = \frac{V_a}{2Z_1 + Z_0}$$

The positive sequence voltage, is thus $V_{a1} = I_{a1}Z_1 = \frac{Z_1}{2Z_1 + Z_0}V_a$

E.2 Line to Line fault

The Connections of the three sequence networks have been shown in Figure E.2. The following equations represent a line to line fault (B-C).

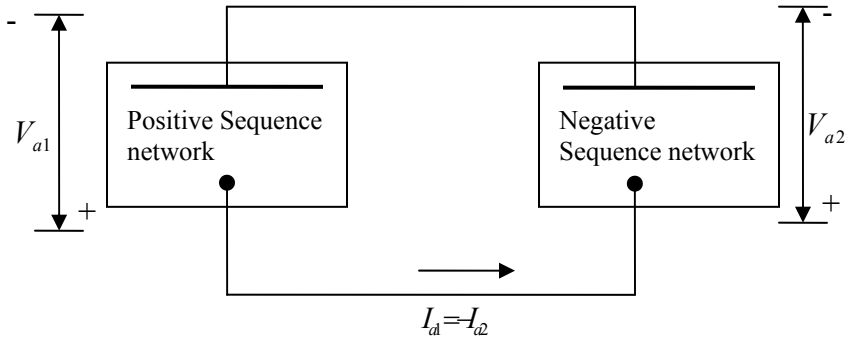

Figure E.2: Sequence Networks for Line to Line Faults

$$V_b = V_c$$

$$I_a = 0$$

$$I_b = -I_c$$

In this case,

$V_{a1} = V_{a2}$ and $I_{a1} = \frac{V_a}{Z_1 + Z_2}$

Since for a transmission line, $Z_1 = Z_2$

Therefore,

$$I_{a1} = \frac{V_a}{2Z_1}$$

The positive sequence voltage, is thus $V_{a1} = I_{a1}Z_1 = \frac{V_a Z_1}{2Z_1} = \frac{V_a}{2}$

E.3 Double Line to Ground fault

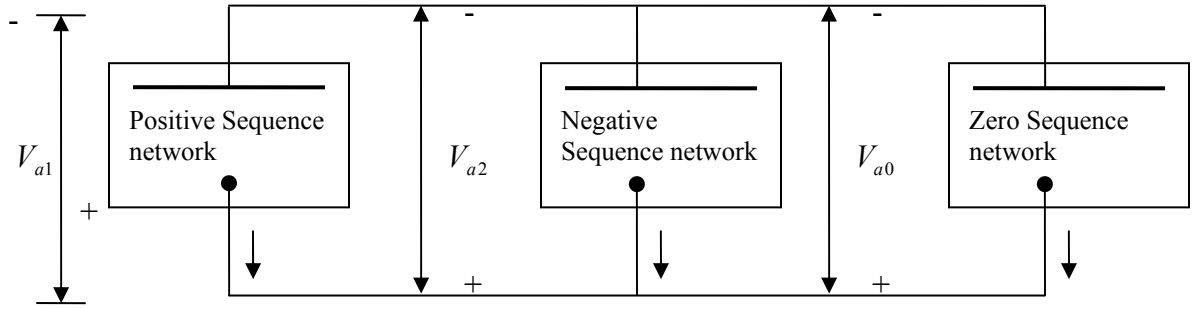

Figure E.3: Sequence Networks for Double Line to Ground Faults

The Connections of the three sequence networks have been shown in Figure E.3. The following equations represent a double line to ground fault (BC-G).

$$V_b = V_c = 0$$

$$I_a = 0$$

In this case, $V_{a1} = V_{a2} = V_{a0}$

Also, $I_{a1} = \dfrac{V_a}{Z_1 + \dfrac{Z_2 Z_0}{Z_2 + Z_0}}$

Now, substituting $Z_1 = Z_2$ for a transmission line,

Therefore,

$$I_{a1} = \frac{V_a}{Z_1 + \dfrac{Z_1 Z_0}{Z_1 + Z_0}} = \frac{V_a (Z_1 + Z_0)}{Z_1^{\,2} + 2 Z_1 Z_0}$$

The positive sequence voltage, is thus $V_{a1} = I_{a1} Z_1 = \dfrac{V_a (Z_1 + Z_0)}{Z_1^{\,2} + 2 Z_1 Z_0} Z_1$

Thus, $V_{a1} = \dfrac{Z_1 + Z_0}{Z_1 + 2Z_0} V_a$

E.4 Three Phase fault

The Connections of the three sequence networks have been shown in Figure E.4. The following equations represent a three phase fault (ABC-G).

$$V_{a1} = I_a Z_1$$

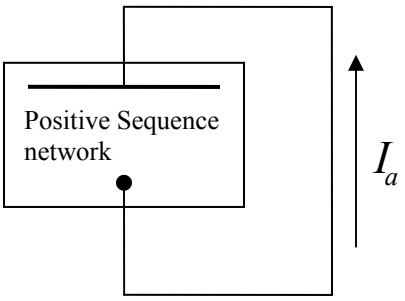

Figure E.4: Sequence Network for Three-Phase Fault

APPENDIX F: NOISY PROCESSED INPUTS

F.1 Signal to Noise Ratio of 30 dB

Figure F.1 show the pre-processed fault pattern for the value of inner diameter (in p.u.) where the ANN is able to perform correctly. A white Gaussian noise with a SNR of 30 dB has been added to both current and voltages and the noisy processed waveforms have been generated in MATLAB. The pre-processed inputs for non-fault pattern have been shown in Figure F.2.

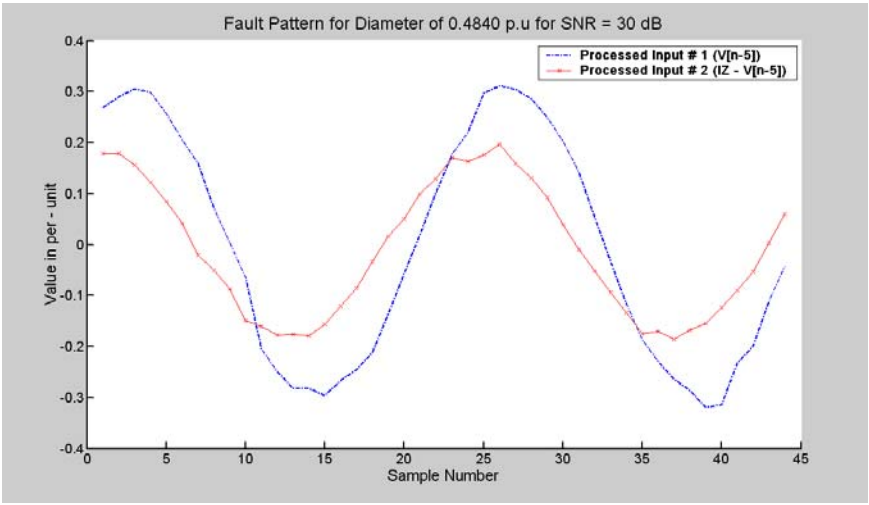

Figure F.1: Processed Inputs for a radius of 0.242 p.u. (inside the relay characteristics) and SNR of 30dB

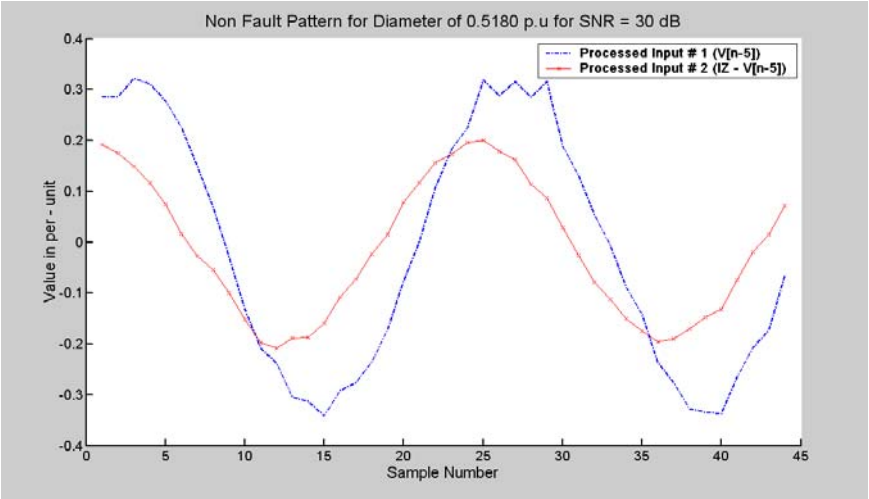

Figure F.2: Processed Inputs for a radius of 0.259 p.u. (outside the relay characteristics) and SNR of 30dB

F.2 Signal to Noise Ratio of 20 dB

Figures F.3 and F.4 show the pre-processed inputs for inner and outer diameters respectively, for the values where the ANN is able to perform correctly. These inputs have been generated after add a white Gaussian noise of a signal to noise ratio of 20 dB to both currents and voltages.

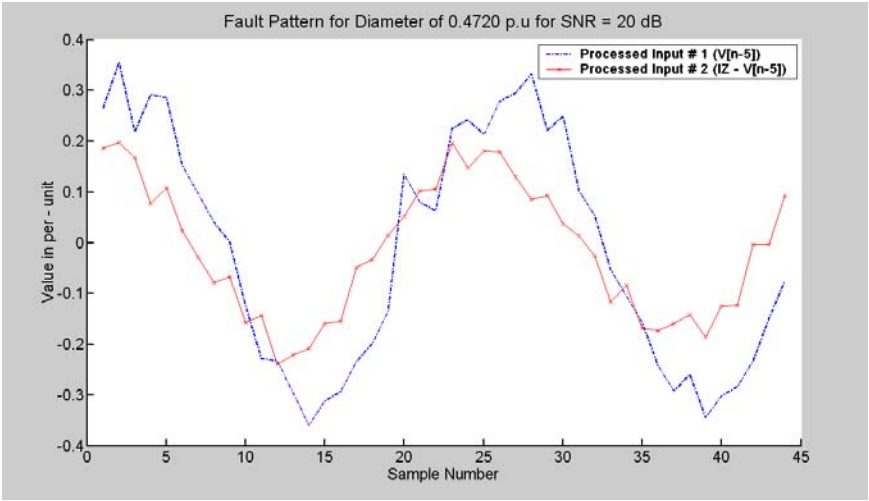

Figure F.3: Processed Inputs for a radius of 0.236 p.u. (inside the relay characteristics) and SNR of 20dB

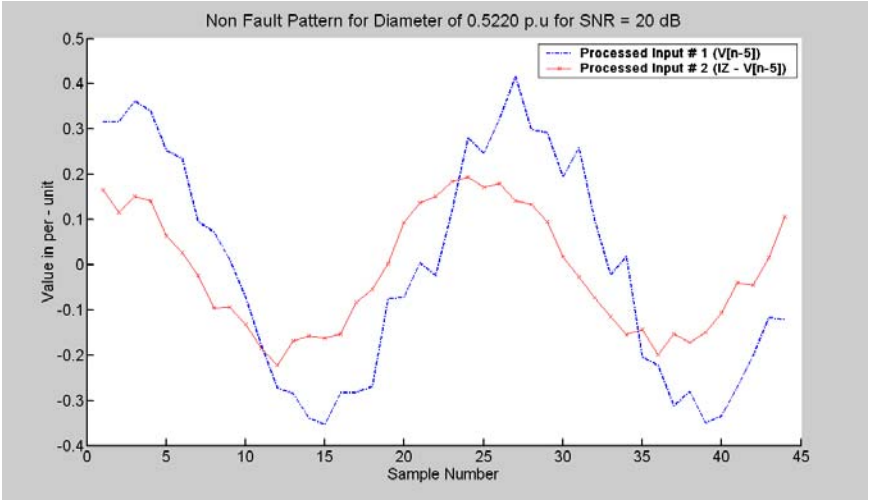

Figure F.4: Processed Inputs for a radius of 0.261 p.u. (outside the relay characteristics) and SNR of 20dB

F.3 Signal to Noise Ratio of 10 dB

In this case, a white Gaussian noise with a SNR of 10 dB has been added to the original inputs in this case. The pre-processed inputs for patterns where the ANN performs correctly have been shown in Figures F.5 and F.6.

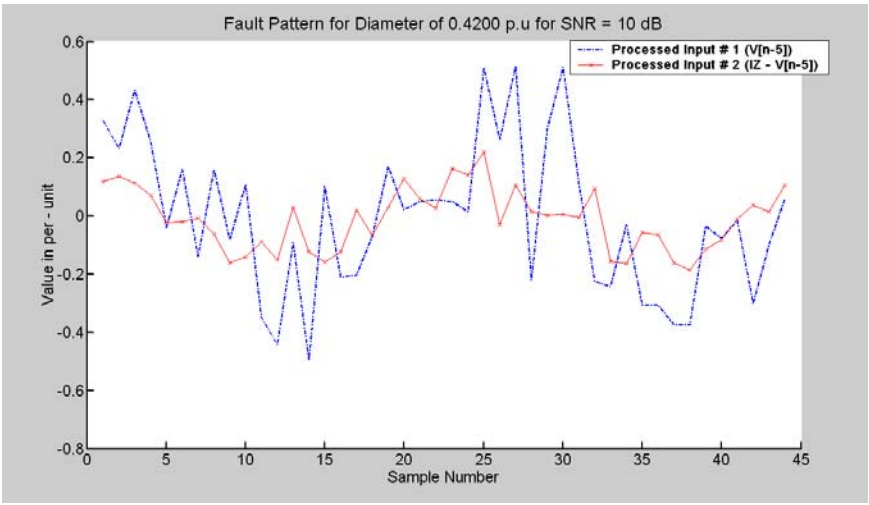

Figure F.5: Processed Inputs for a radius of 0.210 p.u. (inside the relay characteristics) and SNR of 10dB

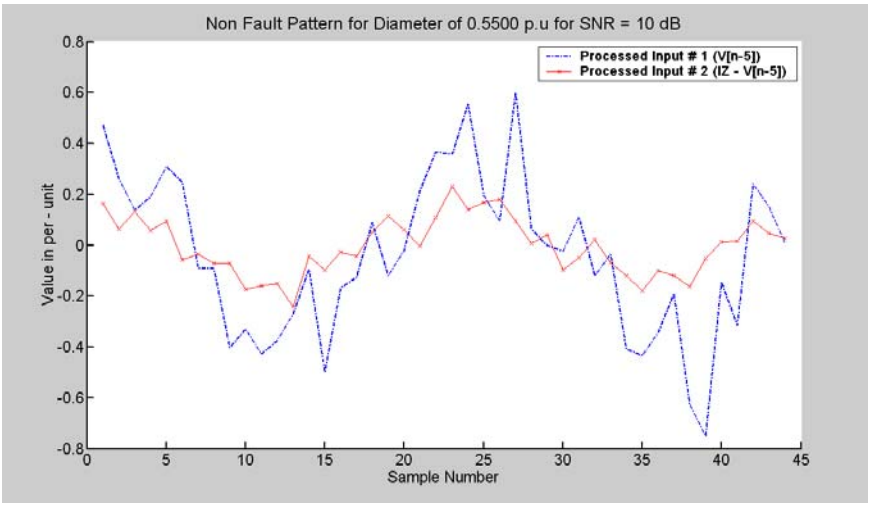

Figure F.6: Processed Inputs for a radius of 0.275 p.u. (outside the relay characteristics) and SNR of 10dB

APPENDIX G: EXTRA RESULTS

Chapter six presented the results for different fault cases for faults primarily at the boundaries of the relay characteristics. This appendix shows the extra results that could not be presented in the main body of the thesis due to space constraints. Below is the list of results and the figures presenting them:

Results	Figure
MHO RELAY	
Single Line to Ground Faults	
- 0° Fault Inception - 90° Fault Inception	Figures G.1 to G.22 Figures G.23 to G.46
Line to Line Faults	
- 0° Fault Inception	Figures G.47 to G.52
Double Line to Ground Faults	
- 0° Fault Inception	Figures G.53 to G.59
Three Line to Ground Faults	
- 0° Fault Inception	Figures G.60 to G.66
QUADRILATERAL RELAY	
Single Line to Ground Faults for 0 Ω Fault Resistance	
- 0° Fault Inception	Figures G.67 to G.73
- 90° Fault Inception	Figures G.74 to G.80
Single Line to Ground Faults for 15 Ω Fault Resistance	
- 0° Fault Inception	Figures G.81 to G.87
- 90° Fault Inception	Figures G.88 to G.94
Single Line to Ground Faults for 50 Ω Fault Resistance	
- 0° Fault Inception	Figures G.95 to G.100
- 90° Fault Inception	Figures G.101 to G.107
Line to Line Faults	
- 0° Fault Inception	Figures G.108 to G.111
Double Line to Ground Faults	
- 0° Fault Inception	Figures G.112 to G.115
Three Line to Ground Faults	
- 0° Fault Inception	Figures G.116 to G.119

Results	Figure
POLARIZATION (MHO RELAY)	
Single Line to Ground Faults	
- 10% Cross Polarization	Figures G.120 to G.128
- 100% Self Memory Polarization	Figures G.129 to G.152
- 75% Self Memory Polarization	Figures G.153 to G.176
- 75% Self Memory + 10% Cross Polarization	Figures G.177 to G.200
- Positive Sequence Memory Polarization	Figures G.201 to G.213
Line to Line Faults	
- 75% Self Memory + 50% Positive Sequence Pol.	Figures G.214 to G.221
Double Line to Ground Faults	
- 75% Self Memory + 50% Positive Sequence Pol.	Figures G.222 to G.229
Three Line to Ground Faults	
- 75% Self Memory + 50% Positive Sequence Pol.	Figures G.230 to G.236

G.1 Results for Admittance Relay

This section presents the results for Admittance relay for different types of fault cases previously discussed in Chapter 6.

G.1.1 Single Line to Ground Faults

a) Zero Degree Fault Inception:

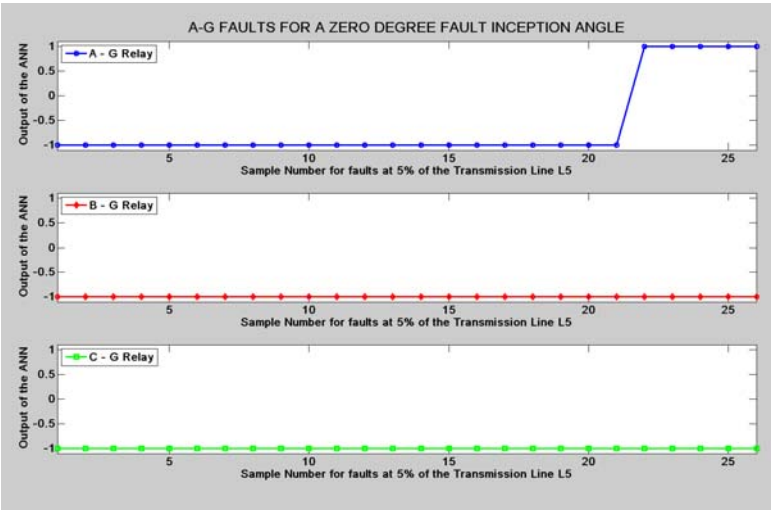

Figure G.1: Mho Relay - SLG Fault at 5% length of L_5

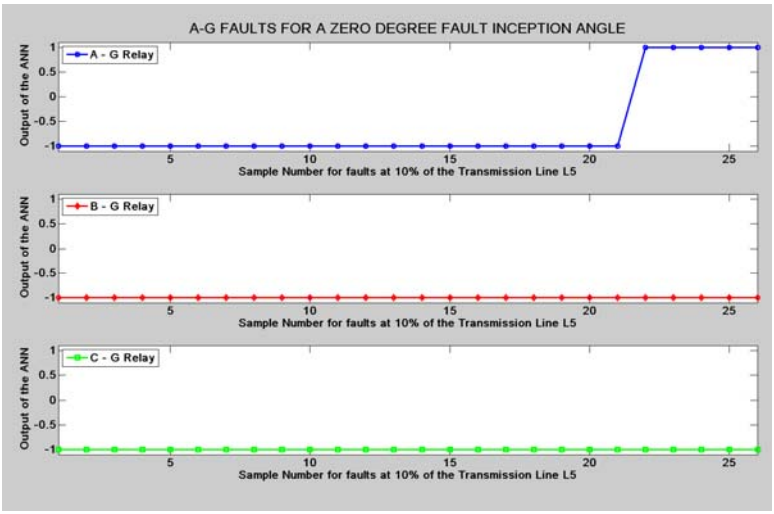

Figure G.2: Mho Relay - SLG Fault at 10% length of L_5

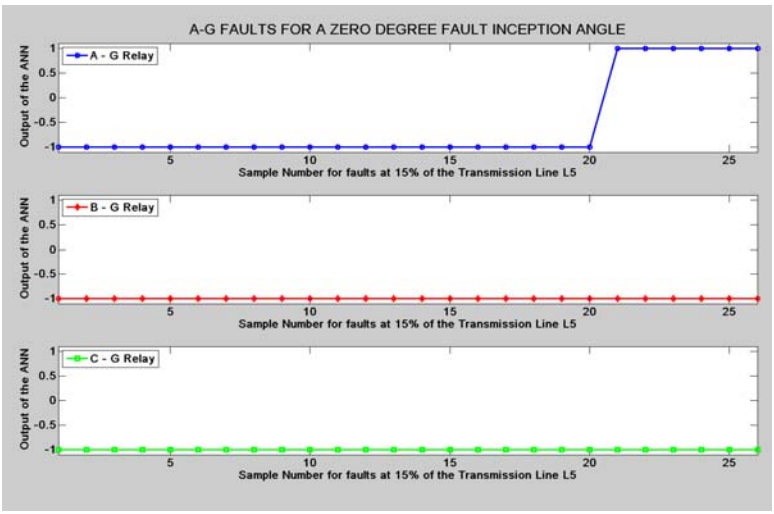

Figure G.3: Mho Relay - SLG Fault at 15% length of L_5

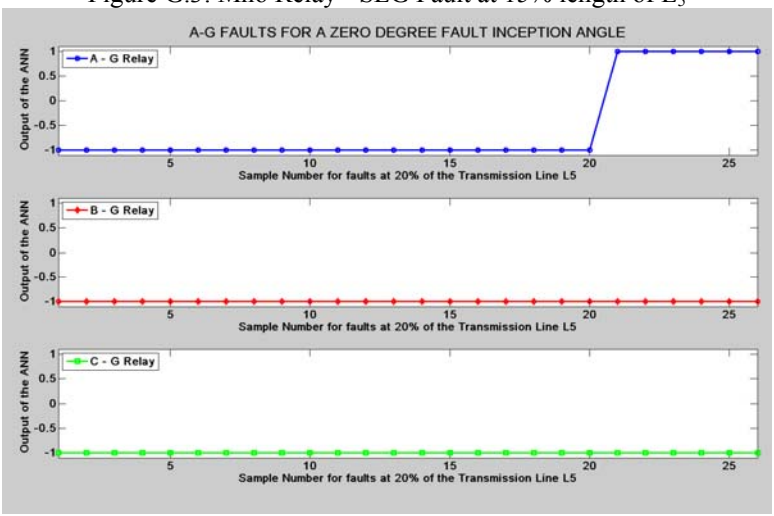

Figure G.4: Mho Relay - SLG Fault at 20% length of L_5

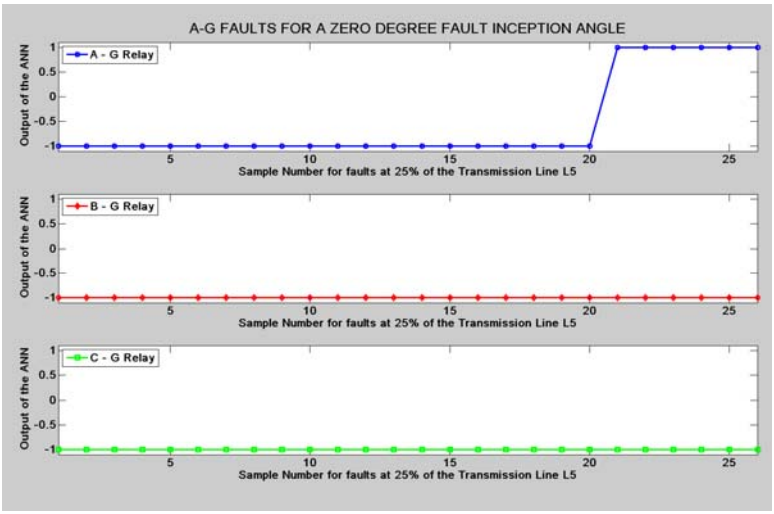

Figure G.5: Mho Relay - SLG Fault at 25% length of L_5,

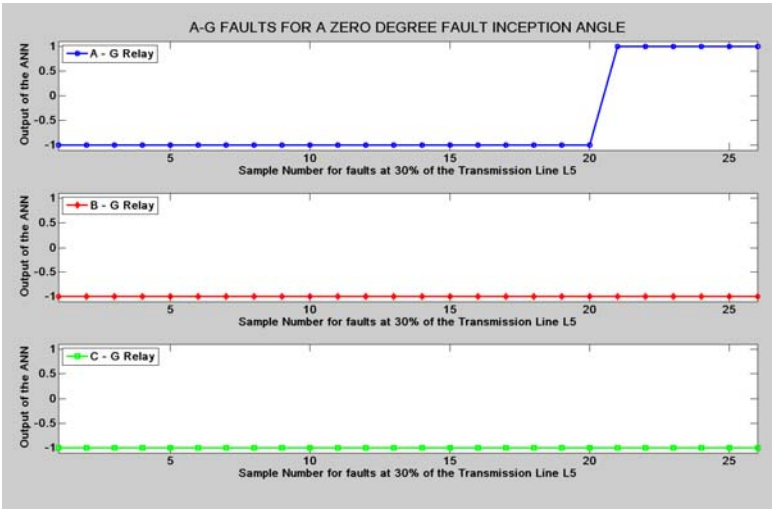

Figure G.6: Mho Relay - SLG Fault at 30% length of L_5

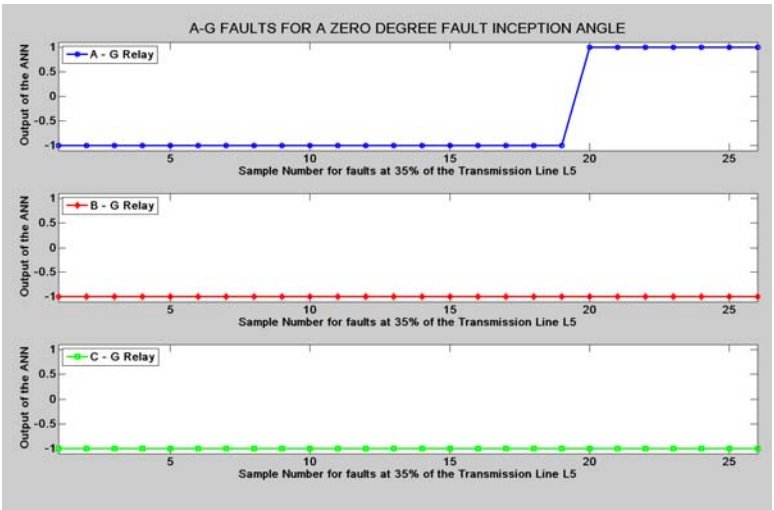

Figure G.7: Mho Relay - SLG Fault at 35% length of L_5

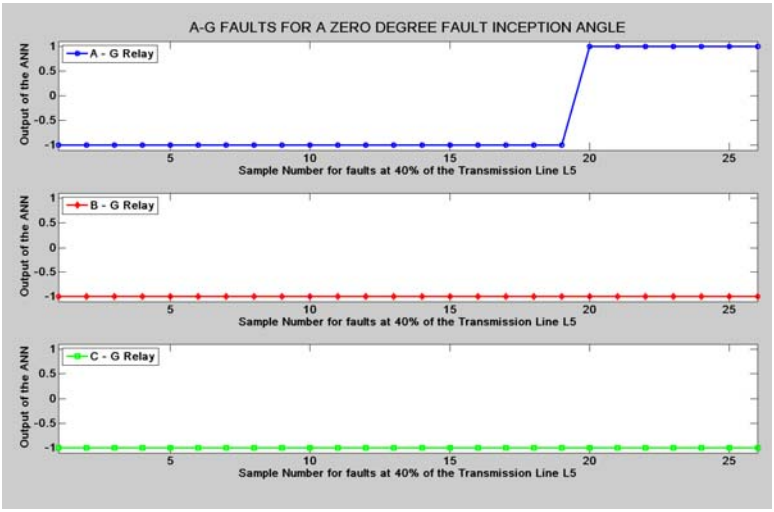

Figure G.8: Mho Relay - SLG Fault at 40% length of L_5

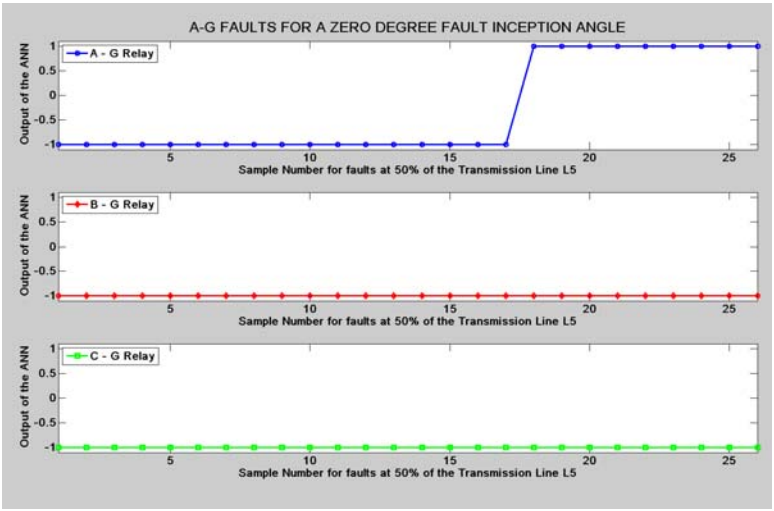

Figure G.9: Mho Relay - SLG Fault at 50% length of L_5

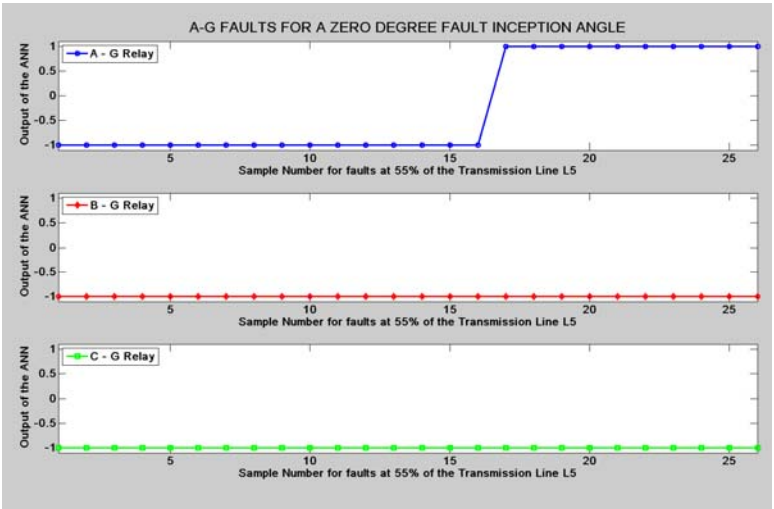

Figure G.10: Mho Relay - SLG Fault at 55% length of L_5

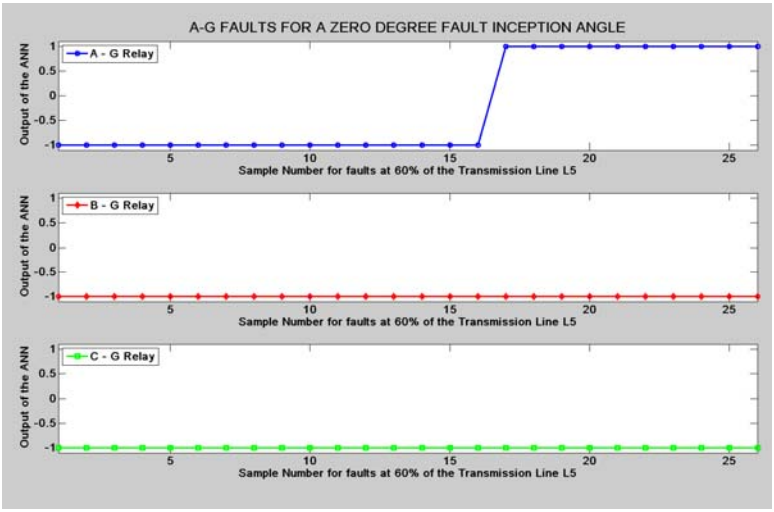

Figure G.11: Mho Relay - SLG Fault at 60% length of L_5

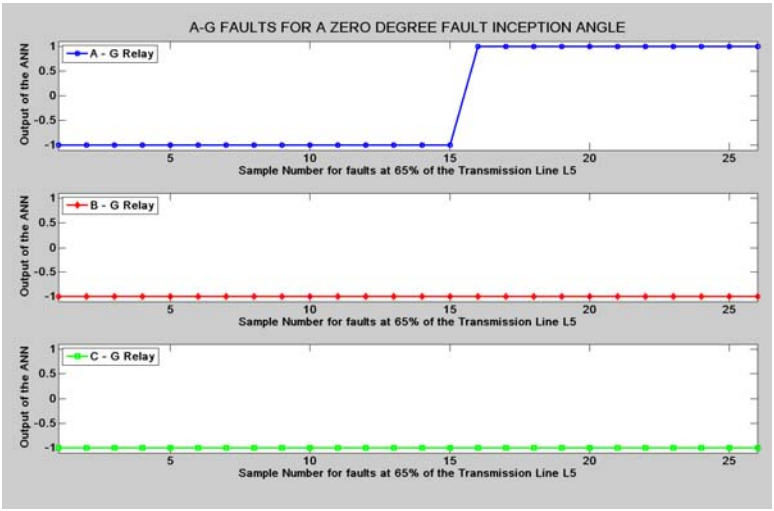

Figure G.12: Mho Relay - SLG Fault at 65% length of L_5

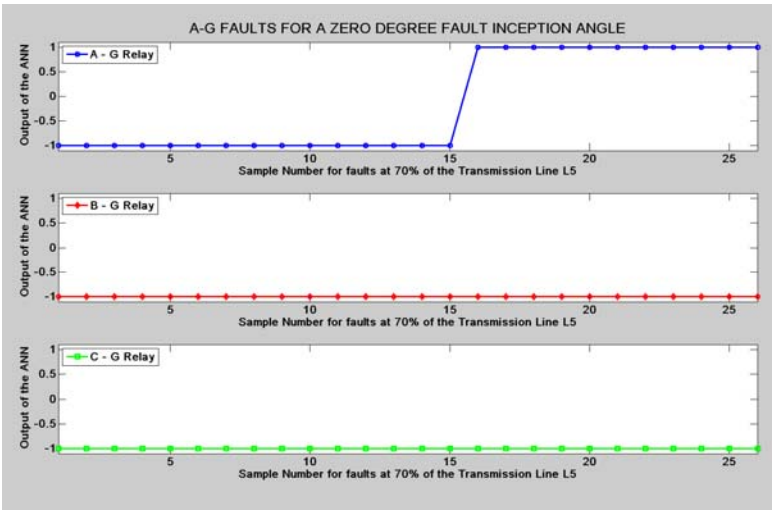

Figure G.13: Mho Relay - SLG Fault at 70% length of L_5

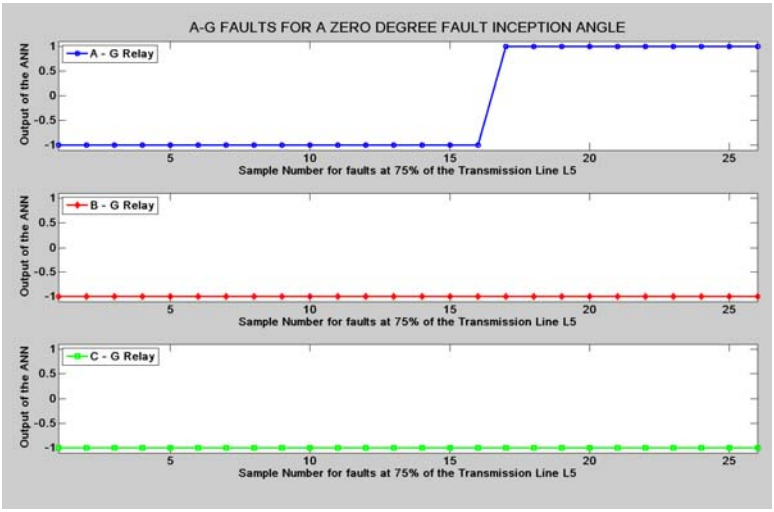

Figure G.14: Mho Relay - SLG Fault at 75% length of L_5

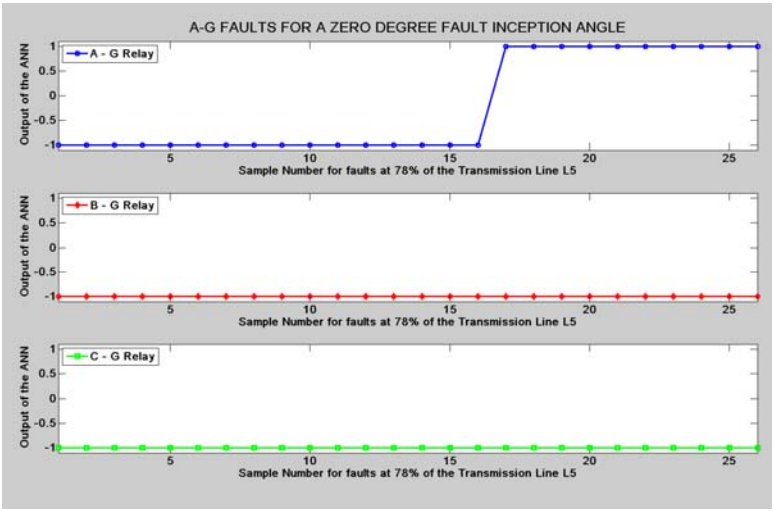

Figure G.15: Mho Relay - SLG Fault at 78% length of L_5

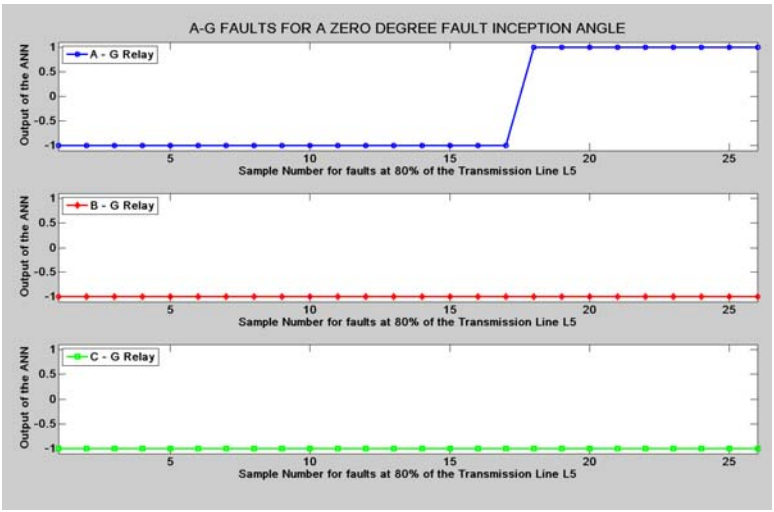

Figure G.16: Mho Relay - SLG Fault at 80% length of L_5

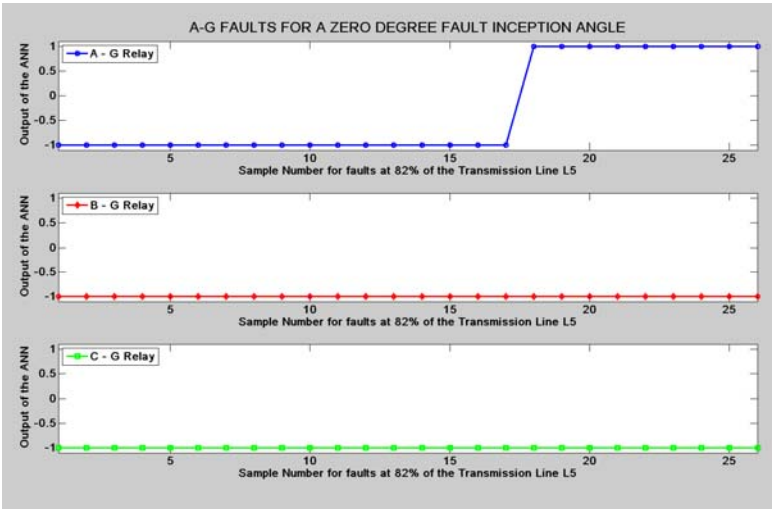

Figure G.17: Mho Relay - SLG Fault at 82% length of L_5

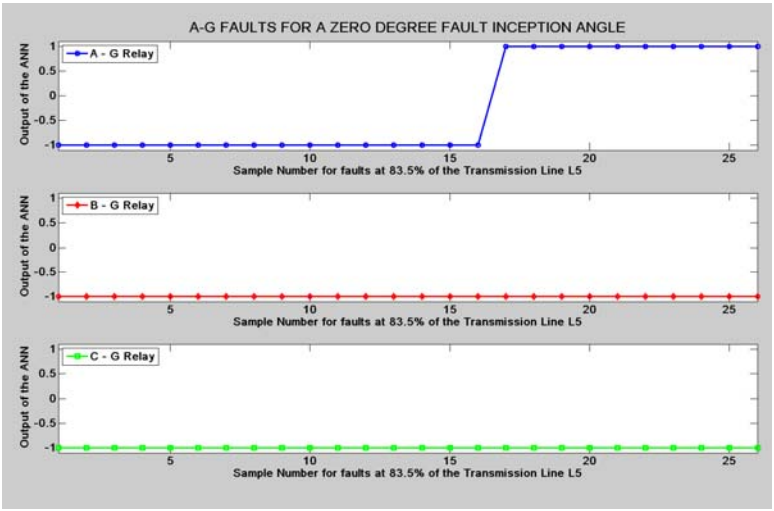

Figure G.18: Mho Relay - SLG Fault at 83.5% length of L_5

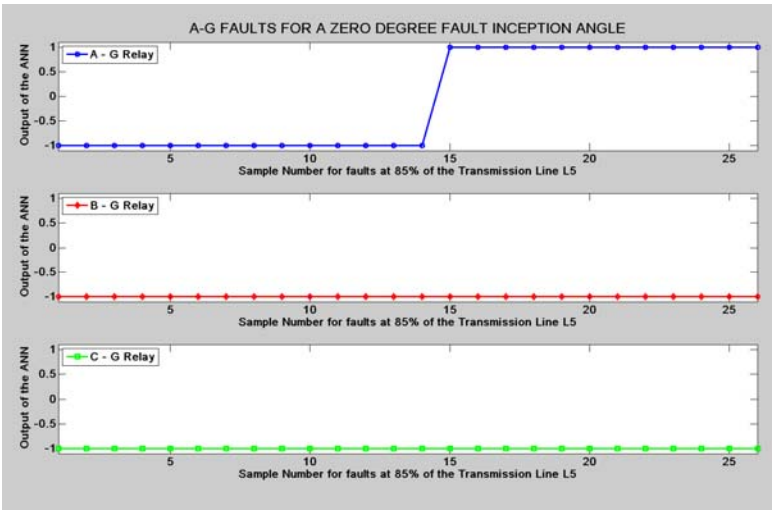

Figure G.19: Mho Relay - SLG Fault at 85% length of L_5

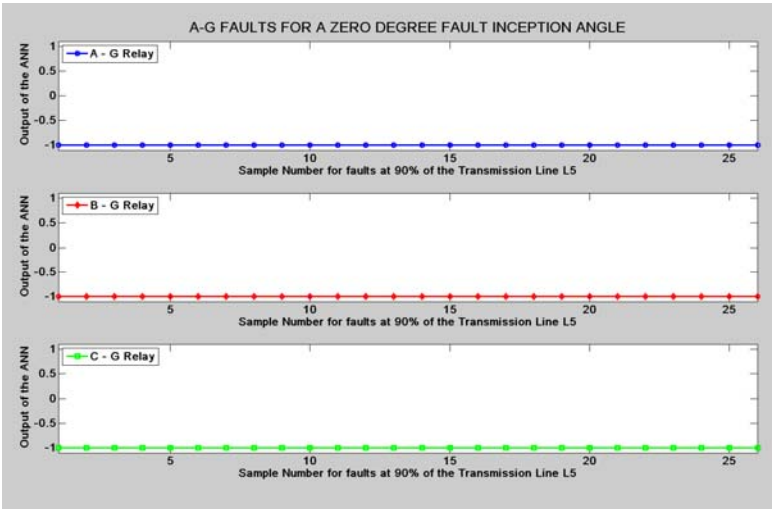

Figure G.20: Mho Relay - SLG Fault at 90% length of L_5

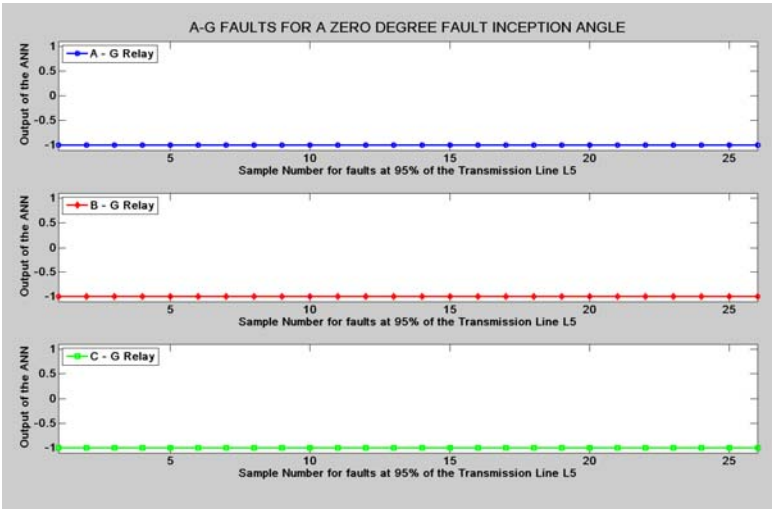

Figure G.21: Mho Relay - SLG Fault at 95% length of L_5

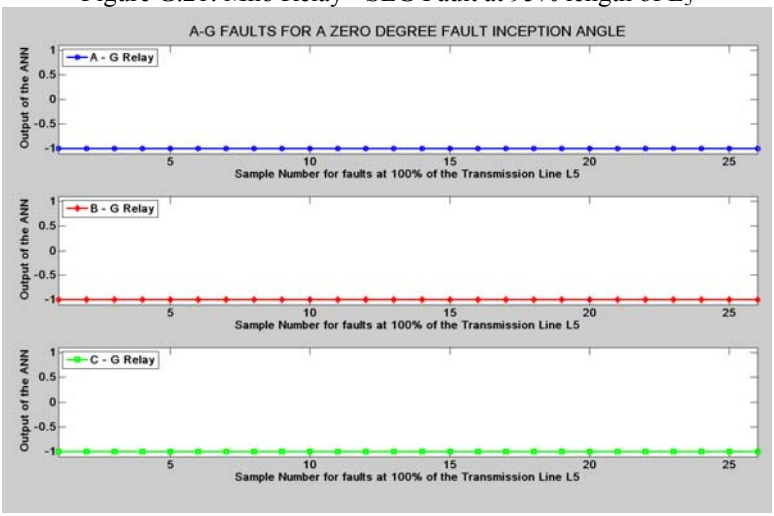

Figure G.22: Mho Relay - SLG Fault at 100% length of L_5

b) Ninety Degree Fault Inception:

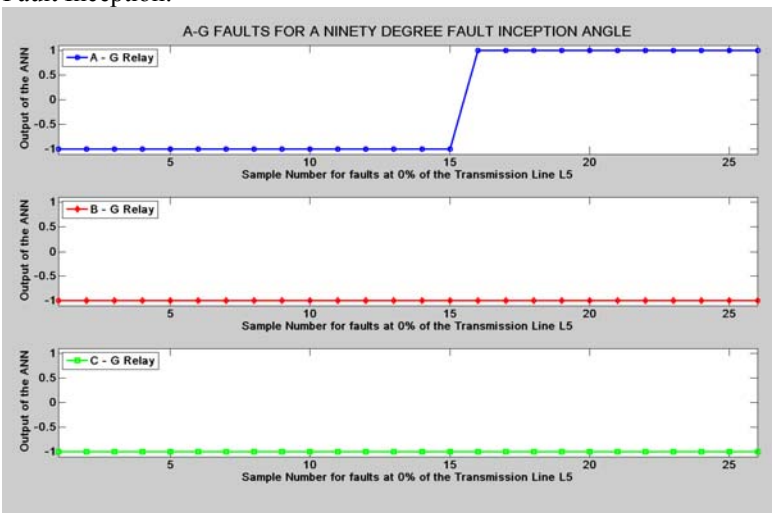

Figure G.23: Mho Relay - SLG Fault at 0% length of L_5

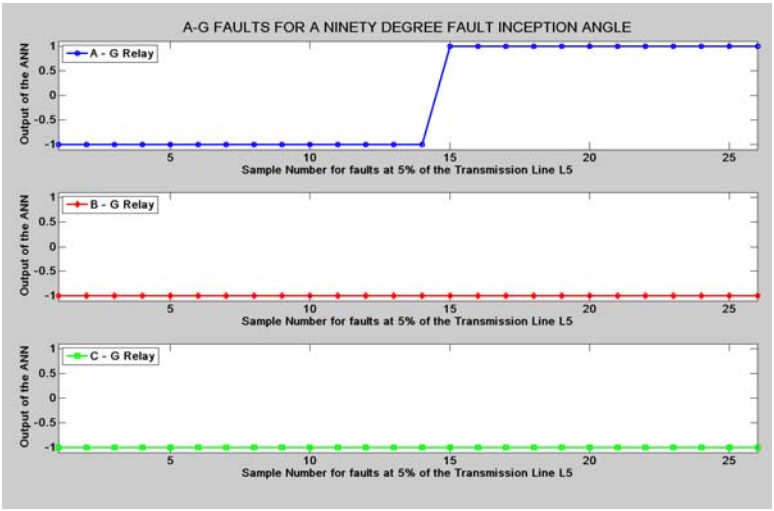

Figure G.24: Mho Relay - SLG Fault at 5% length of L_5,

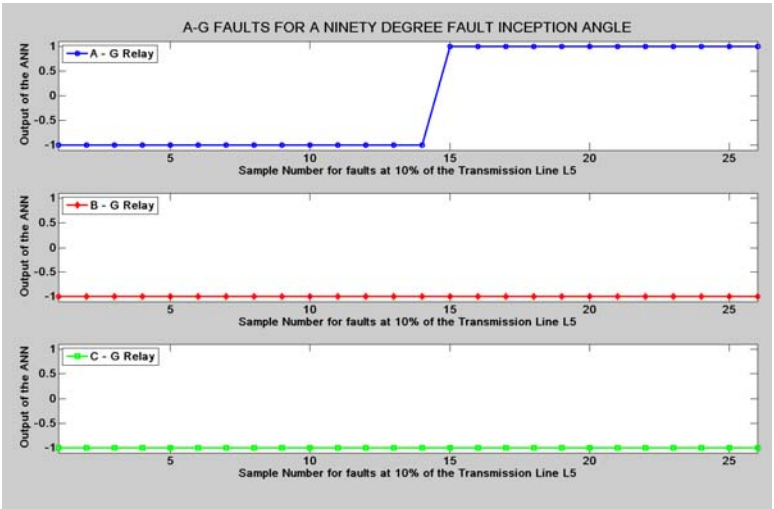

Figure G.25: Mho Relay - SLG Fault at 10% length of L_5

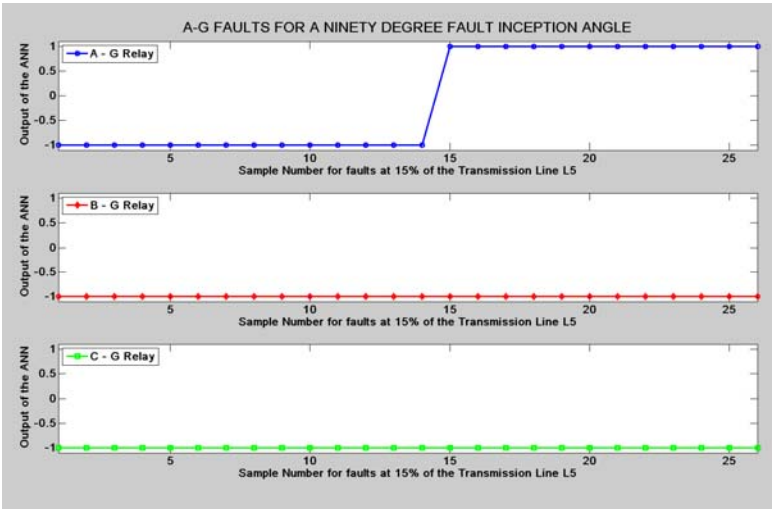

Figure G.26: Mho Relay - SLG Fault at 15% length of L_5

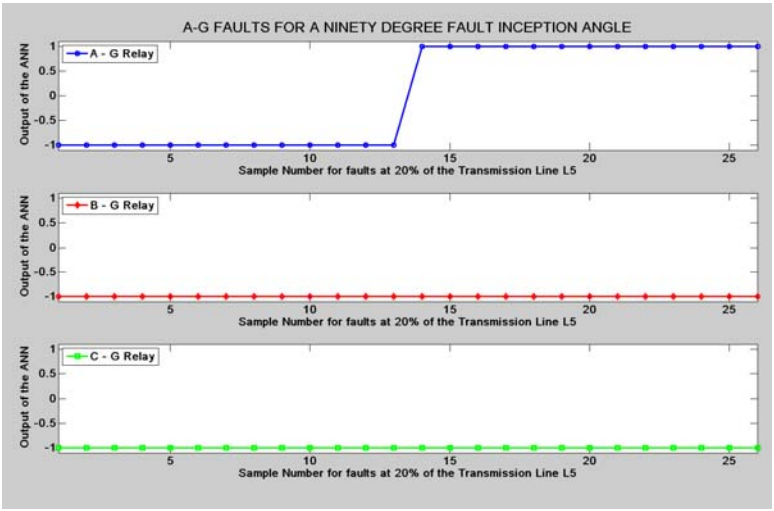

Figure G.27: Mho Relay - SLG Fault at 20% length of L_5,

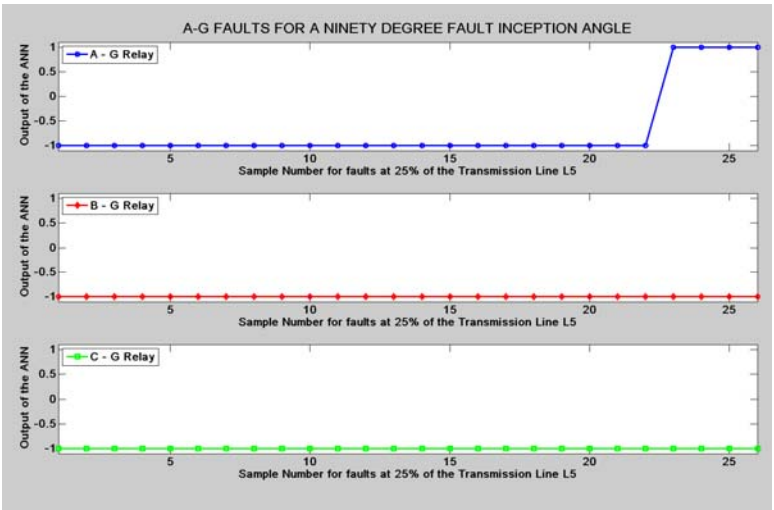

Figure G.28: Mho Relay - SLG Fault at 25% length of L_5

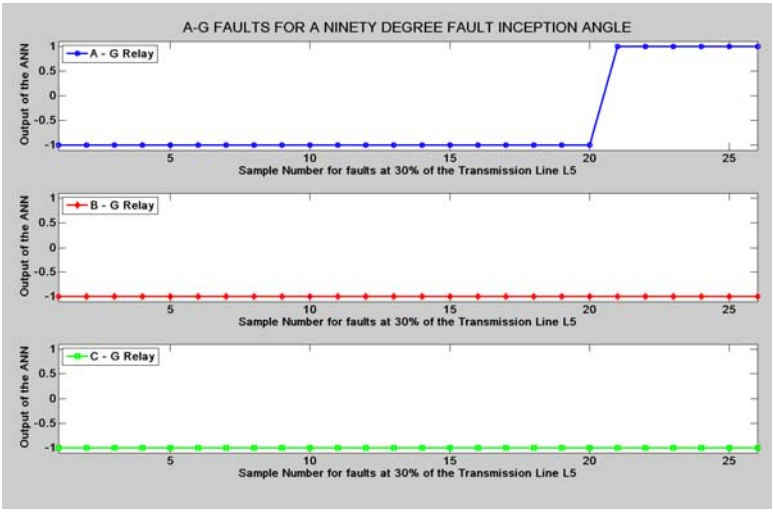

Figure G.29: Mho Relay - SLG Fault at 30% length of L_5

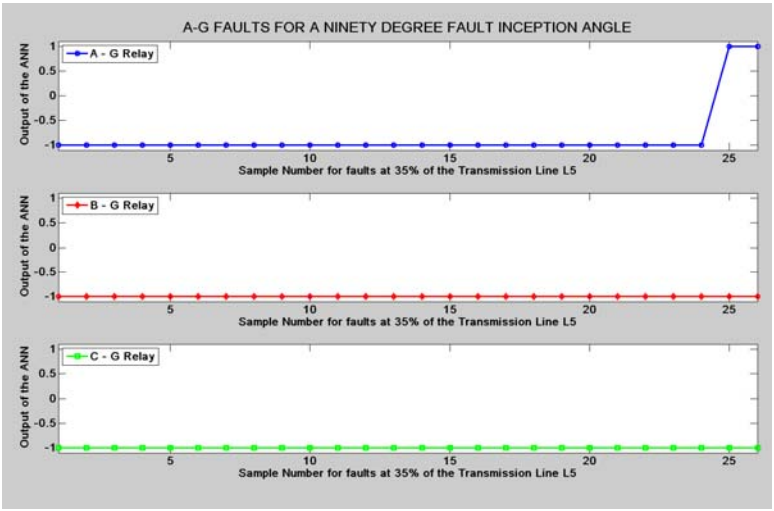

Figure G.30: Mho Relay - SLG Fault at 35% length of L_5

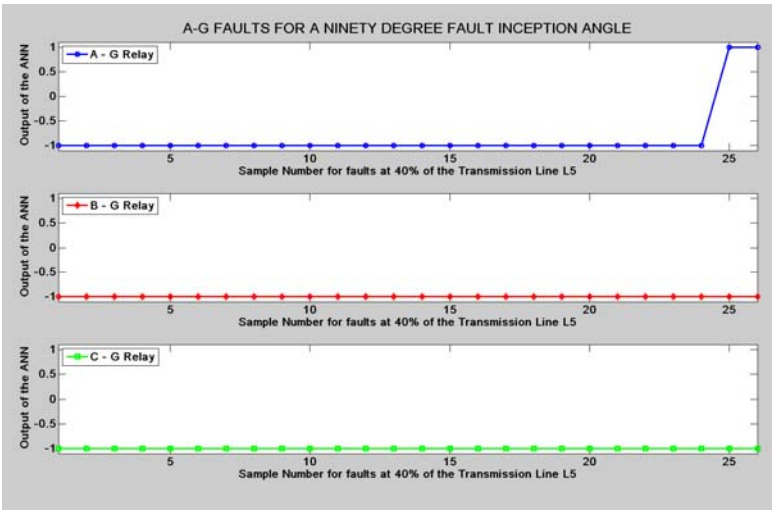

Figure G.31: Mho Relay - SLG Fault at 40% length of L_5

Figure G.32: Mho Relay - SLG Fault at 45% length of L_5

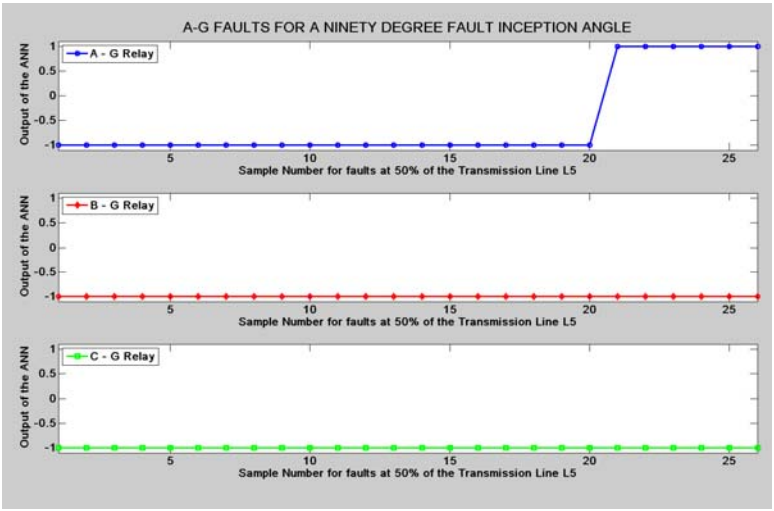

Figure G.33: Mho Relay - SLG Fault at 50% length of L_5

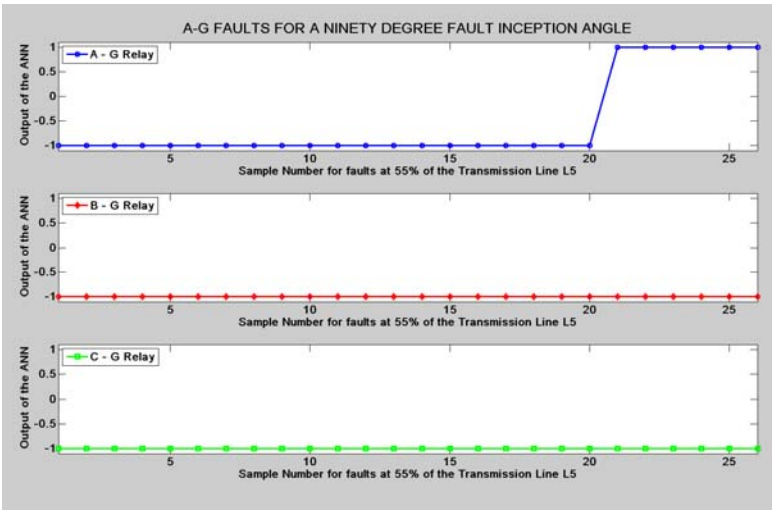

Figure G.34: Mho Relay - SLG Fault at 55% length of L_5

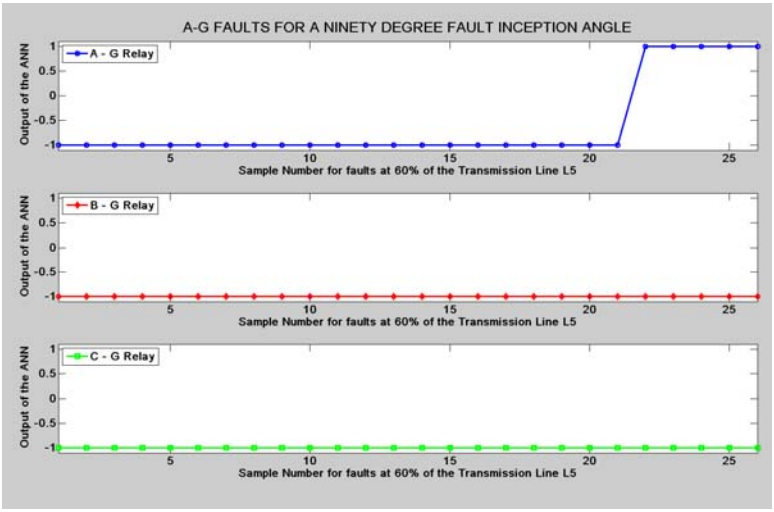

Figure G.35: Mho Relay - SLG Fault at 60% length of L_5

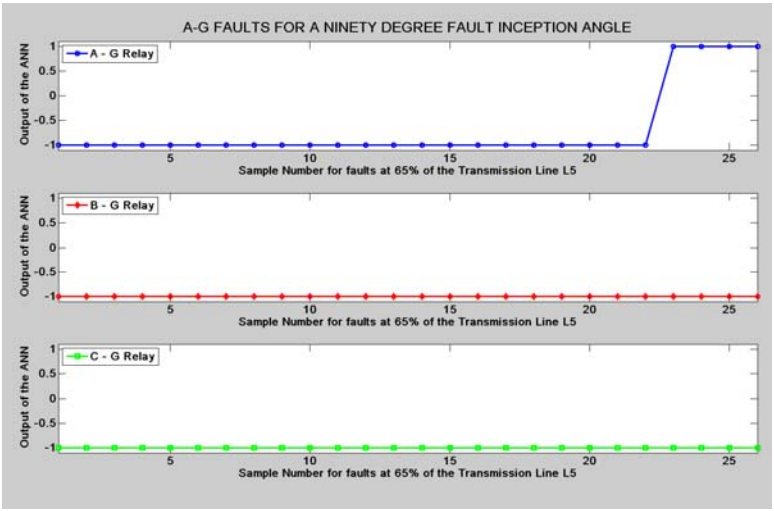

Figure G.36: Mho Relay - SLG Fault at 65% length of L_5

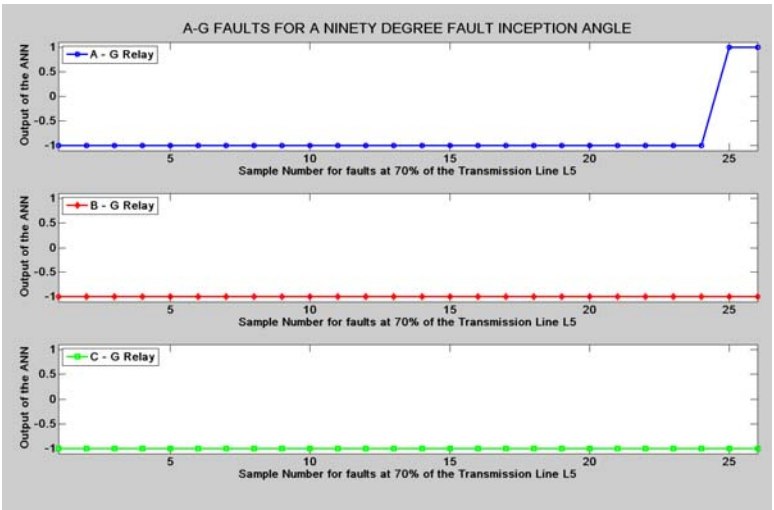

Figure G.37: Mho Relay - SLG Fault at 70% length of L_5

Figure G.38: Mho Relay - SLG Fault at 75% length of L_5

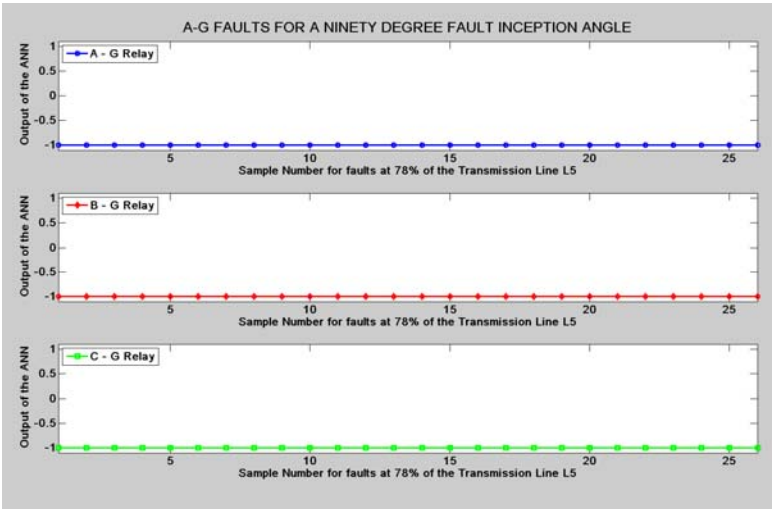

Figure G.39: Mho Relay - SLG Fault at 78% length of L_5

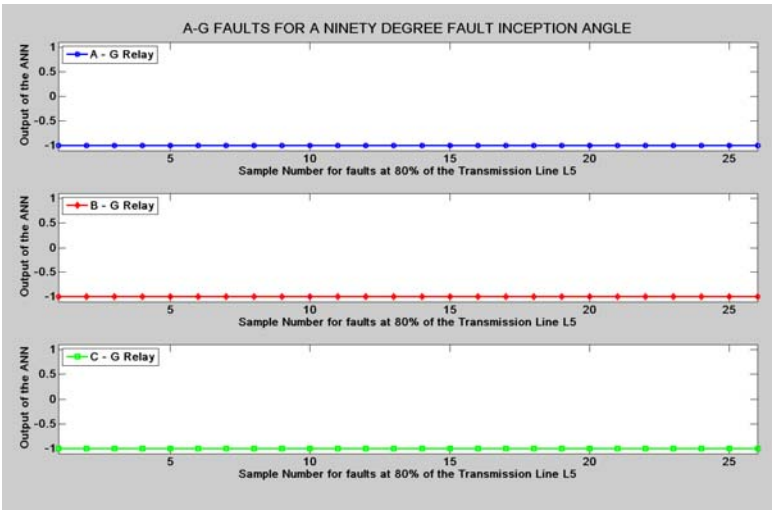

Figure G.40: Mho Relay - SLG Fault at 80% length of L_5

Figure G.41: Mho Relay - SLG Fault at 82% length of L_5

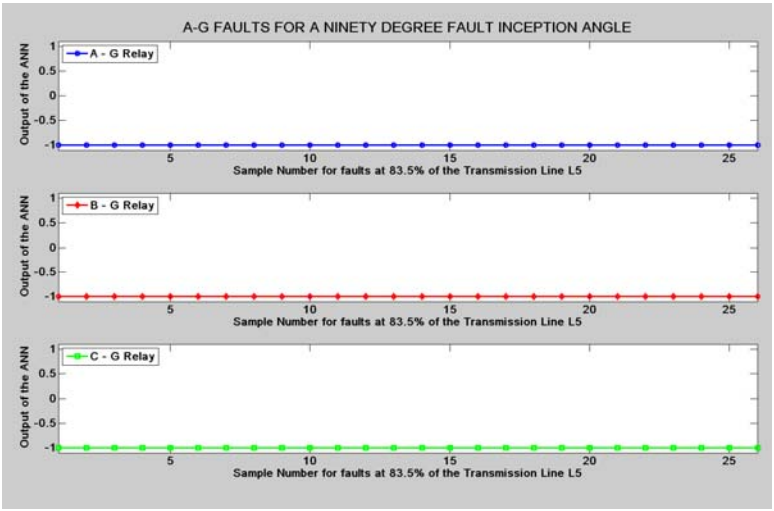

Figure G.42: Mho Relay - SLG Fault at 83.5% length of L_5

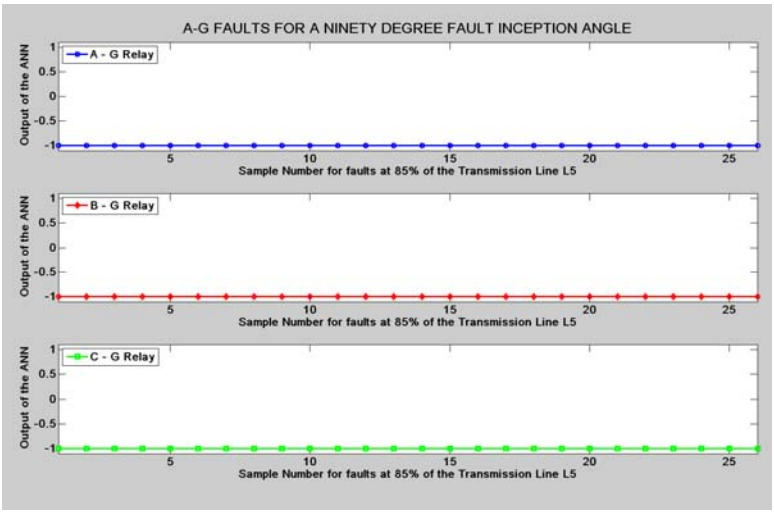

Figure G.43: Mho Relay - SLG Fault at 85% length of L_5

Figure G.44: Mho Relay - SLG Fault at 90% length of L_5

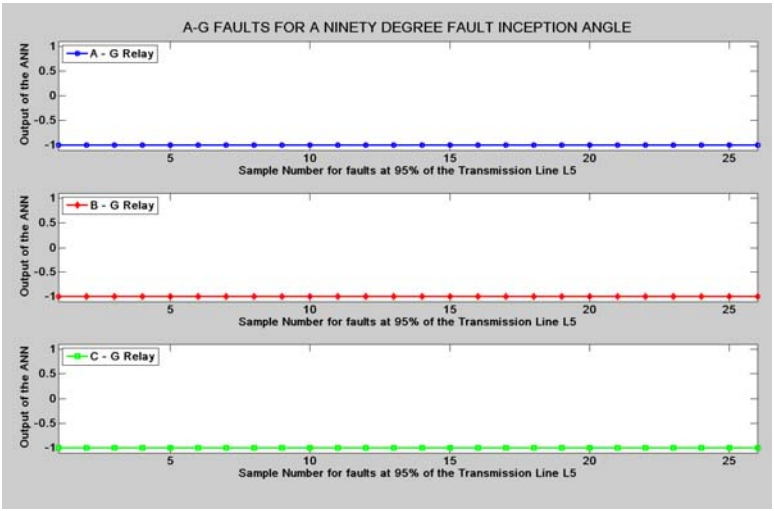

Figure G.45: Mho Relay - SLG Fault at 95% length of L_5

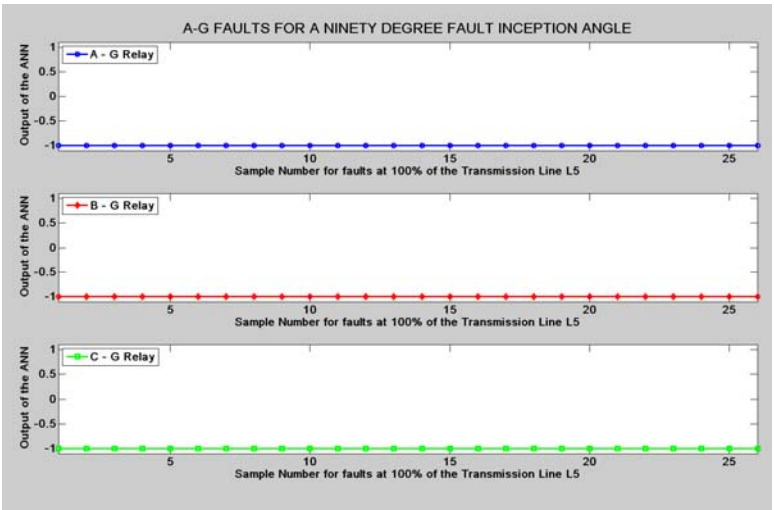

Figure G.46: Mho Relay - SLG Fault at 100% length of L_5

G.1.2 Two and Three Phase Faults

This section presents the results for line to line, double line to ground and three phase faults for zero degree fault inception angle.

a) Zero Degree Fault Inception:

Following are the results for line to line faults using self polarizing inputs.

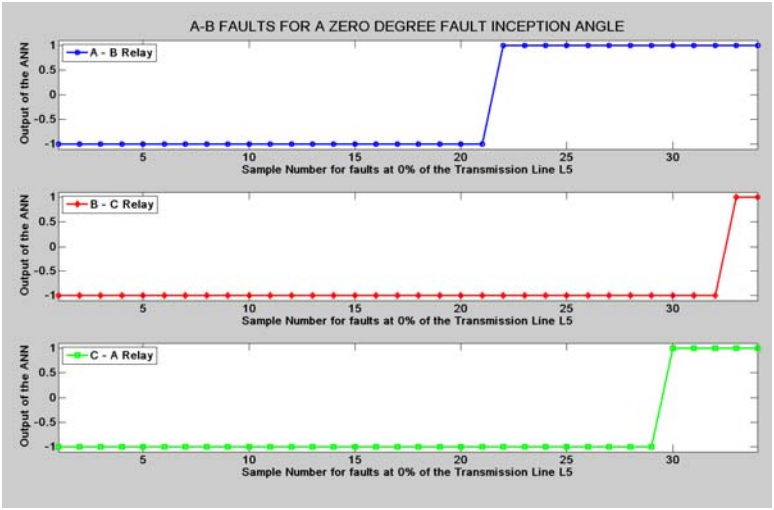

Figure G.47: Mho Relay - Line to Line Fault at 0% length of L5

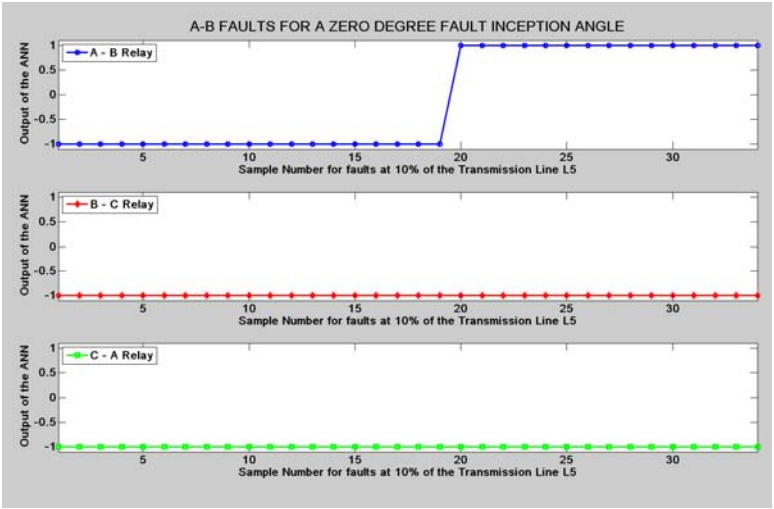

Figure G.48: Mho Relay - Line to Line Fault at 10% length of L_5

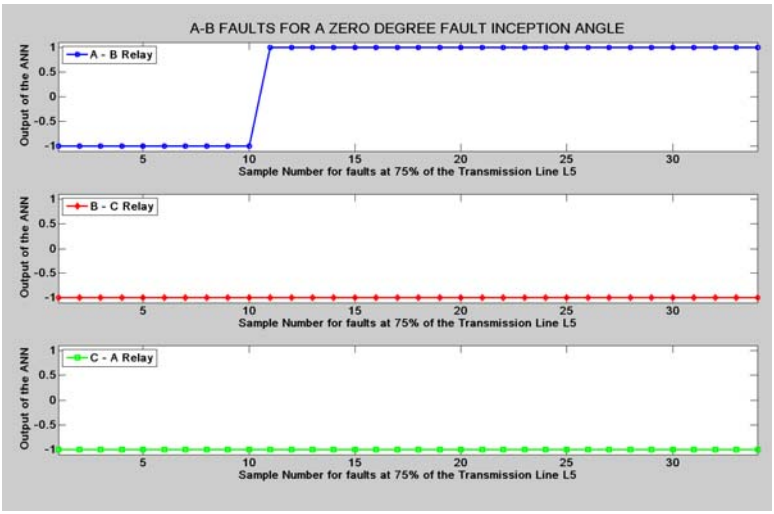

Figure G.49: Mho Relay - Line to Line Fault at 75% length of L_5

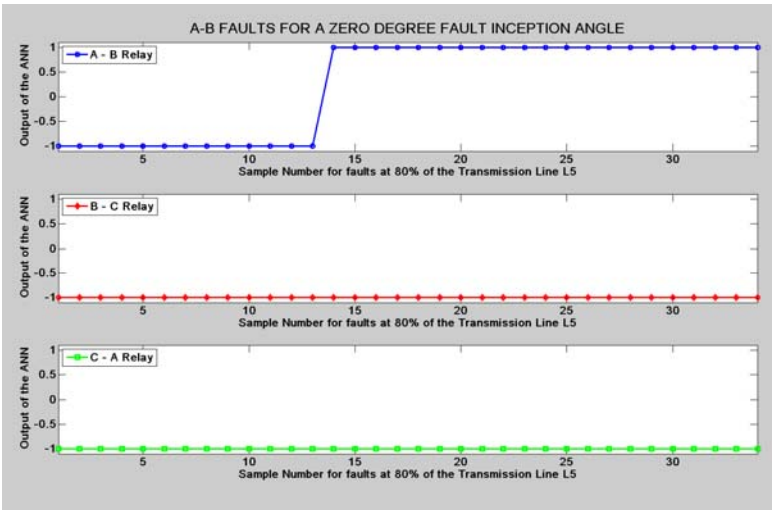

Figure G.50: Mho Relay - Line to Line Fault at 80% length of L_5

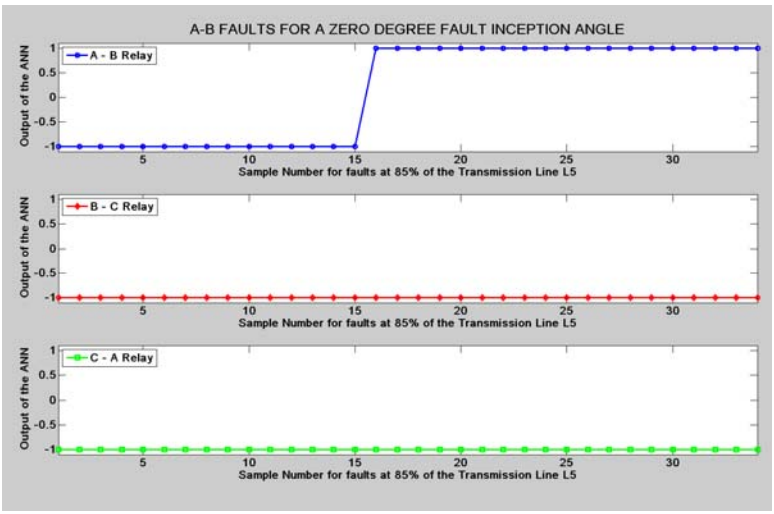

Figure G.51: Mho Relay - Line to Line Fault at 85% length of L_5

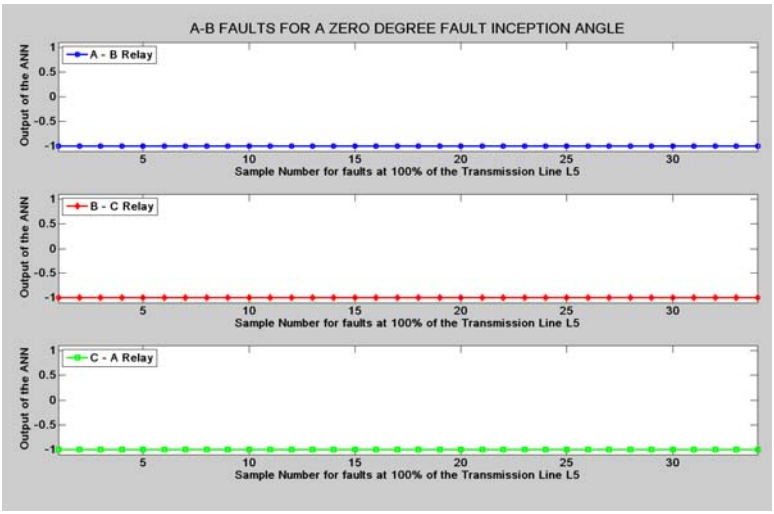

Figure G.52: Mho Relay - Line to Line Fault at 100% length of L_5

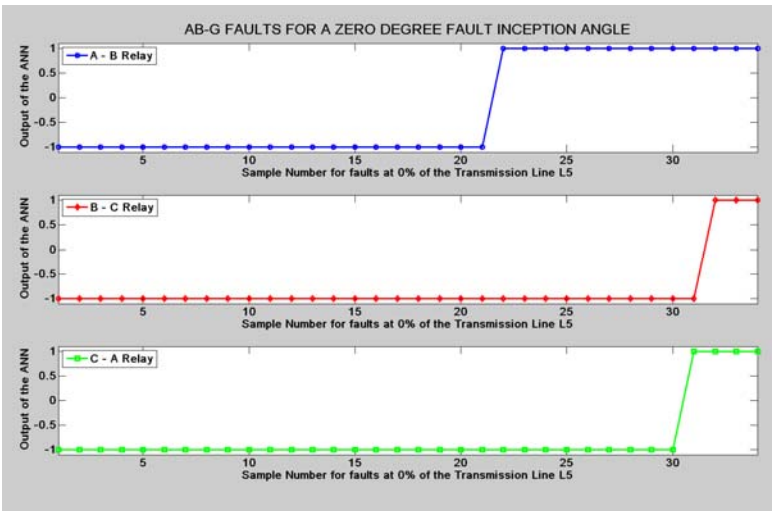

Figure G.53: Mho Relay – Double Line to Ground Fault at 0% length of L_5

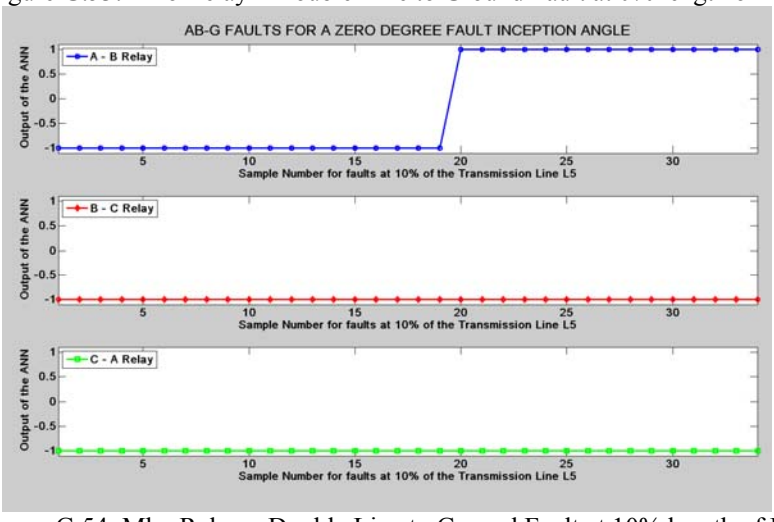

Figure G.54: Mho Relay – Double Line to Ground Fault at 10% length of L_5

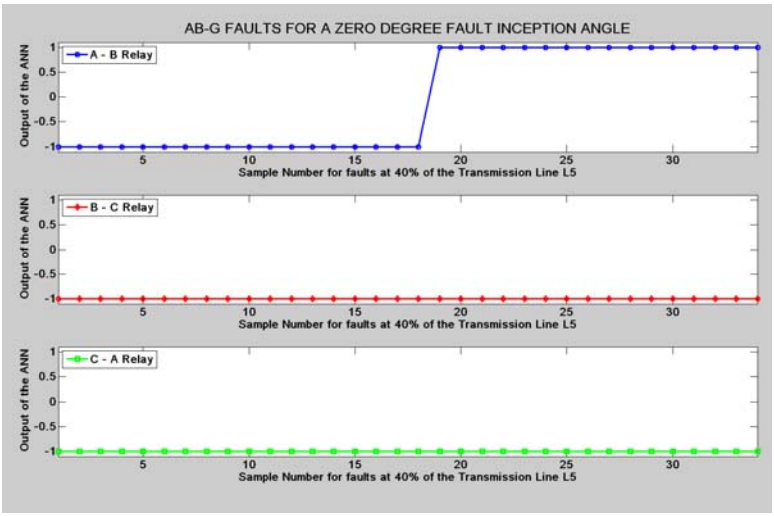

Figure G.55: Mho Relay – Double Line to Ground Fault at 40% length of L_5

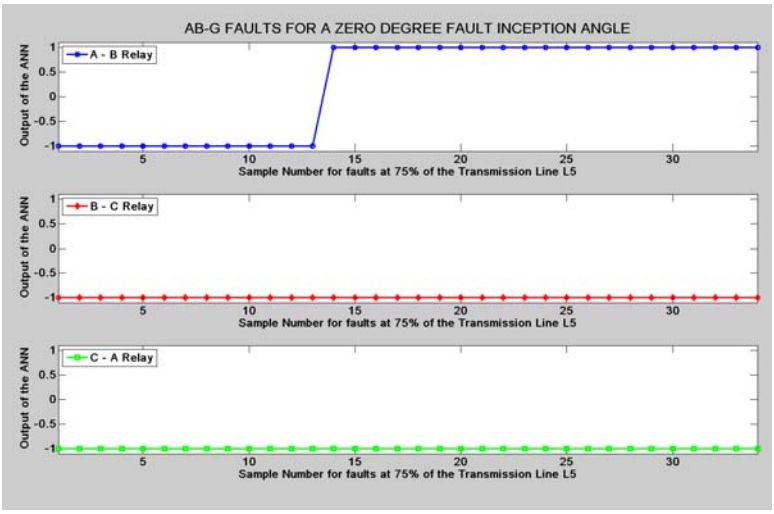

Figure G.56: Mho Relay – Double Line to Ground Fault at 75% length of L_5

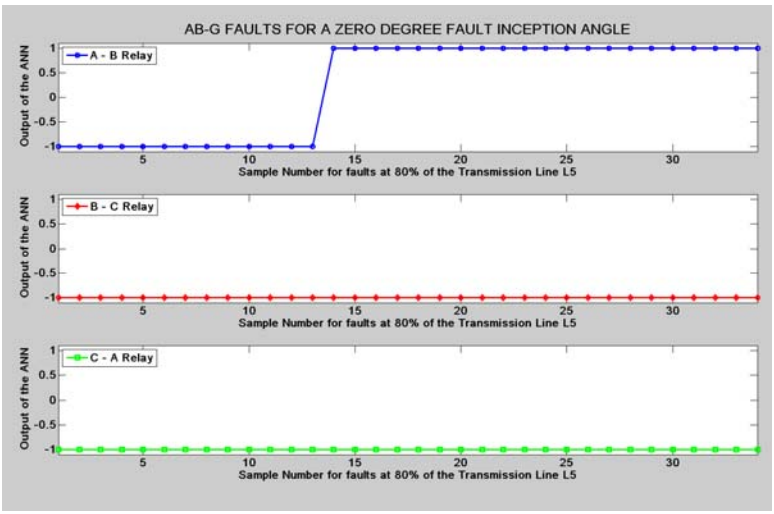

Figure G.57: Mho Relay – Double Line to Ground Fault at 80% length of L_5

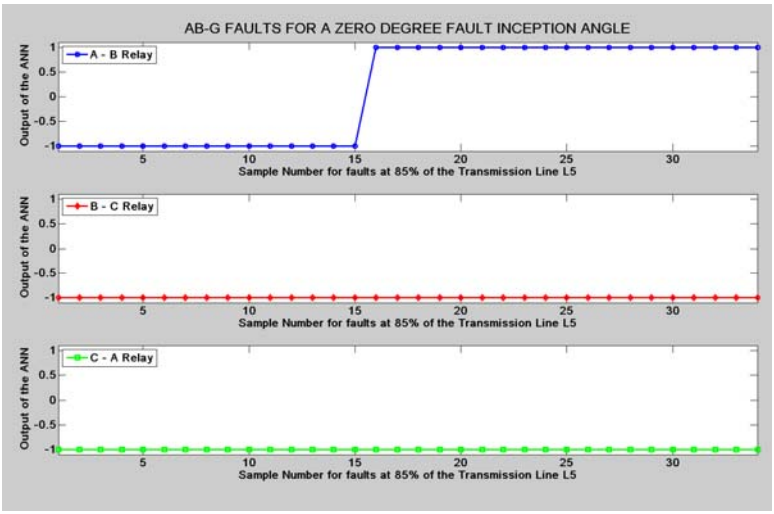

Figure G.58: Mho Relay – Double Line to Ground Fault at 85% length of L_5

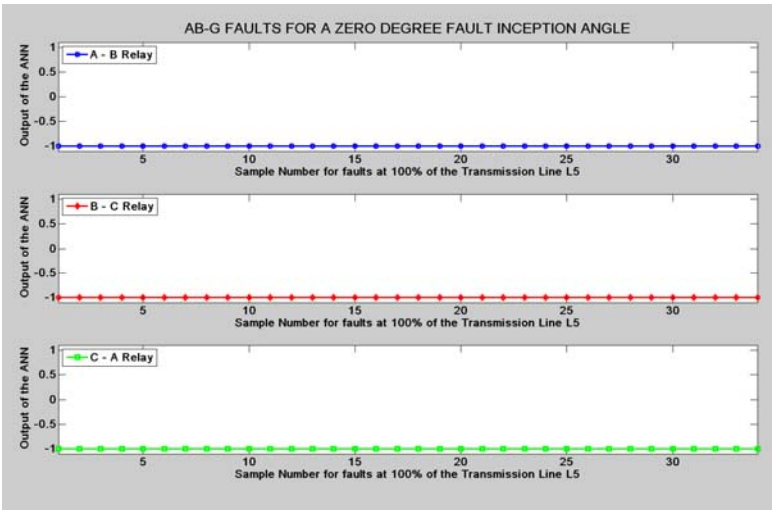

Figure G.59: Mho Relay – Double Line to Ground Fault at 100% length of L_5

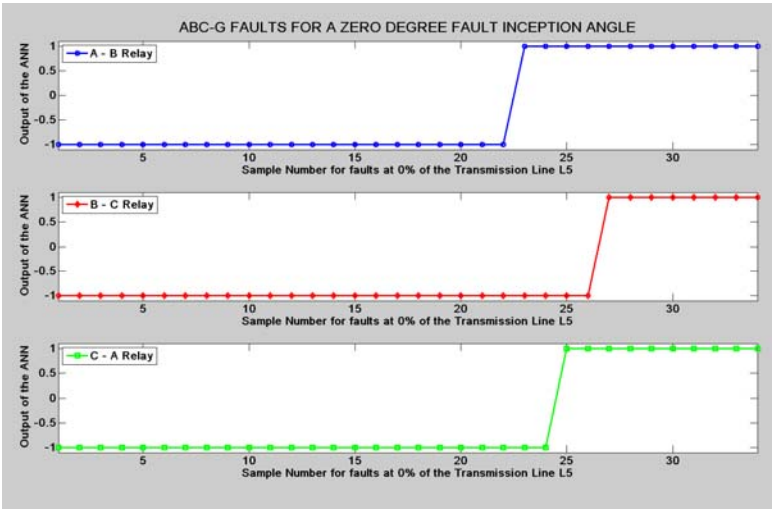

Figure G.60: Mho Relay – Three Line to Ground Fault at 0% length of L_5

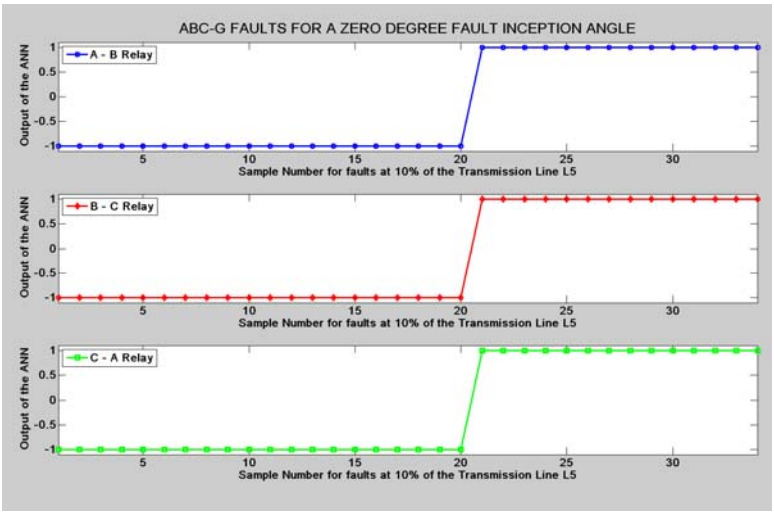

Figure G.61: Mho Relay – Three Line to Ground Fault at 10% length of L_5

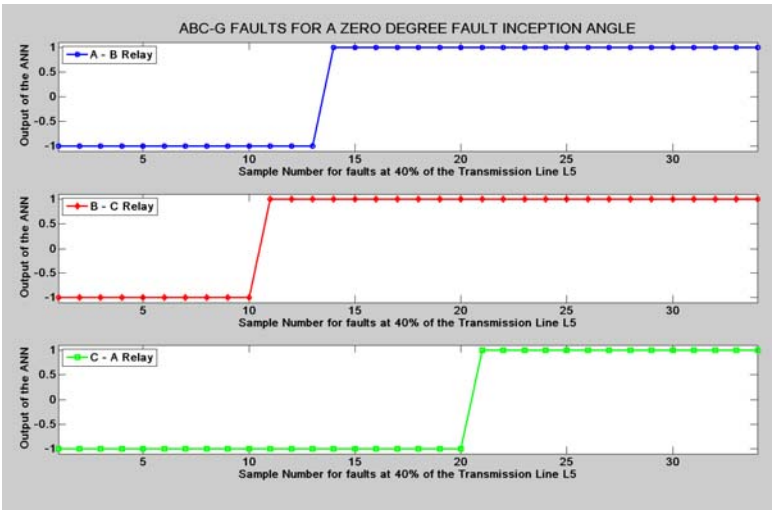

Figure G.62: Mho Relay – Three Line to Ground Fault at 40% length of L_5

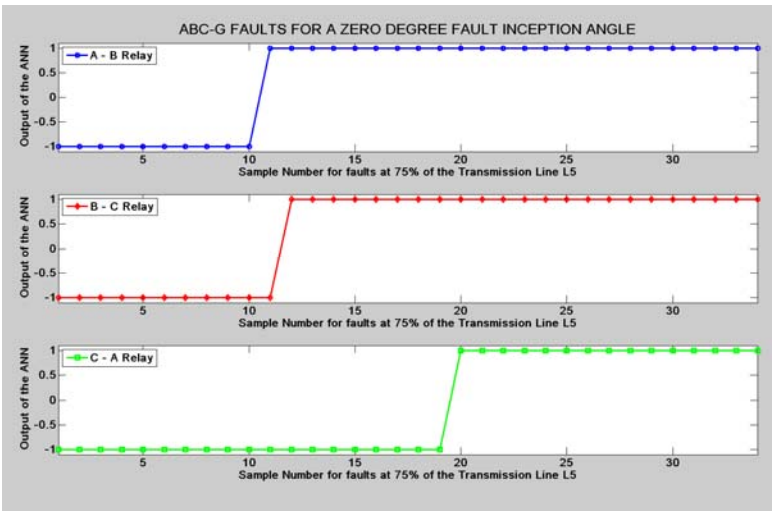

Figure G.63: Mho Relay – Three Line to Ground Fault at 75% length of L_5

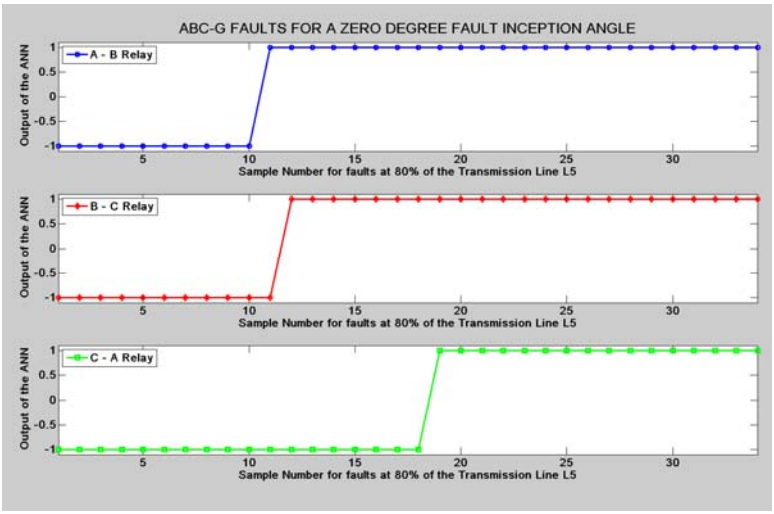

Figure G.64: Mho Relay – Three Line to Ground Fault at 80% length of L_5

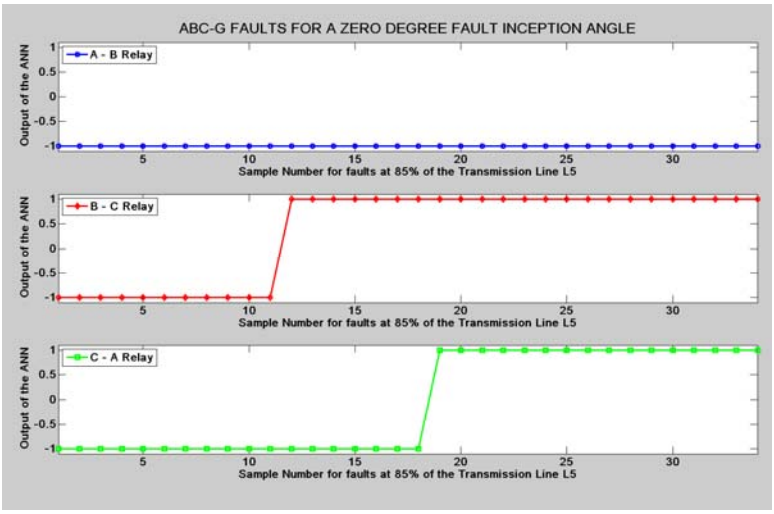

Figure G.65: Mho Relay – Three Line to Ground Fault at 85% length of L_5

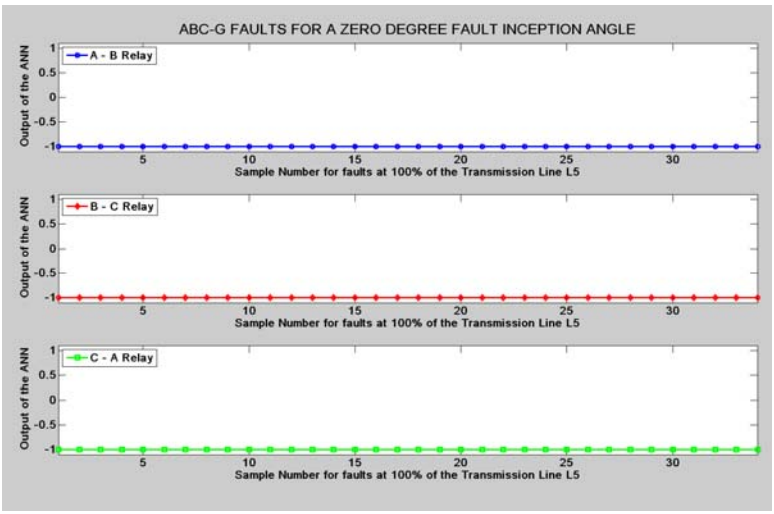

Figure G.66: Mho Relay – Three Line to Ground Fault at 100% length of L_5

G.2 Results for Quadrilateral Relay

This section presents the results for Quadrilateral relay for different types of fault cases previously discussed in Chapter 6.

G.2.1 Single Line to Ground Faults

(a) Zero Ohms Fault Resistance - Zero Degree Fault Inception and Ninety Degree Fault Inception:

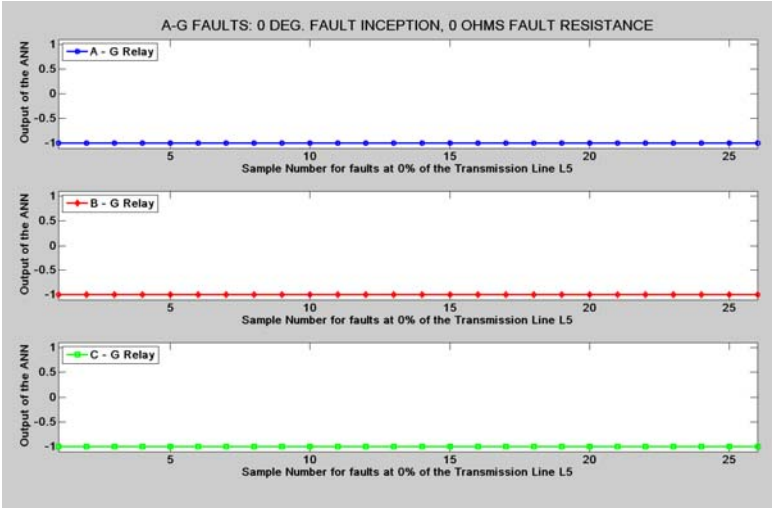

Figure G.67: Quadrilateral Relay – SLG Fault at 0% length of L_5, 0º Inception, 0 Ω Fault Resistance

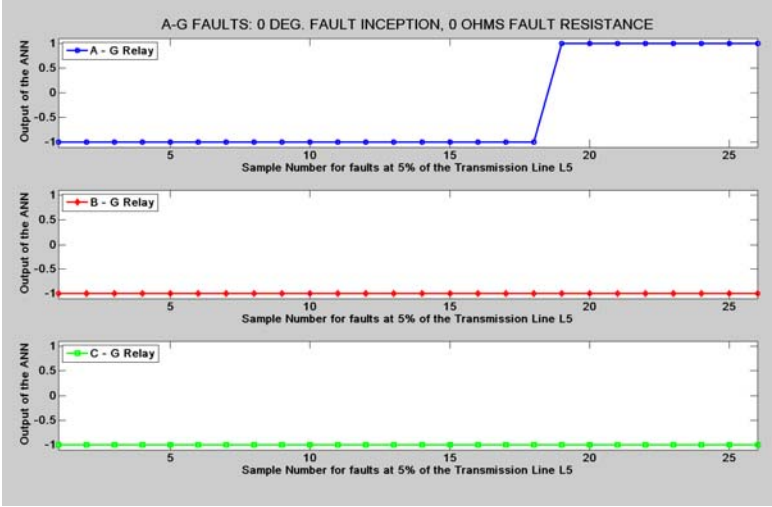

Figure G.68: Quadrilateral Relay – SLG Fault at 5% length of L_5, 0º Inception, 0 Ω Fault Resistance

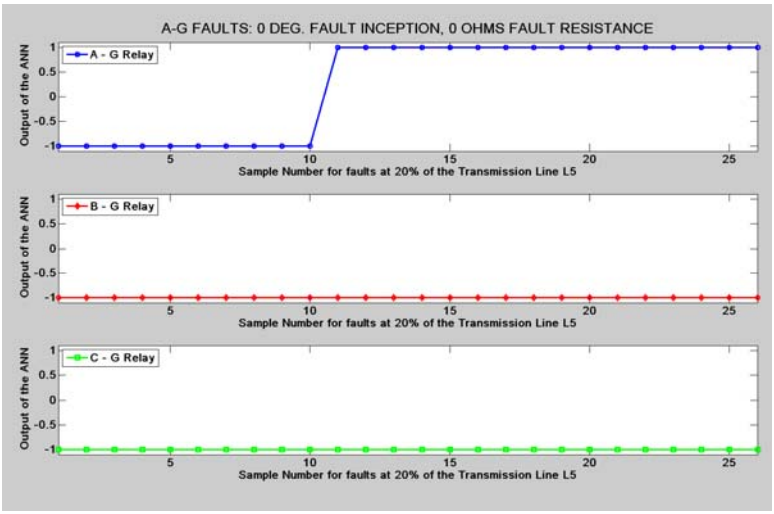

Figure G.69: Quadrilateral Relay – SLG Fault at 20% length of L_5, 0º Inception, 0 Ω Fault Resistance

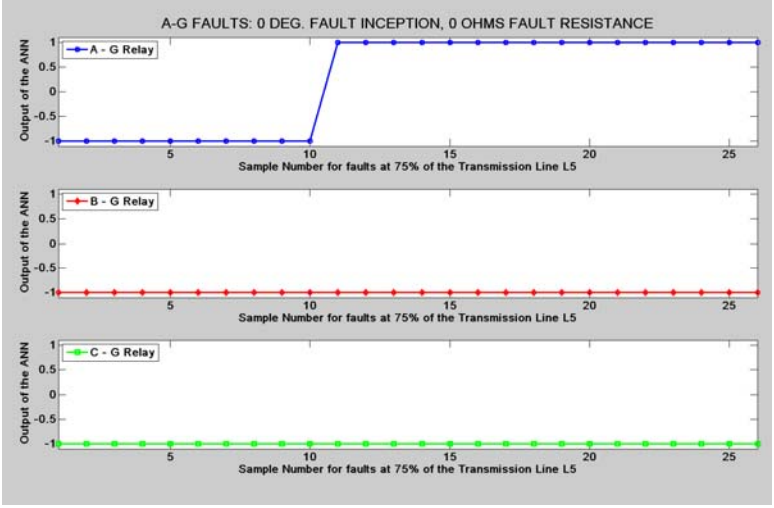

Figure G.70: Quadrilateral Relay – SLG Fault at 75% length of L_5, 0º Inception, 0 Ω Fault Resistance

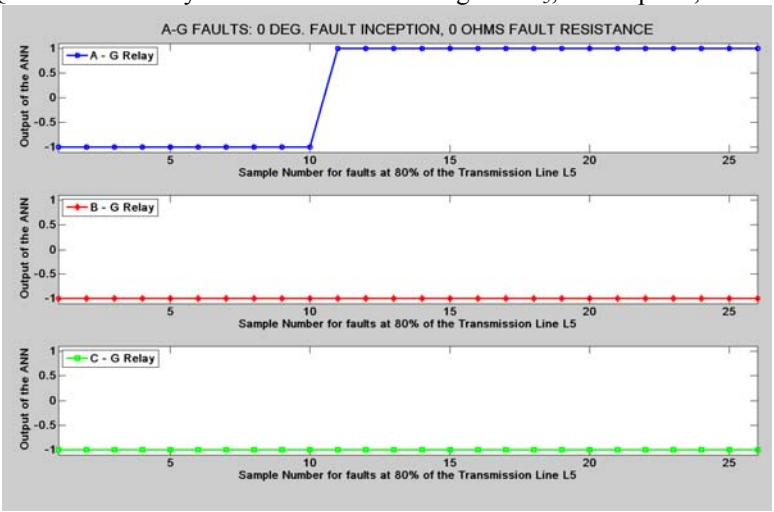

Figure G.71: Quadrilateral Relay – SLG Fault at 80% length of L_5, 0º Inception, 0 Ω Fault Resistance

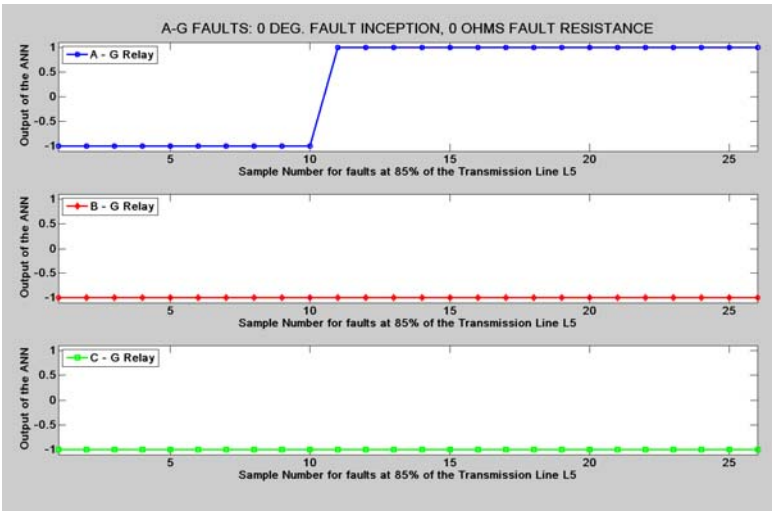

Figure G.72: Quadrilateral Relay – SLG Fault at 85% length of L_5, 0º Inception, 0 Ω Fault Resistance

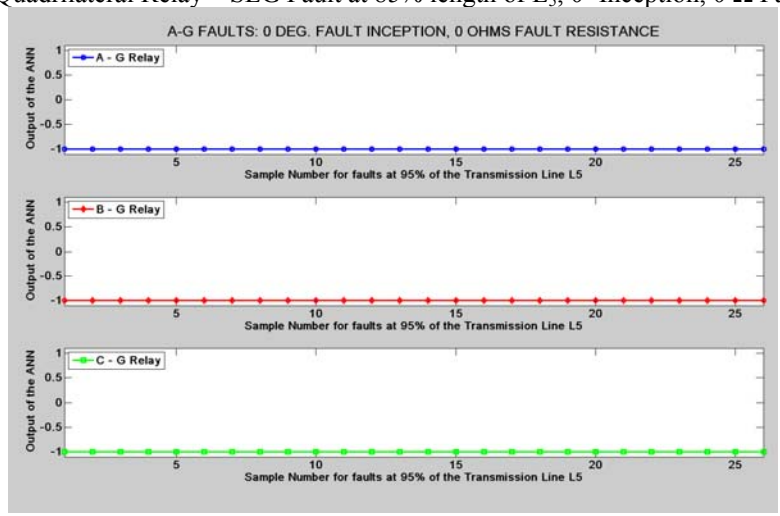

Figure G.73: Quadrilateral Relay – SLG Fault at 95% length of L_5, 0º Inception, 0 Ω Fault Resistance

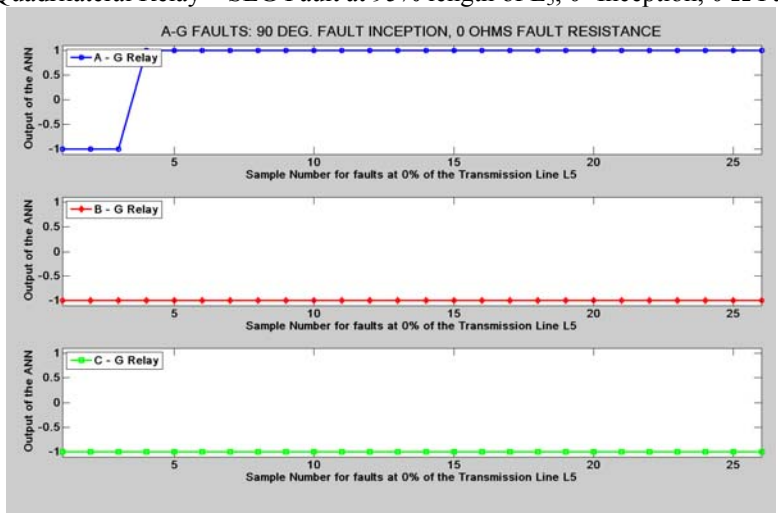

Figure G.74: Quadrilateral Relay – SLG Fault at 0% length of L_5, 90º Inception, 0 Ω Fault Resistance

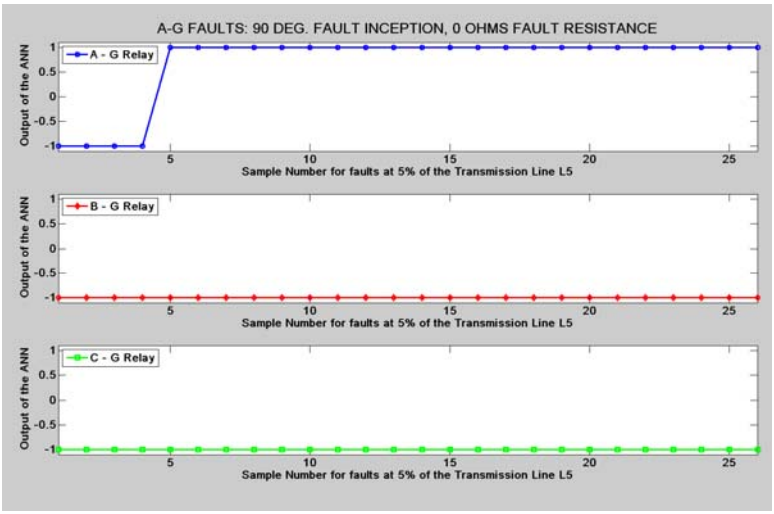

Figure G.75: Quadrilateral Relay – SLG Fault at 5% length of L_5, 90º Inception, 0 Ω Fault Resistance

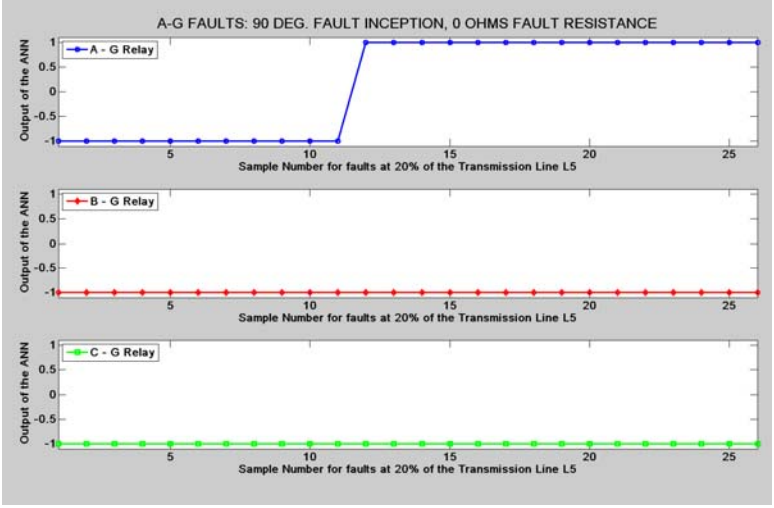

Figure G.76: Quadrilateral Relay – SLG Fault at 20% length of L_5, 90º Inception, 0 Ω Fault Resistance

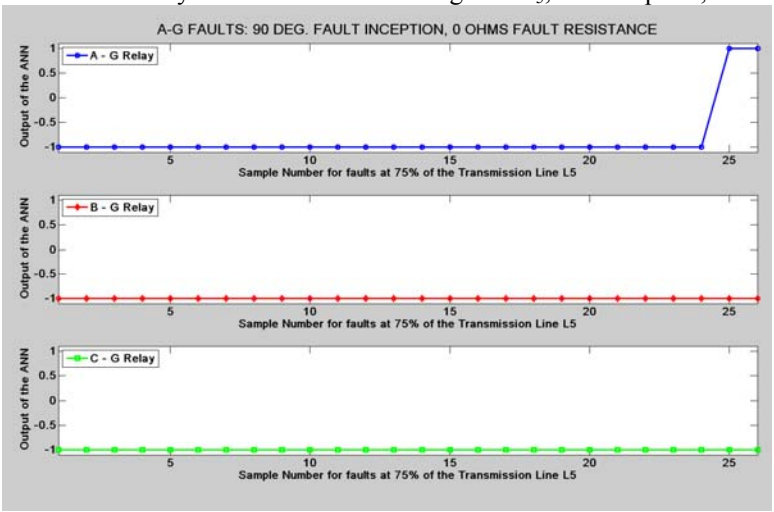

Figure G.77: Quadrilateral Relay – SLG Fault at 75% length of L_5, 90º Inception, 0 Ω Fault Resistance

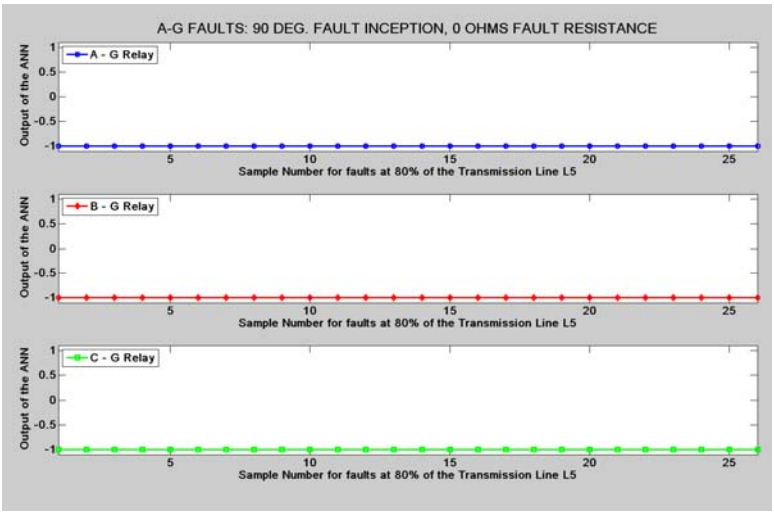

Figure G.78: Quadrilateral Relay – SLG Fault at 80% length of L_5, 90º Inception, 0 Ω Fault Resistance

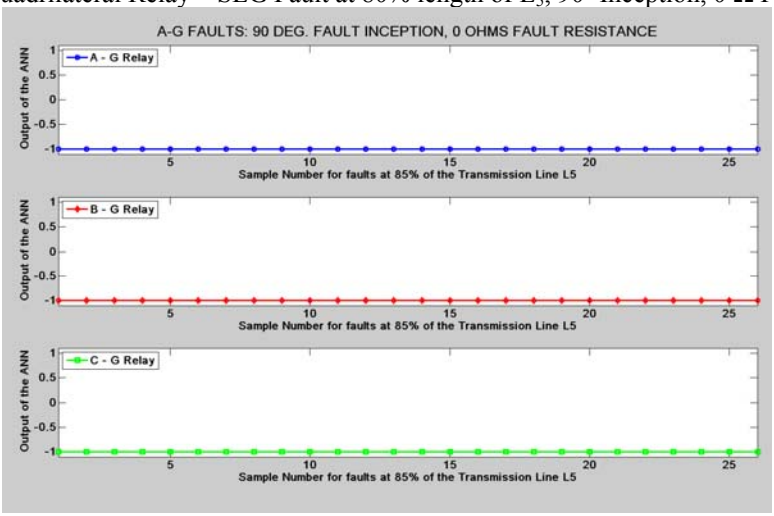

Figure G.79: Quadrilateral Relay – SLG Fault at 85% length of L_5, 90º Inception, 0 Ω Fault Resistance

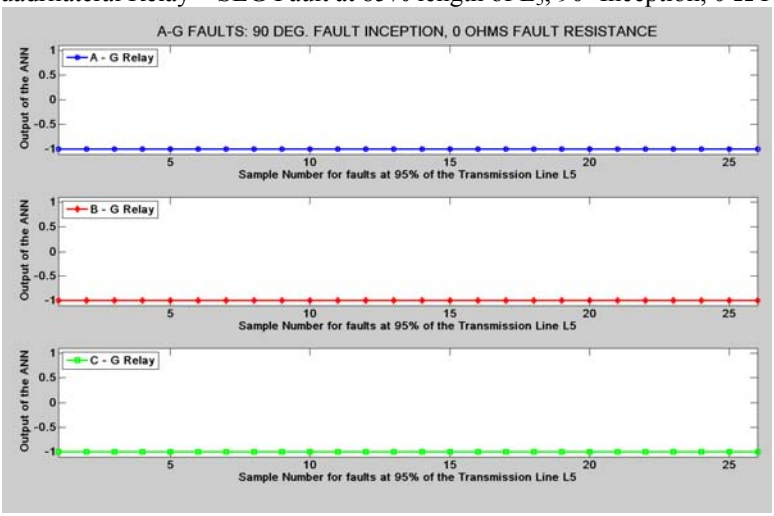

Figure G.80: Quadrilateral Relay – SLG Fault at 95% length of L_5, 90º Inception, 0 Ω Fault Resistance

(b) 15Ω Fault Resistance - Zero Degree and Ninety Degree Fault Inception:

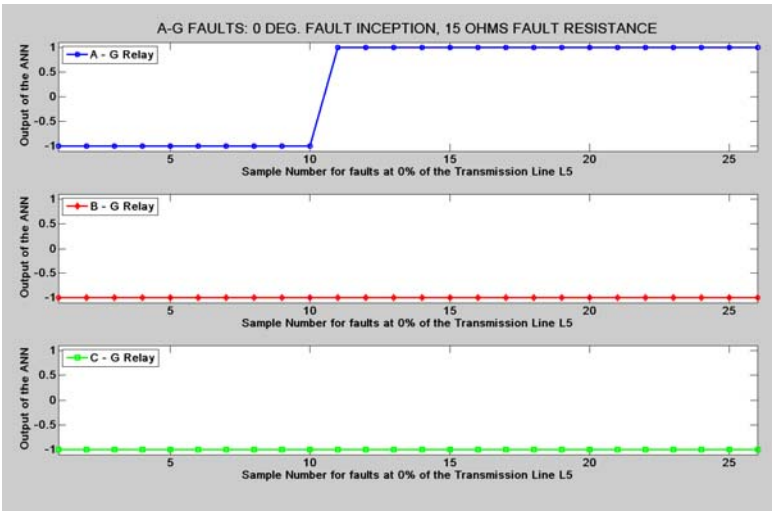

Figure G.81: Quadrilateral Relay – SLG Fault at 0% length of L_5, 0º Inception, 15 Ω Fault Resistance

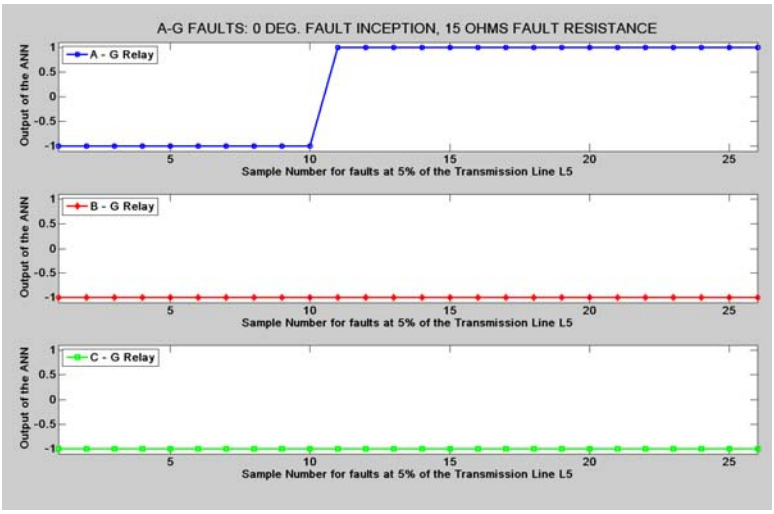

Figure G.82: Quadrilateral Relay – SLG Fault at 5% length of L_5, 0º Inception, 15 Ω Fault Resistance

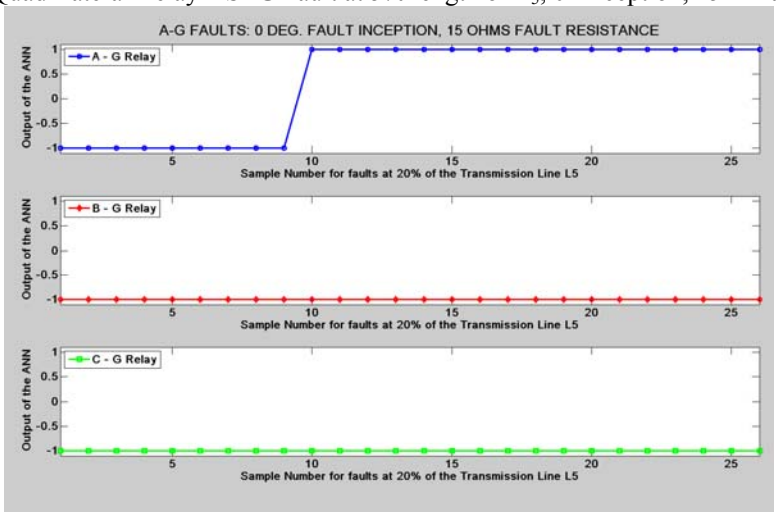

Figure G.83: Quadrilateral Relay – SLG Fault at 20% length of L_5, 0º Inception, 15 Ω Fault Resistance

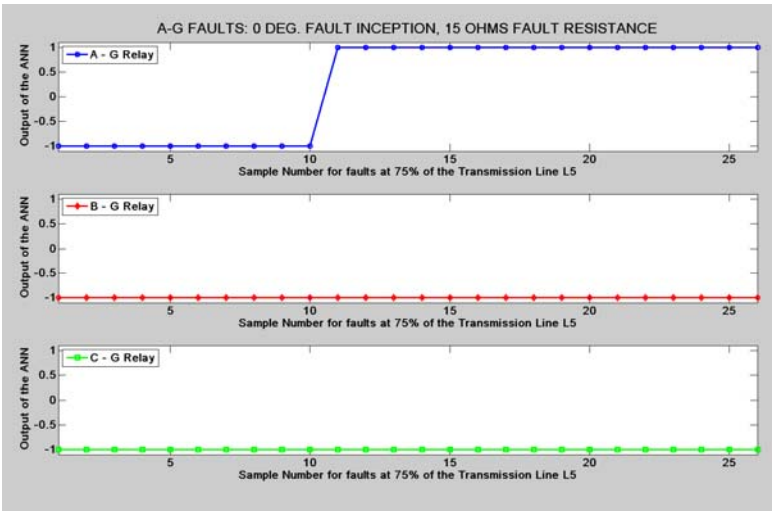

Figure G.84: Quadrilateral Relay – SLG Fault at 75% length of L_5, 0º Inception, 15 Ω Fault Resistance

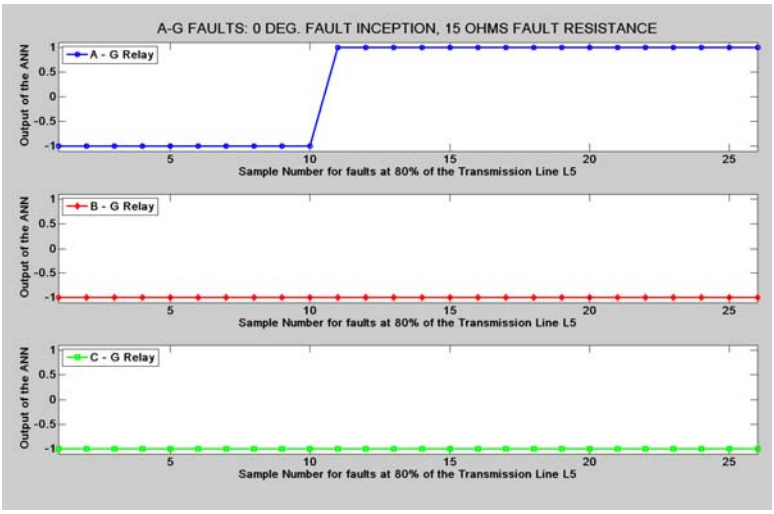

Figure G.85: Quadrilateral Relay – SLG Fault at 80% length of L_5, 0º Inception, 15 Ω Fault Resistance

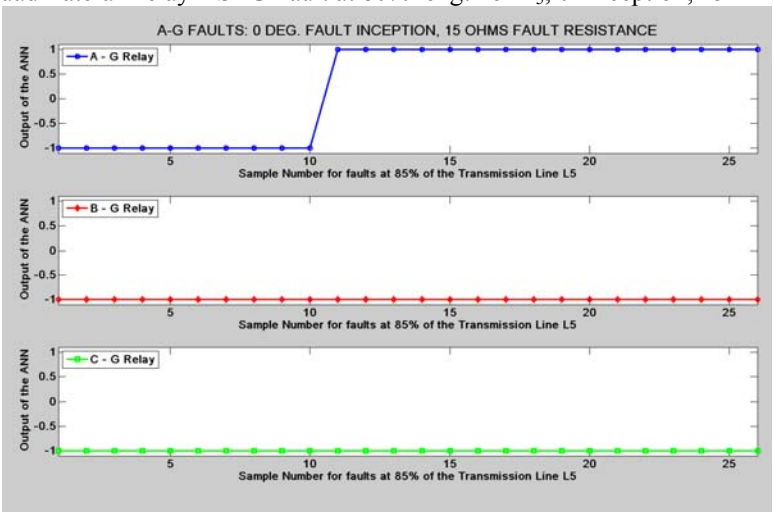

Figure G.86: Quadrilateral Relay – SLG Fault at 85% length of L_5, 0º Inception, 15 Ω Fault Resistance

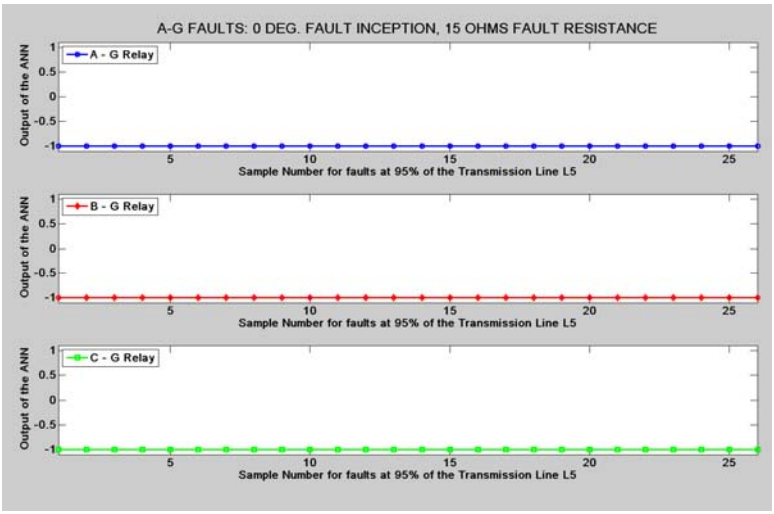

Figure G.87: Quadrilateral Relay – SLG Fault at 95% length of L_5, 0º Inception, 15 Ω Fault Resistance

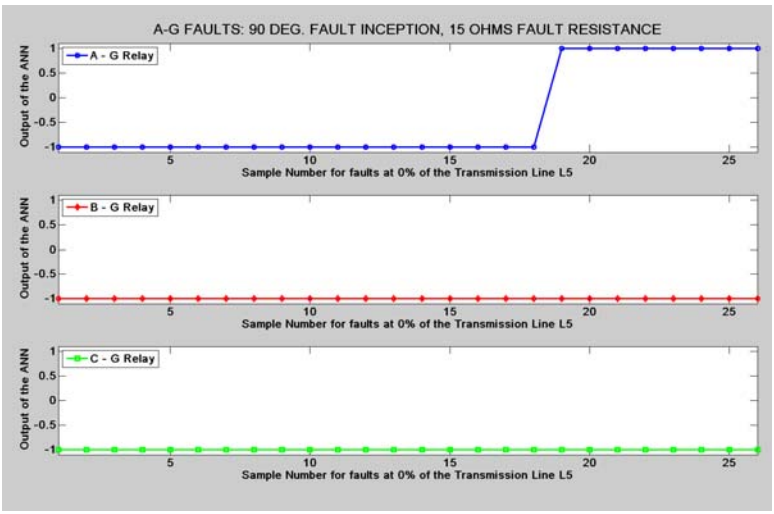

Figure G.88: Quadrilateral Relay – SLG Fault at 0% length of L_5, 90º Inception, 15 Ω Fault Resistance

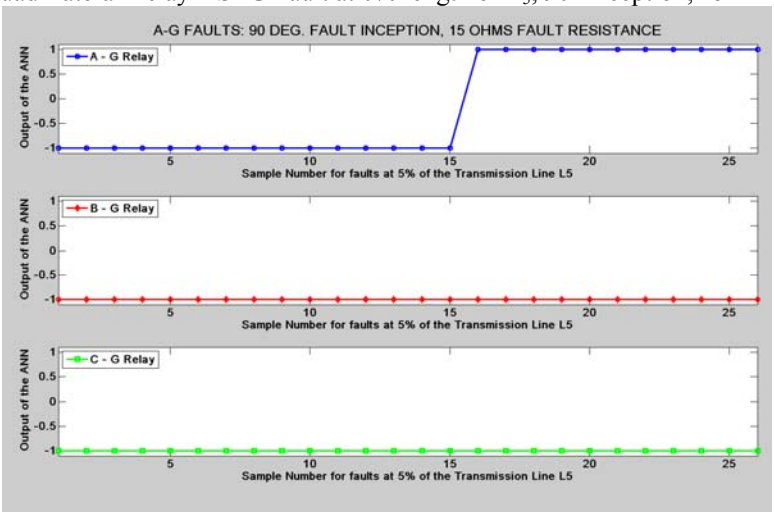

Figure G.89: Quadrilateral Relay – SLG Fault at 5% length of L_5, 90º Inception, 15 Ω Fault Resistance

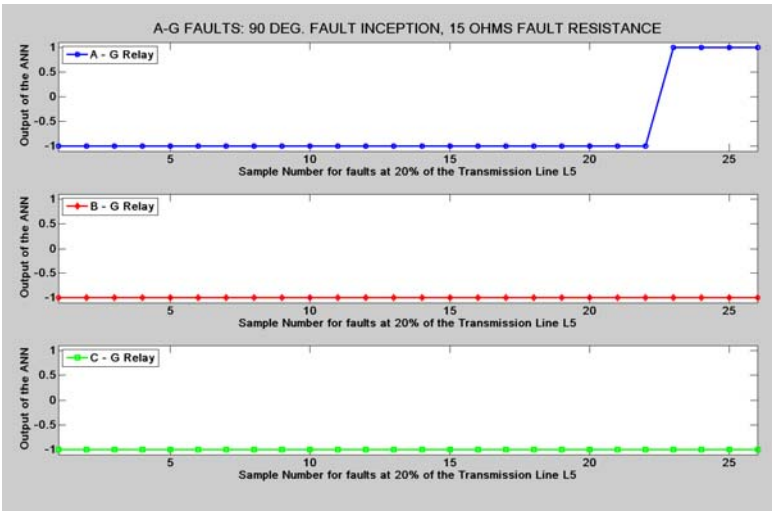

Figure G.90: Quadrilateral Relay – SLG Fault at 20% length of L_5, 90º Inception, 15 Ω Fault Resistance

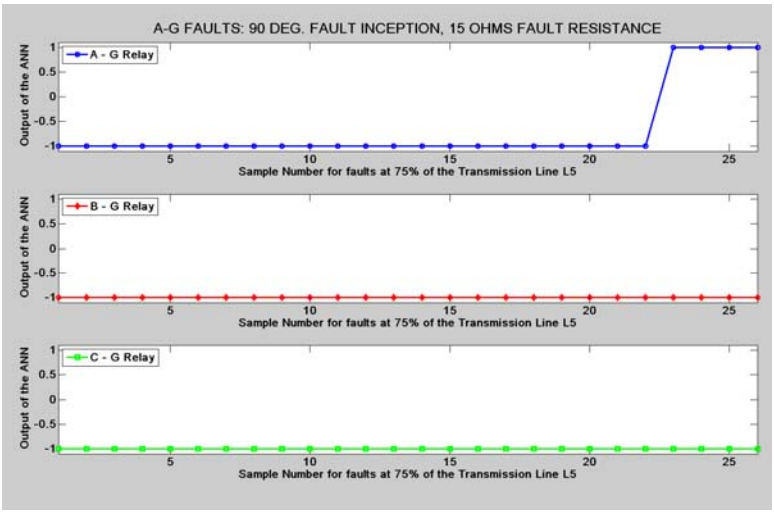

Figure G.91: Quadrilateral Relay – SLG Fault at 75% length of L_5, 90º Inception, 15 Ω Fault Resistance

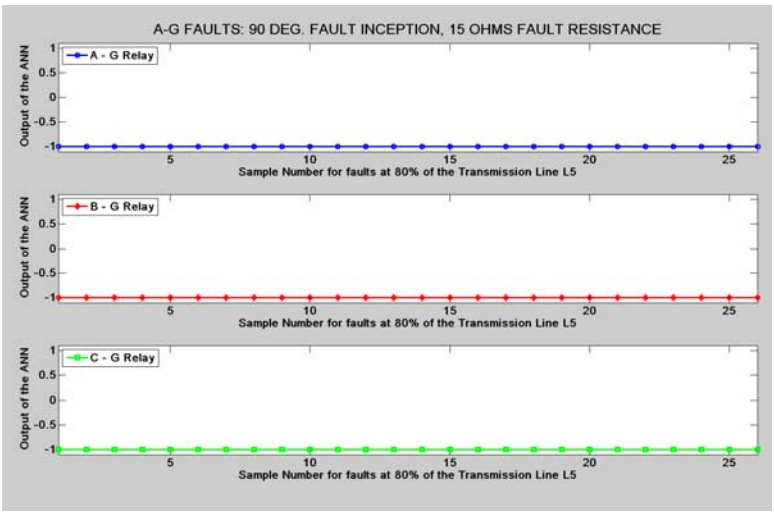

Figure G.92: Quadrilateral Relay – SLG Fault at 80% length of L_5, 90º Inception, 15 Ω Fault Resistance

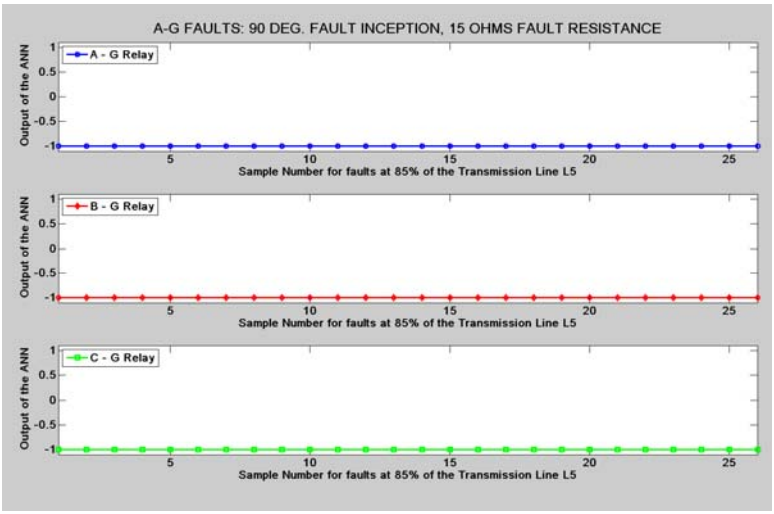

Figure G.93: Quadrilateral Relay – SLG Fault at 85% length of L_5, 90º Inception, 15 Ω Fault Resistance

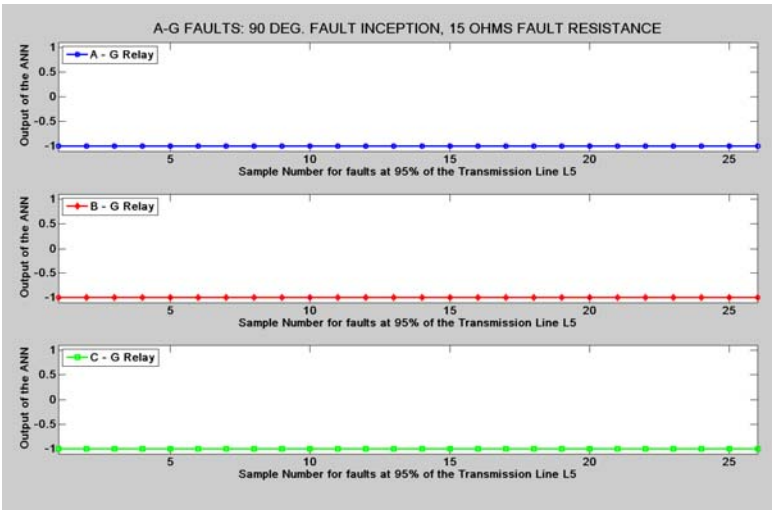

Figure G.94: Quadrilateral Relay – SLG Fault at 95% length of L_5, 90º Inception, 15 Ω Fault Resistance

(c) 50 Ω Fault Resistance - Zero Degree and Ninety Degree Fault Inception:

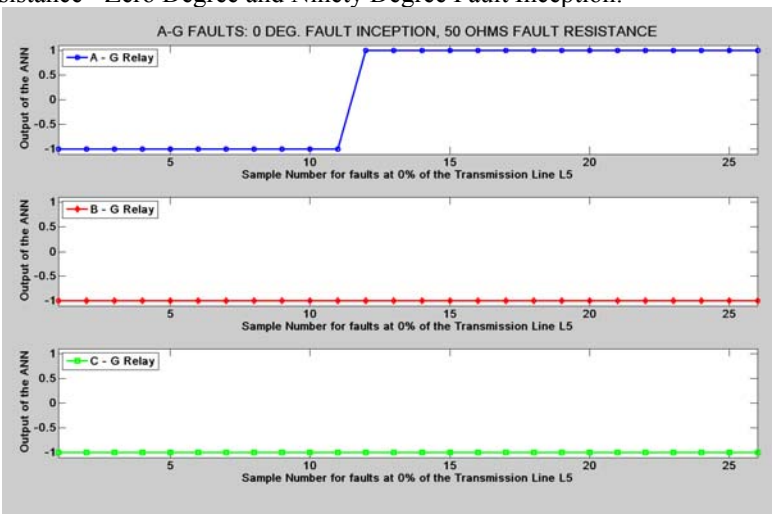

Figure G.95: Quadrilateral Relay – SLG Fault at 0% length of L_5, 0º Inception, 50 Ω Fault Resistance

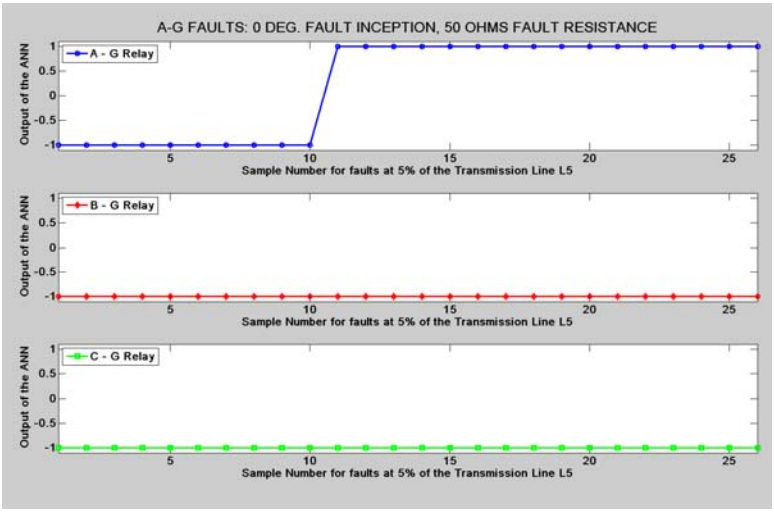

Figure G.96: Quadrilateral Relay – SLG Fault at 5% length of L_5, 0º Inception, 50 Ω Fault Resistance

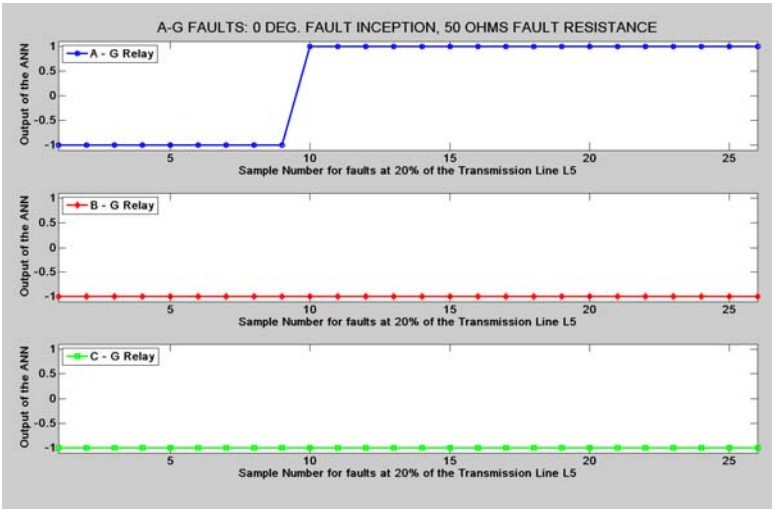

Figure G.97: Quadrilateral Relay – SLG Fault at 20% length of L_5, 0º Inception, 50 Ω Fault Resistance

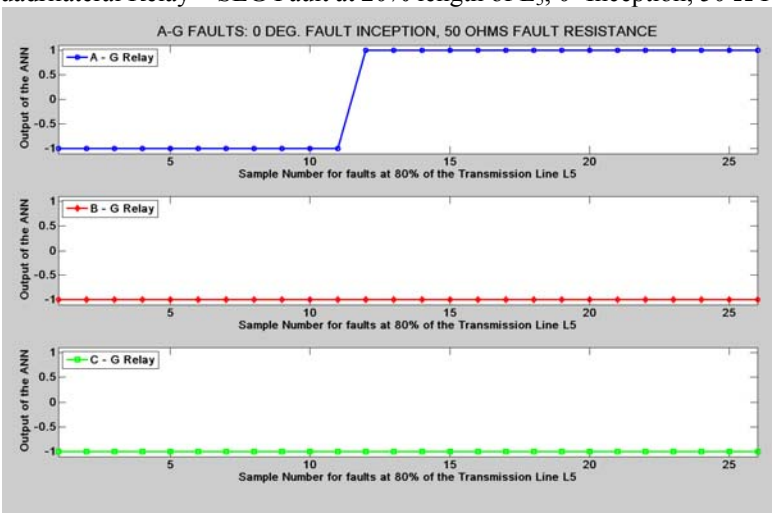

Figure G.98: Quadrilateral Relay – SLG Fault at 80% length of L_5, 0º Inception, 50 Ω Fault Resistance

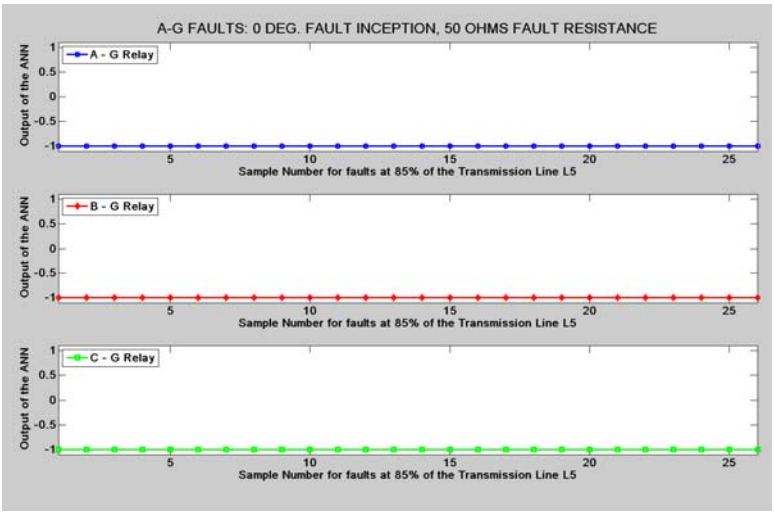

Figure G.99: Quadrilateral Relay – SLG Fault at 85% length of L_5, 0º Inception, 50 Ω Fault Resistance

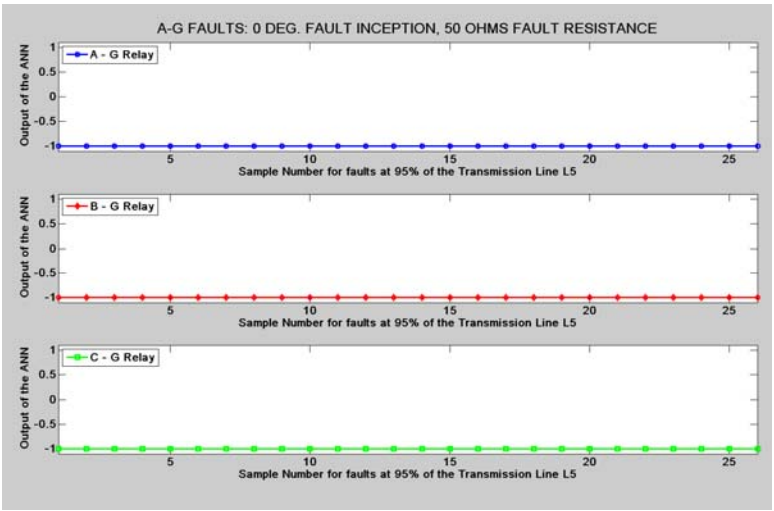

Figure G.100: Quadrilateral Relay – SLG Fault at 95% length of L_5, 0º Inception, 50 Ω Fault Resistance

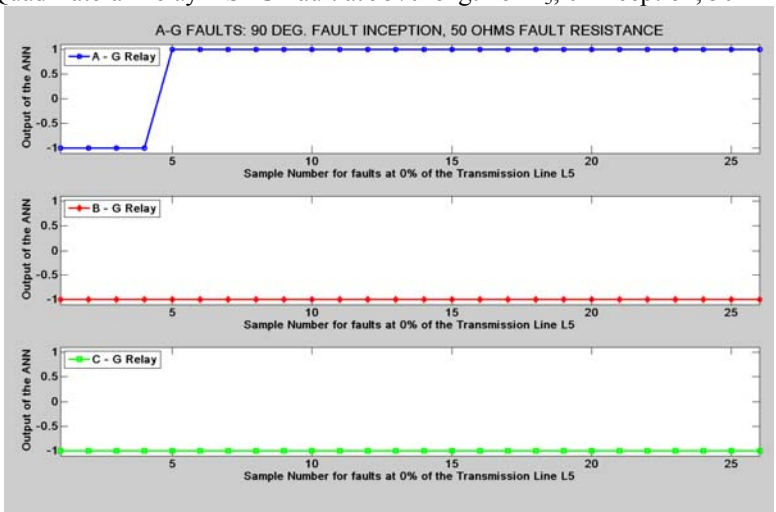

Figure G.101: Quadrilateral Relay – SLG Fault at 0% length of L_5, 90º Inception, 50 Ω Fault Resistance

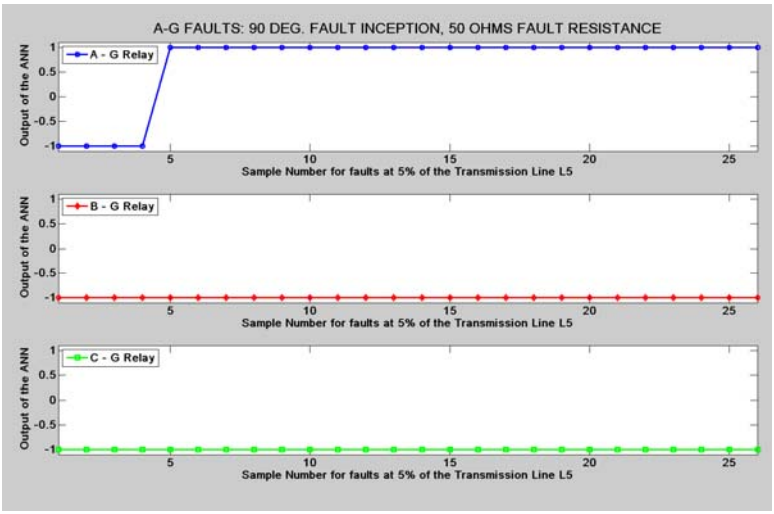

Figure G.102: Quadrilateral Relay – SLG Fault at 5% length of L_5, 90º Inception, 50 Ω Fault Resistance

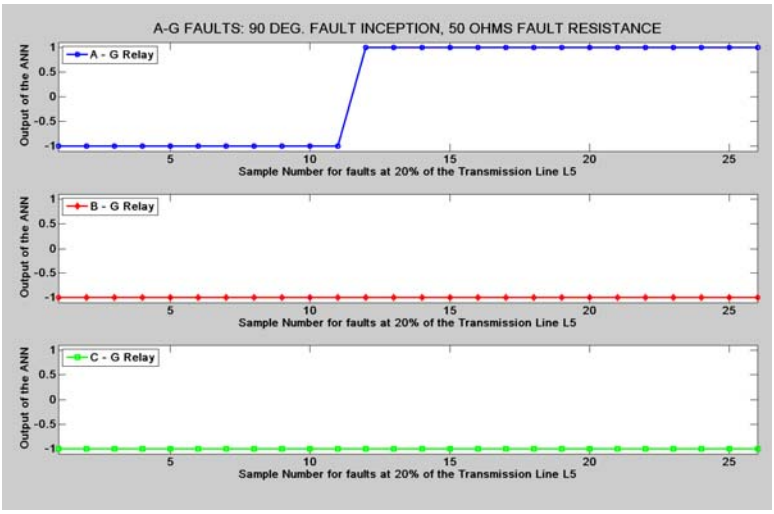

Figure G.103: Quadrilateral Relay – SLG Fault at 20% length of L_5, 90º Inception, 50 Ω Fault Resistance

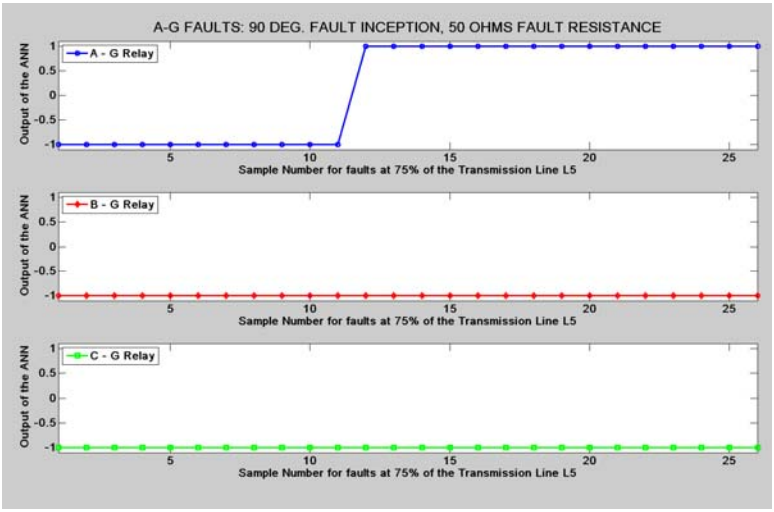

Figure G.104: Quadrilateral Relay – SLG Fault at 75% length of L_5, 90º Inception, 50 Ω Fault Resistance

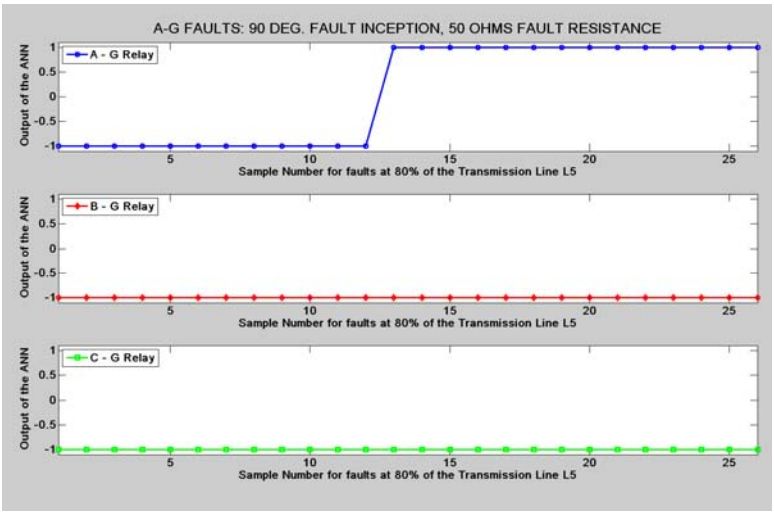

Figure G.105: Quadrilateral Relay – SLG Fault at 80% length of L_5, 90º Inception, 50 Ω Fault Resistance

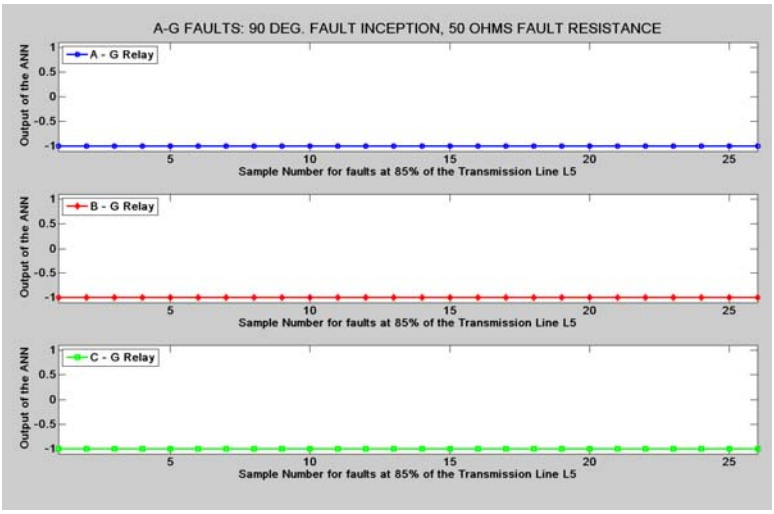

Figure G.106: Quadrilateral Relay – SLG Fault at 85% length of L_5, 90º Inception, 50 Ω Fault Resistance

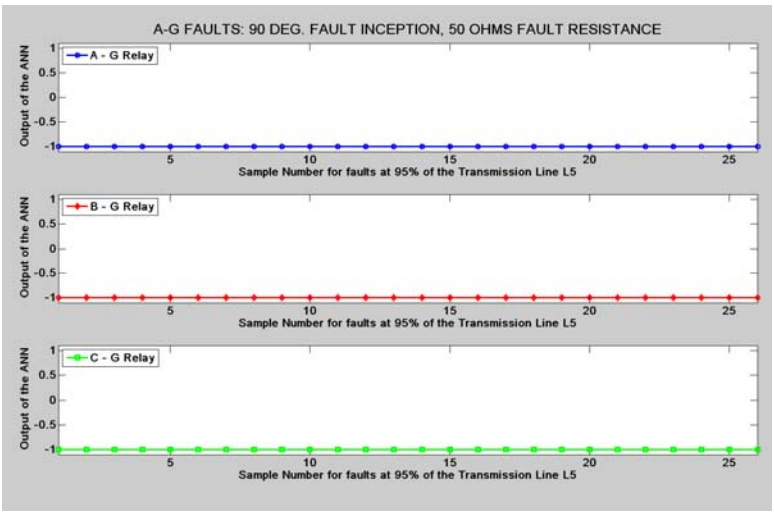

Figure G.107: Quadrilateral Relay – SLG Fault at 95% length of L_5, 90º Inception, 50 Ω Fault Resistance

(c) Two Phase and Three Phase Faults:

The next three figures show the results for line to line, double line to ground and three phase results for fault outside the relay boundary of a quadrilateral relay.

Figure G.108: Quadrilateral Relay – Line to Line Fault at 0% and 5% length of L_5 respectively

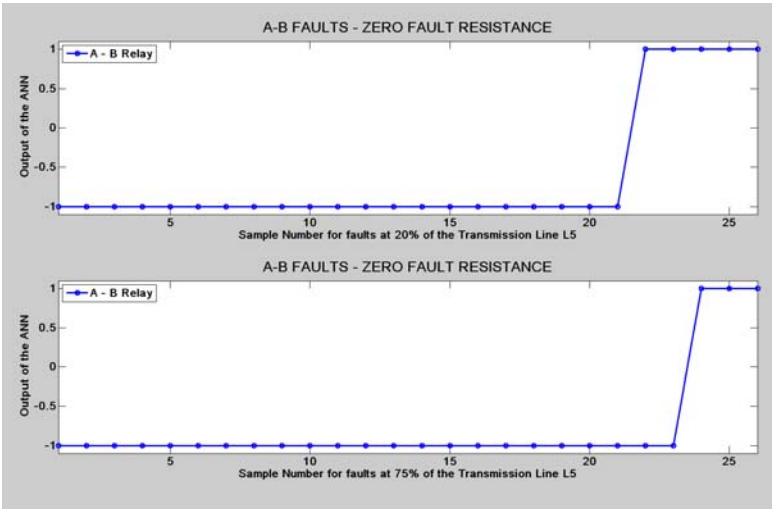

Figure G.109: Quadrilateral Relay – Line to Line Fault at 20% and 75% length of L_5 respectively

Figure G.110: Quadrilateral Relay – Line to Line Fault at 80% and 85% length of L_5 respectively

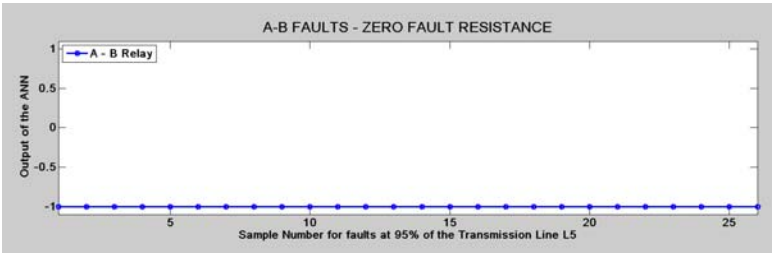

Figure G.111: Quadrilateral Relay – Line to Line Fault at 95% length of L_5

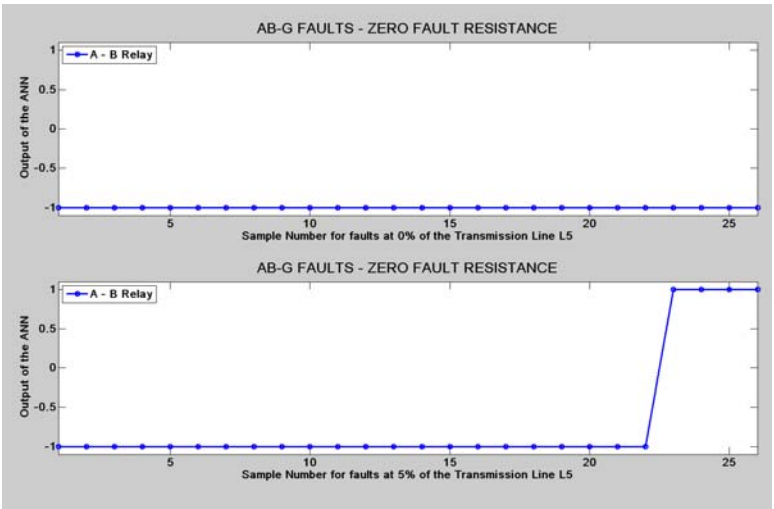

Figure G.112: Quadrilateral Relay – Double Line to Ground Fault at 0% and 5% length of L_5 respectively

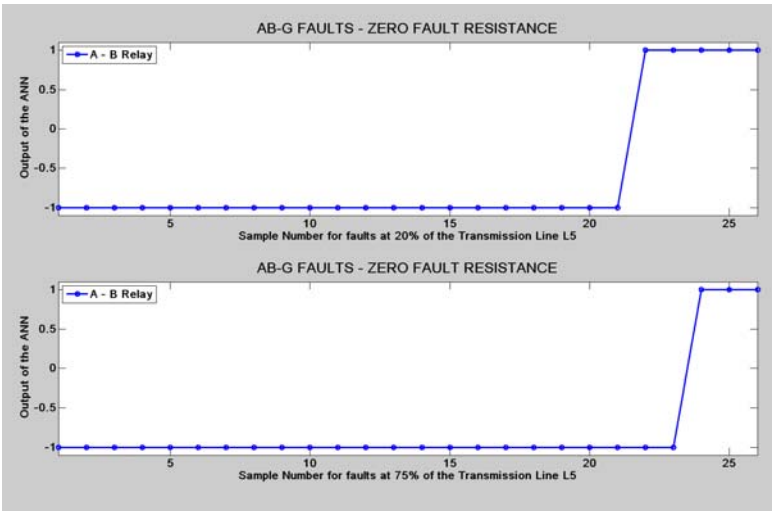

Figure G.113: Quadrilateral Relay – Double Line to Ground Fault at 20% and 75% length of L_5 respectively

Figure G.114: Quadrilateral Relay – Double Line to Ground Fault at 80% and 85% length of L_5 respectively

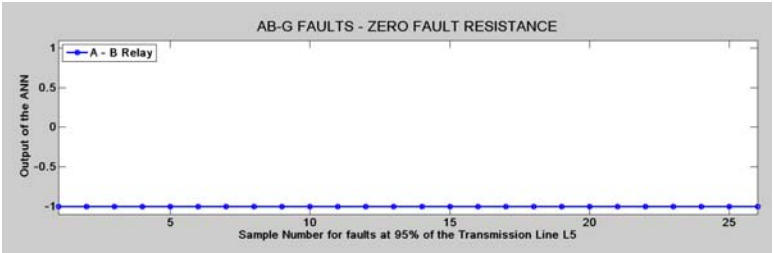

Figure G.115: Quadrilateral Relay – Double Line to Ground Fault at 95% length of L_5

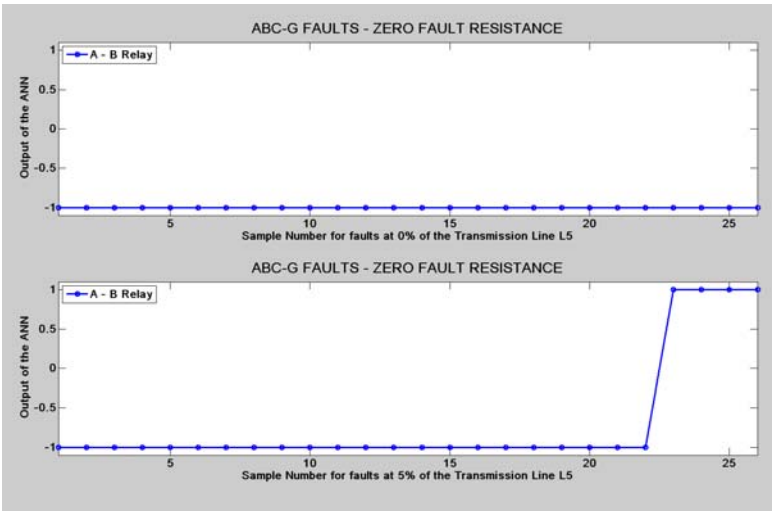

Figure G.116: Quadrilateral Relay – Three Line to Ground Fault at 0% and 5% length of L_5 respectively

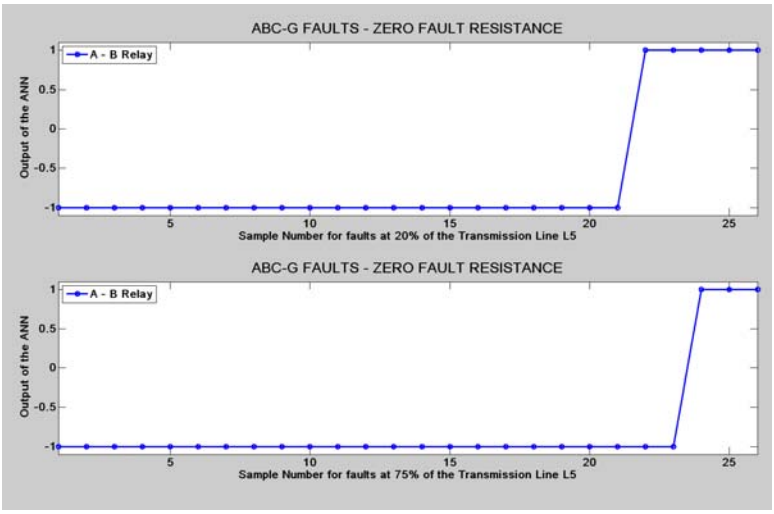

Figure G.117: Quadrilateral Relay – Three Line to Ground Fault at 20% and 75% length of L_5 respectively

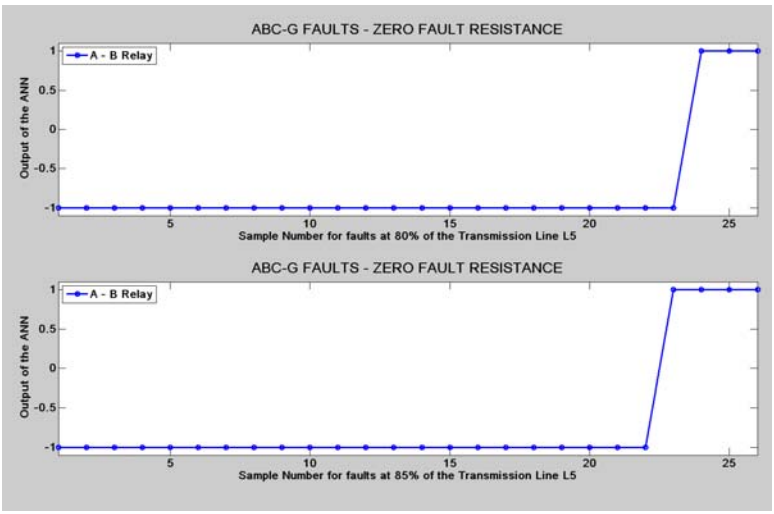

Figure G.118: Quadrilateral Relay – Three Line to Ground Fault at 80% and 85% length of L_5 respectively

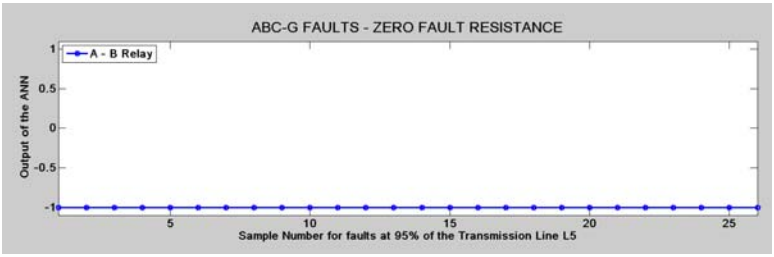

Figure G.119: Quadrilateral Relay – Three Line to Ground Fault at 95% length of L_5

G.3 Polarization Results for Admittance Relay

This section shows the extra polarization results for all cases that have been previously discussed in Chapter 6. All these results are for faults either well within or well outside the relay boundaries.

G.3.1 Polarization Results for Single line to ground faults

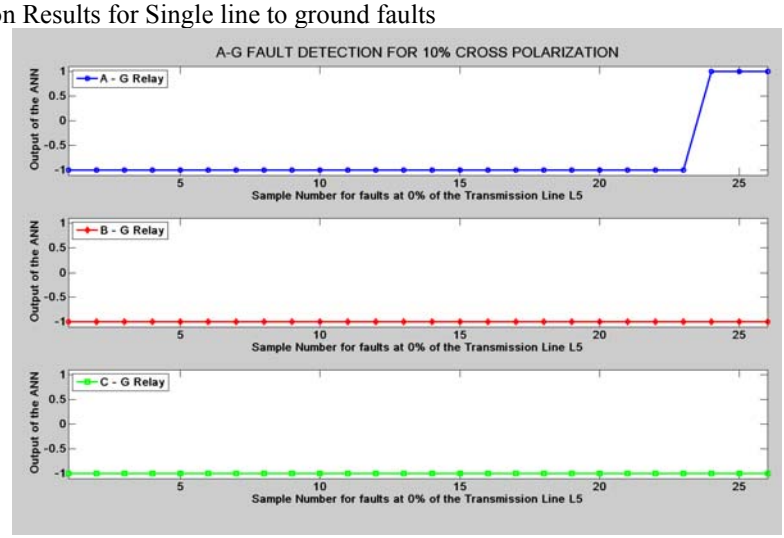

Figure G.120: Mho Relay – SLG Fault at 0% length of L_5 with 10% Cross Polarization

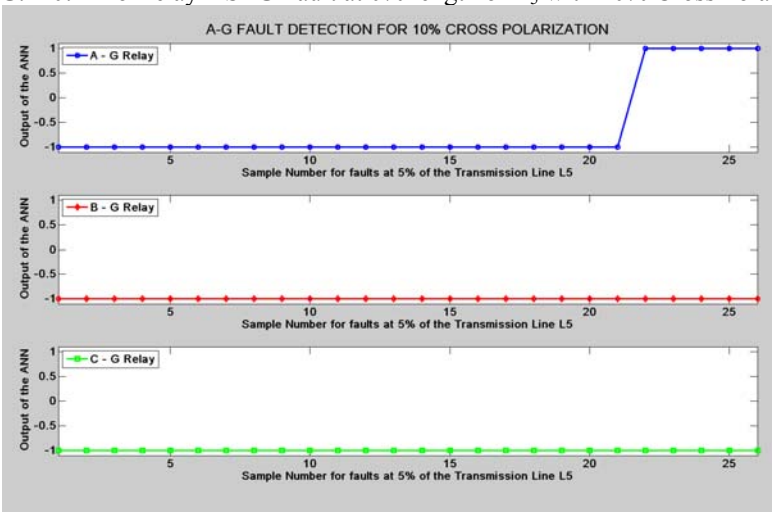

Figure G.121: Mho Relay – SLG Fault at 5% length of L_5 with 10% Cross Polarization

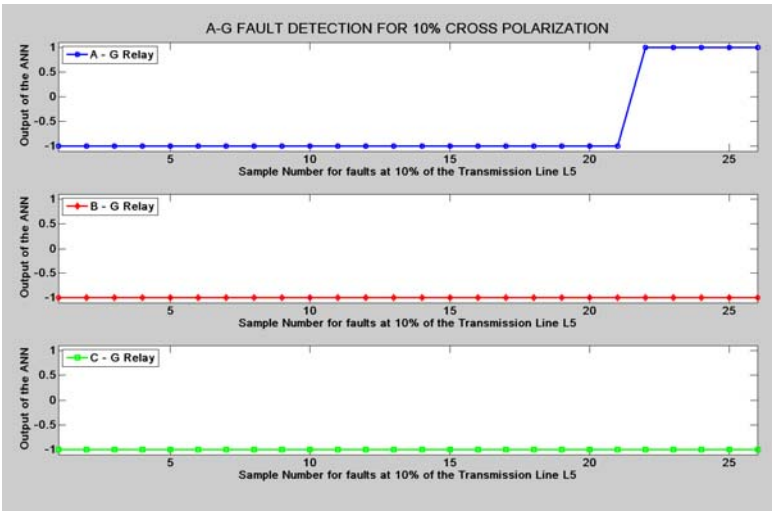

Figure G.122: Mho Relay – SLG Fault at 10% length of L_5 with 10% Cross Polarization

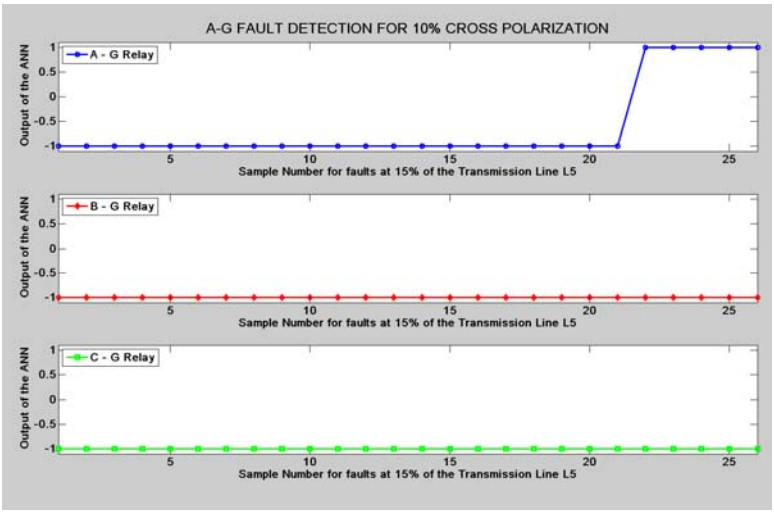

Figure G.123: Mho Relay – SLG Fault at 15% length of L_5 with 10% Cross Polarization

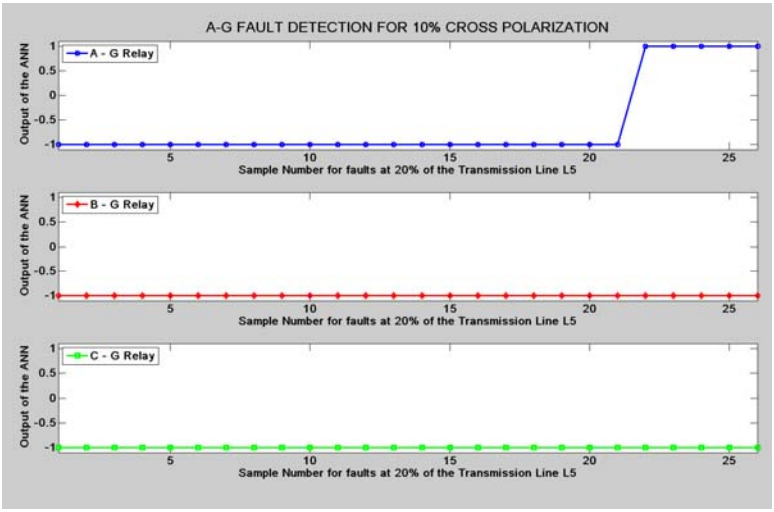

Figure G.124: Mho Relay – SLG Fault at 20% length of L_5 with 10% Cross Polarization

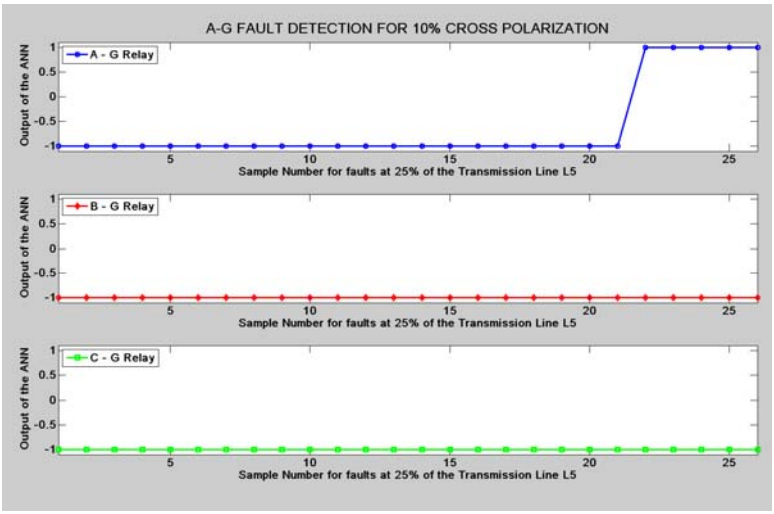

Figure G.125: Mho Relay – SLG Fault at 25% length of L_5 with 10% Cross Polarization

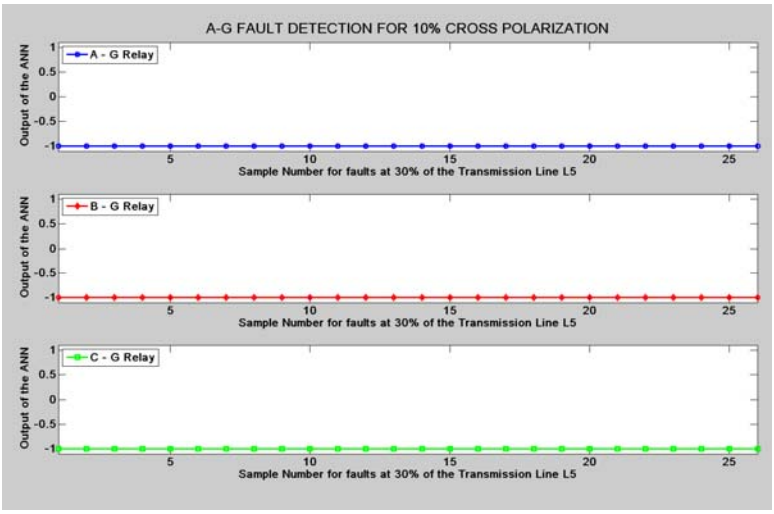

Figure G.126: Mho Relay – SLG Fault at 30% length of L_5 with 10% Cross Polarization

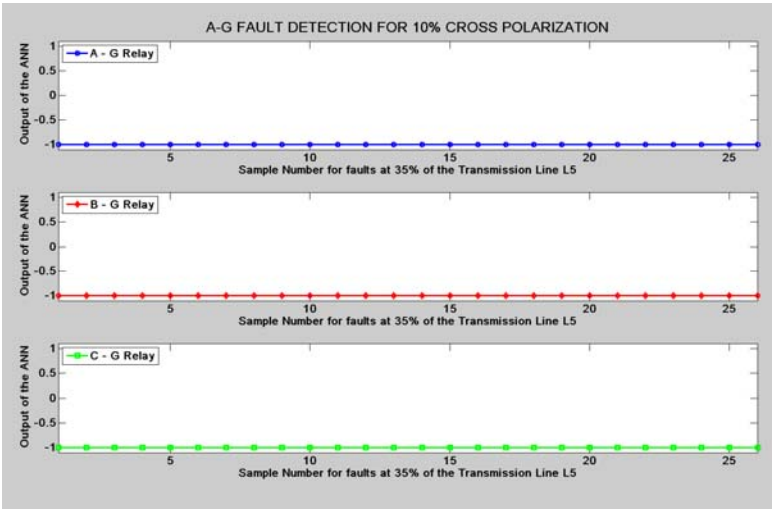

Figure G.127: Mho Relay – SLG Fault at 35% length of L_5 with 10% Cross Polarization

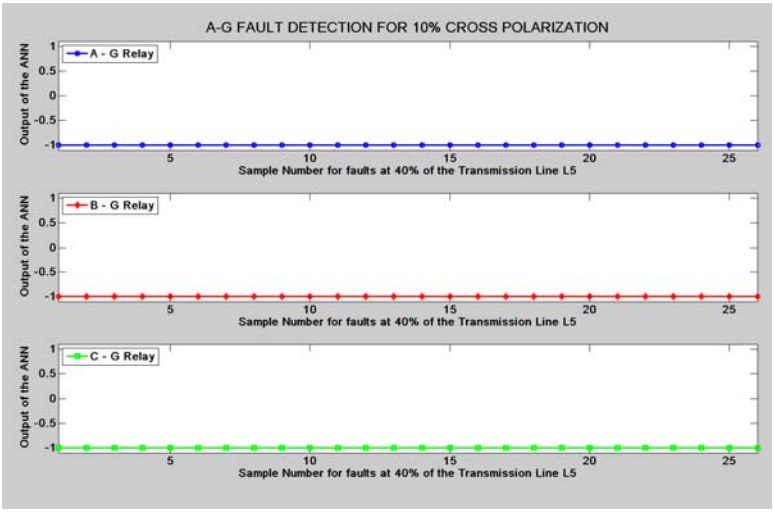

Figure G.128: Mho Relay – SLG Fault at 40% length of L_5 with 10% Cross Polarization

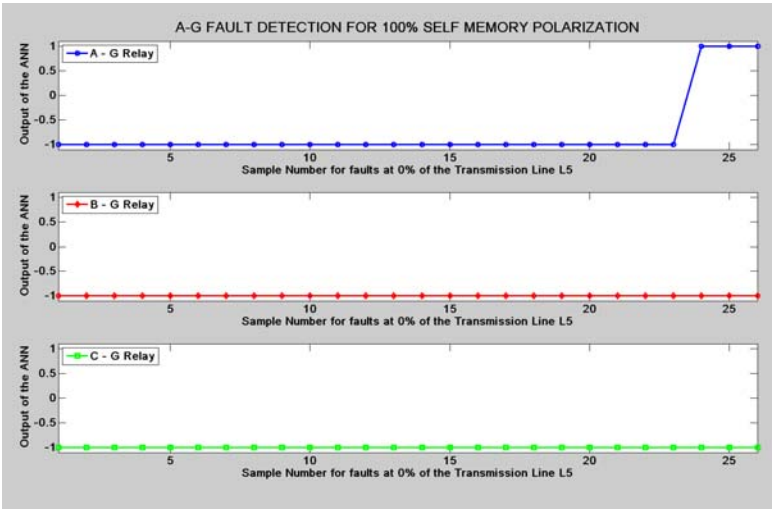

Figure G.129: Mho Relay – SLG Fault at 0% length of L_5 with 100% Self Memory Polarization

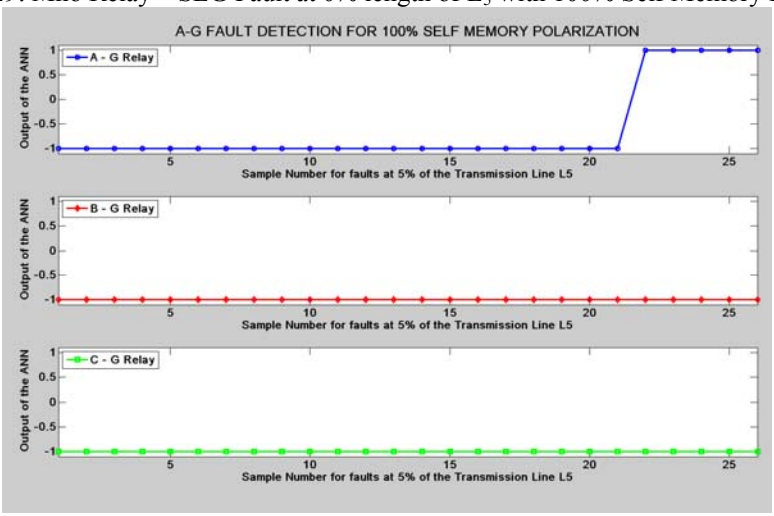

Figure G.130: Mho Relay – SLG Fault at 5% length of L_5 with 100% Self Memory Polarization

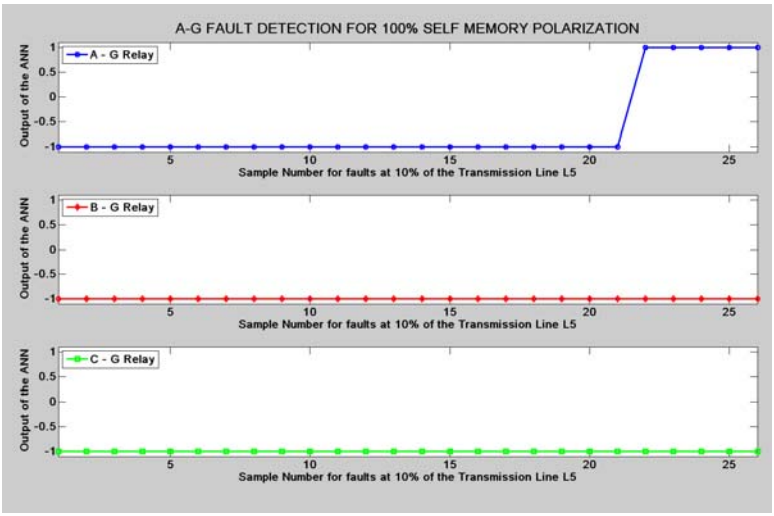

Figure G.131: Mho Relay – SLG Fault at 10% length of L_5 with 100% Self Memory Polarization

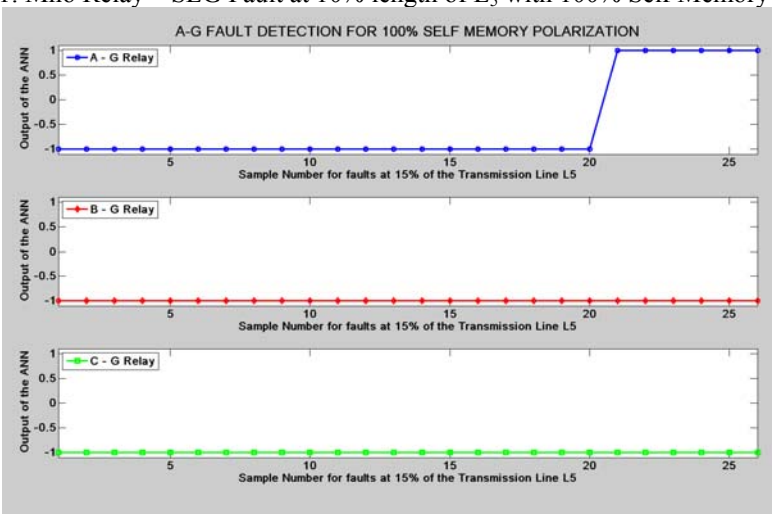

Figure G.132: Mho Relay – SLG Fault at 15% length of L_5 with 100% Self Memory Polarization

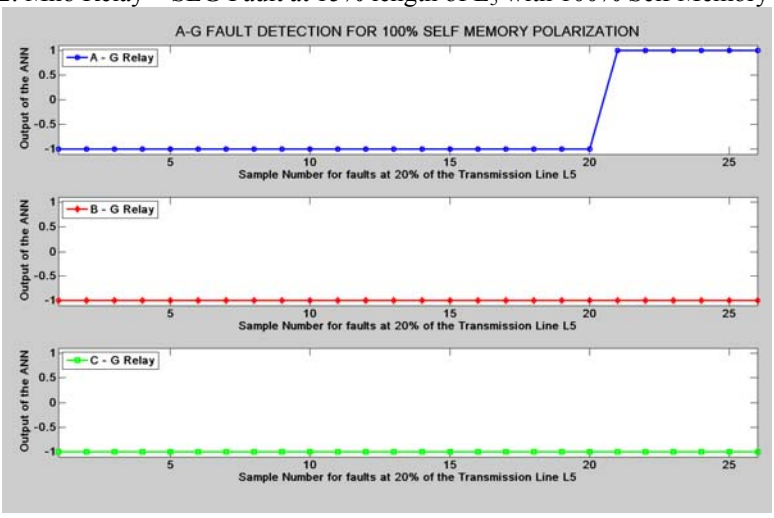

Figure G.133: Mho Relay – SLG Fault at 20% length of L_5 with 100% Self Memory Polarization

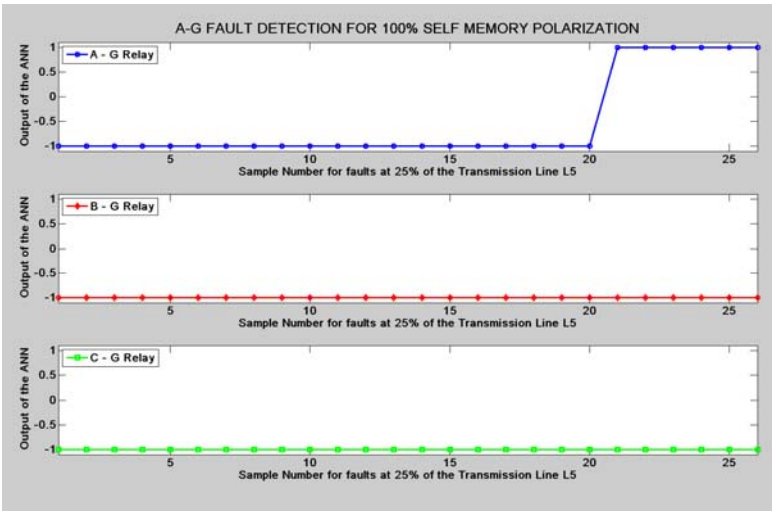

Figure G.134: Mho Relay – SLG Fault at 25% length of L_5 with 100% Self Memory Polarization

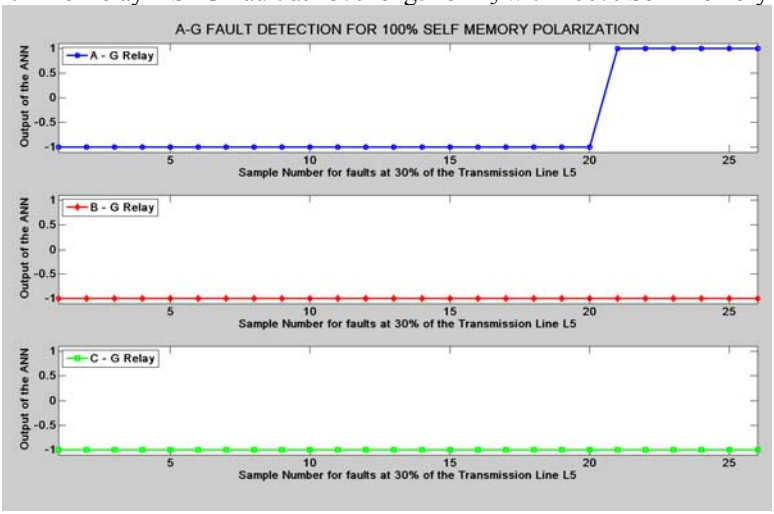

Figure G.135: Mho Relay – SLG Fault at 30% length of L_5 with 100% Self Memory Polarization

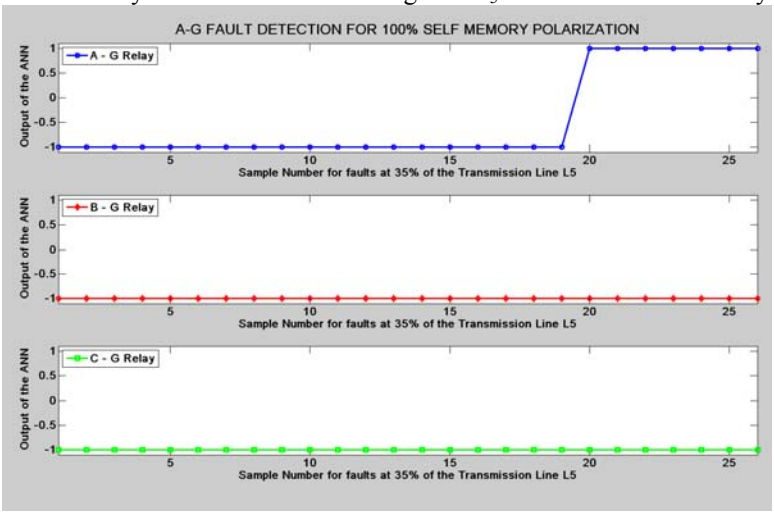

Figure G.136: Mho Relay – SLG Fault at 35% length of L_5 with 100% Self Memory Polarization

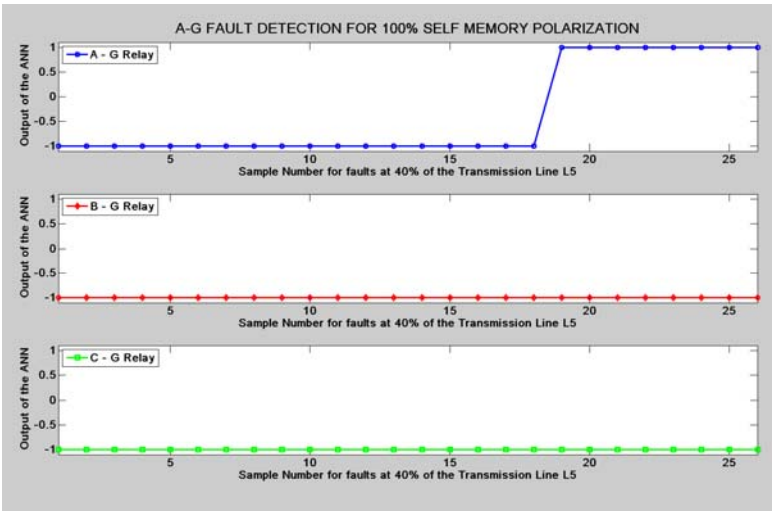

Figure G.137: Mho Relay – SLG Fault at 40% length of L_5 with 100% Self Memory Polarization

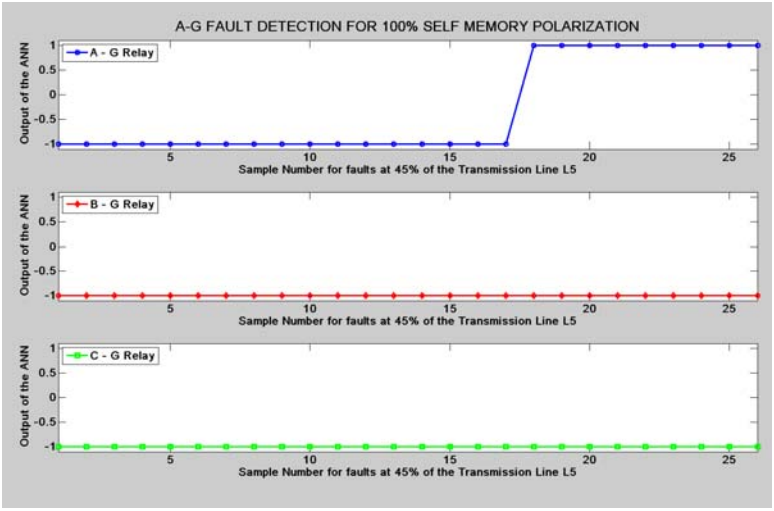

Figure G.138: Mho Relay – SLG Fault at 45% length of L_5 with 100% Self Memory Polarization

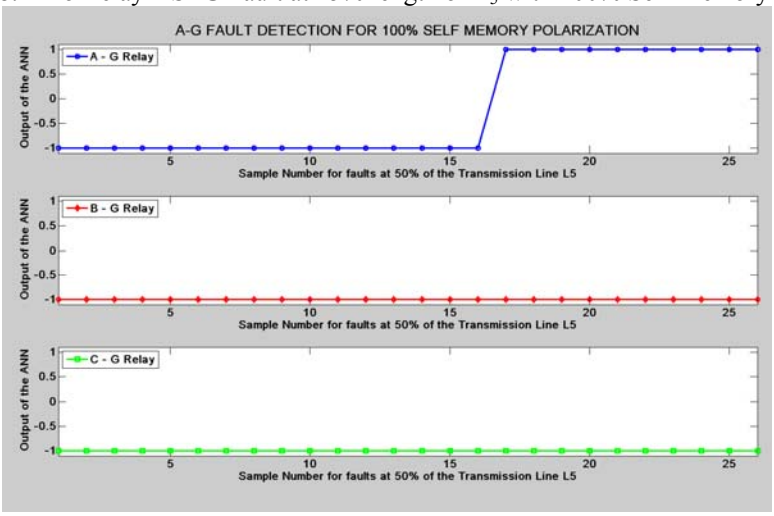

Figure G.139: Mho Relay – SLG Fault at 50% length of L_5 with 100% Self Memory Polarization

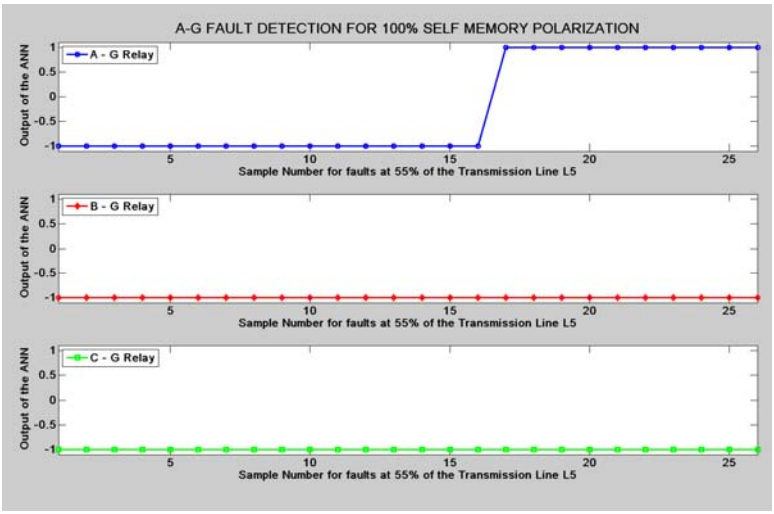

Figure G.140: Mho Relay – SLG Fault at 55% length of L_5 with 100% Self Memory Polarization

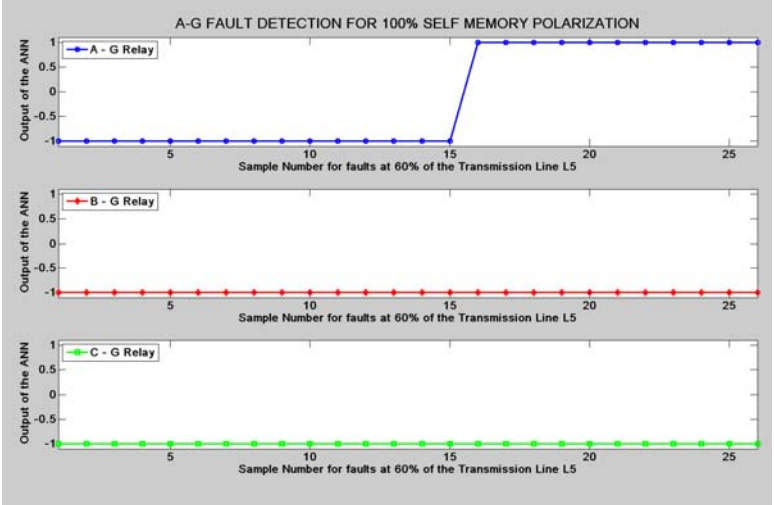

Figure G.141 Mho Relay – SLG Fault at 60% length of L_5 with 100% Self Memory Polarization

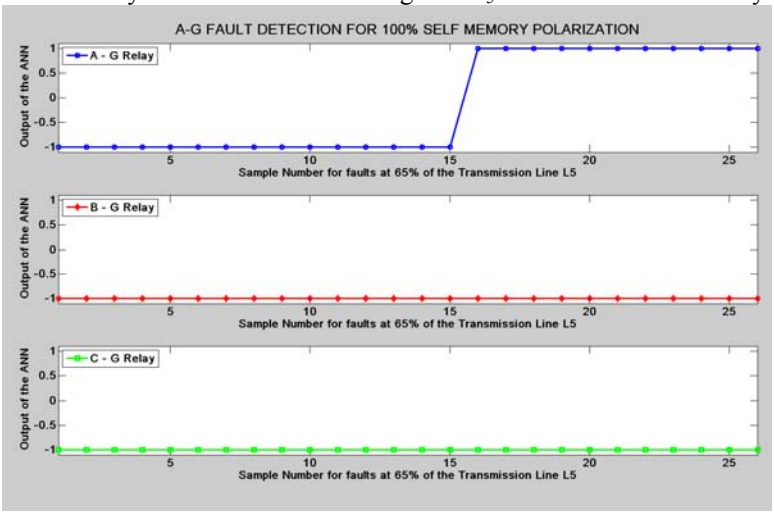

Figure G.142: Mho Relay – SLG Fault at 65% length of L_5 with 100% Self Memory Polarization

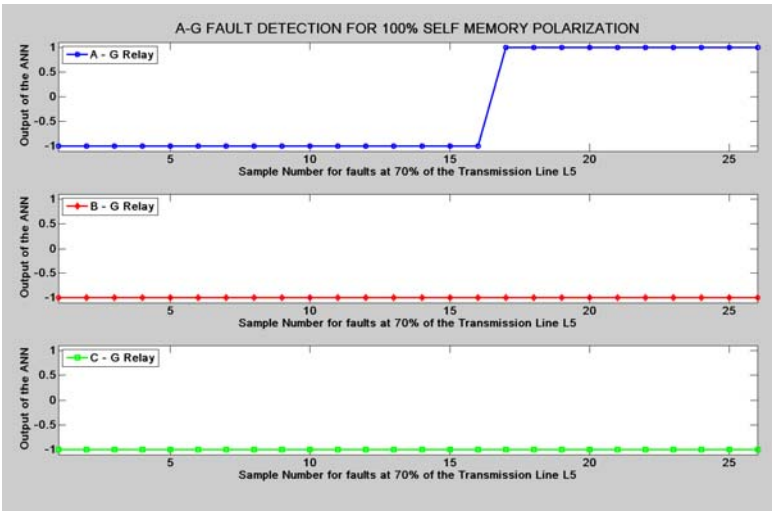

Figure G.143: Mho Relay – SLG Fault at 70% length of L_5 with 100% Self Memory Polarization

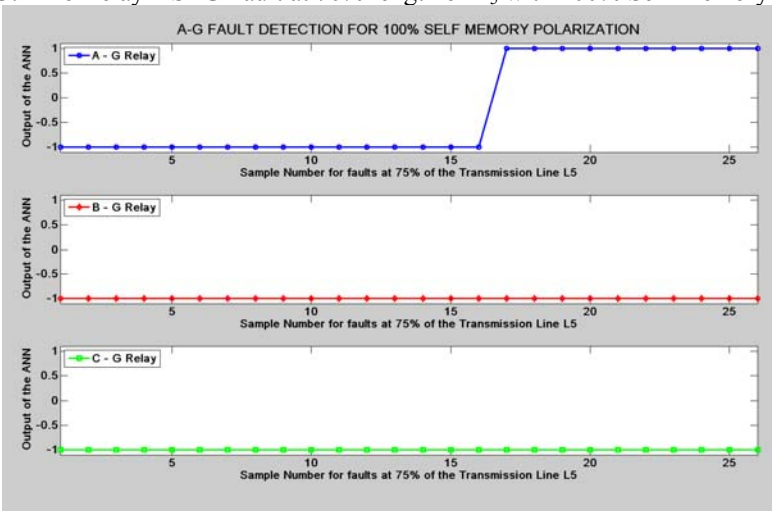

Figure G.144: Mho Relay – SLG Fault at 75% length of L_5 with 100% Self Memory Polarization

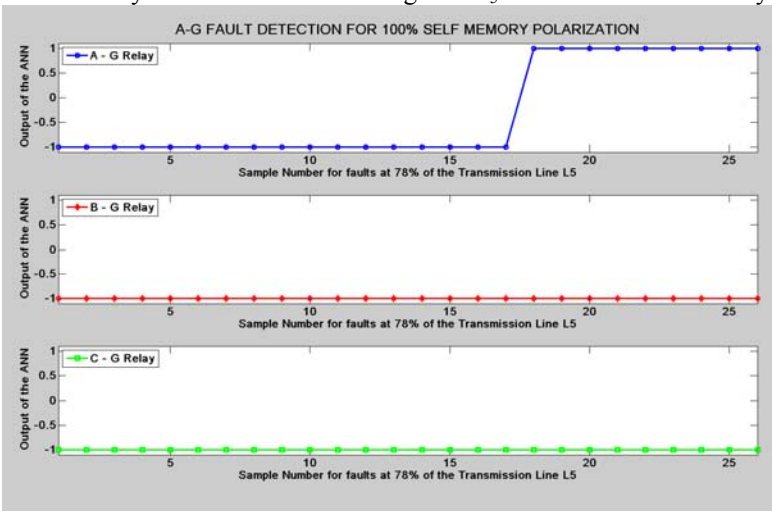

Figure G.145: Mho Relay – SLG Fault at 78% length of L_5 with 100% Self Memory Polarization

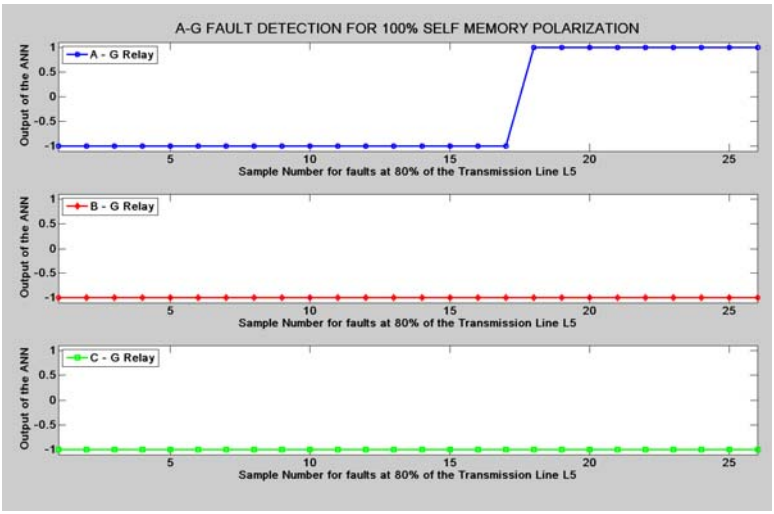

Figure G.146: Mho Relay – SLG Fault at 80% length of L_5 with 100% Self Memory Polarization

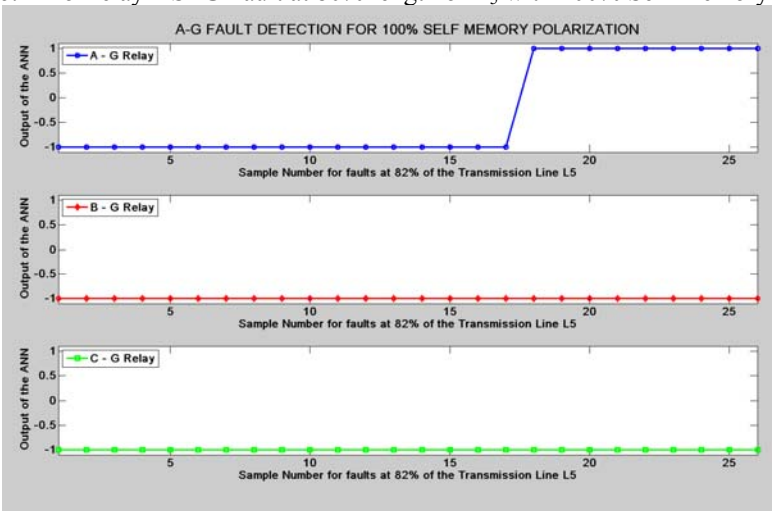

Figure G.147: Mho Relay – SLG Fault at 82% length of L_5 with 100% Self Memory Polarization

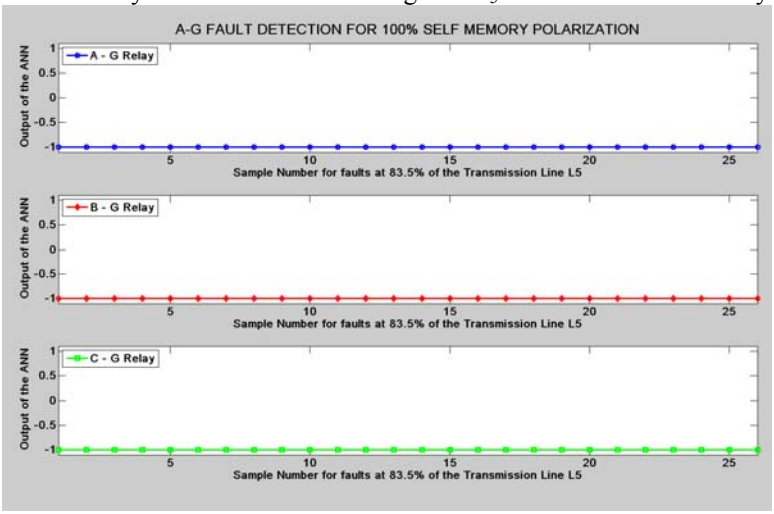

Figure G.148: Mho Relay – SLG Fault at 83.5% length of L_5 with 100% Self Memory Polarization

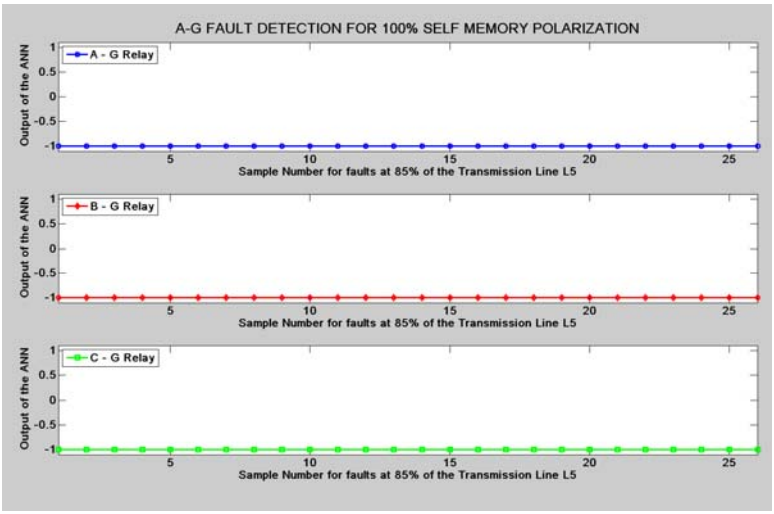

Figure G.149: Mho Relay – SLG Fault at 85% length of L_5 with 100% Self Memory Polarization

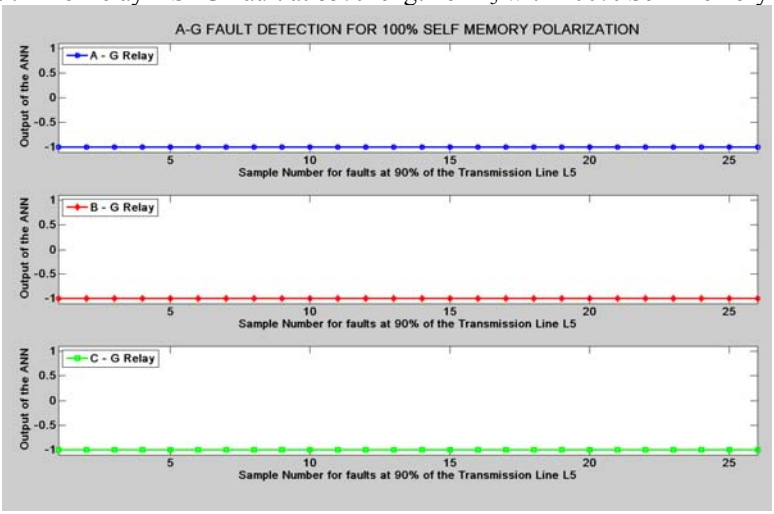

Figure G.150: Mho Relay – SLG Fault at 90% length of L_5 with 100% Self Memory Polarization

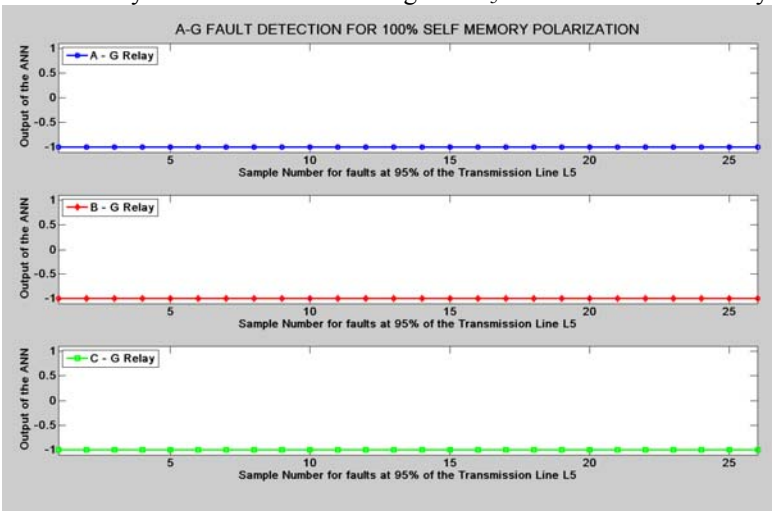

Figure G.151: Mho Relay – SLG Fault at 95% length of L_5 with 100% Self Memory Polarization

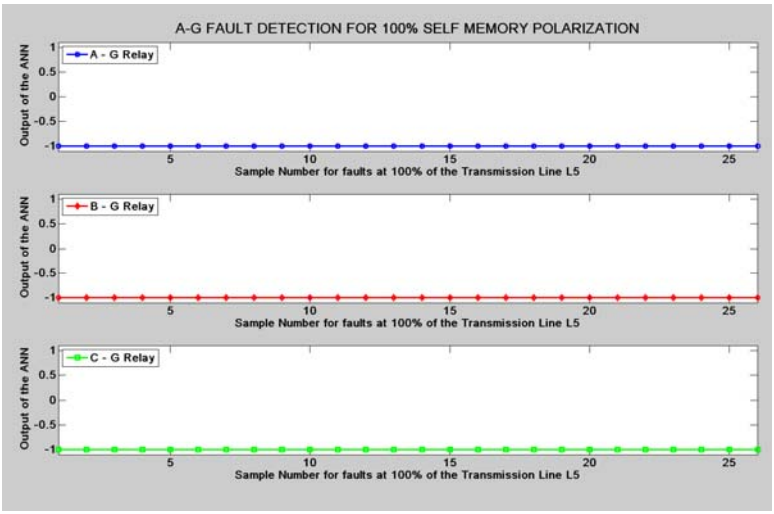

Figure G.152: Mho Relay – SLG Fault at 100% length of L_5 with 100% Self Memory Polarization

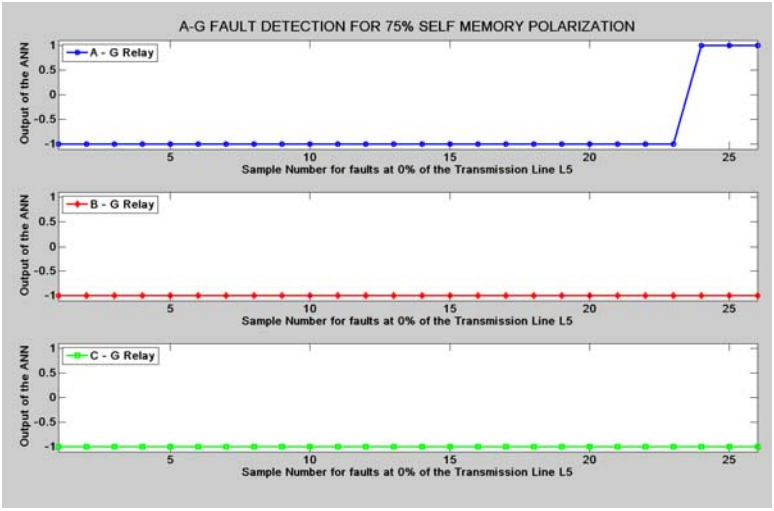

Figure G.153: Mho Relay – SLG Fault at 0% length of L_5 with 75% Self Memory Polarization

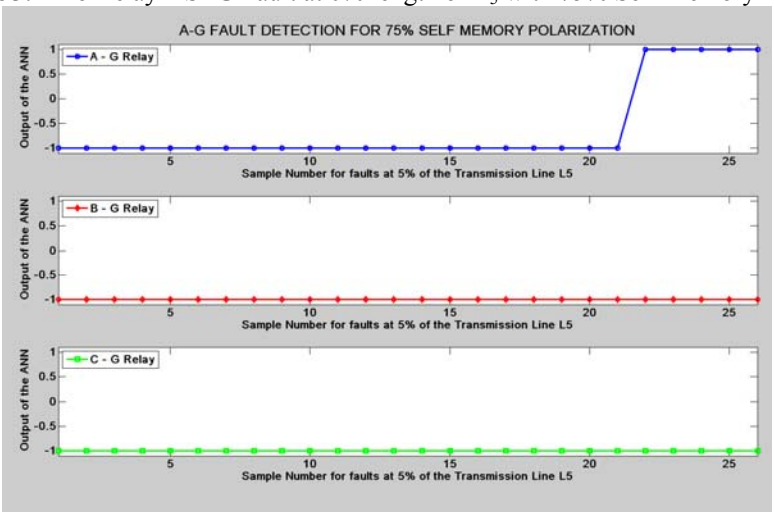

Figure G.154: Mho Relay – SLG Fault at 5% length of L_5 with 75% Self Memory Polarization

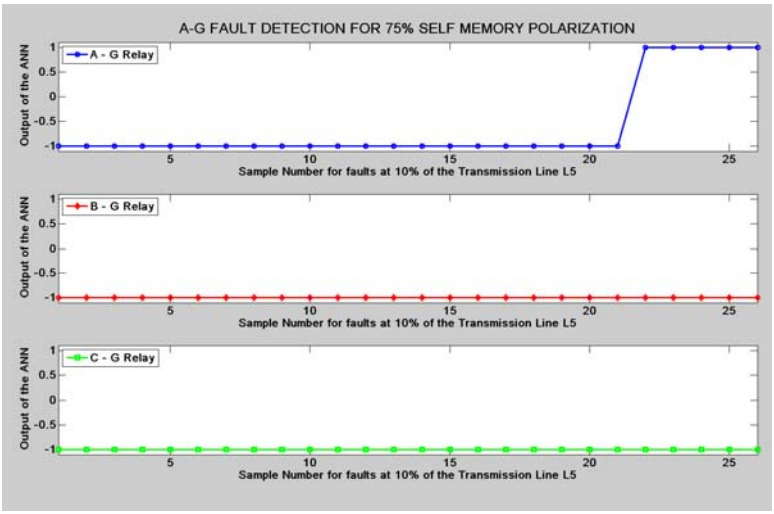

Figure G.155: Mho Relay – SLG Fault at 10% length of L_5 with 75% Self Memory Polarization

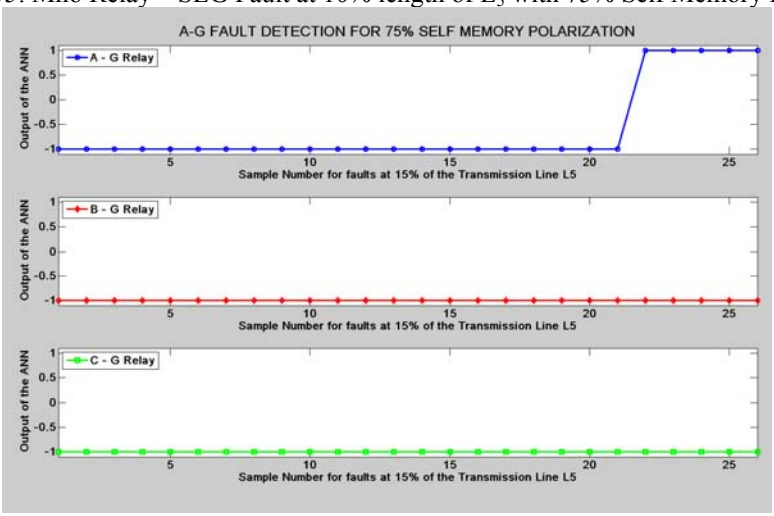

Figure G.156: Mho Relay – SLG Fault at 15% length of L_5 with 75% Self Memory Polarization

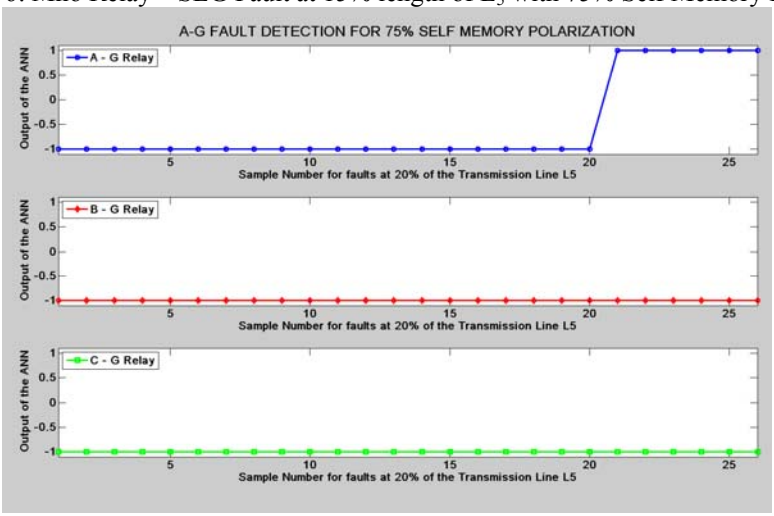

Figure G.157: Mho Relay – SLG Fault at 20% length of L_5 with 75% Self Memory Polarization

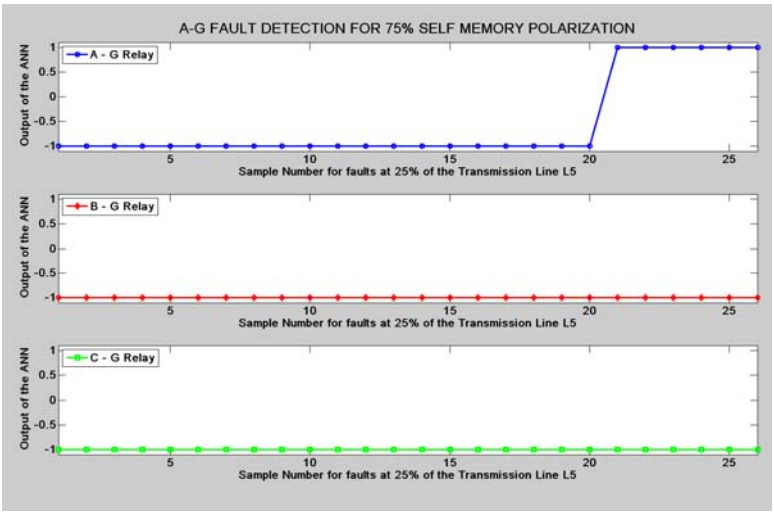

Figure G.158: Mho Relay – SLG Fault at 25% length of L_5 with 75% Self Memory Polarization

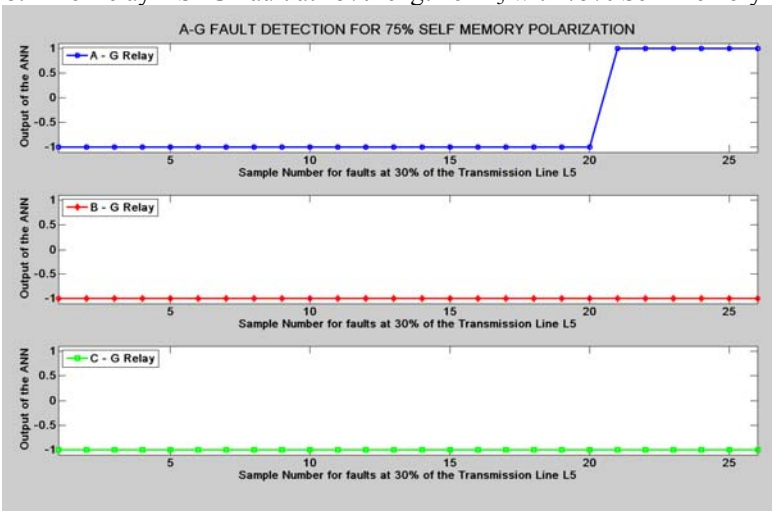

Figure G.159: Mho Relay – SLG Fault at 30% length of L_5 with 75% Self Memory Polarization

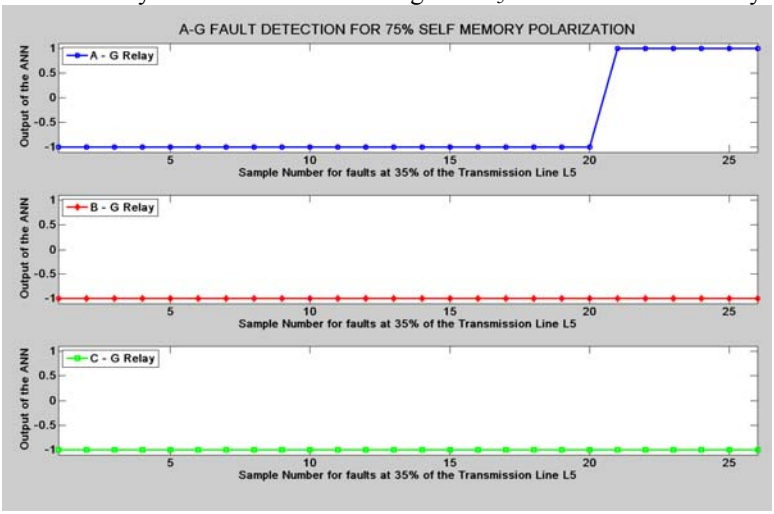

Figure G.160: Mho Relay – SLG Fault at 35% length of L_5 with 75% Self Memory Polarization

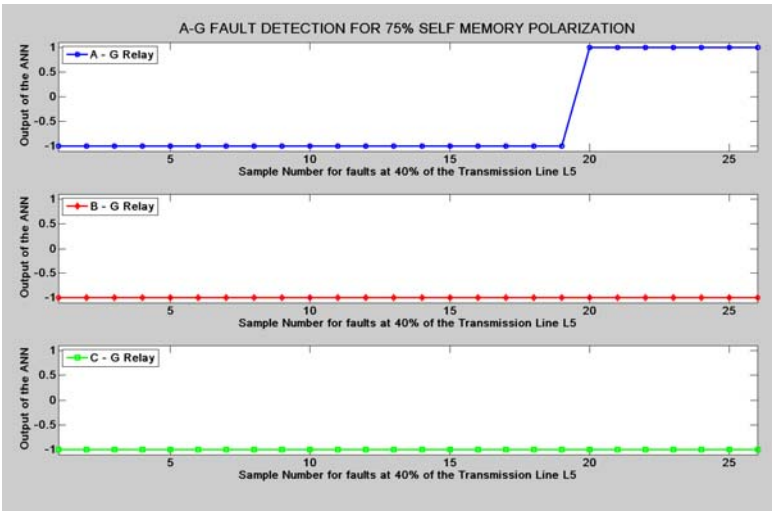

Figure G.161: Mho Relay – SLG Fault at 40% length of L_5 with 75% Self Memory Polarization

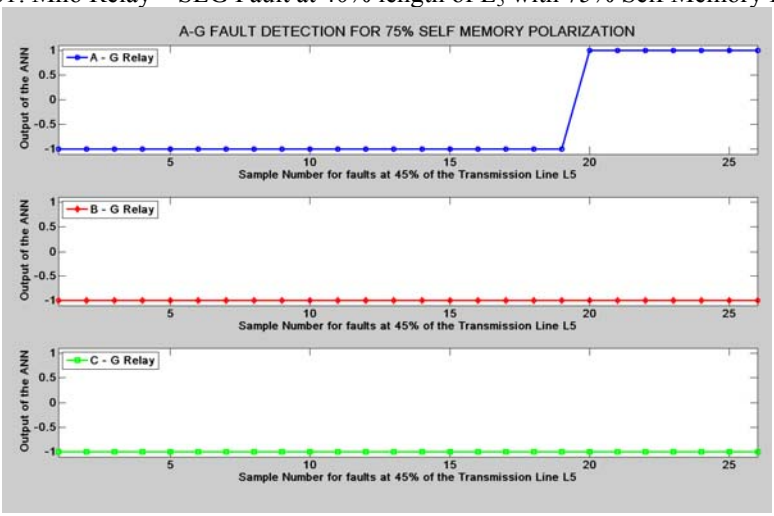

Figure G.162: Mho Relay – SLG Fault at 45% length of L_5 with 75% Self Memory Polarization

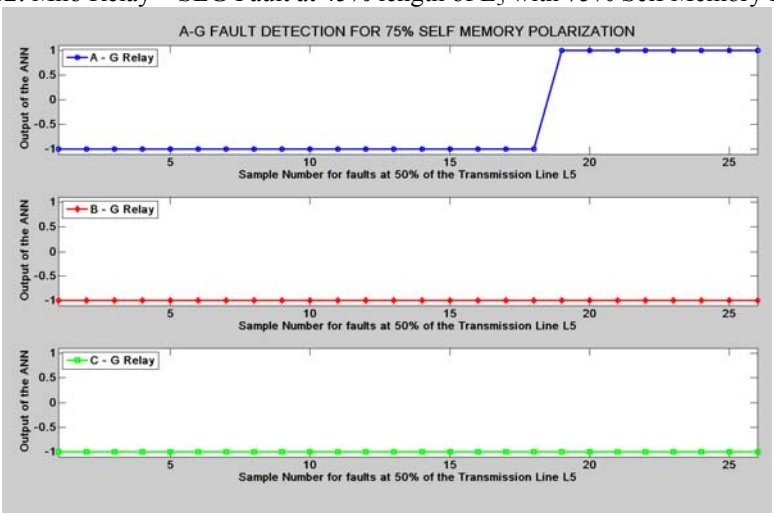

Figure G.163: Mho Relay – SLG Fault at 50% length of L_5 with 75% Self Memory Polarization

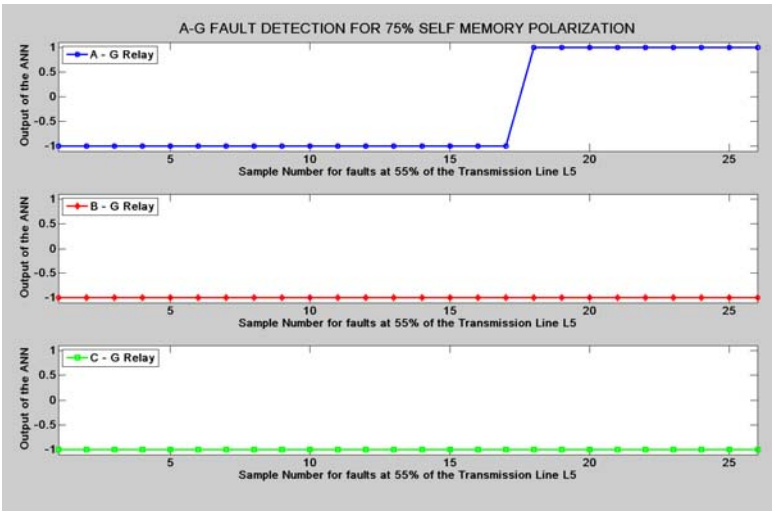

Figure G.164: Mho Relay – SLG Fault at 55% length of L_5 with 75% Self Memory Polarization

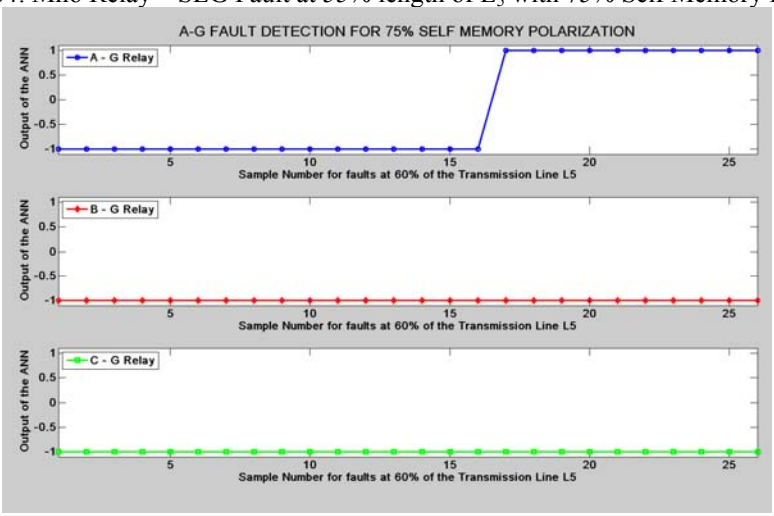

Figure G.165: Mho Relay – SLG Fault at 60% length of L_5 with 75% Self Memory Polarization

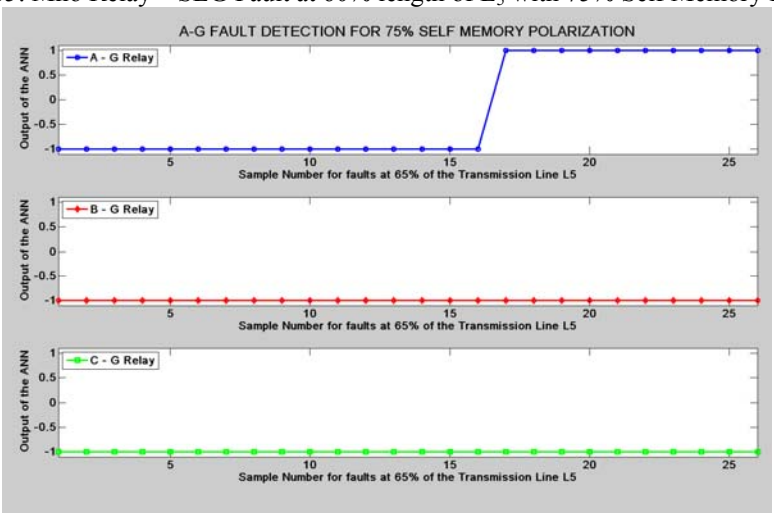

Figure G.166: Mho Relay – SLG Fault at 65% length of L_5 with 75% Self Memory Polarization

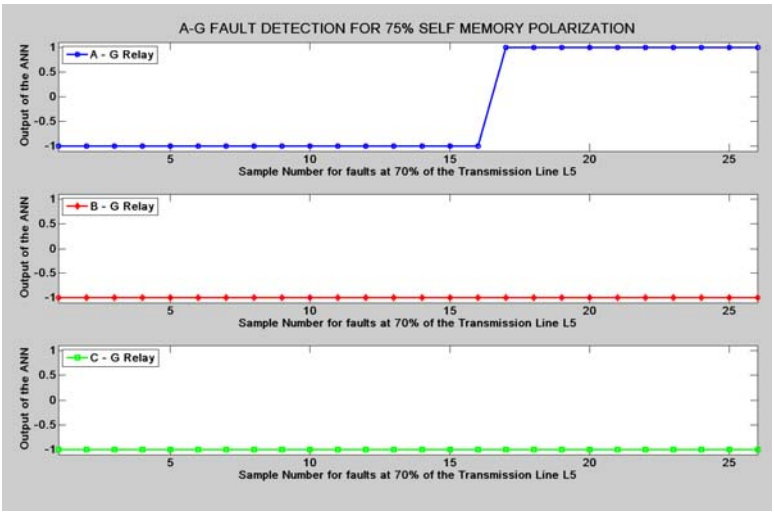

Figure G.167: Mho Relay – SLG Fault at 70% length of L_5 with 75% Self Memory Polarization

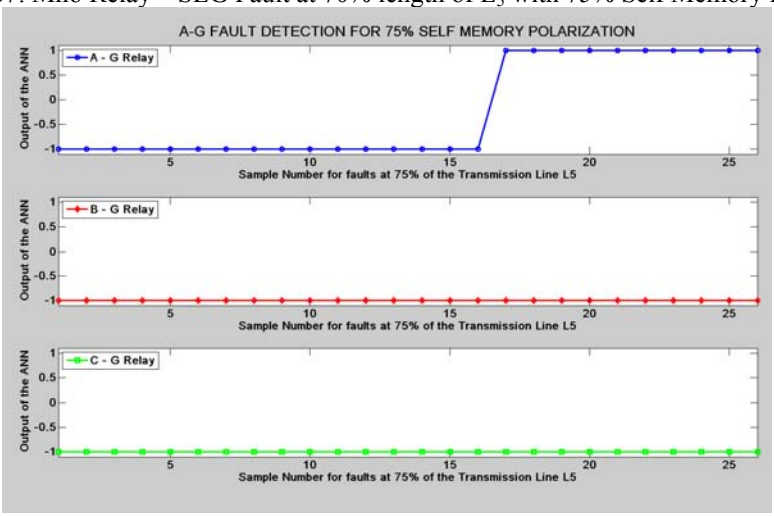

Figure G.168: Mho Relay – SLG Fault at 75% length of L_5 with 75% Self Memory Polarization

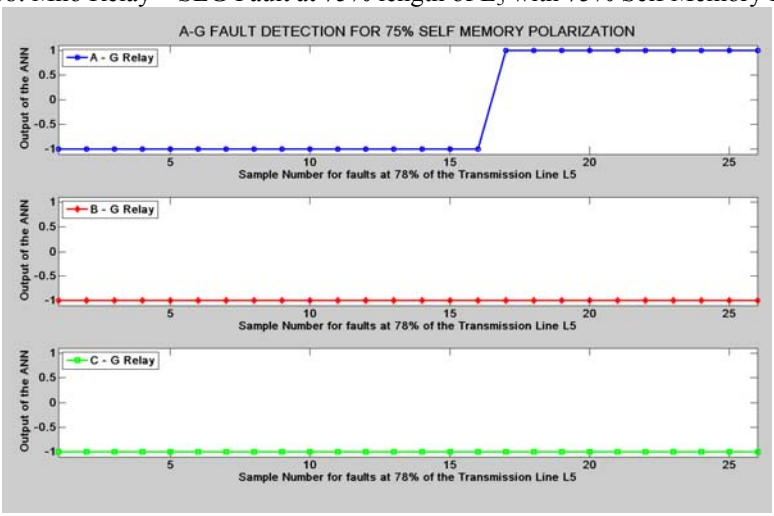

Figure G.169: Mho Relay – SLG Fault at 78% length of L_5 with 75% Self Memory Polarization

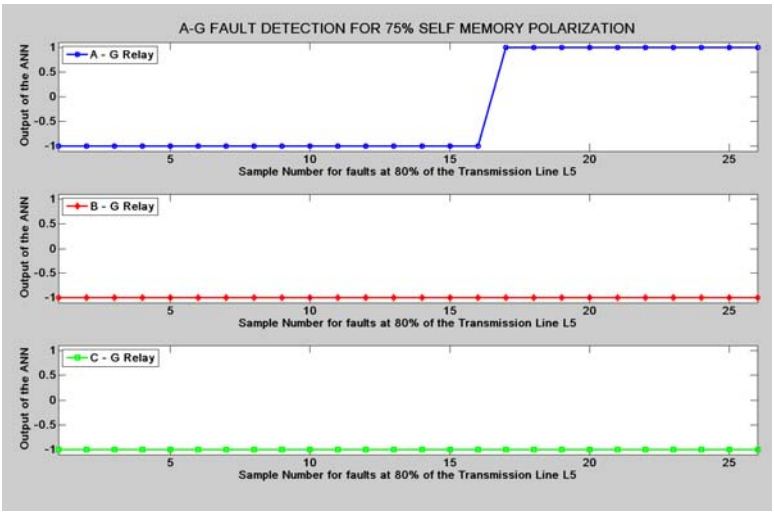

Figure G.170: Mho Relay – SLG Fault at 80% length of L_5 with 75% Self Memory Polarization

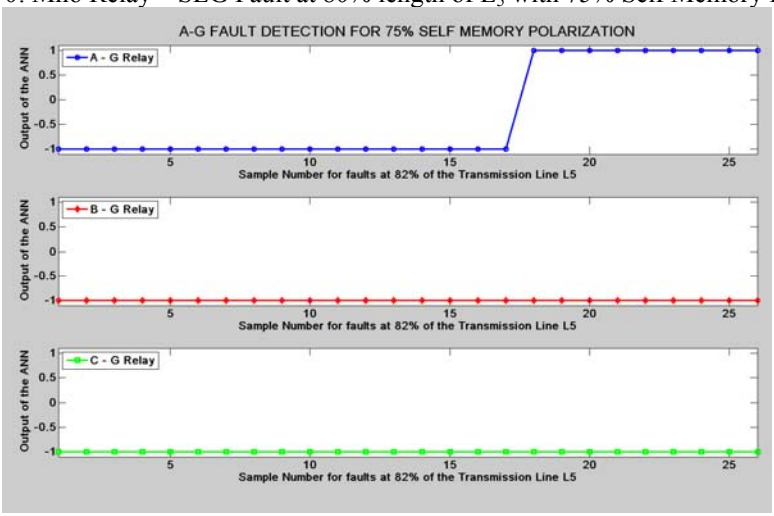

Figure G.171: Mho Relay – SLG Fault at 82% length of L_5 with 75% Self Memory Polarization

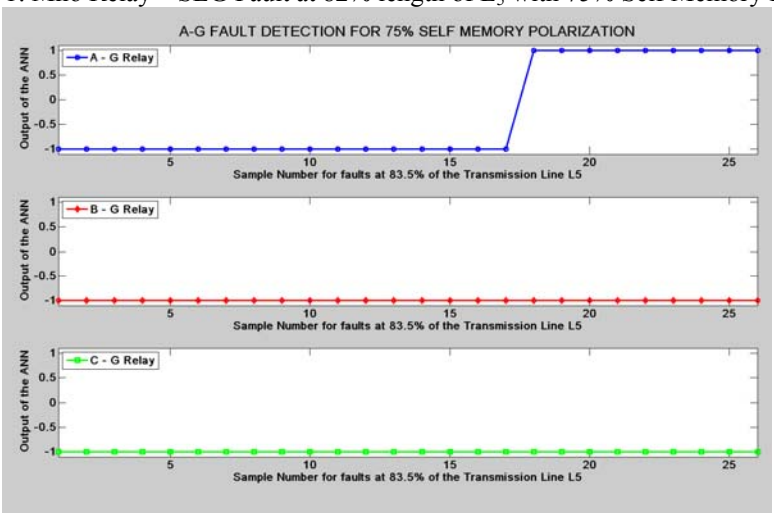

Figure G.172: Mho Relay – SLG Fault at 83.5% length of L_5 with 75% Self Memory Polarization

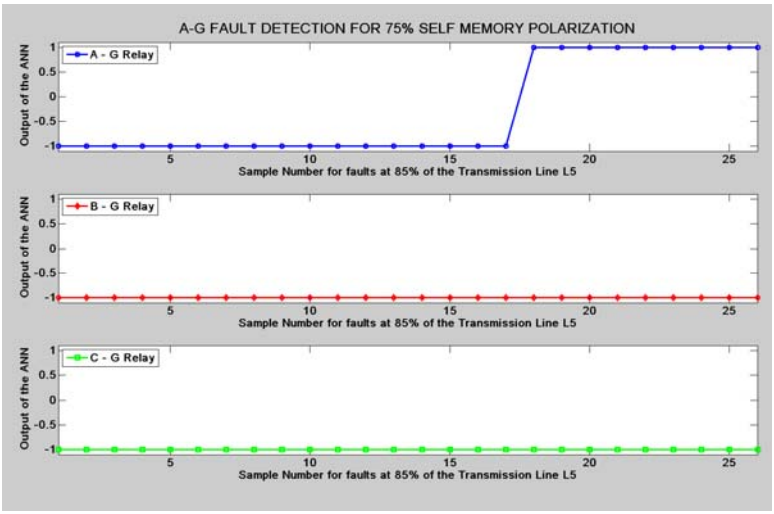

Figure G.173: Mho Relay – SLG Fault at 85% length of L_5 with 75% Self Memory Polarization

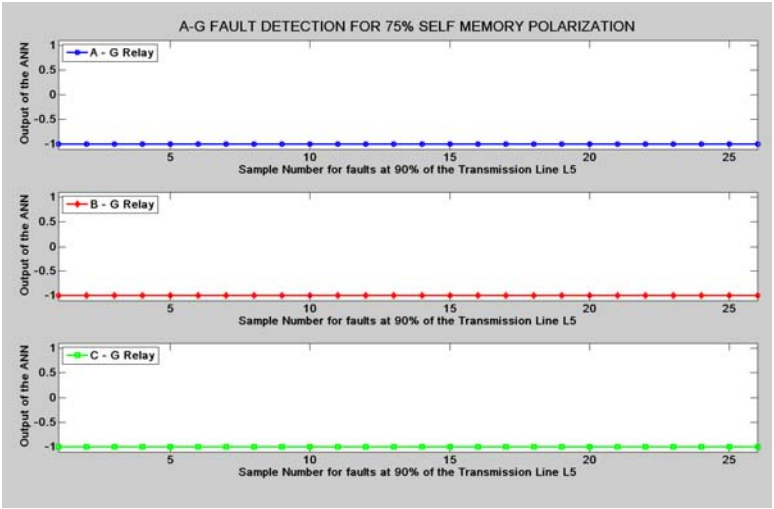

Figure G.174: Mho Relay – SLG Fault at 90% length of L_5 with 75% Self Memory Polarization

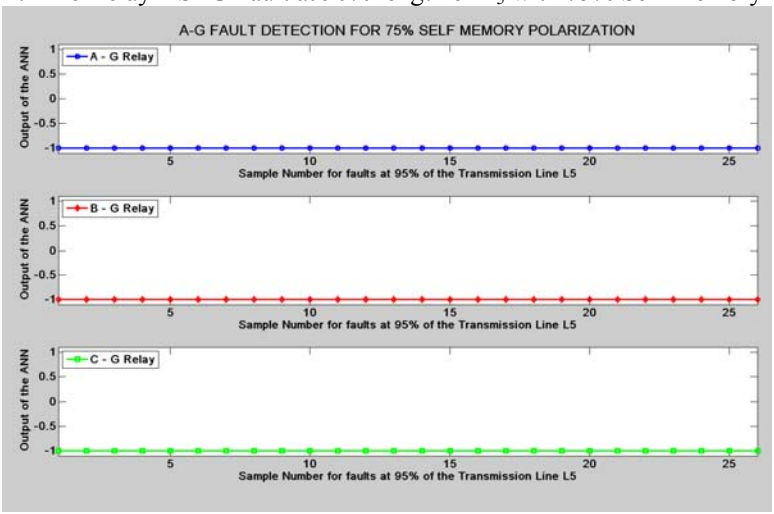

Figure G.175: Mho Relay – SLG Fault at 95% length of L_5 with 75% Self Memory Polarization

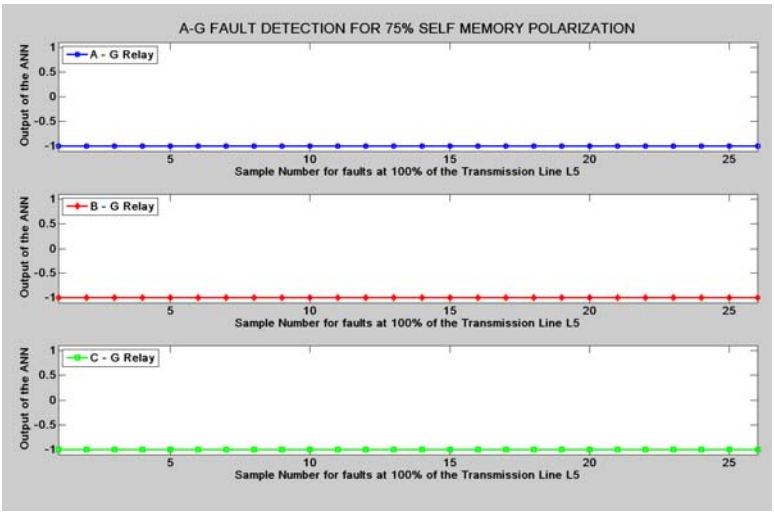

Figure G.176: Mho Relay – SLG Fault at 100% length of L_5 with 75% Self Memory Polarization

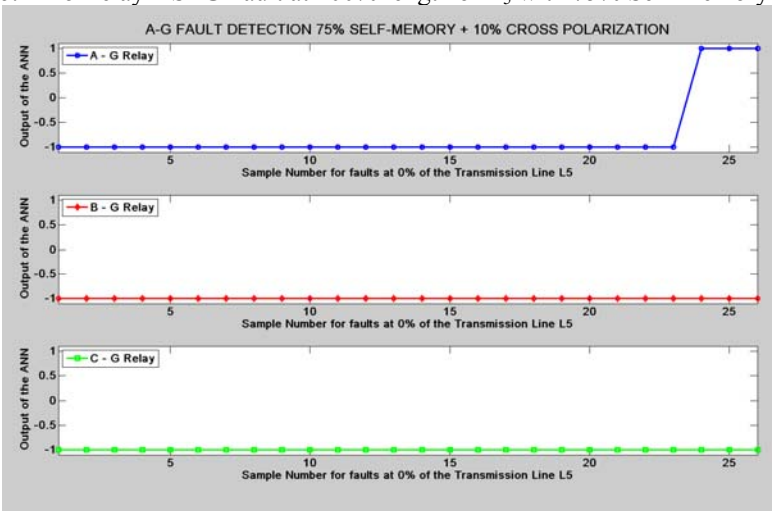

Figure G.177: Mho Relay – SLG Fault at 0% length of L_5 with 75% Self Memory + 10% Cross Polarization

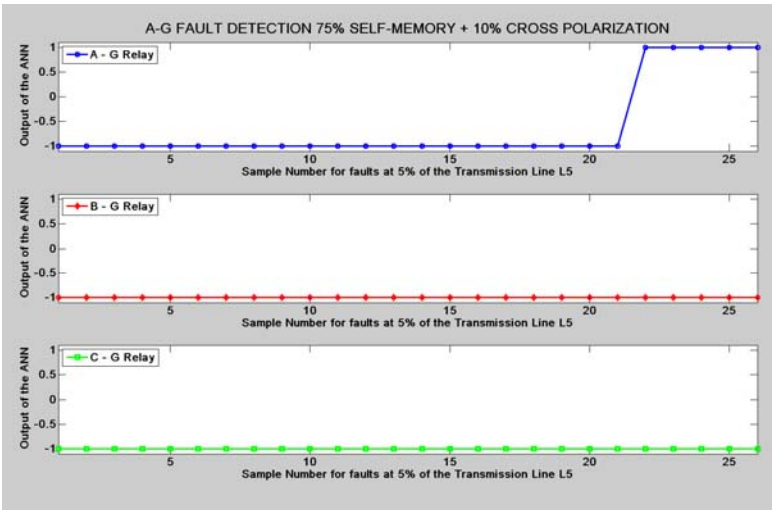

Figure G.178: Mho Relay – SLG Fault at 5% length of L_5 with 75% Self Memory + 10% Cross Polarization

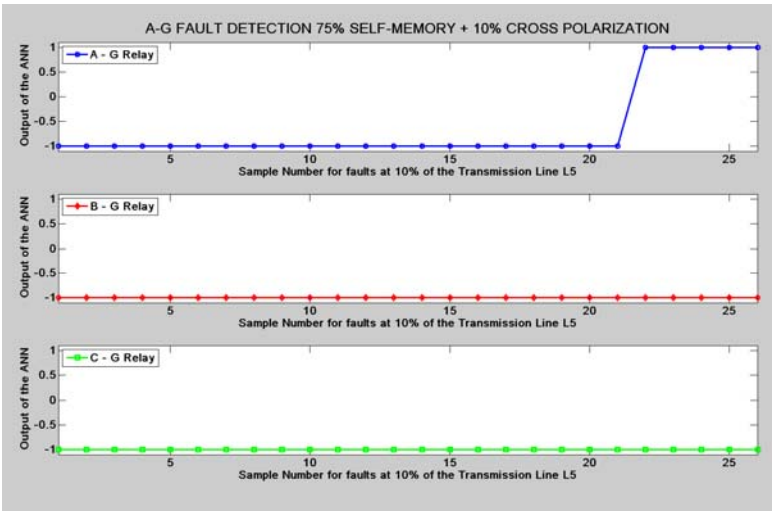

Figure G.179: Mho Relay – SLG Fault at 10% length of L_5 with 75% Self Memory + 10% Cross Polarization

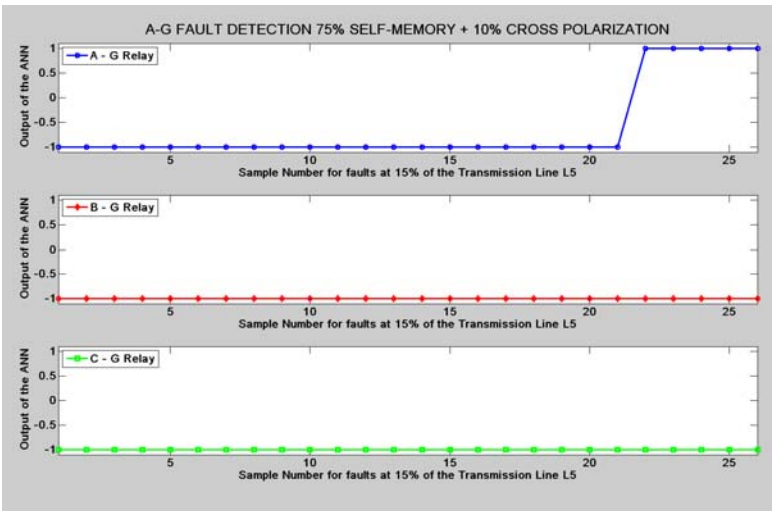

Figure G.180: Mho Relay – SLG Fault at 15% length of L_5 with 75% Self Memory + 10% Cross Polarization

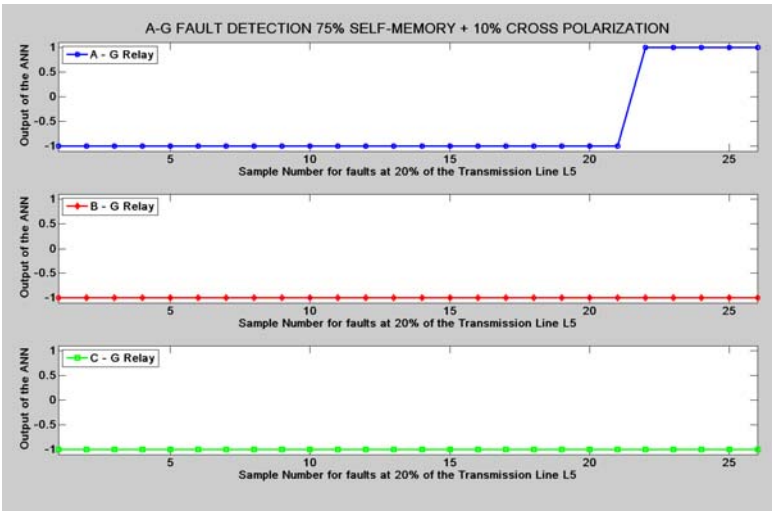

Figure G.181: Mho Relay – SLG Fault at 20% length of L_5 with 75% Self Memory + 10% Cross Polarization

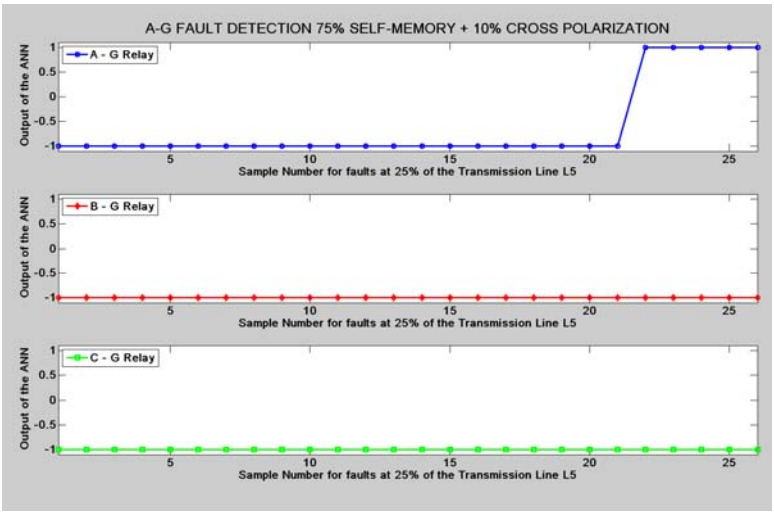

Figure G.182: Mho Relay – SLG Fault at 25% length of L_5 with 75% Self Memory + 10% Cross Polarization

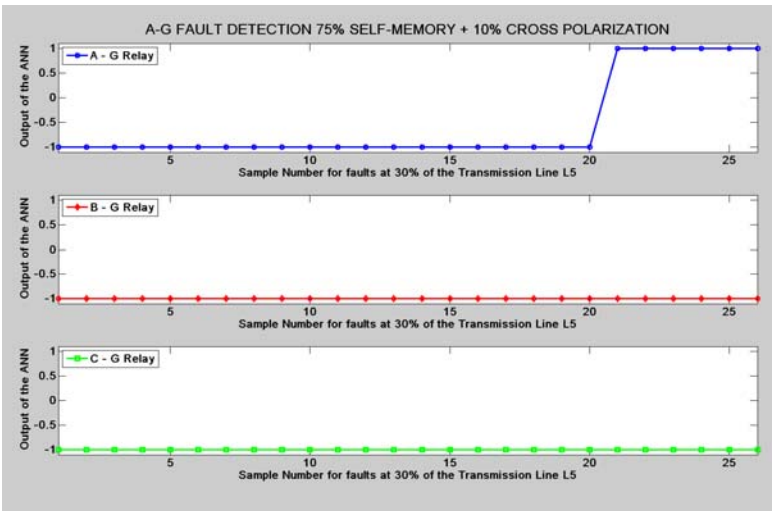

Figure G.183: Mho Relay – SLG Fault at 30% length of L_5 with 75% Self Memory + 10% Cross Polarization

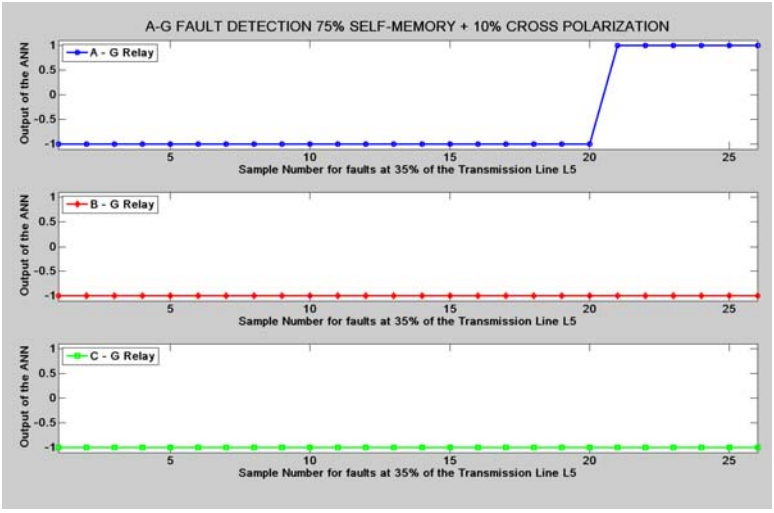

Figure G.184: Mho Relay – SLG Fault at 35% length of L_5 with 75% Self Memory + 10% Cross Polarization

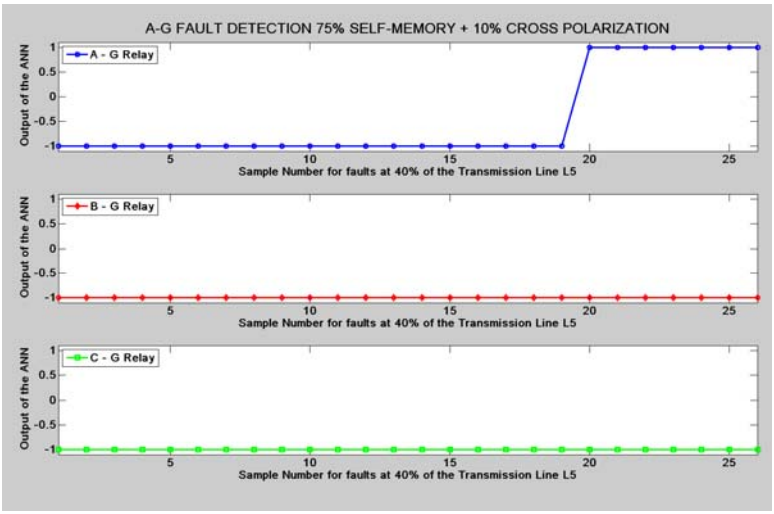

Figure G.185: Mho Relay – SLG Fault at 40% length of L_5 with 75% Self Memory + 10% Cross Polarization

Figure G.186: Mho Relay – SLG Fault at 45% length of L_5 with 75% Self Memory + 10% Cross Polarization

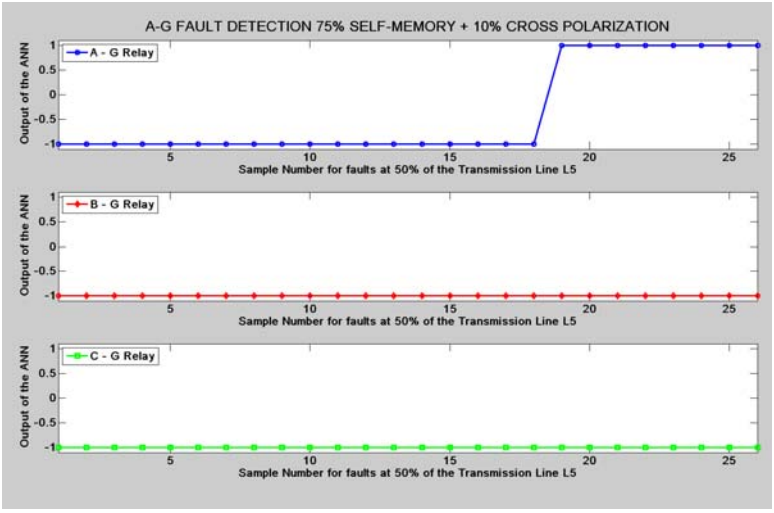

Figure G.187: Mho Relay – SLG Fault at 50% length of L_5 with 75% Self Memory + 10% Cross Polarization

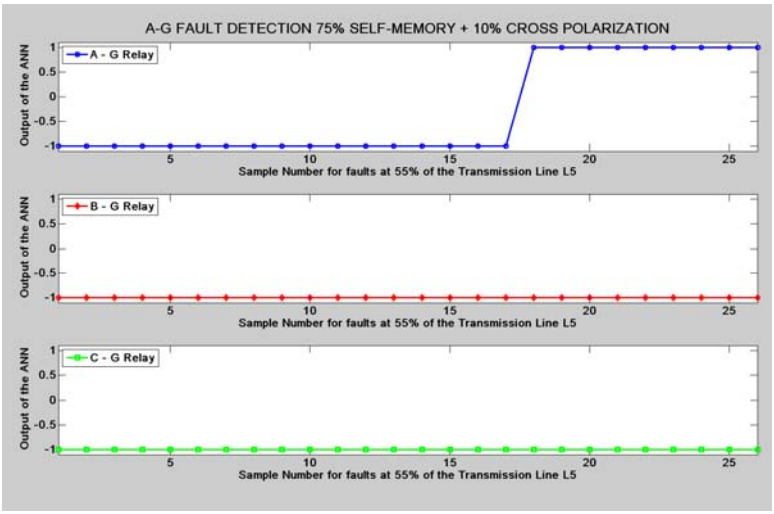

Figure G.188: Mho Relay – SLG Fault at 55% length of L_5 with 75% Self Memory + 10% Cross Polarization

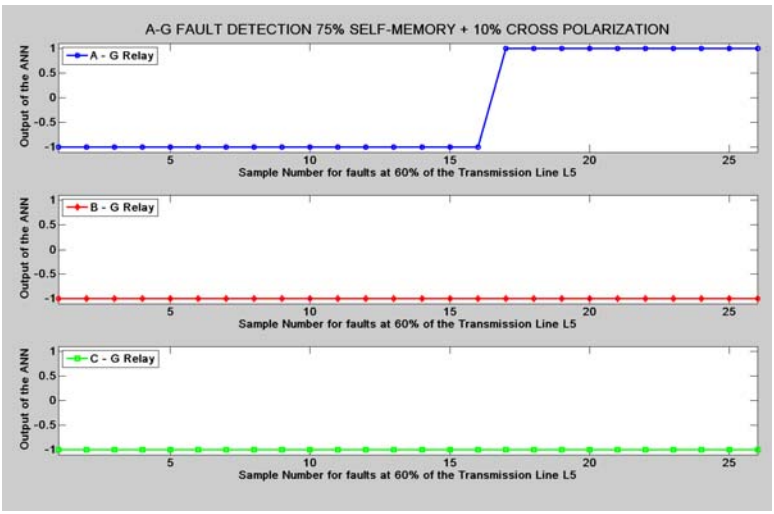

Figure G.189: Mho Relay – SLG Fault at 60% length of L_5 with 75% Self Memory + 10% Cross Polarization

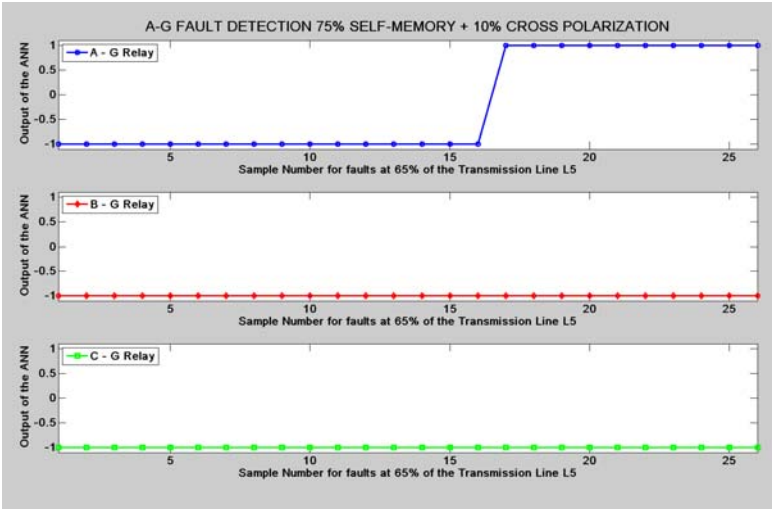

Figure G.190: Mho Relay – SLG Fault at 65% length of L_5 with 75% Self Memory + 10% Cross Polarization

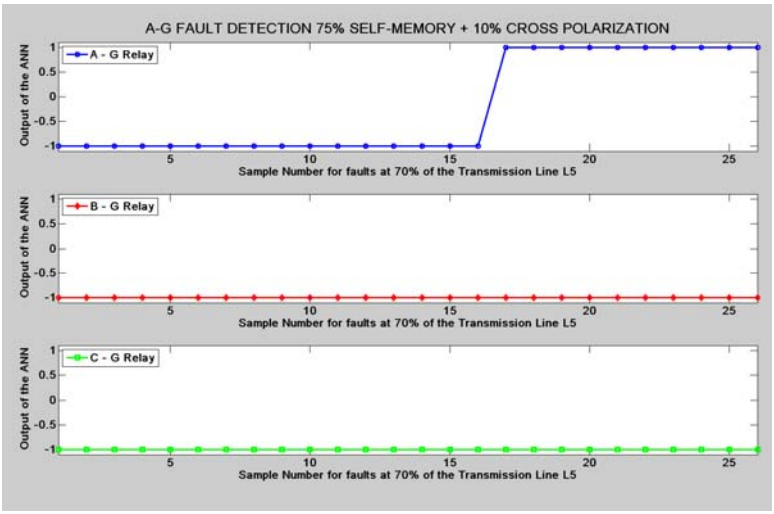

Figure G.191: Mho Relay – SLG Fault at 70% length of L_5 with 75% Self Memory + 10% Cross Polarization

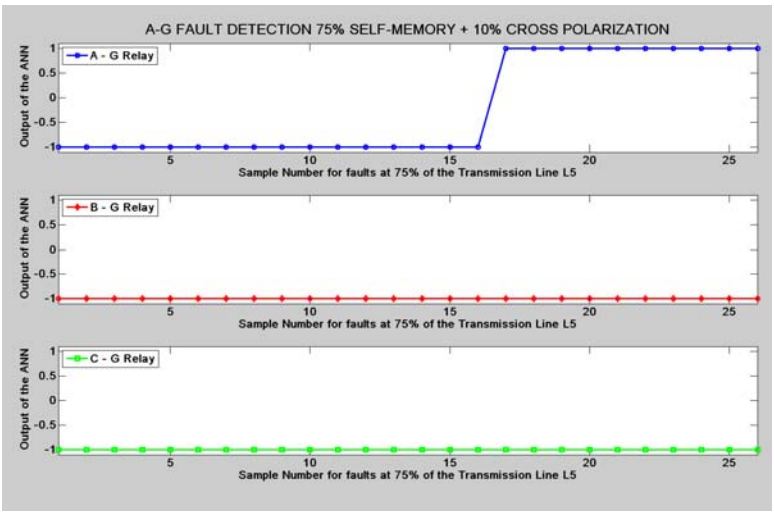

Figure G.192: Mho Relay – SLG Fault at 75% length of L_5 with 75% Self Memory + 10% Cross Polarization

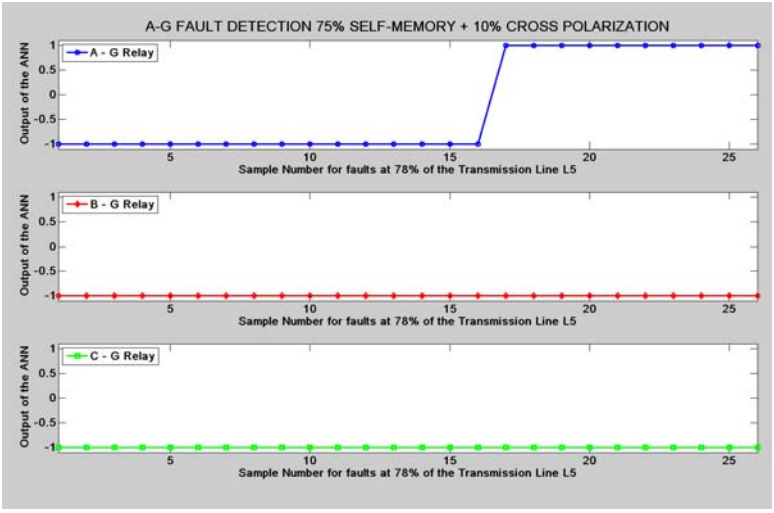

Figure G.193: Mho Relay – SLG Fault at 78% length of L_5 with 75% Self Memory + 10% Cross Polarization

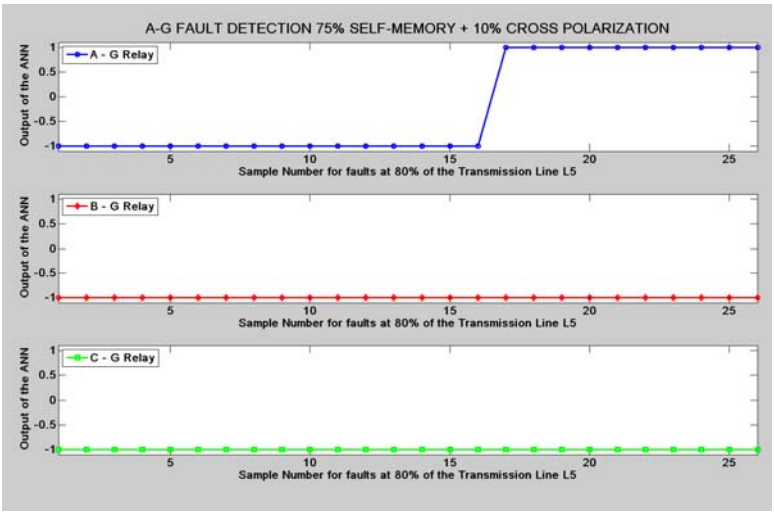

Figure G.194: Mho Relay – SLG Fault at 80% length of L_5 with 75% Self Memory + 10% Cross Polarization

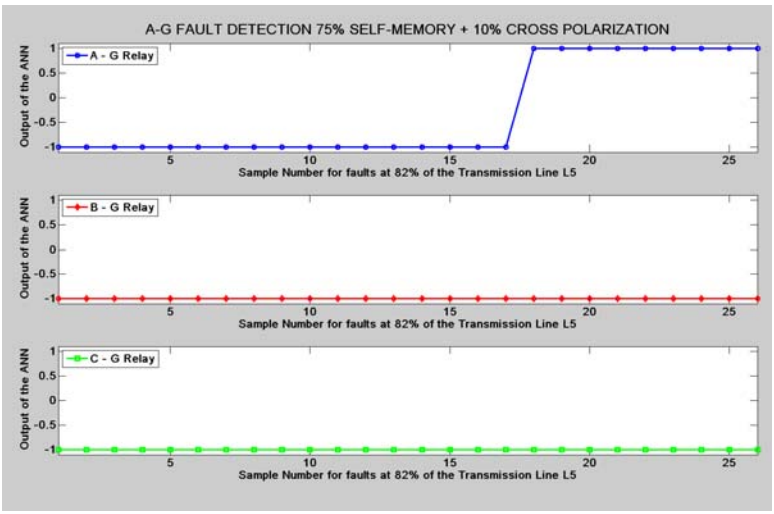

Figure G.195: Mho Relay – SLG Fault at 82% length of L_5 with 75% Self Memory + 10% Cross Polarization

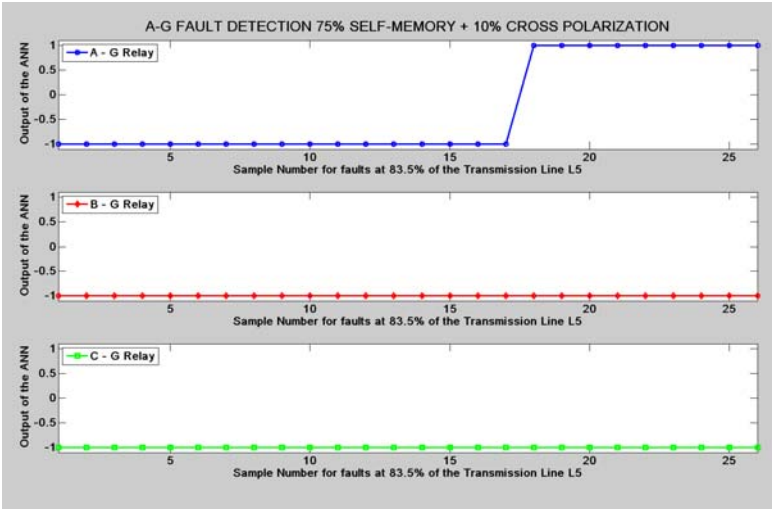

Figure G.196: Mho Relay – SLG Fault at 83.5% length of L_5 with 75% Self Memory + 10% Cross Polarization

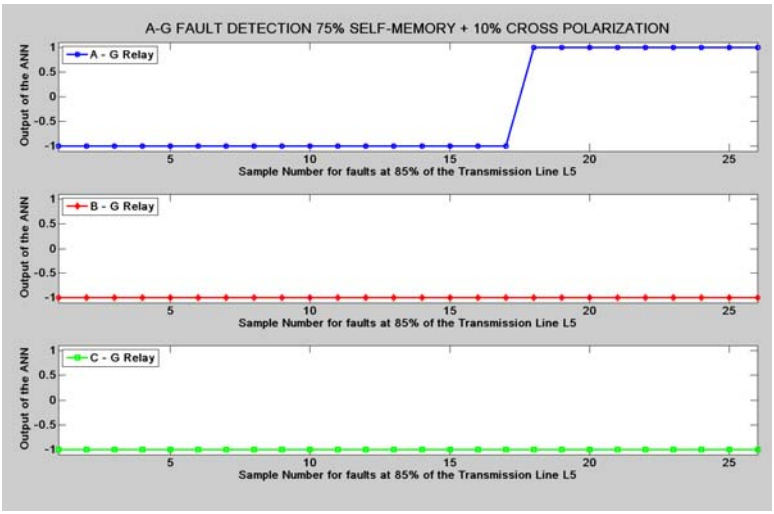

Figure G.197: Mho Relay – SLG Fault at 85% length of L_5 with 75% Self Memory + 10% Cross Polarization

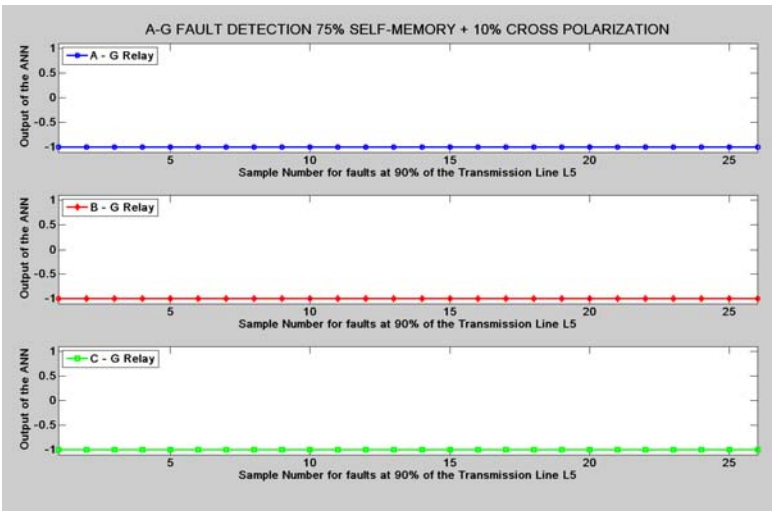

Figure G.198: Mho Relay – SLG Fault at 90% length of L_5 with 75% Self Memory + 10% Cross Polarization

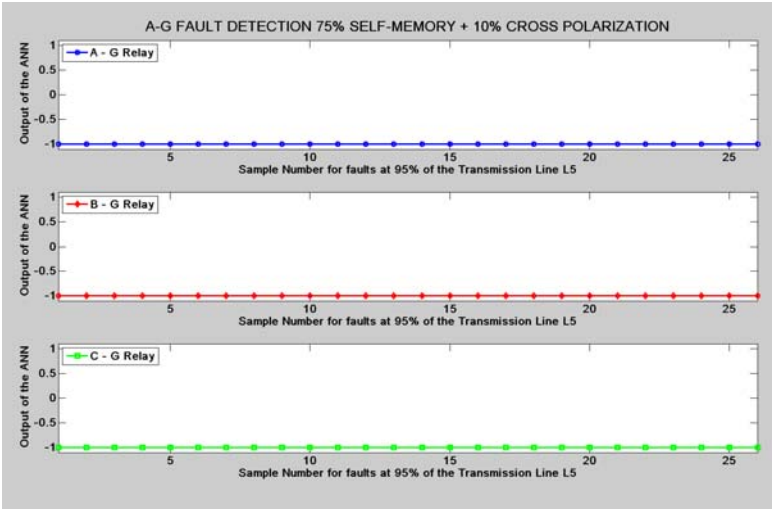

Figure G.199: Mho Relay – SLG Fault at 95% length of L_5 with 75% Self Memory + 10% Cross Polarization

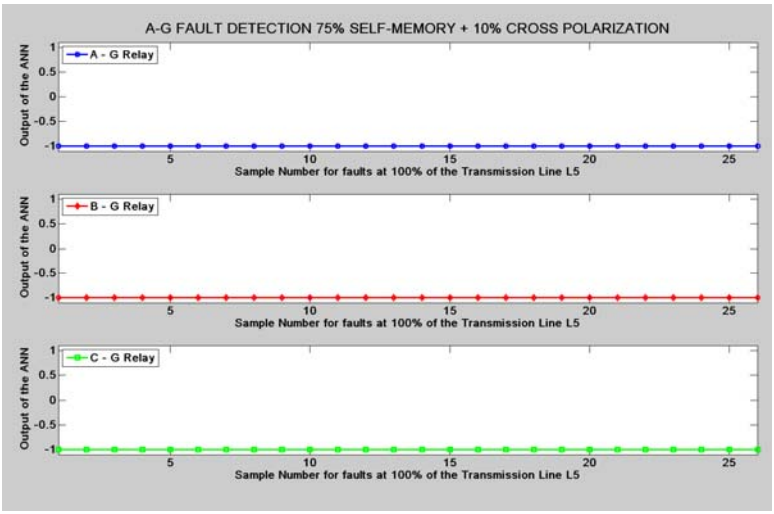

Figure G.200: Mho Relay – SLG Fault at 100% length of L_5 with 75% Self Memory + 10% Cross Polarization

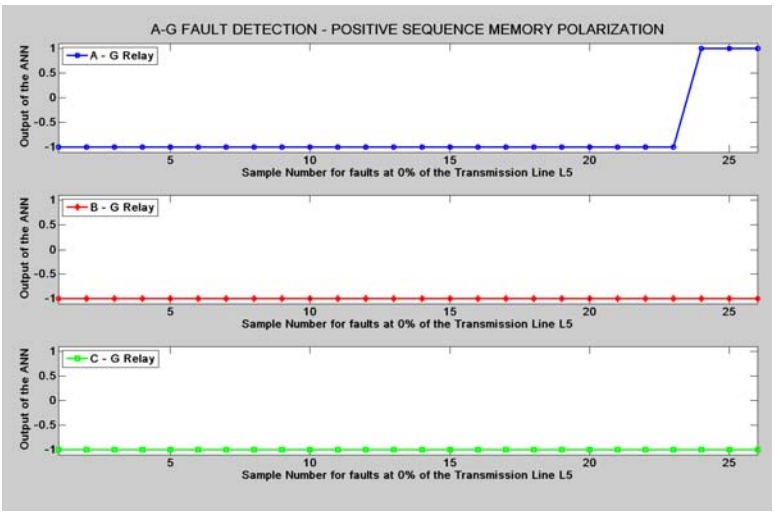

Figure G.201: Mho Relay – SLG Fault at 0% length of L_5 with Positive Sequence Memory Polarization

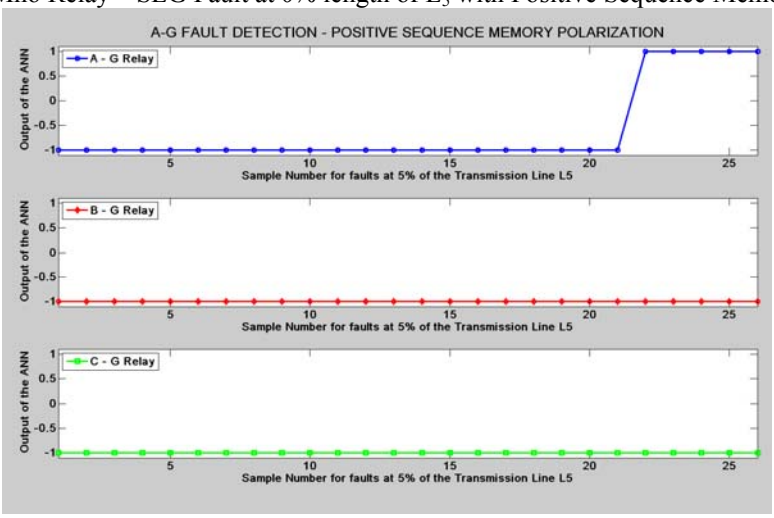

Figure G.202: Mho Relay – SLG Fault at 5% length of L_5 with Positive Sequence Memory Polarization

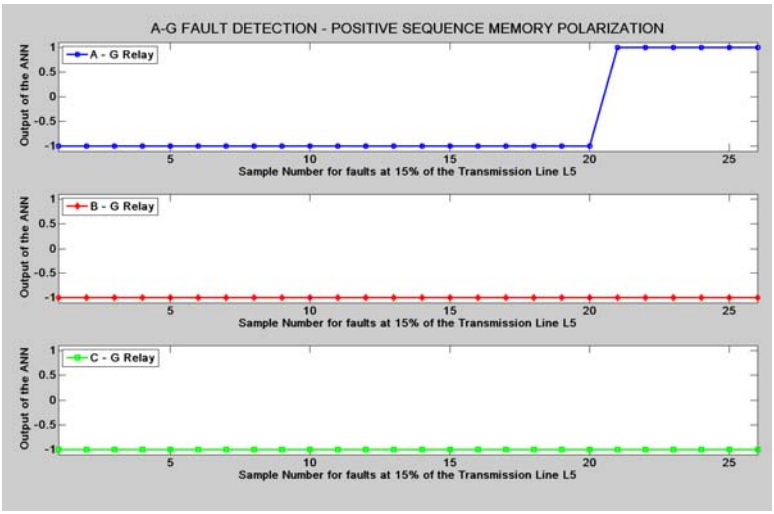

Figure G.203: Mho Relay – SLG Fault at 15% length of L_5 with Positive Sequence Memory Polarization

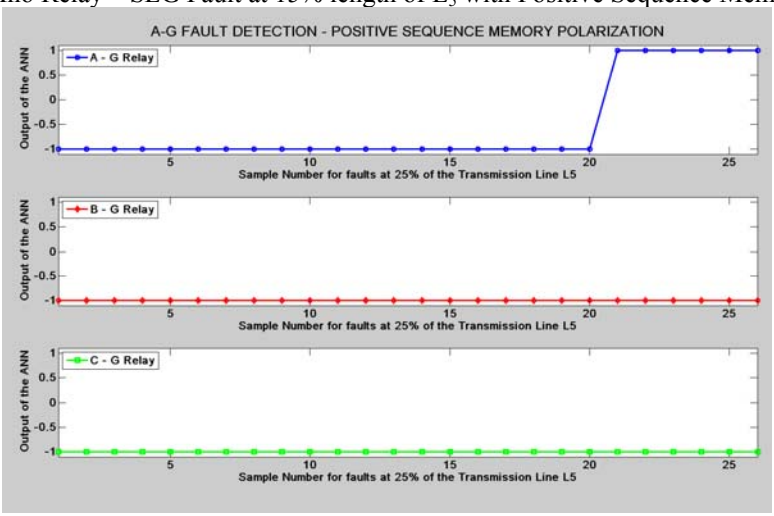

Figure G.204: Mho Relay – SLG Fault at 25% length of L_5 with Positive Sequence Memory Polarization

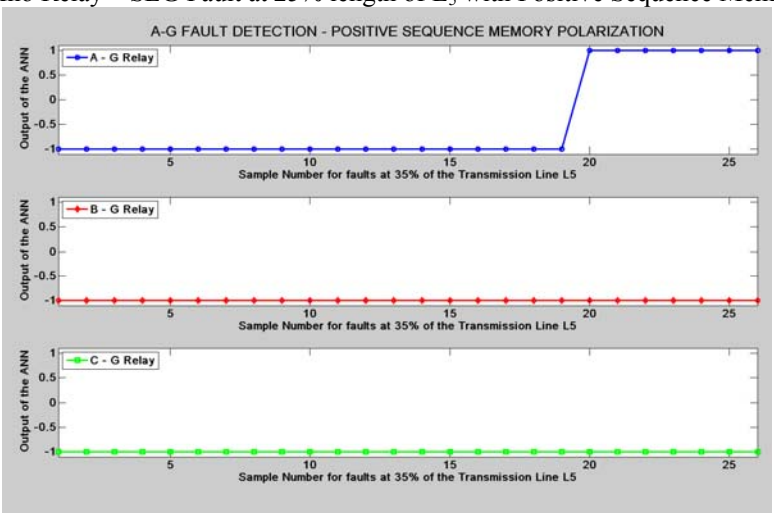

Figure G.205: Mho Relay – SLG Fault at 35% length of L_5 with Positive Sequence Memory Polarization

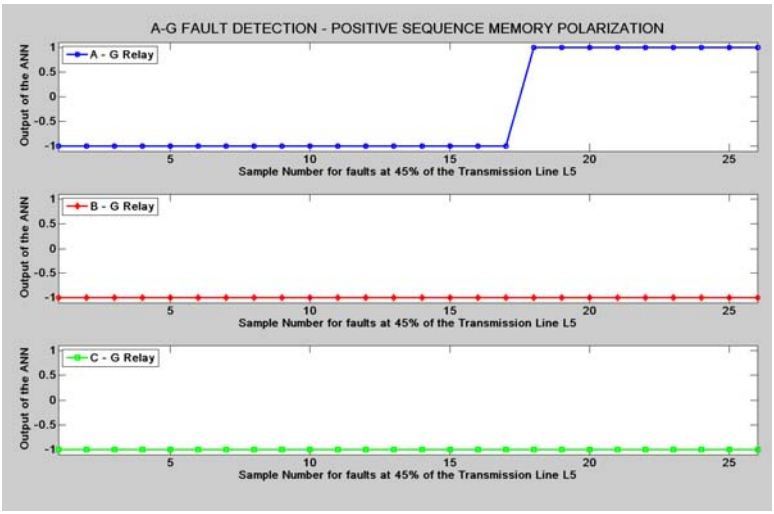

Figure G.206: Mho Relay – SLG Fault at 45% length of L_5 with Positive Sequence Memory Polarization

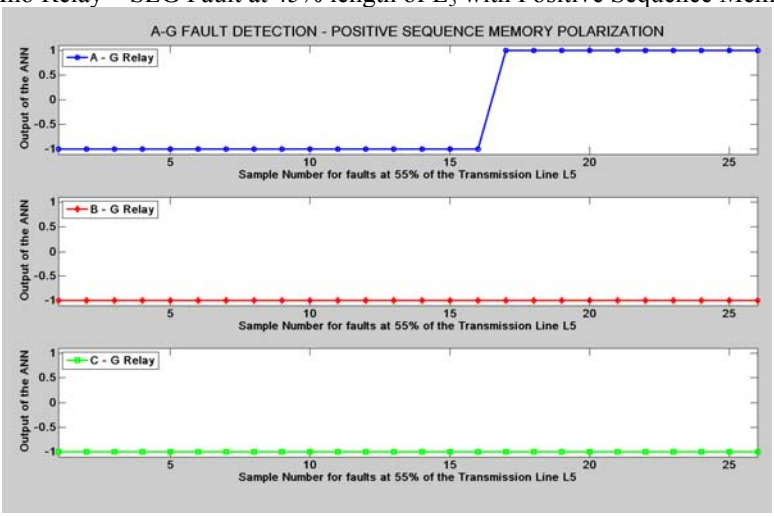

Figure G.207: Mho Relay – SLG Fault at 55% length of L_5 with Positive Sequence Memory Polarization

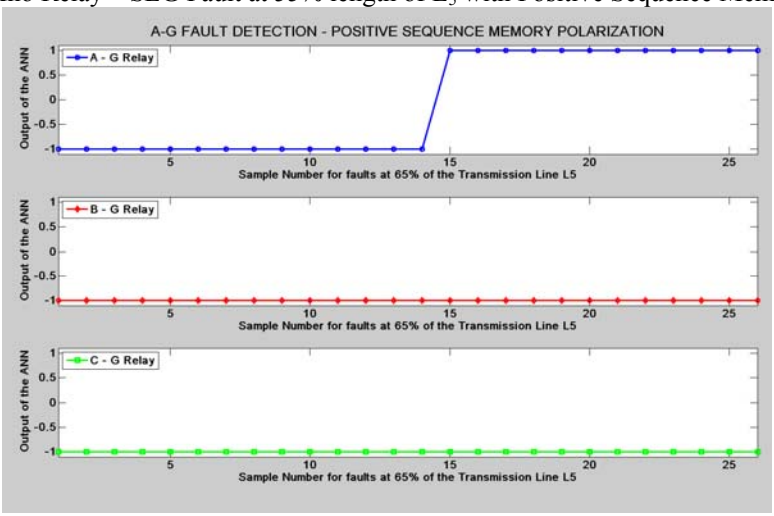

Figure G.208: Mho Relay – SLG Fault at 65% length of L_5 with Positive Sequence Memory Polarization

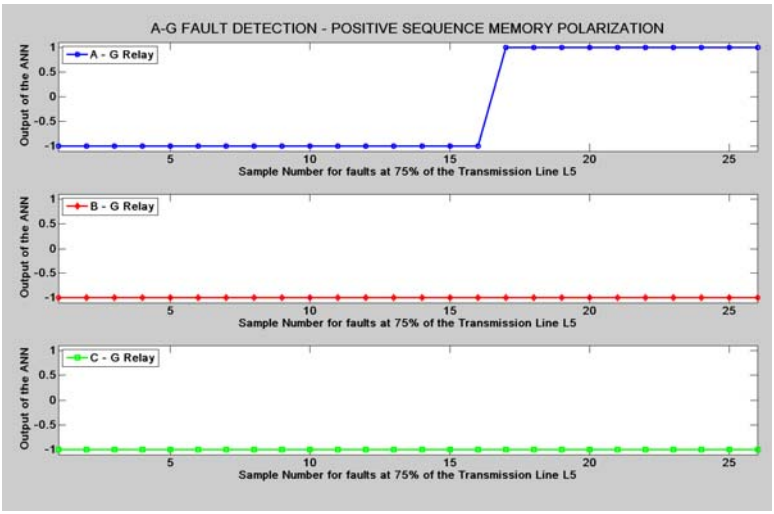

Figure G.209: Mho Relay – SLG Fault at 75% length of L_5 with Positive Sequence Memory Polarization

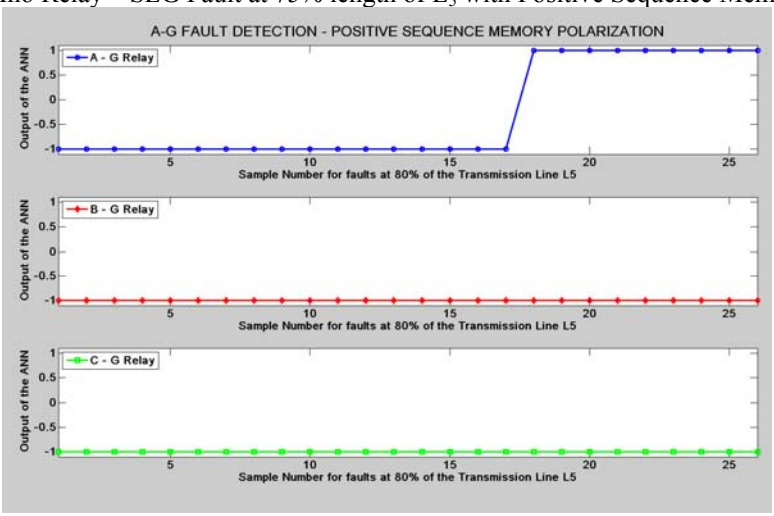

Figure G.210: Mho Relay – SLG Fault at 80% length of L_5 with Positive Sequence Memory Polarization

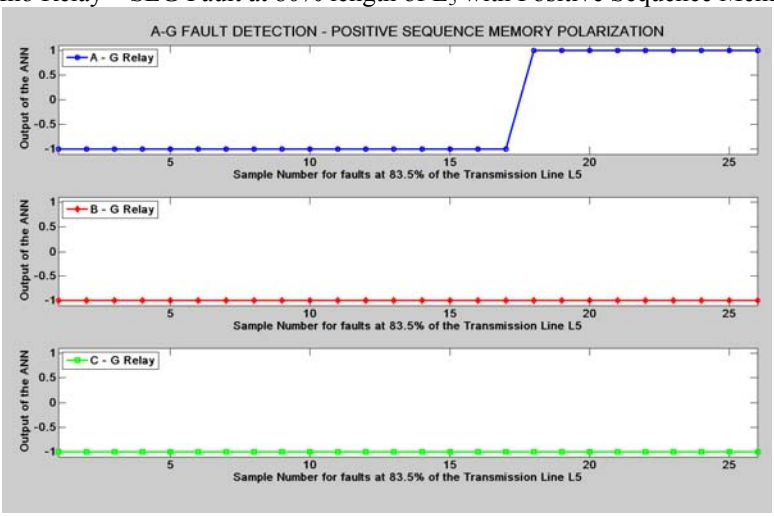

Figure G.211: Mho Relay – SLG Fault at 83.5% length of L_5 with Positive Sequence Memory Polarization

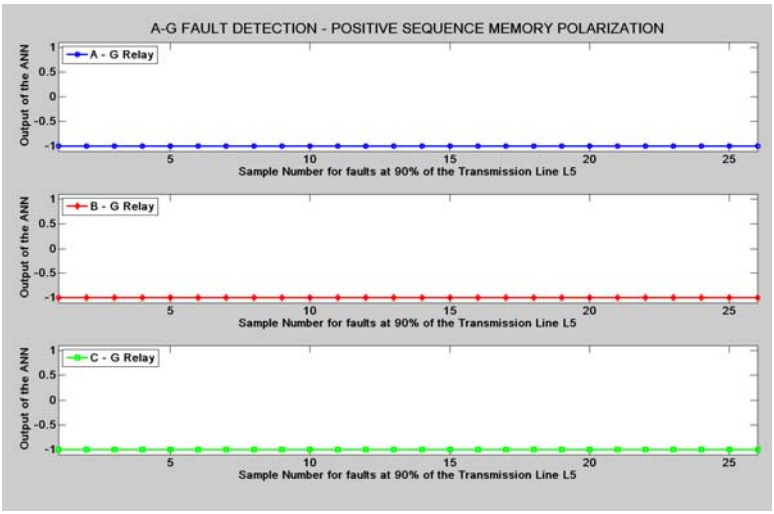

Figure G.212: Mho Relay – SLG Fault at 90% length of L_5 with Positive Sequence Memory Polarization

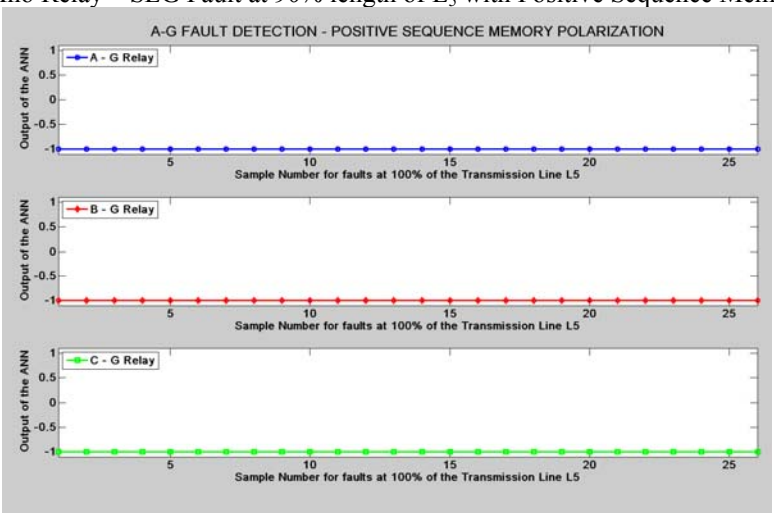

Figure G.213: Mho Relay – SLG Fault at 100% length of L_5 with Positive Sequence Memory Polarization

G.3.2 Application of Polarization Techniques for Two and Three Phase faults

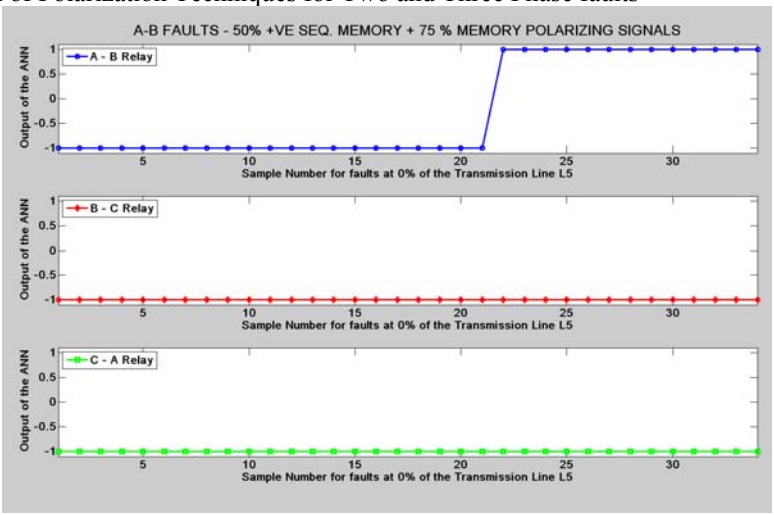

Figure G.214: Mho Relay – Line to Line Fault at 0% length of L_5 with 75% Self Memory + 50% Positive Sequence Memory Polarization

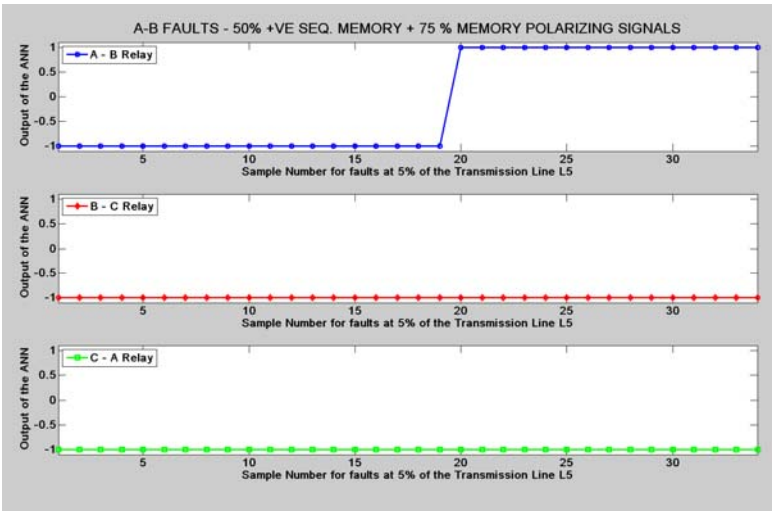

Figure G.215: Mho Relay – Line to Line Fault at 5% length of L_5 with 75% Self Memory + 50% Positive Sequence Memory Polarization

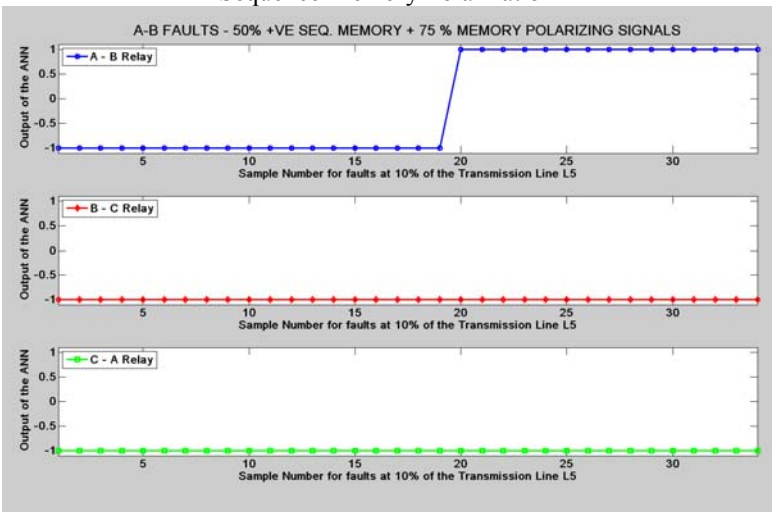

Figure G.216: Mho Relay – Line to Line Fault at 10% length of L_5 with 75% Self Memory + 50% Positive Sequence Memory Polarization

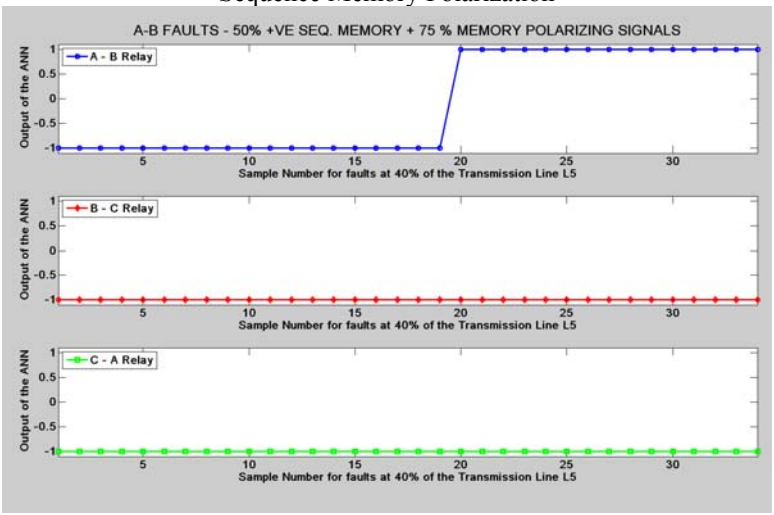

Figure G.217: Mho Relay – Line to Line Fault at 40% length of L_5 with 75% Self Memory + 50% Positive Sequence Memory Polarization

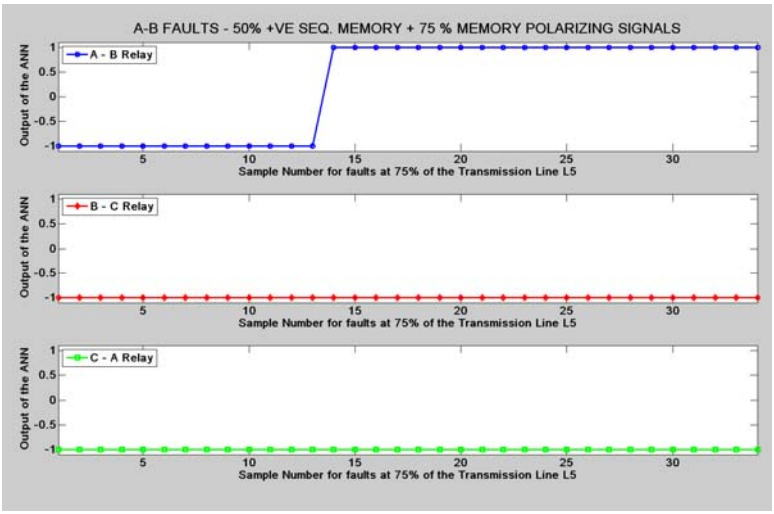

Figure G.218: Mho Relay – Line to Line Fault at 75% length of L_5 with 75% Self Memory + 50% Positive Sequence Memory Polarization

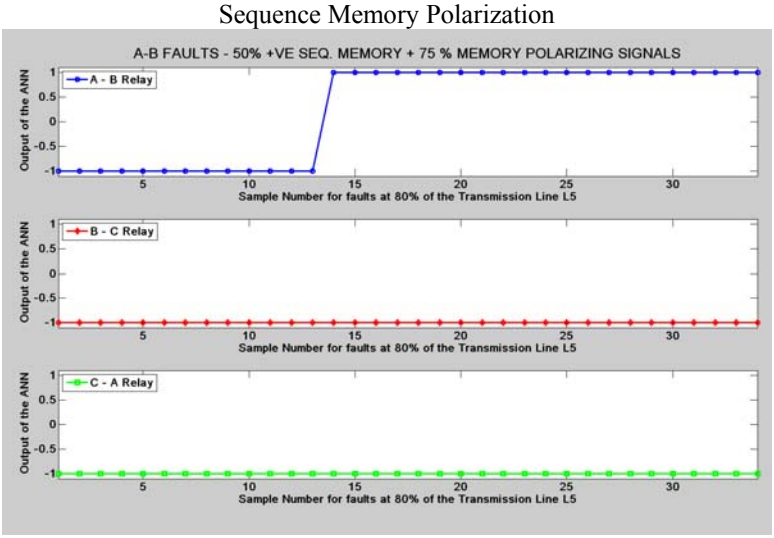

Figure G.219: Mho Relay – Line to Line Fault at 80% length of L_5 with 75% Self Memory + 50% Positive Sequence Memory Polarization

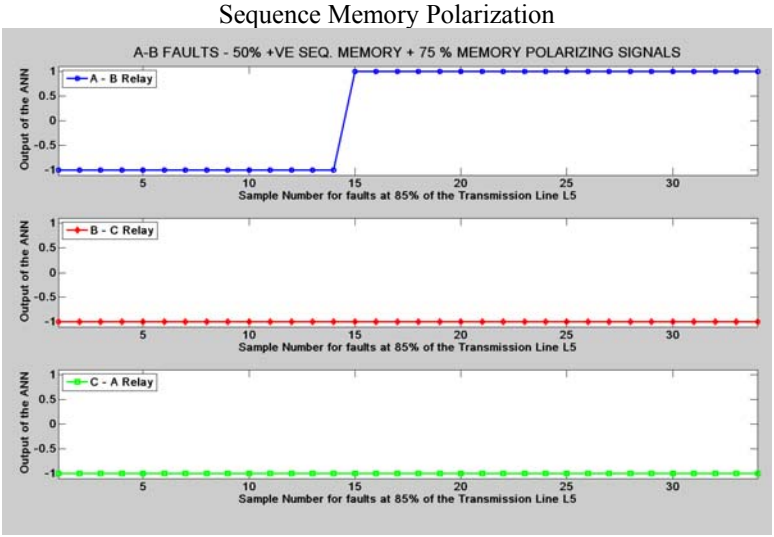

Figure G.220: Mho Relay – Line to Line Fault at 85% length of L_5 with 75% Self Memory + 50% Positive Sequence Memory Polarization

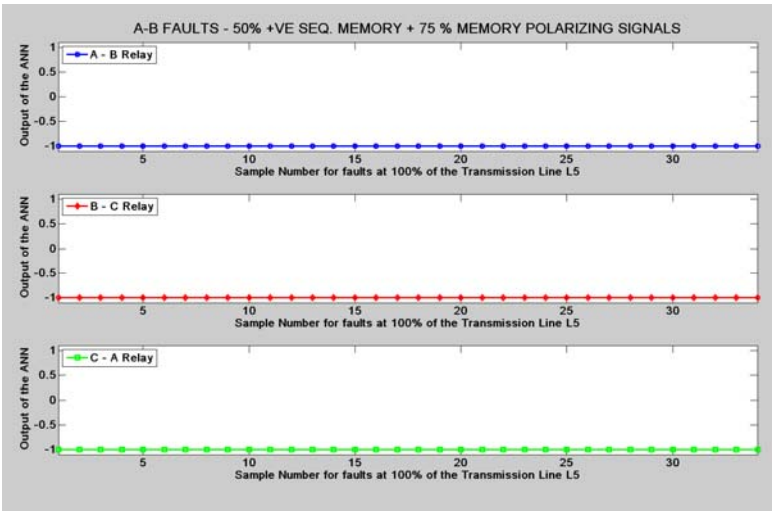

Figure G.221: Mho Relay – Line to Line Fault at 100% length of L_5 with 75% Self Memory + 50% Positive Sequence Memory Polarization

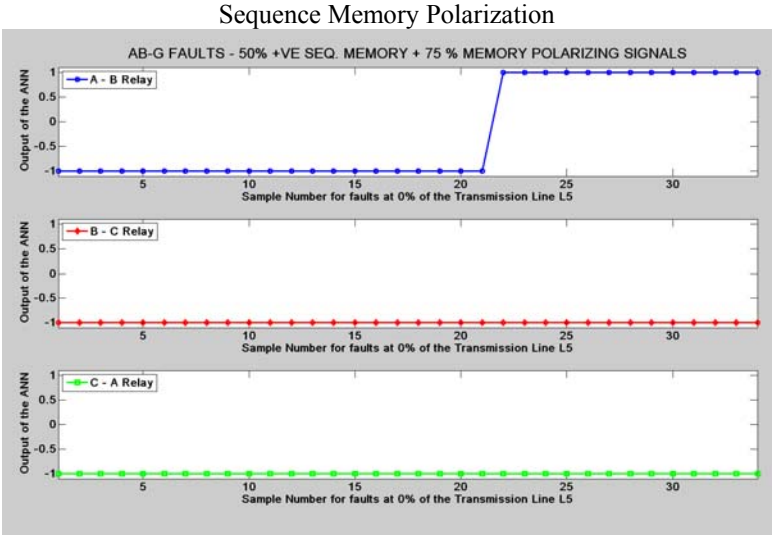

Figure G.222: Mho Relay – Double Line to Ground Fault at 0% length of L_5 with 75% Self Memory + 50% Positive Sequence Memory Polarization

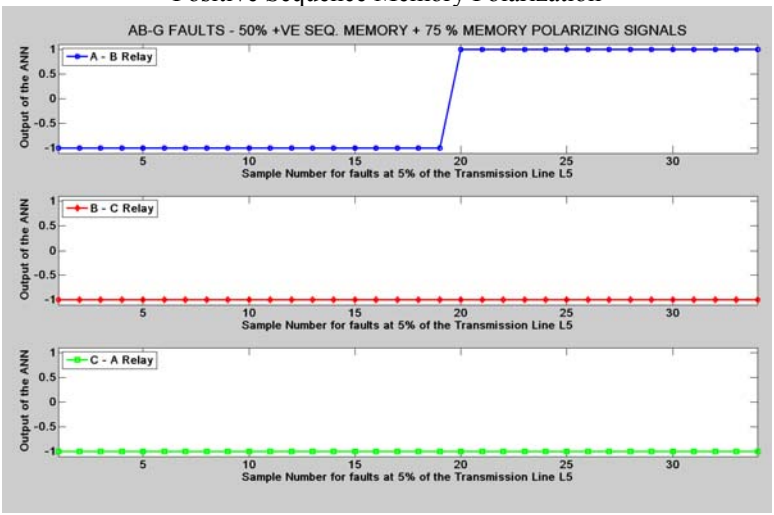

Figure G.223: Mho Relay – Double Line to Ground Fault at 5% length of L_5 with 75% Self Memory + 50% Positive Sequence Memory Polarization

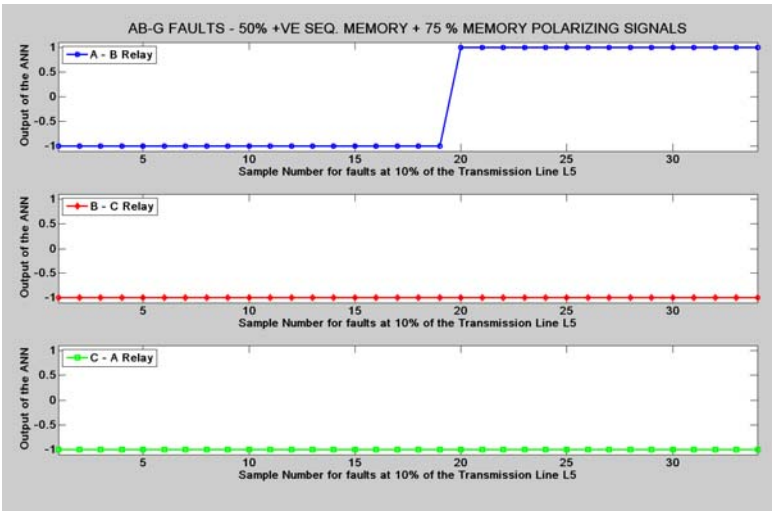

Figure G.224: Mho Relay – Double Line to Ground Fault at 10% length of L_5 with 75% Self Memory + 50% Positive Sequence Memory Polarization

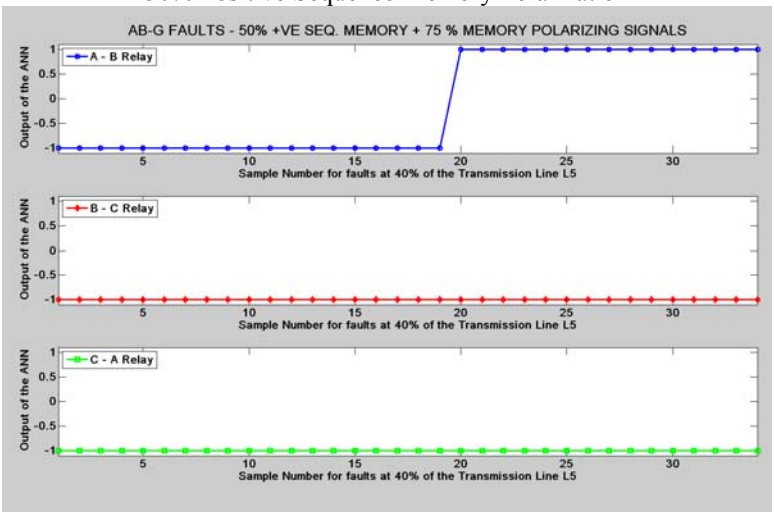

Figure G.225: Mho Relay – Double Line to Ground Fault at 40% length of L_5 with 75% Self Memory + 50% Positive Sequence Memory Polarization

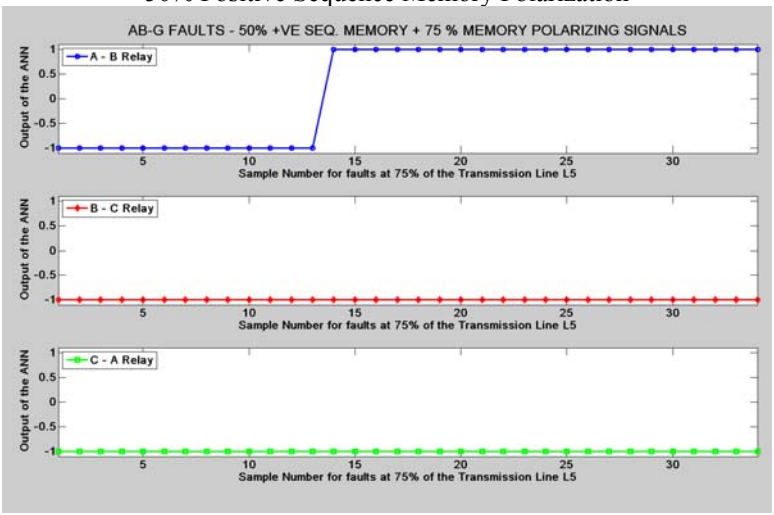

Figure G.226: Mho Relay – Double Line to Ground Fault at 75% length of L_5 with 75% Self Memory + 50% Positive Sequence Memory Polarization

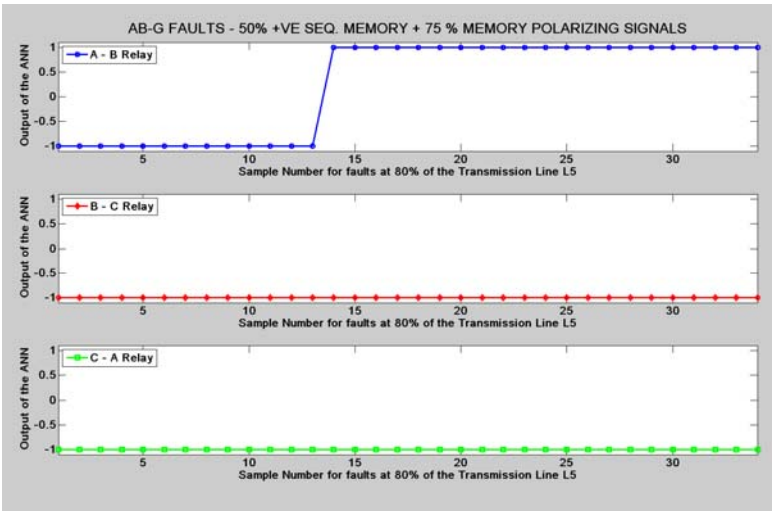

Figure G.227: Mho Relay – Double Line to Ground Fault at 80% length of L_5 with 75% Self Memory + 50% Positive Sequence Memory Polarization

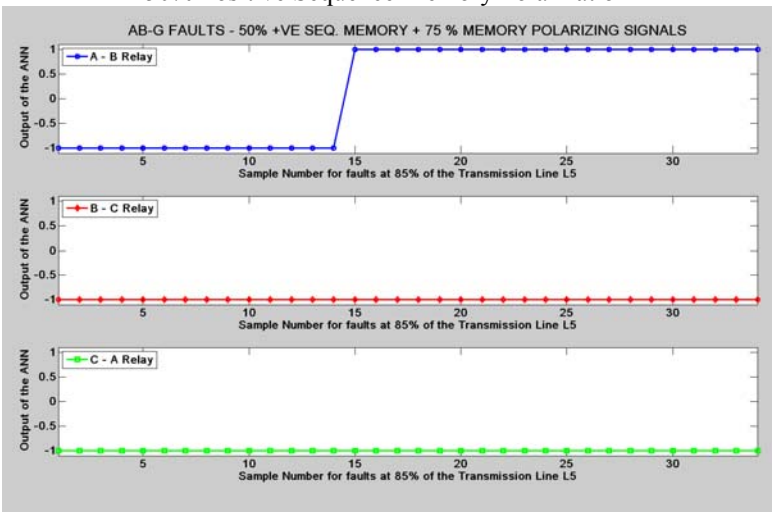

Figure G.228: Mho Relay – Double Line to Ground Fault at 85% length of L_5 with 75% Self Memory + 50% Positive Sequence Memory Polarization

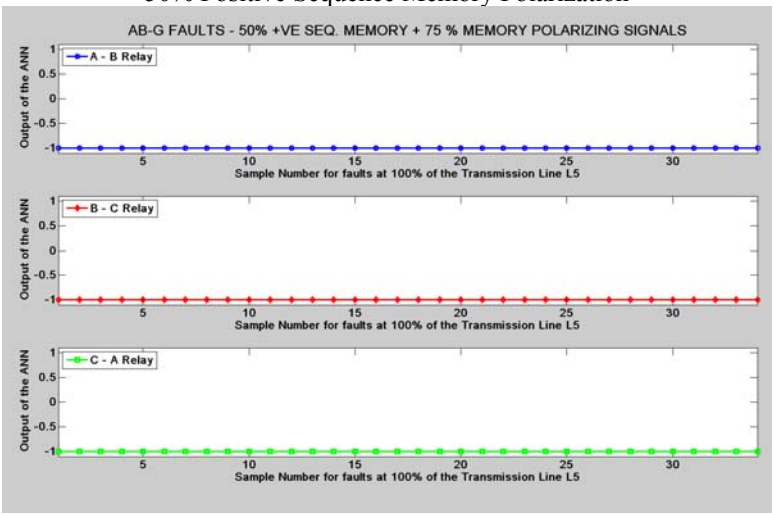

Figure G.229: Mho Relay – Double Line to Ground Fault at 100% length of L_5 with 75% Self Memory + 50% Positive Sequence Memory Polarization

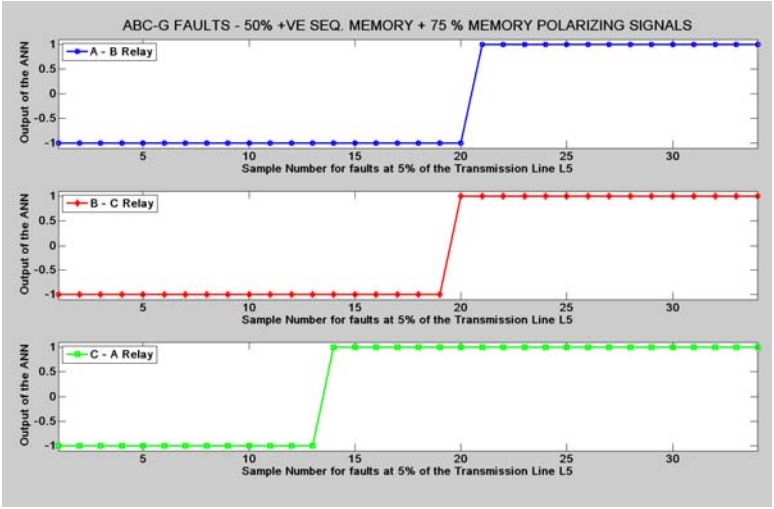

Figure G.230: Mho Relay – Three Line to Ground Fault at 5% length of L_5 with 75% Self Memory + 50% Positive Sequence Memory Polarization

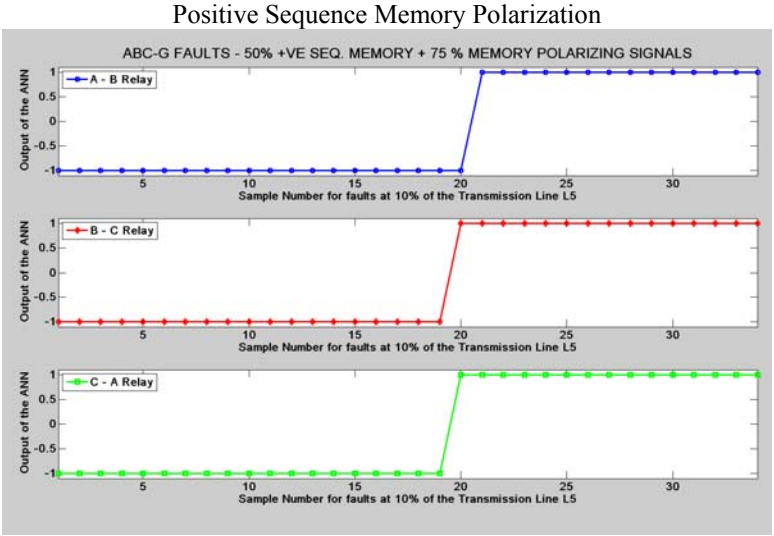

Figure G.231: Mho Relay – Three Line to Ground Fault at 10% length of L_5 with 75% Self Memory + 50% Positive Sequence Memory Polarization

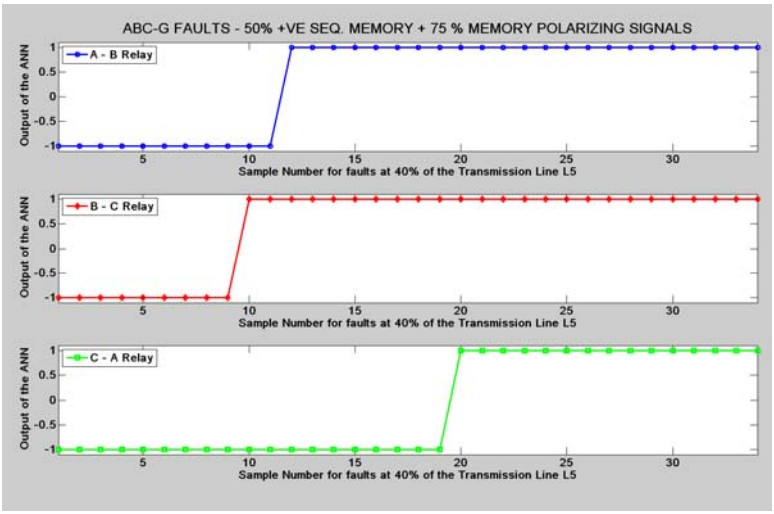

Figure G.232: Mho Relay – Three Line to Ground Fault at 40% length of L_5 with 75% Self Memory + 50% Positive Sequence Memory Polarization

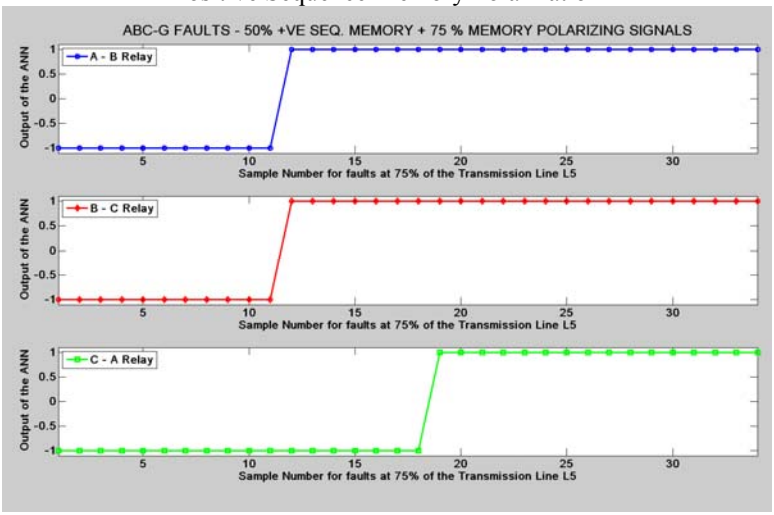

Figure G.233: Mho Relay – Three Line to Ground Fault at 75% length of L_5 with 75% Self Memory + 50% Positive Sequence Memory Polarization

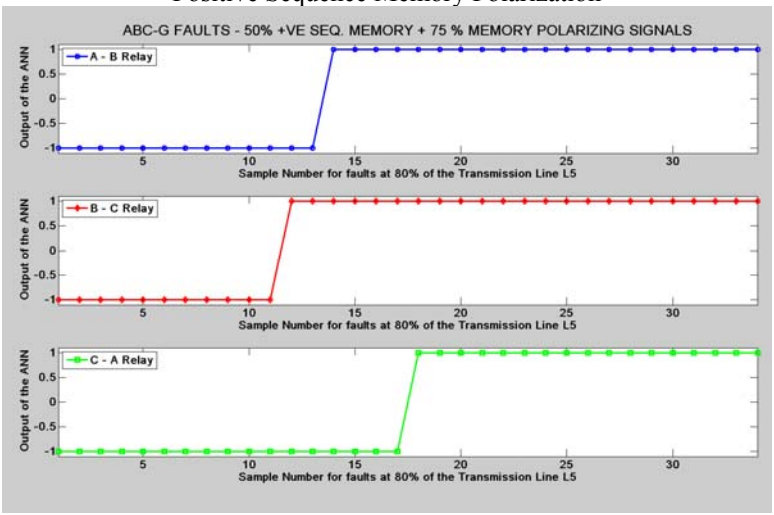

Figure G.234: Mho Relay – Three Line to Ground Fault at 80% length of L_5 with 75% Self Memory + 50% Positive Sequence Memory Polarization

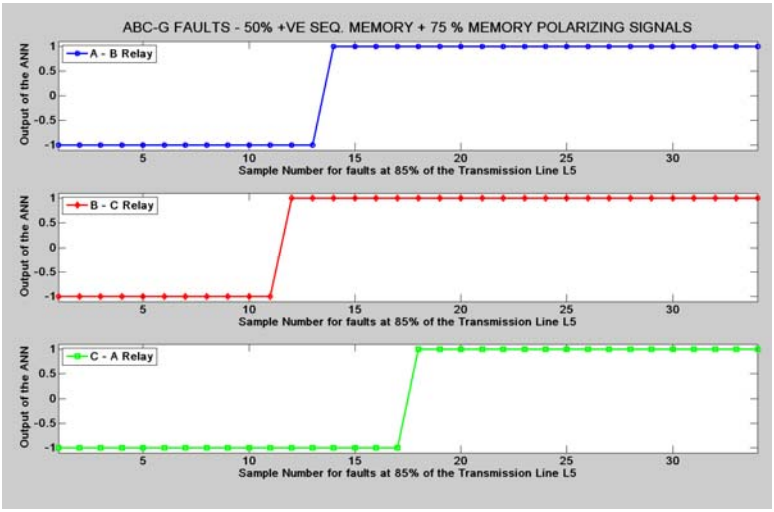

Figure G.235: Mho Relay – Three Line to Ground Fault at 85% length of L_5 with 75% Self Memory + 50% Positive Sequence Memory Polarization

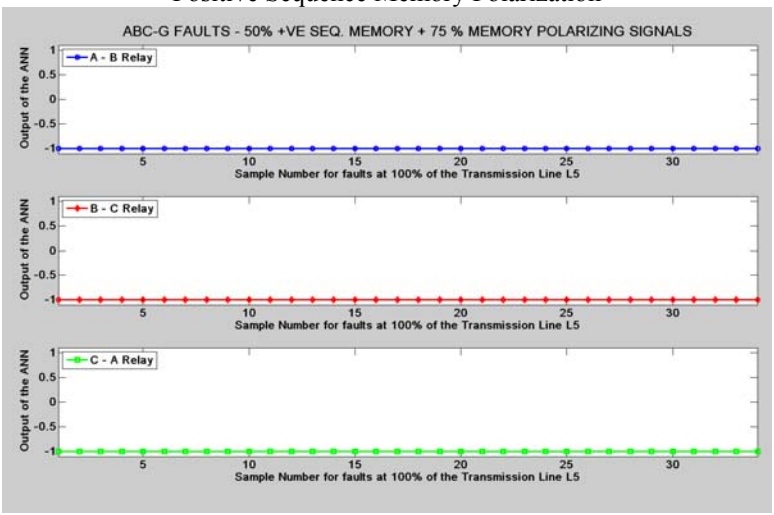

Figure G.236: Mho Relay – Three Line to Ground Fault at 100% length of L_5 with 75% Self Memory + 50% Positive Sequence Memory Polarization